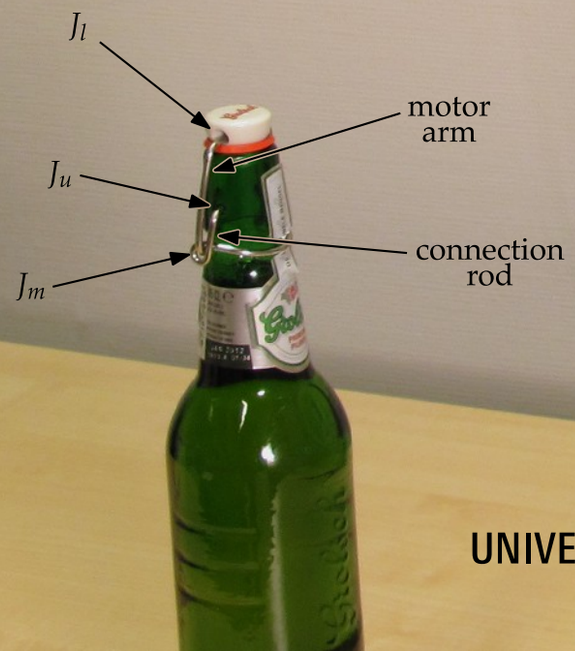

UNIVERSITEIT TWENTE.

Analysis, Control and Design of Walking Robots

Gijs van Oort

Analysis, Control and Design of Walking Robots

Gijs van Oort

Analysis, Control and Design of Walking Robots

Gijs van Oort

Promotiecommissie

Voorzitter/secr.	prof. dr. ir. A. J. Mouthaan	Universiteit Twente
Promotor	prof. dr. ir. S. Stramigioli	Universiteit Twente
Overige leden	prof. dr. A. Ruina	Cornell University
	dr. ir. M. Wisse	Technische Univ. Delft
	prof. dr. ir. P. P. Jonker	Technische Univ. Eindhoven
	prof. dr. ir. H. F. J. M. Koopman	Universiteit Twente
	prof. dr. ir. J. van Amerongen	Universiteit Twente

Paranimfen	Edwin Dertien
	Wietse Balkema

The research described in this thesis has been conducted at the Department of Electrical Engineering, Math, and Computer Science at the University of Twente, and has been financially supported by the IMPACT institute and the VIACTORS project, supported by the European Commission under the 7th Framework Programme.

The research is part of the research program of the Dutch Institute of Systems and Control (DISC). The author has successfully completed the educational program of the Graduate School DISC.

Cover picture: The design of the knee lock for the walking robot Dribbel was inspired by the mechanism of the swing top bottle (see chapter 9).

ISBN 978-90-365-3264-8
DOI 10.3990/1.9789036532648

Printed by Wöhrmann Print Service, Zutphen, The Netherlands.

ANALYSIS, CONTROL AND DESIGN OF WALKING ROBOTS

PROEFSCHRIFT

ter verkrijging van
de graad van doctor aan de Universiteit Twente,
op gezag van de rector magnificus,
prof. dr. H. Brinksma
volgens besluit van het College voor Promoties
in het openbaar te verdedigen
op woensdag 26 oktober 2011 om 14.45 uur

door

Gijs van Oort
geboren op 29 november 1978
te Nijmegen, Nederland

Dit proefschrift is goedgekeurd door

Prof. dr. ir. S. Stramigioli, promotor

ISBN 978-90-365-3264-8

DOI 10.3990/1.9789036532648

Samenvatting

Lopende robots zijn cool. De aanblik van zo'n mooi stukje voortstappend techniek spreekt velen tot de verbeelding. Momenteel worden lopende robots dan ook regelmatig ingezet in de entertainmentindustrie. Behalve leuk kunnen lopende robots ook nuttig zijn: in de toekomst kunnen ze bijvoorbeeld taken overnemen in het huishouden, in kantooromgevingen en in de zorg. Onderzoek naar lopende robots heeft, behalve voor het maken van lopende robots zelf, nog meer nut. Zo kunnen verschillende onderzoeksgebieden die betrekking hebben op lopende robots (bijvoorbeeld de analyse van multi-body-dynamica en contactmodellen), direct toegepast worden op andere vlakken van de robotica zoals het aansturen van (industriële) robotarmen en het ontwikkelen van grijpers. Ook leren we door het onderzoek veel over menselijk lopen; die kennis wordt toegepast bij revalidatie en het maken van protheses en orthoses.

In dit proefschrift worden vijf onderzoeksvragen beantwoord die van belang zijn voor de ontwikkeling van tweebenige (*bipedal*) lopende robots. De onderzoeksvragen zijn gecategoriseerd in drie hoofdonderwerpen: *analyse*, *regeling en aansturing* en *ontwerp*. De onderzoeksvragen worden hieronder besproken. De hoofdstukken van dit proefschrift zijn ieder gebaseerd op een artikel dat is gepubliceerd bij of verzonden naar een conferentie.

DEEL I: Analyse

Hoe kunnen we het gedrag analyseren van een 2D passief-dynamische loper die over oneffen terrein loopt?
Een bekende analyse-tool voor 2D passief-dynamische lopers[1] is de *post-impact Poincaré-sectie*: het 'vlak' in de toestandsruimte bestaande uit alle mogelijke toestanden[2] van de loper direct na de voet-impact op vlakke vloer. Dit concept kan

[1] *2D loper*: een lopertje dat niet naar links en rechts kan omvallen; alleen naar voren en achteren (de bewegingsruimte is gereduceerd tot een tweedimensionaal vlak). *Passief-dynamische loper*: maakt gebruik van het natuurlijke (passieve) zwaaigedrag van de benen; hierdoor is voor het naar voren zwaaien van het been geen energie nodig.

[2] *Toestand*: de positie en snelheid van alle ledematen van de robot (Engels: *state*).

echter niet gebruikt worden als de loper op oneffen terrein loopt. In dit proefschrift wordt hiervoor een oplossing geboden in de vorm van een *mapping* die met iedere mogelijke post-impact toestand op oneffen terrein een punt op de Poincaré-sectie associeert (hoofdstuk 2).

Kunnen we, door middel van een 'andere kijk' op de robot, meer inzicht krijgen in de dynamica?
Om de toestand van een robot numeriek te representeren (zodat ermee gerekend kan worden) maken we vaak gebruik van *coördinaten*. Er bestaan vele verschillende coördinaatrepresentaties (b.v. absolute hoeken, of juist relatieve) van een toestand; welke representatie het meest geschikt is hangt af van het specifieke probleem dat opgelost moet worden. Sommige problemen kunnen ook zonder het gebruik van coördinaten (*geometrisch*) worden opgelost.

Voor lopende robots wordt vaak een coördinaatrepresentatie gekozen waarbij de torso het referentielichaam is. In dit proefschrift wordt aangetoond dat dit niet altijd de meest geschikte keuze is; soms is de standvoet als referentielichaam beter. De vergelijkingen die de bewegingen van de robot beschrijven worden dan eenvoudiger en door deze te bestuderen kan men beter inzicht krijgen in de robotdynamica (hoofdstuk 3).

In dit proefschrift wordt een methode beschreven om, gegeven de grondcontactwrench (de kracht die de grond uitoefent op de voet van de robot), op een coordinaat-vrije manier de positie te bepalen van het Zero-Moment Point[3] (ZMP). In plaats van wiskundige vergelijkingen wordt er gebruik gemaakt van geometrische relaties, wat het inzicht in de materie verhoogt (hoofdstuk 4).

Vaak helpt het om voor de analyse een versimpeld model van de robot te gebruiken. In dit proefschrift wordt zo'n model besproken: het *locked inertia model*. Hierin wordt de robot voorgesteld als zijnde één star lichaam. De wiskundige vergelijkingen van het model zijn veel eenvoudiger dan die van de robot zelf en kunnen gebruikt worden als startpunt voor analyse van de dynamica van de robot (hoofdstuk 5).

DEEL II: Regeling en aansturing

Hoe kunnen we een robot regelen om hem te stabiliseren in de laterale (zijwaartse) richting?
In dit proefschrift worden twee regelaars besproken die dit kunnen bewerkstelligen. Beide maken gebruik van 'laterale voetplaatsing': door de voet iets meer naar links of rechts neer te zetten, kan gezorgd worden dat de robot niet naar links of rechts omvalt.

Bij de eerste methode (toegepast op een zeer simpel loper-model) wordt precies

[3]De positie van dit punt (op de vloer) geeft een indicatie of de standvoet stevig op de grond staat.

halverwege de stap (*mid-stance*) de zijwaartse snelheid van de heup gemeten en via een lineaire P-regelaar teruggekoppeld naar de zijwaartse positie van de voet. Er wordt numeriek aangetoond dat deze regelaar een stabiel systeem oplevert met een grote robuustheid tegen verstoringen (hoofdstuk 6).

De tweede methode gebruikt het *Extrapolated Center of Mass*[4] (XCOM) als invoer voor de (lineaire) regelaar. Deze methode is geïmplementeerd in TUlip[5]. Testresultaten laten zien dat de robot met de regelaar inderdaad stabiel is in laterale richting (hoofdstuk 7).

Hoe kunnen we de actuatoren verbeteren om een minimaal energieverbruik te verkrijgen?
De actuatoren ('motoren') die in de meeste lopende robots zitten zijn niet erg energiezuinig. In dit proefschrift wordt een concept voor een nieuw type actuator geïntroduceerd dat negatieve arbeid mechanisch kan opslaan en later hergebruiken. De actuator bestaat uit een DC motor, een rem om de motoras vast te zetten, een spiraalveer en een 'oneindig variabele transmissie' (IVT) (hoofdstuk 8).

DEEL III: Ontwerp

Hoe kunnen we het knie- en enkelgewricht van een lopende robot verbeteren?
Het kniegewricht van Dribbel[6] en het enkelgewricht van TUlip voldeden niet aan onze verwachtingen. Door veel aandacht te besteden aan het formuleren van de precieze eisen van de gewrichten, kwamen we tot creatieve ontwerpoplossingen.

Het eerste ontwerp is een innovatief knie-blokkeermechanisme, dat ervoor zorgt dat het standbeen van de robot gestrekt blijft. Het is gebaseerd op een 'vierstangenmechanisme' (*four-bar linkage*) en blokkeert door middel van een *mechanische singulariteit*: een bepaalde stand van het mechanisme waarin één bewegingsrichting van het mechanisme geblokkeerd wordt. Het geblokkeerd houden van de knie kost geen energie terwijl het deblokkeren zeer gemakkelijk gaat. Het ontwerp is succesvol toegepast in de 2D loper Dribbel (hoofdstuk 9).

Het tweede ontwerp is een twee-graden-van-vrijheid enkelbesturing. In plaats van het gebruik van één motor voor het actueren van de x-as en één voor de y-as, zijn beide motoren gemonteerd in een *differentieelopstelling*. Draaien de motoren beide in dezelfde richting, dan wordt de x-as geactueerd; draaien ze in tegengestelde richting, dan wordt de y-as geactueerd. Voordeel hiervan is dat de kracht van beide motoren samen gebruikt kan worden voor de enkelafzet tijdens het lopen, waardoor kleine motoren kunnen volstaan (hoofdstuk 10).

[4] De positie van dit punt (op de vloer) geeft een indicatie van waar de voet neergezet moet worden om de robot in één stap tot stilstand te brengen.

[5] *TUlip*, een 3D lopende robot, is ontwikkeld in een samenwerkingsproject van de Universiteit Twente (vakgroep Control Engineering), en de Technische Universiteiten van Delft en Eindhoven.

[6] *Dribbel*, een 2D lopende robot, is ontwikkeld op de vakgroep Control Engineering van de Universiteit Twente.

Summary

Walking robots are cool. The appearance of such a beautiful piece of technology that moves around in the way that we humans do, is appealing to many. Consequently, walking robots are regularly being used in the entertainment industry. Apart from being fun, walking robots can also be useful: in the future they can for example take over tasks in household, office environments and the health care sector. Research on walking robots is, except for making the walking robots themselves, of more use. Several research areas related to walking robots (such as analysis of multi-body dynamics and contact models) can be directly applied in other robotics fields such as the control of (industrial) robot arms and the development of grippers. Also, by researching walking robots, we learn a lot about human walking; this knowledge is being applied in rehabilitation and the development of prostheses and orthoses.

In this thesis five research questions are discussed that are related to the development of two-legged (*bipedal*) walking robots. The research questions are categorized in three main topics: *analysis*, *control and actuation* and *design*. The research questions are discussed below. Each chapter of this thesis is based on an article which was published at or submitted to a conference.

PART I: Analysis

How can we analyze the behavior of a 2D passive dynamic walker that is walking on rough terrain?
A well-known analysis tool for 2D passive dynamic walkers[1] is the *post-impact Poincaré section*: the 'plane' in the state space consisting of all possible states[2] of the walker directly after foot-impact on a flat floor. This concept however can not be used if the walker is walking on rough terrain. In this thesis a solution to this

[1] *2D walker*: a walking system that cannot fall sideways; only forward and backward (the motion space is reduced to a two-dimensional plane). *Passive dynamic walker*: utilizes the natural (passive) swinging motion of the legs; because of this no energy is required to swing the leg forward.

[2] *State*: the position and velocity of all parts of the body.

is given by providing a *mapping* that associates with each possible post-impact state on rough terrain a point on the Poincaré section (chapter 2).

By looking at the robot from a different 'perspective', can we gain more insight in its dynamics?
In order to represent the state of a robot numerically (to be able to do calculations with it), we often make use of *coordinates*. There exist many different coordinate representations (*e.g.*, absolute angles, or relative ones) of a state; which of the representations is most suitable depends on the exact problem that needs to be solved. Some problems can also be solved without the use of coordinates, *i.e.*, in a *geometric* manner.

For walking robots usually a coordinate representation is chosen in which the torso is the reference body. In this thesis it is shown that this is not always the best choice; sometimes it is more convenient to take the stance foot as the reference body. The equations that describe the motions of the robot become simpler and by studying these, one can gain better insight in the robot dynamics (chapter 3).

In this thesis a method is presented for determining the position of the Zero-Moment Point[3] (ZMP) in a coordinate-free way, given the ground reaction wrench (the force the ground exerts on the foot of the robot). Instead of using mathematical equations, the method uses geometrical relations, which gives more insight in the material (chapter 4).

It is often helpful to use a simplified model of the robot. In this thesis such a model is discussed: the *locked inertia model*. In this model the robot is represented as a single rigid body. The mathematical equations of this model are much simpler than those of the robot itself and can be used as a starting point for analysis of the dynamics of the robot (chapter 5).

PART II: Control and actuation

How can we control a walking robot in order to stabilize it in the lateral (sideways) direction?
In this thesis two controllers are discussed that can achieve this. Both controllers make use of 'lateral foot placement': positioning the foot a little to the left or right, which prevents the robot from falling sideways.

In the first method (applied to a very simple walker model), the sideways velocity of the hip is measured, exactly halfway the step (at *mid-stance*). This velocity is then, through a linear P-controller, fed back to the lateral position of the foot. It is shown numerically that this controller yields a stable system with a large

[3]The position of this point (on the floor) gives an indication whether the stance foot is firmly standing on the ground.

robustness margin (chapter 6).

The second method uses the *Extrapolated Center of Mass*[4] (XCOM) as input of the (linear) controller. This method was implemented in TUlip[5]. Experimental results show that the robot is indeed stabilized in the lateral direction (chapter 7).

How can we improve the actuators in order to get minimum energy consumption?
The actuators ('motors') commonly used in walking robots are not very energy efficient. In this thesis a concept is introduced for a new type of actuator which can store negative work mechanically and re-use it later. The actuator consists of a DC motor, a clutch to fix the motor axis, a rotational spring and an 'infinitely variable transmission' (IVT) (chapter 8).

PART III: Design

How can we improve the knee and ankle joints of a walking robot?
The knee joint of Dribbel[6] and the ankle joint of TUlip did not meet our expectations. By paying much attention to formulating the exact requirements of these joints, we came up with creative design solutions.

The first design is an innovative knee locking mechanism, which keeps the stance leg of the robot stretched. It is based on a *four-bar linkage* and locks by means of a *mechanical singularity*: a certain configuration of the mechanism in which one direction of motion of the mechanism is locked. Keeping the knee locked does not require any energy, and unlocking goes easily. The design was successfully applied on the 2D walker Dribbel (chapter 9).

The second design is a two-degrees-of-freedom ankle actuation system. Instead of using one motor for actuating the x-axis and one for the y-axis, both motors are mounted in a *differential setup*. When both motors turn in the same direction, the x-axis is actuated; if they turn in opposite direction, the y-axis is actuated. The advantage of this is that the force of both motors together can be used for ankle push-off, which allows the use of smaller motors (chapter 10).

[4]The position of this point (on the floor) gives an indication of where the foot should be placed in order to bring the robot to a stand-still in one step.

[5]*TUlip*, a 3D walking robot, was developed in a collaboration project of University of Twente (the Control Engineering group) and the Technical Universities of Delft and Eindhoven.

[6]*Dribbel*, a 2D walking robot, was developed at the Control Engineering group of the University of Twente.

Contents

Chapter 1

Introduction

1.1 The field of walking robots

Walking robots are fascinating machines. They beautifully combine advanced technology on the one side, and basic human-like behavior on the other. Scientifically, walking robots can also be seen as interesting research objects. One of the reasons for that is that many different disciplines are needed in order to be able to build them and make them walk properly. Walking robots themselves and the research conducted on it will be focused upon in more detail below.

1.1.1 Walking robots

There are different types of walking robots. The most appealing are walking robots that are roughly shaped like a human: two legs, two arms, a torso and a head. These are called *humanoid robots*. Robots that have two legs (but are not necessarily) humanly shaped are called *bipedal robots*. Opposed to that are *multi-legged robots*, which are usually inspired by some animal. Some of the smaller multi-legged robots are very capable of negotiating rough terrain such as debris of collapsed buildings. Therefore, they are sometimes used in search and rescue operations to find casualties.

Some of the walking robots that exist today are shown in figure 1.1. It should be noted that only a small part of all existing robot designs are actually commercially available; most are prototypes from universities or spin-off companies. This thesis discusses bipedal walking only, therefore, the rest of this section will focus on bipedal robots.

Humanoid robots gradually find their way into the entertainment industry. Now-

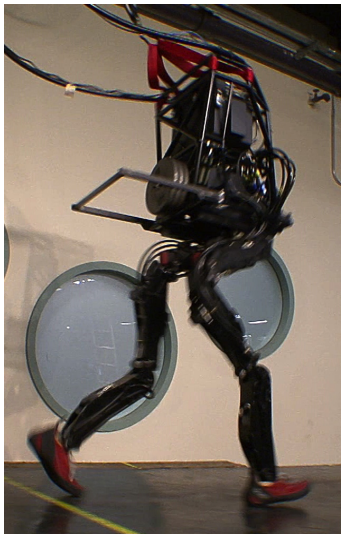

a

b

c

d

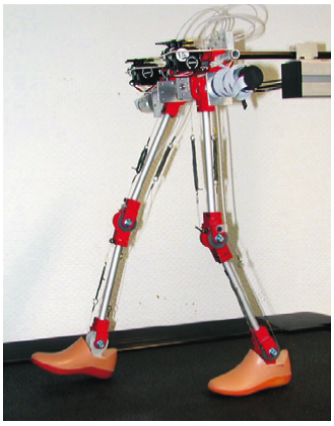

e

Figure 1.1: Various walking robots:
a) PetProto, the precursor to Petman, Boston Dynamics,
b) TUlip, collaboration between University of Twente, Delft University of Technology and Eindhoven University of Technology,
c) HRP-4C, National Institute of Advanced Industrial Science and Technology (AIST) (Nakaoka et al., 2009).
Picture: courtesy of AIST, http://www.aist.go.jp,
d) RHex, Kod*lab, University of Pennsylvania (Komsuoglu et al., 2010),
e) Jena Walker II, University of Jena (Seyfarth et al., 2009).

adays, they are often exhibited at technological fairs, at which they receive much attention. Still, they can only perform their act in a very-well structured environment, such as a specially prepared stage. Their capabilities grow year by year however, and the author expects that the first shows of a humanoid robot walking among the crowd will emerge in the near future.

A second use of bipedal (in particular: humanoid) robots will be in household, office and elderly care environments. The expectation is that at first these robots will assist humans in delivering things (*e.g.*, bringing the mail), and later simple manipulation tasks such as pouring in water or (un)locking a door can be done. Compared to walking robots, wheeled robots are much easier to manufacture and control. However, as our daily environment is optimized for walking, wheeled robots may easily get into problems when they come across an obstacle such as a door step or a staircase.

A commonly heard objection to humanoid nursing robots is "I don't want a robot at my bed, I want a human being!". In the author's opinion however, these robots should (and will) not become a replacement for the human nurses. Instead, they assist the human nurses by doing the 'annoying jobs' such that the nurses get time again for the real interaction with the patients.

1.1.2 Research on walking robots

Apart from the walking robots themselves, research being conducted on walking robots has more value. Many problems that are studied for usage in walking robots appear in other fields of science as well. Below some examples are discussed. Note that this thesis is limited to the dynamics of walking only, so things like artificial intelligence (when should the humanoid robot do what) are out of the scope of this list.

Walking robots are usually modeled as *multi-body systems*. They are more complex than most conventional multi-body systems (such as robotic arms) because they are non-stationary (*i.e.*, no fixed base) and may be considered having 'changing end effectors'. With the latter it is meant that sometimes the left foot is the 'end of the kinematic chain', and sometimes the right foot is. If we consider a humanoid robot, having also a head (usually including one or two cameras) and two arms, we clearly have multiple end-effectors. The research being done on describing this kind of systems can be used in for example multi-arm robot arms.

While walking, the feet of the robot periodically make *contact* with the ground. This contact can be modeled in two different ways: either as a *compliant contact* (approximation by a spring-damper) or as a *rigid contact* (approximation by an infinitely stiff connection), (Gilardi and Sharf, 2002). Both are used often in walking

robots. Compliant models are easy to implement, but usually make the model 'stiff' (*i.e.*, very high as well as very low eigenfrequencies within the model), which results in long simulation times. Rigid contact models do not suffer from this problem, but are hard to implement. Especially when multiple points are in contact at the same time, it is complex to figure out if contact loss occurs at any of the contacts (Ruspini and Khatib, 1997; Duindam, 2006). Other robotic fields in which contacts play a role, such as grasping or object stacking, can use the same strategies for coping with contacts as in walking robots.

The *actuation* of almost all walking robots that are being built today is done by electrical motors. Although this type of actuators has reached a high level of maturity, it is questionable whether this is, in the long term, the best actuator type for walking robots. In order to make motors really suitable for walking, a few properties have to be 'faked' by control (see section 1.3.2). The control methods developed for this purpose can also be used in other fields of research, in particular in robots that interact with humans. A few experiments are being conducted around the world on making walking robots with actuators that are not based on DC motors (Verrelst et al., 2005; Kratz et al., 2007). Once more knowledge is obtained on how to use these actuators in walking robots, the actuators can also be implemented in other types of robots.

The same holds for the *mechanical design* of walking robots. Due to the high demands on the mechanics (small and light to fit in the human-like shape, yet strong and accurate to ensure performance), innovative concepts are used in walking robot design. These concepts may be useful for other robots in other fields as well.

Most robotics applications, such as industrial robot arms, use tight trajectory *control algorithms*, meaning that at each instant in time, the system should be as close as possible to a desired trajectory. For walking robots the exact trajectory of each joint is usually not so important; there are only bounds on the behavior. As an example, in order to not topple over, the center of pressure of the robot should be within the foot area, but where it is exactly does not matter (see chapter 4). This freedom could be exploited in new control algorithms that eventually can also be used in other fields of robotics.

Lastly, research on the dynamics of walking will lead to more insight in *how humans walk*. By either synthesizing or analyzing the gait of a robot that has more or less the same shape as a human, we can learn the principles behind walking: how exactly can we cope with disturbances and asymmetries, what if one of the joints is limited in its agility, *etc*. Using a simple robot with only a few degrees of freedom and a simple (known) controller, gives us the possibility to isolate and study specific effects that influence the gait. The lessons learned can then be used for rehabilitation, orthoses and prostheses.

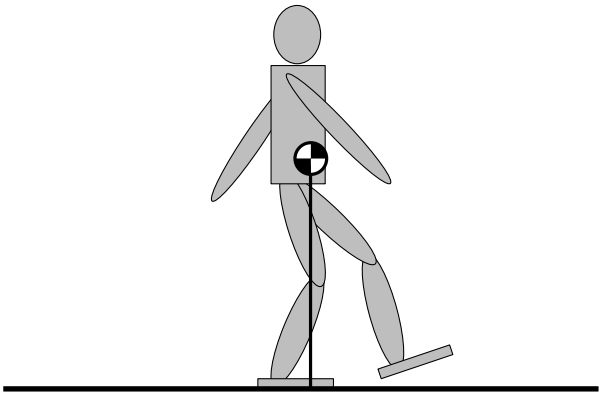

Figure 1.2: 'Static walking'. As long as the center of mass of the robot is above the supporting foot and the movements are so slow that any dynamic effects can be neglected, the robot will not fall.

1.1.3 Different types of walking

Generally, the field of walking robots can be divided into two categories. Giving an adequate name to these categories is hard, and will become harder in the future, as both categories tend to integrate more and more (which is a good development). The two categories, which will be termed *Zero-Moment Point walking* and *limit cycle walking* in this thesis, will be explained below, together with a discussion of the various names that are in use of the categories.

Zero-Moment Point walking

The easiest way to control a walking robot is by making sure that it is always in *static equilibrium*. This is the case if

1. the center of mass (COM) of the robot is above the supporting foot, *i.e.*, the vertical projection of the COM onto the ground plane is within the convex hull of the supporting foot (called the *support polygon*) as in figure 1.2, and

2. the movements of the robot are so slow that any dynamic effects can be neglected.

As soon as the vertical projection of the COM gets outside the support polygon, the foot will start to rotate (topple over) and the entire robot will fall. A good term for this type of walking would be *static walking*.

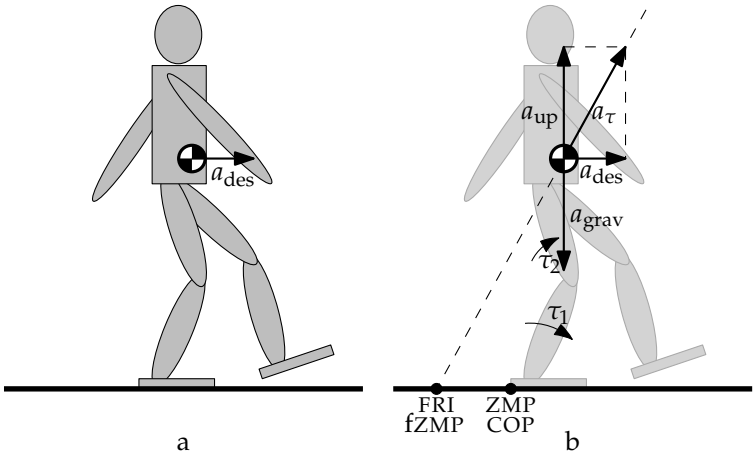

Figure 1.3: A 2D sketch showing the idea of extending static walking to include dynamics. a) A robot and the desired acceleration of the COM. b) All accelerations involved and the projection of the COM along a_τ onto the ground plane (resulting in the FRI or (f)ZMP). In this case, the FRI lies outside the convex hull of the support foot so the foot will start to rotate about its rear edge. The ZMP or COP cannot leave the support polygon and coincides with the rear edge of the foot in this case. It is assumed that there is no change in angular momentum of the system.

The above can be extended by incorporating dynamics, in particular the acceleration of the center of mass. Assume that we want to accelerate the COM of a robot with acceleration a_{des}, as shown in figure 1.3. In order to do that, we need torques τ on the joints that result in an acceleration a_τ, being the combination of:

1. the desired acceleration a_{des}, and
2. an acceleration component a_{up} to counteract the gravitational acceleration a_{grav}.

For the sake of simplicity, we assume that there is no change in angular momentum of the system. Now instead of projecting the COM of the robot straight down onto the ground plane, we project it along the vector a_τ. The projection point is known as the *Foot Rotation Indicator* (FRI), (Goswami, 1999) or *(fictitious) Zero-Moment Point*[1] ((f)ZMP), (Vukobratović and Borovac, 2004). Similarly to the static case, if this point is outside the support polygon, the foot will start to rotate. Contrary to the static case however, there is no direct link between the FRI being outside the support polygon and falling of the robot (Pratt and Tedrake, 2006).

[1] If the point is within the support polygon, it is called Zero-Moment Point (ZMP). If the point is outside the support polygon, it is called fictitious Zero-Moment Point (fZMP) and the ZMP is the point on the support polygon closest to the fZMP.

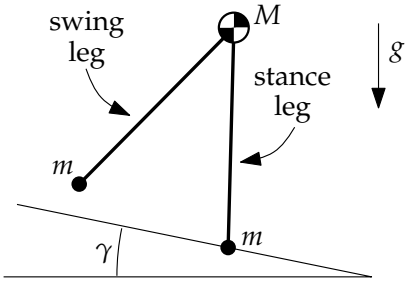

Figure 1.4: The 'simplest passive dynamic walker': three point masses connected with two massless links, placed on a slope.

This has been (and probably will remain) a critical point of misunderstanding (Ito et al., 2008). The reason why this fact gives so much confusion is probably because if the foot is rotating about one of its edges, the robot is underactuated (there is no actuator on the rotation edge of the foot) which makes precise control very hard, but not impossible. Note that when we look at the static case ($a_{\text{des}} = 0$) this dynamic extension reduces to static walking again.

Many researchers, especially those working with many-degree-of-freedom walkers, use the above concept. In order to keep the control simple, they choose to make the supporting foot always stay firmly on the ground. This is done by ensuring that the FRI never leaves the support polygon (*e.g.*, by choosing COM accelerations that are not too large). In that case we can always speak of the ZMP when referring to the point (instead of the fZMP), hence the name for this type of walking: ZMP walking.

The Zero-Moment Point was introduced by Vukobratović and Juričić (1969). Since then, a large number of extensions and refinements have been made to the concept in different directions, including 'preview control' (using the future reference trajectory as control input) (Kajita et al., 2003; Park and Youm, 2007), walking on stairs (Fu and Chen, 2008; Hirukawa et al., 2006) and irregular terrain (Sardain and Bessonnet, 2004; Huang et al., 2008).

Limit cycle walking

There exist simple mechanisms that, when carefully started on a gentle slope, exhibit natural walking behavior. They do this without any form of control, even without any power source other than gravity. This fact has been known for more than a century (Fallis, 1888). It is generally assumed that McGeer (1989, 1990a,b,c) was the first to bring this notion into the scientific world, and since then many researchers have dived into this subject.

Consider a 2D mechanical structure as shown in figure 1.4: a 'hip mass' M, connected to two 'foot masses' m by rigid links. The structure is put on a gentle slope γ and gravity g is acting on the system. Collisions between the feet and ground are considered fully inelastic and rigid. Friction is high enough to prevent slipping. Each of the legs is either in the role of *stance leg* or in the role of *swing leg*.

At the start of each step the rear leg leaves the ground and swings forward as a pendulum. If we allow 'foot scuffing' (that is, allow the swing foot to temporarily penetrate the ground while swinging forward), the swing foot will end up in front of the stance foot, impacting the ground. Due to the rigidity and inelasticity of the collision, the rear foot will immediately leave the ground, starting a new step. During each step, the walker converts potential energy (it walks down the slope) to kinetic energy. At the end of the step, during foot impact, some of the kinetic energy of the walker is dissipated. Besides very naturally looking, this type of walking is very energy efficient.

There exist hip and foot trajectories such that after one complete step the state of the walker is exactly the same as it was before (only translated along the slope), *i.e.*, if we denote the system state at the start of step k as x_k, we have $x_{k+1} = x_k$ for all k. Such a set of hip and foot trajectories is called a *limit cycle*. For a narrow set of parameters, the limit cycle of the walker is even stable: there is a small region around the limit cycle, called the *basin of attraction* (BOA), such that, when the walker is started within the BOA, the walker converges to the limit cycle and shows a stable walking gait. This type of walking is called *passive dynamic walking*: it utilizes only the passive dynamics of the system. It should be noted that the robustness of these passive dynamic walkers is very poor: if the walker is not started very close to the limit cycle, it will fall inevitably.

Many researchers have investigated passive dynamic walkers in different forms: with or without knees, with point feet or arc-shaped feet, with or without torso, 2D or 3D *etc.* (Goswami et al., 1996; Collins et al., 2001; Wisse et al., 2004; Chen, 2007; Kuo, 1999).

A natural extension to true passive dynamic walkers would be to add some form of actuation. There are mainly two reasons to do so:

1. to provide the energy needed for walking, such that walking on a horizontal floor ($\gamma = 0$) becomes possible,

2. to provide some means of control to increase robustness or versatility.

A common place for the actuator is between the legs in the hip (Wisse and van Frankenhuyzen, 2003; Beekman, 2004). This way, the actuator can help the swing leg to swing forward (provide energy for walking) and it can precisely position the leg in order to increase robustness (control). Another common place for the actuator is in the ankles (Hobbelen and Wisse, 2008), such that a push-off force

can be generated. However, the potential of increasing robustness by control of the ankle actuator is much less than it is with hip actuation. Dribbel, the first walking robot developed at the Control Engineering Group at the University of Twente, has both hip and ankle actuation (Franken, 2007).

This field of research suffers from an interesting conflict: on the one hand we want to leave the walker alone in order not to disturb the nice passive dynamic behavior, on the other hand, we want to actively control it in order to maximize the robustness of the walker. Moreover, in order to keep the walker energy efficient, the controller action should be as low as possible.

Fortunately, the passive dynamics in the system can also help here. When a disturbance occurs, mechanical work should be done in order to restore the balance. However, it is not necessary that the actuator itself does all the work. Ideally, the actuator only changes the 'shape' of the system by a minimum control action, such that the passive dynamics result in the rebalancing of the system energy. As an example, consider the case where a walker has experienced a disturbance which has reduced the kinetic energy of the hip (*i.e.*, it slowed down the forward motion of the hip). Now instead of actively accelerating the hip by applying a large ankle torque, we could control the swing leg position such that a smaller step is made than normal. This reduces the energy lost at the next foot impact, so the total energy of the system is restored.

As already stated, the terms for different types of walking have become a little confusing. Especially the group of walkers that are based on passive dynamic walking but do have actuation are referred to by many different terms. Below, a few are listed and the pitfalls are explained.

- As the 'passive' in 'passive dynamic walking' actually refers to the dynamics being passive (not the walker), it can be argued that *passive dynamic walking* is a good term for the walkers considered, even if they are active. The risk to confusion however is obvious, and therefore the use of this term should be avoided.

- Following up on the previous term and its confusion, a term sometimes seen is the paradoxical but correct *powered passive dynamic walking* (Camp, 1997; Mitobe et al., 2010).

- As the walkers considered are not passive anymore, people tend to simply omit the word 'passive', resulting in the term *dynamic walking* (Kuo, 2007). This term is not incorrect (the walkers *are* walking in a dynamical fashion), but so are the ZMP-walkers! Therefore, this term does not distinguish between these two types and the use of this term should be avoided.

- The safe way is just describing the field instead of giving a direct name:

walking based on passive dynamic walking (Wisse and van Frankenhuyzen, 2003; Collins et al., 2005), or, a little shorter, *passivity-based walking* (Hass et al., 2006; Wang et al., 2008).

- Probably the best solution — the one that the author favors — is to completely abandon the words passive and dynamic and use the term *limit cycle walking* instead (Hosoda and Narioka, 2007; Hobbelen, 2008). This term exactly indicates the essence of all walkers in the category: the use of the natural limit cycle.

The walking cycle of a limit cycle walker is dependent on the system dynamics of the walker. Generally, only one limit cycle (*i.e.*, one combination of step length, step time, ground clearance *etc.*) comes naturally with a walker. This is a limitation, because normally one wants to be able to make a robot exhibit different gaits (at the very first, it should be able to transition from a 'standing still gait' to a walking gait). Similarly to the control case described above, one can extend the capabilities of a limit cycle walker in two ways: either by making the actuators constantly do work to push the walker into a different 'artificial' limit cycle, or by using the actuator to change the dynamics so that a different natural limit cycle appears. As an example of the latter, consider a passive dynamic walker with a variable stiffness torsional spring between its legs. By having an actuator increase the stiffness, the natural swing frequency of the swing leg increases, putting the walker in a different (faster) limit cycle (Kuo, 2002).

Closing the gap

Humans are a good example of the combination of both strategies. Obviously, they have an enormous dexterity, which is due to the fact that they learned to do full control on all limbs when needed. Also, when walking normally, the energy consumption of humans is very low, suggesting that in that case extensive use is made of the passive dynamics.

In order for future humanoid robots to be useful, they need both strategies as well. They need the versatility from ZMP walkers to be able to start and stop walking, turn and walk at different velocities, and they need the energy efficiency of limit cycle walkers (having the naturally looking gait of limit cycle walkers can be seen as a bonus). It is believed that, to reach the full potential of walking in robots, both fields should merge into one integrated strategy. First attempts to closing the gap for walking robots are being made (Hobbelen et al., 2008; Mitobe et al., 2010).

2D and 3D walkers

In the world of walking robots, a clear distinction is made between two-dimensional (2D) and three-dimensional (3D) walkers. With a two-dimensional walker (also called a *planar walker*) a walker is meant that can move in the sagittal plane (forwards and backwards) but does not have any degrees of freedom to move in the lateral plane (sideways). The reason to study two-dimensional walkers (both in theory and in practice) is to split the complex problem of understanding walking into smaller problems: first concentrate only on the fore–aft motion, and only then add the sideways motion.

In analysis and control, reducing the number of dimensions from three to two reduces the complexity of locomotion to much less than 2/3rd of the original complexity. Firstly, restricting to two dimensions reduces the number of directions to which a robot can fall; it cannot fall sideways. Secondly, in the 3D case, the robot can rotate around its vertical axis and there exists complex coupling between motions in the sagittal and lateral plane, which does not exist in 2D. Finally, the number of degrees of freedom of a 2D walker is generally much less, which results in equations of motion that are actually manageable.

Building a 2D robot is a different story. As we live in a 3D world, any real robot is essentially a 3D robot. In order to restrict its movements to two dimensions, three methods are available:

1. mounting a two-legged robot on the end of a boom in such a way that it can walk on the perimeter of a circle (figure 1.5a). This is a quite simple construction, but takes a lot of lab-space;

2. mounting a two-legged robot on a suspension that inhibits movements in sideways direction and rotation around the unwanted axes (figure 1.5b). Care must be taken that the suspension does not influence the dynamics of the walker too much. Therefore, it should not be too heavy and have as little friction as possible;

3. building a free-walking four-legged robot with all its legs in line. The outer legs are paired, as are the inner legs (figure 1.5c). The challenge in this type of design is to make the paired legs identical, such that any sideways motion is really impossible. The big advantage is that the robot is mobile so it can easily be demonstrated anywhere.

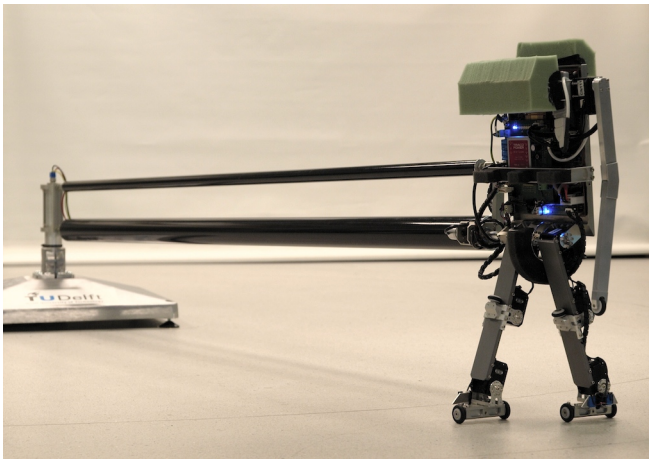

a

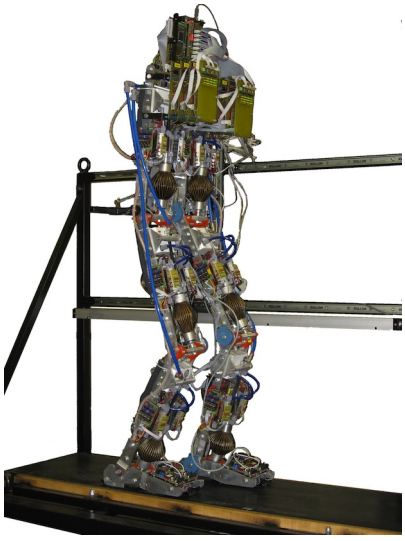

b

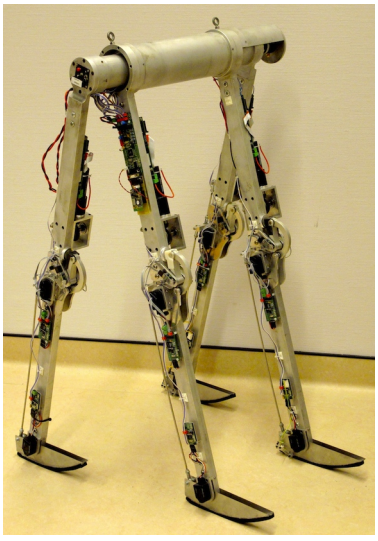

c

Figure 1.5: Examples of 2D walking robots:
a) LEO, Delft University of Technology (Schuitema et al., 2010),
b) Lucy, Vrije Universiteit Brussel (Vanderborght, 2007),
c) Dribbel, University of Twente (Dertien, 2005).

1.2 The VIACTORS project

Most industrial robots are manufactured as rigid as possible: in order to be accurate, control should be stiff and the deformation of the links of the robot should be minimal. Consequently, the robots need to be heavy and the actuators need to be extremely powerful in order to achieve the desired accelerations. As long as no humans are close to the robot, nothing is wrong with that, except perhaps the relatively large energy consumption. However, for robots operating in the vicinity of humans (think of a robotic arm mounted on a wheel chair of disabled person, or a humanoid robot walking around in the same room as humans), this is not a good choice. The problem is safety. The stiff controllers make that as soon as a slight deviation is found between the desired end-effector trajectory and the actual one, enormous forces are exerted. Moreover, as the impulse of a part of the robot scales linearly with its mass, a heavy part will have a large impulse when moving. Both can be dangerous if the robot accidentally comes in contact with a human.

To solve the problem, one could use sensors to detect any accidental contact and then, by very quick (thus stiff) control, react on the sensory information to minimize damage. If the system was designed well, this may be a good solution. However, if the sensor or controller fails, the robot is still dangerous.

Another way to cope with the problem is by not making the robot stiff in the first place; instead use light constructions (and compensate for deformation by control) and use a special type of actuators that can be adapted to the task at hand: strong if they need to but compliant if they can. Such actuators are called *variable-impedance actuators*.

The VIACTORS project, a project supported by the European Commission under the 7th Framework Programme, addresses the development and use of safe, energy-efficient, and highly dynamic variable-impedance actuation systems.

One of the 'work packages', WP5, focuses on *locomotion with variable-impedance actuation*, in particular (Viactors, 2011): analysis, simulation and development of legged locomotion systems which are, at the same time, robust, in terms of the ability of the system to stabilize its motion under substantial disturbances, and energy efficient, in terms of minimization of the energy consumptions. Focus points are:

- Morphological analysis and definition of metrics for "locomotion controllability";
- Implementation of developed actuators and control in humanoid robots;
- Modeling and simulations of (new actuation for) robust and energy efficient

legged locomotion;

- Experiments of (new actuation for) robust and energy efficient legged locomotion.

The following partners are in the consortium of VIACTORS: German Aerospace Center (DLR), University of Pisa, University of Twente, Imperial college London, Italian Institute of Technology and Free University of Brussels. The author's Ph.D. position at the University of Twente has been financed for 40 % by VIACTORS.

1.3 Main topics of the thesis

Building walking robots is a multi-disciplinary job; it requires knowledge from different research areas to succeed. For this thesis it was chosen to take a look at various disciplines instead of focusing on one aspect only. The thesis contains three parts, which are discussed in more detail below.

1.3.1 Analysis

Analysis is the art of studying the behavior of a (complex) system and trying to find rules that explain the behavior, in order to gain understanding of the system. An important aspect of analysis is the modeling of the system: the process of making a (mathematical) system description in which only the relevant aspects of the system are included. As an example, for general kinematics and dynamics analysis of a walking robot, it is often sufficient to make a *rigid body model*, in which each link of the robot is represented as an infinitely stiff mass and the connections between the links are represented as ideal prismatic or revolute joints. For different research questions, different aspects of a robot may be important, therefore different models should be used.

Many 'tools' are available for model making and analysis of the model. For very simple walkers, typically 2D limit cycle walkers with three or less degrees of freedom, the equations of motion may be simple enough to analyze analytically. This can lead to basic but important conclusions such as the fact that for the 'simplest walker model' the swing foot velocity just before foot impact does not influence the dynamics for the next step (see chapter 2). For slightly larger models, the equations of motion are already too complex, and one must resort to analyzing numerical trends or specific properties of the equations of motion, such as the Poincaré section, the step-to-step function and its eigenvalues (Goswami et al., 1996).

When the walkers become even more complex, typically the ZMP walkers that have many degrees of freedom, the analysis tools described above do not work anymore (the models are too complex to do such analysis and for ZMP walkers the limit cycle analysis is irrelevant anyway). In those cases one can resort to analysis tools like the center of mass (COM), extrapolated center of mass (XCOM)[2] (Hof, 2008), center of pressure (COP), Zero-Moment Point (ZMP), locked inertia and others. These are all concepts that 'transform' the full high-dimensional state of the system to a meaningful two- or three-dimensional point in Euclidean space.

Often it is helpful to 'look at the walker from a different point of view'. For example, when calculating the result of an inelastic collision between two bodies, it makes more sense to look at the impulses of the bodies than at their velocities: the equations become simpler just by taking different look. This can also be done for walking robots. By using different mathematics (*e.g.*, *Screw theory*, (Ball, 1900) instead of classical mechanics), analysis of the model can become much simpler.

Because walking robots are very complex systems with highly non-linear behavior, proper analysis tools are a necessity for building good robots. Without them, it is simply impossible to figure out whether a robot will be able to walk or not. In order to understand increasingly better the walking behavior of walking robots, new analysis tools constantly need to be developed.

1.3.2 Control and actuation

If there are actuators in a walking robot, these actuators should be steered in some way: a controller is needed. The non-linearity of the robots, as well as their very limited margin of robustness (if any), may put high demands on the controllers.

For ZMP walkers, tight trajectory control is often used. Low-level feed-forward controllers cancel out all internal dynamics and impose the accelerations obtained from the desired trajectories while linear feed-back controllers compensate for model mismatch and disturbances.

For limit cycle walkers, it is usually tried to make the controllers as simple as possible, in order not to disturb the passive dynamic behavior too much. Often ordinary linear feedback controllers are used. By choosing the input and output of the controller carefully, very nice results can be achieved, even with linear controllers (see chapter 6).

The controller inside a walking robot can make or break the robot's performance. Where a simple controller could barely keep a robot walking, a slight improvement (or even proper tuning) may improve the gait a lot. Therefore, research on proper control is vital for walking robots.

[2] Also known as the Instantaneous Capture Point (Pratt et al., 2006; Koolen, 2011).

An ideal actuator is a lossless *converter of energy* from one domain (*e.g.*, electrical) into mechanical energy (and vice versa), which does not influence the dynamics of the joint, other than by the actuation torque. Electrical motors, the most-used actuators for walking robots, are unfortunately far from ideal. Firstly, because of the series resistance in the electrical part of the motor, electrical energy is dissipated when a force is generated, even if no mechanical work is done. Secondly, the motor's moment of inertia and friction (especially the gearbox) heavily influence the dynamics of the joint (*i.e.*, the motor is not *backdrivable*). Especially for limit cycle walkers, this is undesired.

Biological muscles are, in some sense, better. Although they are certainly not lossless (Whipp and Wasserman, 1969), their backdrivability (in uncontracted condition) is much better than DC motors. Furthermore, muscles can exert high peak forces, which allows for quick disturbance rejection. The benefits of muscles are clearly seen in many walking organisms: their locomotion is highly energy efficient and robust. It is the author's strong belief that, until an entirely new class of (muscle-like) actuators is mature enough for usage, we will not be able to build humanoid robots that are as versatile and robust against disturbances as humans.

As long as we still have to work with electric motors, there are ways to 'fake' ideality of some aspects of the actuator. Especially backdrivability (*i.e.*, acting as a pure force source) can be mimicked by embedding the motor in a *series elastic actuator* and applying appropriate control (Pratt and Williamson, 1995). This concept can be extended to a more versatile type of actuator, as discussed in chapter 8.

1.3.3 Design

Thanks to the recent improvements of materials and manufacturing techniques (3D printing for example) and to the miniaturization of electronics, humanoid robots start to look better and better. In some cases (*e.g.*, HRP-4C, figure 1.1c) the developers have succeeded to compress all the hardware into the posture of a normal human being. Still, the robots lack functionality that is needed for really useful behavior. For example, in order to reduce weight, each hand of HRP-4C is only provided with 2 degrees of freedom (Kaneko et al., 2009). So, future developments in design will be necessary for improving this.

For limit cycle walkers the design criteria are different than for ZMP walkers. As the internal dynamics of the system are important, this has to be taken into consideration much more than in ZMP walkers. As an example, for a good gait the mass ratio between upper and lower leg should be approximately 10:1 (Franken et al., 2008), which limits freedom of putting heavy actuators in the lower leg. Creative designs can help in such cases; by combining existing technology in innovative ways, solutions can be generated for the problems. In this way, clever design can help increasing the potential of limit cycle walkers.

1.4 Thesis outline

1.4.1 Research goals

In this thesis a number of questions are addressed, all relevant to walking robots:

1. How can we analyze the behavior of a 2D passive dynamic walker that is walking on rough terrain?
2. By looking at the robot from a different 'perspective', can we gain more insight in its dynamics?
3. How can we control a walking robot in order to stabilize it in the lateral (sideways) direction?
4. How can we improve the actuators in order to get minimum energy consumption?
5. How can we improve the knee and ankle joints of a walking robot?

1.4.2 Contents of each chapter

Each chapter in this thesis is based on a paper which has been published at or submitted to a conference (with the exception of chapter 3, which has not been published before). The contents of each chapter is mostly identical to the original paper, but at some points the chapters in this thesis are more extensive: they contain content that was originally removed from the paper to get it within the conference's six-page limit (with the exception of chapter 7, which has undergone a major revision). Because of the fact that the chapters are based on separate papers, the contents of the chapters overlaps in some places. Below a short description is given of each chapter, and it is indicated to which research goal the chapter contributes.

PART I: Analysis

Chapter 2 addresses question 1 from the research goals. A standard way of analyzing the behavior of a 2D walker is by using the so-called Poincaré map: a function which, given the walker's state x_k^+ at the start of step k, returns the new state x_{k+1}^+ at the start of step $k+1$. In this chapter it is shown that this method can not be used for walkers on an irregular floor. An extension to this theory is proposed that does make it possible. Furthermore, the relation is shown between

different types of disturbances and curves on the Poincaré section, introducing a new way of analyzing the walker's behavior.

Chapter 3 addresses question 2 from the research goals. The configuration of a walking robot can be described as the pose (position and orientation) of one of the rigid bodies (called the 'reference body') of the robot plus all internal joint angles. It is customary to take the torso as reference body. In this chapter it is shown that in some cases it is more convenient to take the stance foot as reference body: the equations become easier. It is also shown how the reference body change (a standard non-linear coordinate transformation) is done on a 3D walking robot.

Chapter 4 addresses question 2 from the research goals. A widely used concept in robot walking is the Zero-Moment Point (ZMP). The theory about ZMP, including equations on how to calculate its position, exists already for over 40 years. In this chapter it is explained how the position of the ZMP can be found geometrically (*i.e.*, in a coordinate-free manner) from the ground contact wrench. In order to arrive at this, general theorems are presented on how one can decompose one wrench W into other wrenches W_1' and W_2'.

Chapter 5 also addresses question 2 from the research goals. It focuses on simplification of the dynamic model of a 3D walker; in particular the approximation of the walker by one single rigid body (the *locked inertia*) rolling over the sole of a curved foot.

PART II: Control and actuation

Chapter 6 addresses question 3 from the research goals. In this chapter a specific 3D walker model is used that, in its limit cycle, exhibits time-symmetrical behavior (*i.e.*, the trajectories played backwards are identical to the trajectories played forwards). In the case of a disturbance, the trajectory becomes asymmetric; the amount of asymmetry is used as an input for a (linear) stabilizing foot placement controller.

Chapter 7 also addresses question 3 from the research goals. In this chapter it is explained how the walking robot 'TUlip' is controlled by means of the *extrapolated center of mass* (XCOM). The XCOM is a projection of the robot's center of mass (COM) onto the ground plane, where the direction of projection is dependent on COM's velocity. Experiments on the real robot are presented.

Chapter 8 addresses question 4 from the research goals. In this chapter a new actuation concept is presented, called the *very versatile energy efficient actuator*, V2E2. An ideal actuator is just an energy converter (*e.g.*, from the electrical to the mechanical domain). The V2E2 has, on top of that, a mechanical energy storage element (a spring) and an 'infinitely variable transmission' (a continuously variable

transmission that can have a positive as well as negative transmission ratio). The power of the V2E2is its ability to store negative work mechanically and release it when positive work is needed.

PART III: Design

Chapter 9 addresses question 5 from the research goals. It describes the design of a new knee locking mechanism for the 2D walking robot Dribbel. The mechanism keeps the leg in extended position while it serves as stance leg. It does this by exploiting a mechanical singularity which, in theory, can withstand arbitrary large torques while consuming no energy. Unlocking however only requires a minimum amount of energy. In this chapter the system is described in detail and experiments are presented that show the benefits of the system.

Chapter 10 also addresses question 5 from the research goals. It describes the analysis, design and control of a new ankle actuation system for the 3D walking robot TUlip. The system consists of two series-elastic actuators (DC-motors with springs in series) that drive both the x-axis (sideways rotation) and y-axis (forward/backward rotation) of the ankle, in a differential set-up. The analysis of this non-linear, coupled series elastic system is treated in this chapter, as well as some control issues following from the series elasticity and non-linearity.

Part I

Analysis

Chapter 2

The Poincaré section and basin of attraction of a 2D passive dynamic walker on an irregular floor

This chapter is based on the following article (van Oort and Stramigioli, 2012):

The Poincaré section and basin of attraction of a 2D passive dynamic walker on an irregular floor
Gijs van Oort and Stefano Stramigioli
Submitted to IEEE International Conference on Robotics and Automation (ICRA'12).

Abstract—**In analysis of passive dynamic walking, one often makes use of the Poincaré section and basin of attraction. In this chapter we show that these methods cannot be used when the walker walks on an irregular floor. As a solution we propose three different mappings (called *stance foot angle mapping*, *rotation mapping* and *integration mapping*) and show that integration mapping is optimal for analysis. Furthermore, we introduce a new way to visualize the relation between disturbances of different magnitude and the states on the Poincaré section. This opens a new way of analyzing the walker's behavior. We show the effectiveness of the proposed methods by means of a simple simulation experiment.**

2.1 Introduction

For more than two decades already people have researched passive dynamic walking. A passive dynamic walker is a mechanical system that, when 'launched' from a gentle slope, can exhibit stable walking behavior (McGeer, 1990b). There are no actuators in the system; all energy needed for walking is obtained from gravity's potential field. For quite a large range of parameters stable walking can be achieved, but the robustness of these walkers is very poor (*i.e.*, if the walker is not started 'close to the periodic trajectory', it falls).

For analyzing the behavior of passive dynamic walkers, the notions of *Poincaré section*, and *basin of attraction* are often used. Although these have been studied intensively in the past (by Goswami et al. (1998); Liu et al. (2007); Schwab and Wisse (2001) and more), we found that they were often only loosely defined; usually just by a sentence that only intuitively makes sense[1].

In this chapter we will define the Poincaré section and the basin of attraction in a more formal manner, and show that this has implications if one wants to use them on irregular floors. Secondly, we show the relation between points on the basin of attraction and various disturbances. This helps in understanding how various disturbances influence the gait.

This chapter is organized as follows. At the end of this introduction, we introduce two walker models that we will use throughout the chapter and spend some words on irregular floors. In section 2.2 we introduce the equations that describe the behavior of the walkers. Then, in section 2.3 we give a definition of the Poincaré section. It also contains the main contribution of this chapter: the description of how to deal with irregular floors and the Poincaré section. In section 2.4 we give a definition of the basin of attraction and discuss the usage of the area of basin of attraction as a measure of robustness. Section 2.5 contains the second contribution of this chapter, being the relation between points on the basin of attraction and various disturbances. Finally, in section 2.6 we show by means of some experiments the usage of the methods.

2.1.1 Test models

In this chapter, we use two different 2D walker models for our simulations. These are described below. The *first walker model* is the model used by Garcia et al. (1998). It is a compass walker model (no knees) with point feet, a unit point mass M at the hip, very small foot mass ($m \ll M$), having unit length legs, walking

[1] A notable exception is the work by Grizzle et al. (2001), which thoroughly defines the Poincaré section. His definition however, is incompatible with irregular floors.

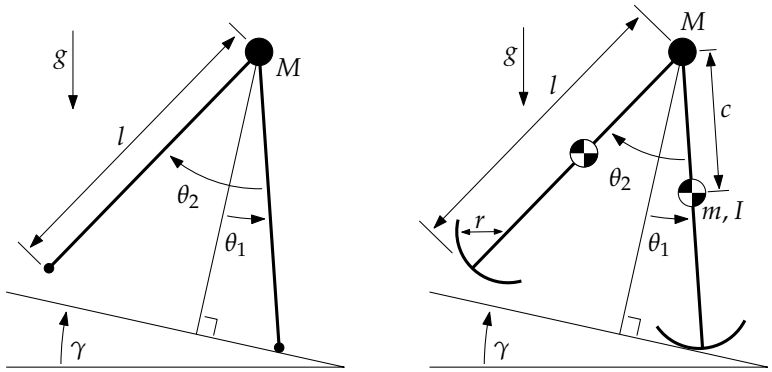

Figure 2.1: The two walker models used in this chapter. a) the 'first walker model'; b) the 'second walker model'.

Parameter	Name	Model 1	Model 2	Unit
Hip mass	M	1	1	kg
Leg mass	m	$10^{-4}/0^*$	0.5	kg
Additional leg inertia	I	0	0.02	kgm^2
Center of mass	c	1	0.5	m
Leg length	l	1	1.2	m
Foot radius	r	0	0.2	m
Gravity	g	1	1	m/s^2
Slope angle	γ	0.009	0.01	rad

* In order to avoid numerical problems, a leg mass of $m = 10^{-4}$ kg was used for the integration of f. For the impact equations g a leg mass of $m = 0$ kg was used (see also section 2.2).

Table 2.1: Parameters of the two walker models used in this chapter (see also figure 2.1)

down a gentle slope in a unit gravity field. Foot scuffing is ignored, ground contact is assumed rigid, and no slip occurs. The walker has no inputs; it is fully autonomous.

The *second walker model* is a slightly extended model, featuring arc-shaped feet, non-negligible leg mass and leg inertia. Note that the first model is a special case of the second model; it can be obtained by setting the appropriate parameters to zero. Figure 2.1 and table 2.1 summarize both models.

We used Matlab to simulate the walkers. Our code is based on Matlab code by Pranav Bhounsule (Ruina, 2010).

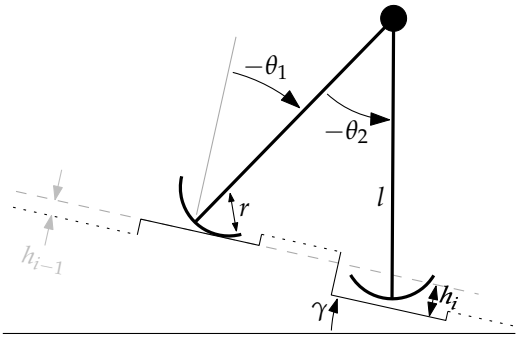

Figure 2.2: The second walker model experiencing a step-down of height h_i on an irregular floor.

2.1.2 Irregular floor

In this chapter, we consider walkers walking on 'irregular floors'. We model the floor as follows. A floor has a fixed slope γ and consists of piecewise constant-height parts, placed such that during stance-phase, the stance foot will always stay on the same part (*i.e.*, it will not roll onto a new part of different height); see figure 2.2. Any parts on which the walker will not step (dotted in the figure) are considered unimportant and are not modeled at all. More specifically, we do not consider collisions between the swing foot and these parts. Hence, the floor is fully specified by one unique slope γ and, for each step, a *step-down* of height $h_i \in \mathbb{R}$, being the height difference between the two parts that will support the walker.

We define a *flat floor* as a floor that has $h_i = 0 \ \forall i$. Note that a flat floor is not necessarily horizontal (it can have a non-zero γ). In our definition, the flat floor is the opposite of an *irregular floor*. We usually will consider a floor that only has one non-zero step-down; and therefore we will omit the subscript i.

2.2 Dynamic equations

The state space of each of the models is $\mathcal{X} = \mathrm{TS}^2$ (the tangent of the 2-sphere S^2), *i.e.*, the state can be denoted as $x = [\theta_1 \ \dot{\theta}_1 \ \theta_2 \ \dot{\theta}_2]^T$.

During swing phase, the evolution of the state can be described by a continuous-time differential equation (the equations of motion):

$$\dot{x} = f(x), \tag{2.1}$$

where f is a nonlinear continuous function. The exact equations of motion for the first model are written out in (Garcia et al., 1998). Note that during normal walking, $\dot{\theta}_1 < 0$. As soon as the swing foot hits the floor ('heelstrike' or 'impact'), the state is instantaneously reset using the impact equations

$$x^+ = g(x^-), \tag{2.2}$$

where x^- and x^+ denote the state just before and just after the moment of impact respectively and g is a continuous function. The impact equations also effectuate the leg-relabeling. The post-impact velocities $\dot{\theta}_1^+, \dot{\theta}_2^+$ are linear in $\dot{\theta}_1^-$ and $\dot{\theta}_2^-$.

On a flat (*i.e.*, non-irregular) floor, the moment of impact is when $x \in \mathcal{S}_0$, where

$$\begin{aligned} \mathcal{S}_0 = \{x \in \mathcal{X} |\ & \theta_2 = 2\theta_1, && \text{both legs on the ground} \\ & -\pi < \theta_2 < 0, && \text{stance foot behind swing foot} \\ & \dot{\theta}_1 < 0, && \text{forward movement} \\ & \dot{\theta}_2 < 2\dot{\theta}_1 && \text{swing foot goes down}\}. \end{aligned} \tag{2.3}$$

In the field of hybrid systems, $\mathcal{S}_0 \subset \mathcal{X}$ is called the *switching surface*, and the impact equations g are seen as a function $g : \mathcal{S}_0 \to \mathcal{X}$. We define $\mathcal{S}_\bullet^\star$ as the image of g when applied to $\mathcal{S}_\bullet$; *i.e.*, by definition $\mathcal{X} \supset \mathcal{S}_0^\star = \{g(x^-) | x^- \in \mathcal{S}_0\}$. In the case of irregular terrain, a step down or obstacles, the switching surface is different. For example, when experiencing a step-down of height h, the moment of impact (and thus the switching surface) for both walker models is

$$\begin{aligned} \mathcal{S}_h = \{x \in \mathcal{X} |\ & (l-r)\cos(\theta_2 - \theta_1) = (l-r)\cos\theta_1 + h, \\ & -\pi < \theta_2 < 0,\ \dot{\theta}_1 < 0, \\ & \sin(\theta_2 - \theta_1)(\dot{\theta}_2 - \dot{\theta}_1) - \sin\theta_1\,\dot{\theta}_1 < 0\}. \end{aligned} \tag{2.4}$$

In order for the impact equations g to be valid always, any switching surface $\mathcal{S}_\bullet$ should be in the domain of g. Therefore we'd rather see g as a function $g : \mathcal{X} \to \mathcal{X}$, meaning that it can return, for *any* state x^- a post-impact state x^+ if the swing foot would hit an object at that particular x^-.

For later reference, we show the impact equations g of the first walker model (contrary to for example the equations by Garcia et al. (1998), this is valid for any $x^- \in \mathcal{X}$):

$$\begin{bmatrix} \theta_1 \\ \dot{\theta}_1 \\ \theta_2 \\ \dot{\theta}_2 \end{bmatrix}^+ = \begin{bmatrix} 1 & 0 & -1 & 0 \\ 0 & \cos\theta_2 & 0 & 0 \\ 0 & 0 & -1 & 0 \\ 0 & \cos\theta_2(1-\cos\theta_2) & 0 & 0 \end{bmatrix} \begin{bmatrix} \theta_1 \\ \dot{\theta}_1 \\ \theta_2 \\ \dot{\theta}_2 \end{bmatrix}^- . \tag{2.5}$$

The impact equations of the second walker model are a much more complex function of θ_2. Around the limit cycle, having $x^- \approx [-0.19\,\text{rad}, -0.26\,\text{rad/s},$

-0.38 rad, -0.016 rad/s$]^T$, the numerical approximation of the impact equations for the second walker model is:

$$\begin{bmatrix}\theta_1\\ \dot\theta_1\\ \theta_2\\ \dot\theta_2\end{bmatrix}^+ = \begin{bmatrix}1 & 0 & -1 & 0\\ 0 & 0.91 & 0 & 0.072\\ 0 & 0 & -1 & 0\\ 0 & 0.20 & 0 & 0.070\end{bmatrix}\begin{bmatrix}\theta_1\\ \dot\theta_1\\ \theta_2\\ \dot\theta_2\end{bmatrix}^- . \tag{2.6}$$

From (2.3) and (2.5) it can be deduced that $\mathcal{S}_0^\star$ has the following properties:

$$\forall x^+ \in \mathcal{S}_0^\star : \quad \begin{array}{ll}\theta_2^+ = 2\theta_1^+, & \text{both legs still on the ground;}\\ \theta_2^+ > 0, & \text{swing foot behind stance foot.}\end{array} \tag{2.7}$$

Moreover, if the inter-leg angle satisfies $-\frac{\pi}{2} < \theta_2^- < 0$ (which is normally the case), then after impact the hip will move forward ($\dot\theta_1^+ < 0$). For $-\pi < \theta_2^- \leq -\frac{\pi}{2}$, the hip will move backwards and the robot will fall. This is a very rare situation. For the other switching maps $\mathcal{S}_\bullet^\star$, properties similar to (2.7) hold.

For certain floor angles γ the walkers show stable walking behavior: as time goes to infinity, the walkers converge towards a specific periodic orbit, called the *limit cycle* (when started close enough to it).

2.3 The Poincaré section

A *Poincaré section* is an open subset $\tilde{\mathcal{X}}$ of a 'slice' of the state space with a dimension one lower than the dimension of the state space $\mathcal{X}$. It should be transversal to the flow of the equations of motion f, *i.e.*, no trajectory generated by f may have two consecutive points on $\tilde{\mathcal{X}}$. If well chosen, the state trajectory of a walker passes the Poincaré section once per cycle. This gives the ability to do analysis on a per-step basis; the k^{th} step gives a point $\tilde{x}_k \in \tilde{\mathcal{X}}$. One can define the *stride function* $St : \tilde{\mathcal{X}} \to \tilde{\mathcal{X}}$, a (Poincaré) map that, given the state $\tilde{x}_k$ of step k, returns the state $\tilde{x}_{k+1}$ of the next step $k+1$, if it exists (McGeer, 1990c). A *fixed point* $\tilde{x}^\star$ is a special point on the Poincaré section, having the property that it is mapped onto itself by the stride function, *i.e.*, $St(\tilde{x}^\star) = \tilde{x}^\star$. By construction, it is the intersection of the Poincaré section and a limit cycle trajectory. More than one fixed point may exist on a Poincaré section.

A convenient and heavily used choice for the Poincaré section is to choose the set of all possible states at the start of a step, *i.e.*, just after impact (denoted $\tilde{\mathcal{X}}^+$). We will refer to this choice of Poincaré section as the *post-impact Poincaré section*. Similarly, a Poincaré section consisting of the set of all possible states at the end of a step, *i.e.*, just before impact, will be referred to as the *pre-impact Poincaré section*

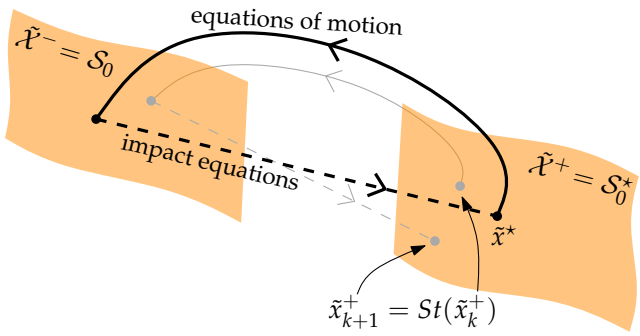

Figure 2.3: The evolution of the walker's state along the limit cycle (black line) consists of two parts: the integration of the equations of motion and the instantaneous impact equations. We consider a flat floor in this figure. The two planes shown are the pre-impact Poincaré section $\tilde{\mathcal{X}}^-$ and post-impact Poincaré section $\tilde{\mathcal{X}}^+$. In gray the application of the stride function St is shown. Note that in reality the whole state space is four-dimensional and the Poincaré sections are three-dimensional.

$\tilde{\mathcal{X}}^-$. For a flat floor (*i.e.*, $\theta_2^- = 2\theta_1^-$) , we have $\tilde{\mathcal{X}}^- = \mathcal{S}_0$ and $\tilde{\mathcal{X}}^+ = \mathcal{S}_0^\star$. In figure 2.3 the limit cycle, Poincaré sections and stride function are visualized.

2.3.1 Poincaré section and irregular terrain

The definition of the post-impact Poincaré section gives difficulty when walking on irregular terrain or when considering step-down disturbances. The problem is that the set of all possible states at the start of the step is different for each step (*i.e.*, $\mathcal{S}_{h1}^\star \neq \mathcal{S}_{h2}^\star$ for $h1 \neq h2$), and because the Poincaré section should be identical for each step, we cannot simply use $\tilde{\mathcal{X}}^+ = \mathcal{S}_\bullet^\star$ (hence the nice and thorough results of Grizzle et al. (2001) will fail in this case). Taking the Poincaré section to be the union of all switch map images $\cup_h \mathcal{S}_h^\star$ (which solves the problem by making all possible post-impact states part of $\tilde{\mathcal{X}}^+$) is neither a solution because this set is not transversal to f anymore (and it is a four-dimensional space instead of three-dimensional).

In order to be able to do post-impact Poincaré analysis even on irregular floors, we need

1. one single Poincaré section $\tilde{\mathcal{X}}^+$ that is used for all steps, and
2. a way to associate (for each floor disturbance h) with each point on $\mathcal{S}_h^\star$ a point on this $\tilde{\mathcal{X}}^+$; in other words, a mapping

$$\Pi_h : \mathcal{S}_h^\star \to \tilde{\mathcal{X}}^+. \tag{2.8}$$

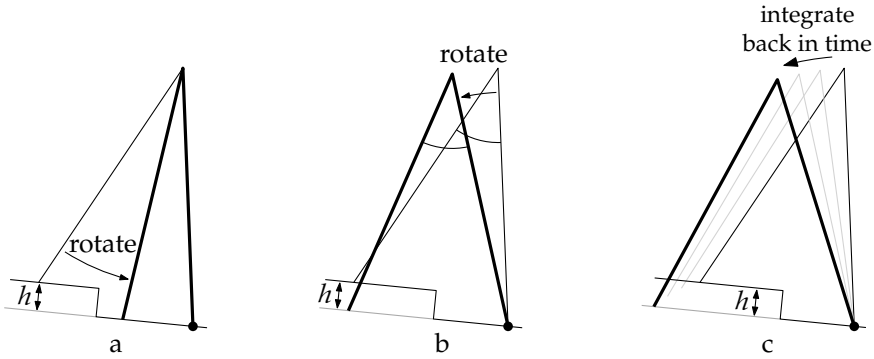

Figure 2.4: Three different mappings from a post-impact state onto the Poincaré section after experiencing a step down h. The thin line represents the walker's state; the thick line the output state of the mapping. a) Stance-foot-angle mapping ΠS: the swing leg is rotated until it hits the ground as if it were flat; b) Rotation projection ΠR: the walker is rotated until the swing foot hits ground; c) Integration projection ΠI: the walker's state is integrated forward or backward in time until the swing foot hits the ground.

A natural choice for $\tilde{\mathcal{X}}^+$ would be to take the Poincaré section for undisturbed steps, thus $\tilde{\mathcal{X}}^+ = \mathcal{S}_0^\star$.

If the sections $\mathcal{S}_h^\star$ and $\tilde{\mathcal{X}}^+$ are close to each other, a simple projection map may suffice. We introduce two possibilities:

- *Stance-foot-angle mapping* ΠS:

$$\Pi S_h = [\theta_1\ \dot{\theta}_1\ \theta_2\ \dot{\theta}_2]^T \mapsto [\theta_1\ \dot{\theta}_1\ 2\theta_1\ \dot{\theta}_2]^T, \tag{2.9}$$

  i.e., we leave the stance foot angle as it is and adjust the inter-leg angle to satisfy the constraints of (2.7).

- *Rotation mapping* ΠR:

$$\Pi R_h = [\theta_1\ \dot{\theta}_1\ \theta_2\ \dot{\theta}_2]^T \mapsto [\tfrac{1}{2}\theta_2\ \dot{\theta}_1\ \theta_2\ \dot{\theta}_2]^T, \tag{2.10}$$

  i.e., we leave the inter-leg angle as it is and rotate the whole walker around the stance foot to satisfy the constraints of (2.7).

From figure 2.4a and b it is obvious that the results of the two mappings may differ significantly, and the rotation mapping looks much better intuitively. Consider a post-impact state $x^+ \in \mathcal{S}_h^\star$ and its image $\tilde{x}^+ = \Pi_h(x^+) \in \tilde{\mathcal{X}}^+$. The best mapping function Π_h would be the function that minimizes the 'distance' between the evolution of the equations of motion f starting at x^+ and the evolution of f starting at $\tilde{x}^+$ for all $x^+ \in \mathcal{S}_h^\star$. Now for $h < 0$ (a step-up), the evolution of

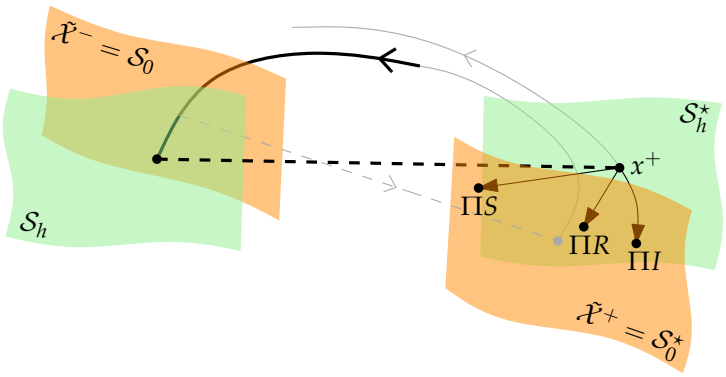

Figure 2.5: State space view of a walker experiencing a step-down. Heelstrike does not occur on the pre-impact Poincaré section $\tilde{\mathcal{X}}^-$, but a little later, on switching surface $\mathcal{S}_h$. Consequently, the post-impact state x^+ will not be at $\tilde{\mathcal{X}}^+$, but at $\mathcal{S}_h^\star$. For Poincaré analysis, we need to map the post-impact state onto $\tilde{\mathcal{X}}^+$. The three different mappings described in the text are shown.

f starting at x^+ crosses the hyperplane $\tilde{\mathcal{X}}^+$. From the intersection point on, the evolution of f starting from that point and continuation of the original trajectory are identical, and therefore the mapping that maps x^+ to the intersection point is the best mapping there is, *i.e.*, it is optimal in this sense. We will call this mapping *integration mapping* ΠI and define it as follows:

$$\Pi I_h = x^+ \mapsto \int_{t0}^{t1} f\left(x(t)\right)\, \mathrm{d}t \tag{2.11}$$

where $x(t_0) = x^+$ and t_1 is the moment $x(t)$ crosses $\tilde{\mathcal{X}}^+$ (*i.e.*, $\theta_2 = 2\theta_1$). In the case of $h > 0$ (step-down), the integration should be done backwards in time, again until $x(t)$ crosses $\tilde{\mathcal{X}}^+$. This is shown in figure 2.4c. Note that all mapping equations are invariant for h and therefore, we will omit the h-subscript from now on. In figure 2.5 the three mappings are shown.

A special case occurs when the walker experiences a step-up but has not enough forward velocity to reach the point where $x(t)$ crosses $\tilde{\mathcal{X}}^+$ (see figure 2.6a). Then the walker will fall and (2.11) has no solution. This situation can be detected by looking for a sign change in the vertical velocity v_{yf} of the swing foot during integration of (2.11); this occurs if

$$v_{yf} = \sin(\theta_2 - \theta_1)(\dot{\theta}_2 - \dot{\theta}_1) - \sin\theta_1\, \dot{\theta}_1 = 0. \tag{2.12}$$

The total structure can be described as a fiber bundle (Bullo and Lewis, 2004), where $\cup_h \mathcal{S}_h^\star$ is the total space, $\tilde{\mathcal{X}}^+$ is the base space and Π is the mapping π

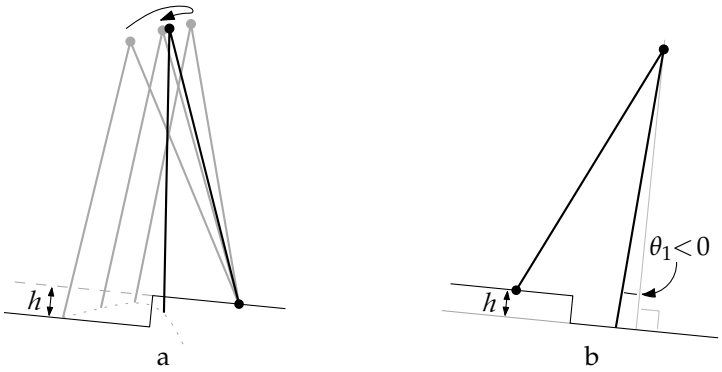

Figure 2.6: a) This walker has experienced a step-up and has not enough velocity to get its swing foot to cross the 'flat floor'. Obviously, the walker will fall. The dashed line is the trajectory of the swing foot. b) This walker has experienced a large step-down and its post-impact state is already past mid-stance. Therefore, during the following step, it will not pass $\tilde{\mathcal{X}}^M$ anymore.

to the base space. In the case of integration mapping, each fiber $\pi^{-1}(x)$ is the evolution of f through x.

Apart from the already mentioned pre-impact and post-impact Poincaré sections, any other Poincaré section can be defined along the trajectory of the walker. An example is the mid-stance Poincaré section $\tilde{\mathcal{X}}^M = \{x \in \mathcal{X} \,|\, \theta_1 = 0, \dot{\theta}_1 < 0\}$ which was used for example by Rummel et al. (2010). In practice, this Poincaré section does not suffer from the problem of needing mappings; all normal steps pass through this section exactly once (an unconventionally high step-down may however cause the walker to have a post-impact state where the stance leg has already past $\theta_1 = 0$ however; see figure 2.6b). This seems like an advantage, but actually there is not much difference: in both cases (post-impact or mid-stance Poincaré section) you have to integrate the equations of motion from the post-impact state to the Poincaré section.

2.3.2 Dimension of the Poincaré section

Generally, the Poincaré section is one dimension smaller than the state space. In the case of our walker having a four-dimensional state space, it is thus three-dimensional. When considering the post-impact Poincaré section of the first walker model however, it can be shown that the part of the post-impact Poincaré section that is actually covered (the image of (2.5)) is only a two-dimensional

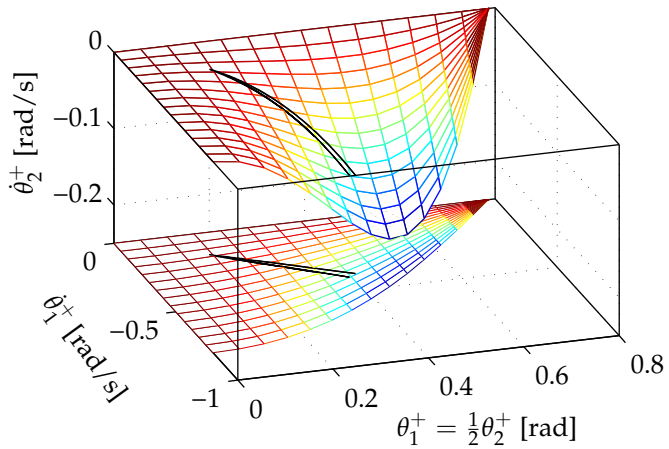

Figure 2.7: For the first walker model walking on a flat floor, the image of the impact equation (2.2) (*i.e.*, the set of actual values that the post-impact state can take) is a two-dimensional slice within the three-dimensional Poincaré section. The mesh shown was obtained by applying (2.5) to a grid of $x^- = [\theta_1\ \dot\theta_1\ 2\theta_1\ 0]^T$ with $\theta_1 \in [-\pi/4 \ldots 0\ \mathrm{rad}]$ and $\dot\theta_1 \in [-0.8 \ldots 0\ \mathrm{rad/s}]$. On top of the mesh the (quite small) basin of attraction is plotted as a black patch. At the bottom of the graph, the projection onto the $(\theta_1^+, \dot\theta_1^+)$ plane is shown. This is the commonly used way of visualizing the BOA.

manifold in the four-dimensional state space if the walker walks on a flat floor[2] (*i.e.*, $\theta_2^- = 2\,\theta_1^-$), being

$$\begin{bmatrix}\theta_1\\ \dot\theta_1\\ \theta_2\\ \dot\theta_2\end{bmatrix}^+ = \begin{bmatrix}-\frac{1}{2}\theta_2^-\\ \cos\theta_2^-\,\dot\theta_1^-\\ -\theta_2^-\\ \cos\theta_2^-\,\left(1-\cos\theta_2^-\right)\dot\theta_1^-\end{bmatrix};\ \begin{matrix}\theta_2^- \in (-\pi, 0)\\ \dot\theta_1^- \in \mathbb{R}^-\end{matrix}\ . \tag{2.13}$$

The shape of the covered part of the Poincaré section is shown in figure 2.7. Also shown is the *basin of attraction*, see section 2.4. The fact that (in the case of a flat floor) only a two-dimensional part of the Poincaré section is covered was also mentioned in other publications, but we have not found any reference to the actual shape of the manifold (for example, Schwab and Wisse (2001) just omitted the third and fourth dimension and described the stride function as a map $[\theta_1^+, \dot\theta_1^+]_{k+1} = St([\theta_1^+, \dot\theta_1^+]_k)$. The value of $\dot\theta_2^+$ was not discussed at all).

[2]Garcia et al. (1998) and Norris et al. (2008) have also mentioned this fact. However, they attribute this to the fact that the matrix in (2.5) can be written as a rank 2 matrix if one assumes that $\theta_2^- = 2\,\theta_1^-$. This is not exactly the truth (the reason is that the matrix itself depends on the variables as well). Although it is a necessary condition to have rank ≤ 2 (if it should be valid for any x^-), it is not sufficient. A necessary and sufficient condition is that there exists a coordinate transformation $z = \Phi_1(x)$ such that g expressed in z depends only on two coordinates and there exists no coordinate transformation $y = \Phi_2(x)$ such that g expressed in y depends only on one coordinate.

Regarding the second walker model, inspection of (2.6) shows us that, at least near the limit cycle, the post-impact state is dependent on $\dot{\theta}_2^-$ as well. This is due to the non-zero moment of inertia of the legs. More precisely, when assuming walking on a flat floor ($\theta_2^- = 2\,\theta_1^-$), we can write the matrix equation (2.6) only as a rank 3 matrix equation, being

$$\begin{bmatrix} \theta_1 \\ \dot{\theta}_1 \\ \theta_2 \\ \dot{\theta}_2 \end{bmatrix}^+ = \begin{bmatrix} 0 & 0 & -1/2 & 0 \\ 0 & 0.91 & 0 & 0.072 \\ 0 & 0 & -1 & 0 \\ 0 & 0.20 & 0 & 0.070 \end{bmatrix} \begin{bmatrix} \theta_1 \\ \dot{\theta}_1 \\ \theta_2 \\ \dot{\theta}_2 \end{bmatrix}^- .$$

Therefore (see also footnote 2), the covered part of the Poincaré section is not two-dimensional anymore; in theory it covers the whole 3D Poincaré space. However, around the limit cycle, $\dot{\theta}_2^-$ is much smaller than $\dot{\theta}_1^-$, and the numbers in the last column of the matrix in (2.6) are much smaller than those in the second column. Therefore, in practice the influence of $\dot{\theta}_2^-$ can be considered small, and the covered part of the Poincaré section for this walker is a thin three-dimensional slice in $\tilde{\mathcal{X}}^+$.

2.4 The basin of attraction

2.4.1 Definition of the basin of attraction

In walking robot literature, two different interpretations of the *basin of attraction* (BOA) are used, which can be defined as follows:

1. The basin of attraction B of a walker is the set of all states in the full state space $\mathcal{X}$ that, when the walker is started in that state, result in an endless forward walking motion, *i.e.*,

   $$B = \{x \in \mathcal{X} | \text{endless walking motion when started in } x\},$$

   and

2. The basin of attraction $\tilde{B}$ of a walker is the set of all states in the Poincaré section $\tilde{\mathcal{X}}$ that, when the walker is started in that state, result in an endless forward walking motion, *i.e.*,

   $$\tilde{B} = \{x \in \tilde{\mathcal{X}} | \text{endless walking motion when started in } x\}.$$

   Note that $\tilde{B} = B \cap \tilde{X}$.

An example of the usage of the first interpretation can be found in Spong and Bhatia (2003); the second interpretation is used in for example Wisse et al. (2004).

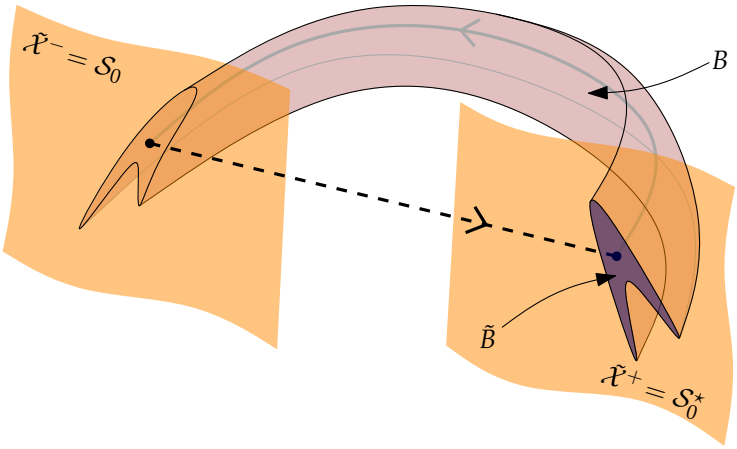

Figure 2.8: The basin of attraction B is a tube around the limit cycle. The intersection with a Poincaré section gives a Poincaré basin of attraction $\tilde{B}$.

In many papers however (*e.g.*, Schwab and Wisse (2001); Hobbelen and Wisse (2007); Liu et al. (2007); Wang et al. (2010)) the two interpretations are mixed up: at first the BOA is introduced using the first interpretation, but then it is used using the second.

Usually, from the context it is clear which definition is being used. In case of doubt, one can use the terms *global basin of attraction* and *Poincaré basin of attraction*. The second definition is the most used, because it allows easy analysis of the system. We will adopt this and we use the Poincaré basin of attraction in the rest of this chapter. Figure 2.8 shows the two different basins of attraction and their relation.

2.4.2 Comparison of basins of attraction

A plot of the basin of attraction may look attractive, but what is its usefulness in judging the robustness of a walker? Many researchers consider the basin of attraction to be some measure of robustness; by comparing two basins of attraction of different walkers, they try to determine which of the two walkers is most robust. Usually it is assumed that a larger basin of attraction implies better robustness, *i.e.*, the 'volume' of the BOA is taken as a measure for this (Jeon et al., 2010; Liu et al., 2007).

In most cases, comparing the basins of attraction of two different walkers is not meaningful: from the basin of attraction one cannot immediately tell which one is 'better'. We can explain this with an easy contradictory example.

Consider two walkers, A and B. Assume that walker B moves twice as fast as walker A and that the basin of attraction of walker B is the same as that of walker A but stretched a factor of two in the velocity direction. If we consider the volume of the BOA's as a measure of robustness, we may conclude that walker B is twice as robust as walker A. However, if we would normalize the plots relatively to the fixed point $\tilde{x}^\star$, we would conclude that both robots are equally robust. Thus, our conclusion depends on our choice of representation and not solely on the walker properties.

Mathematically speaking, considering the volume of the BOA makes no sense at all. This is because the BOA is a subset of $\mathcal{X} = \mathrm{TS}^2$, and a thing as a volume is not defined on TS^2. We could abuse the fact that TS^2 is locally homeomorphic to $\mathbb{R}^4$ to define a volume for a small part of the domain, but then the volume will be dependent on the homeomorphism used. In the case of our simple walkers (figure 2.7), the unit of the volume (assuming the mis-use of the homeomorphism) is $\mathrm{rad}^3/\mathrm{s}^2$, which is physically not something meaningful. Furthermore, if we would use different coordinates, the volume measurement would change too. In other words, the 'volume' of the BOA is not an intrinsic property of the walker, it is influenced by the choice of coordinates. Even worse: by sticking strictly to this 'definition', we would conclude that the first walker is not robust at all because the volume of its basin of attraction is zero (a 2D surface in a 3D space has no volume).

In practice however, in some cases it may still be meaningful to compare two different basins of attraction: if two very similar walkers have the same fixed point $\tilde{x}^\star$ and the same coordinates and homeomorphism are used. An example is if we have one robot and test different closed-loop controllers on it. It is required then, however, that all controllers act identically when the walker is in its limit cycle (otherwise, the different set-ups still have different fixed points).

2.5 Relation between BOA and disturbances

The assumption is often made that a larger basin of attraction directly implies a more robust walker. Intuitively this sounds reasonable: if a larger part of all possible states is inside the BOA, then the chances are higher that the visited states are inside. The thing that we are interested in however, is not purely 'how much of the states' is within the BOA, but much more something like 'how much of the important states' is within the BOA. In other words: it does not help to make the basin of attraction larger if the majority of the added states is never reached

anyway. Therefore, it is interesting to know which part of the Poincaré section is covered during normal walking (with disturbances). Below we present a new way of visualizing the relation between the Poincaré BOA and disturbances: a curve on the Poincaré section, associated with the disturbance.

Let us investigate some disturbance (*e.g.*, an impulsive torque around the stance ankle just after the start of the step, or a step-down) with magnitude $d \in \mathbb{R}$. When experiencing a disturbance (*i.e.*, $d \neq 0$), the walker will deviate from its limit cycle, and thus cross the post-impact Poincaré section at a point $\tilde{x}(d) \neq \tilde{x}^\star$. We can draw a curve consisting of all points $\{\tilde{x}(d) | d \in \mathbb{R}\}$. By definition, this curve fully lies in the covered part of the Poincaré section and it includes the fixed point $\tilde{x}^\star$ (for $d = 0$). If and only if the disturbance is such that the walker will not fall, then the point $\tilde{x}(d)$ lies within the basin of attraction. For large disturbances, the walker cannot complete a full step (*e.g.*, for a large step-up the swing foot will never reach the floor level after foot-scuffing), so not for each d there exists a $\tilde{x}(d)$.

As an example we inspect the following disturbances on the walker:

- An impulsive torque $p \in \mathbb{R}$ around stance ankle just after the start of the step; the maximum value P such that the walker survives a constant impulsive torque of each $-P < p < P$ is said to be a measure of robustness; the larger P, the more robust the walker against this type of disturbance. This disturbance can also be interpreted as being an impulsive backward push at the hip just after the start of the step.

- A step-down $h \in \mathbb{R}$; The maximum value H such that the walker survives a step down of each $-H < h < H$ is said to be a measure of robustness; the larger H, the more robust the walker against this disturbance. In order to use the Poincaré section, we used the integration mapping ΠI.

Figure 2.9 shows the curves of the two types of disturbance on top of the basin of attraction of the second walker model. By using this method, we immediately see that when considering these two disturbances, only a small part of the basin of attraction is important for the practical robustness of the walker; the whole lower-right part is never reached by any of the disturbances.

So we learned that if we want to make the walker more robust against these disturbances by extending the basin of attraction (*e.g.*, by applying control), then we should focus on extending the top part.

The relation between basin of attraction and permanent disturbances (such as parameter change, joint friction or a different slope) can not be investigated through this method. The reason is that a walker with a permanent disturbance has a different limit cycle and a different basin of attraction than the original walker. Therefore, comparison of the disturbance to the original basin of attraction has no meaning.

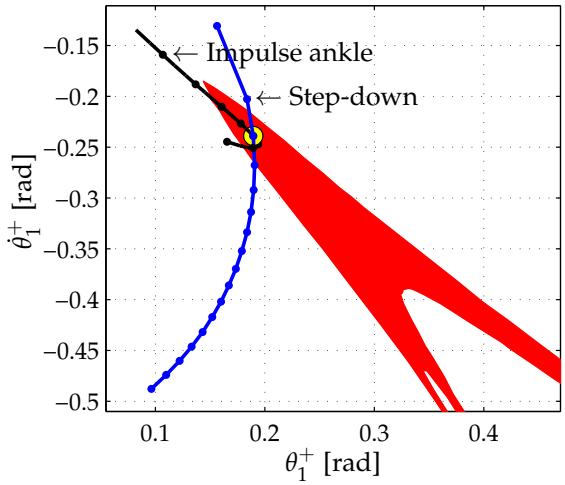

Figure 2.9: The relation between post-impact basin of attraction (red) and disturbances of different type and magnitude on our second walker model. The basin of attraction is actually a three-dimensional volume (not a slice); shown here is the projection onto the $\theta_1^+\dot{\theta}_1^+$-plane. It can be observed that only a small part of the basin of attraction is actually visited when considering these disturbances. The fixed point is encircled in the plot.

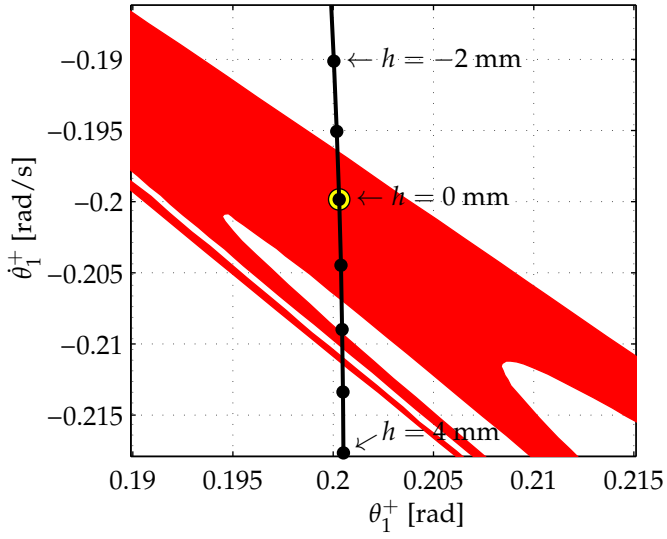

Figure 2.10: The covered part of the basin of attraction of the first walker model, with overlaid the line representing all states corresponding to a step-down (using the integration mapping method). The thick points on the line correspond to $h = \{\ldots, -2, -1, 0, 1, 2, \ldots\}$ mm.

2.6 Experiments

In order to test the above ideas, we investigated the step-down event of the first walker model (which is known to have bad robustness against step-downs) in more detail. Firstly, we made a one-step simulation of different step-downs in the range of -0.01 to 0.01 m and overlaid it on the basin of attraction. The result is shown in figure 2.10. It can be observed that the major part of the step-downs leads to a fall. An interesting thing is that the intersection of the line and the basin of attraction seems to be non-continuous; it spans the following ranges: $[-0.7 \ldots 1.5$ mm], [2.1 ... 2.3 mm] and a very small region around 2.5 mm. In order to verify this, we simulated two walkers experiencing a step-down of 1.8 mm (should fall) and 2.2 mm (should walk) respectively. The walkers were started from the fixed point and after a few steps the step-down was applied. Figures 2.11 and 2.12 show the results. Indeed the expected behavior can be observed. Note that this behavior is consistent with results from Hobbelen and Wisse (2007).

2.7 Conclusions and future work

In this chapter we have introduced a way to deal with Poincaré sections in the case of an irregular floor. We have shown that the image of the switching surface $S^\star$ can not be used as a Poincaré section in that case, because for each drop in floor height h this surface is different. We introduced three different mappings from any switching surface $\mathcal{S}_h^\star$ to some Poincaré surface $\mathcal{X}^+ = \mathcal{S}_0^\star$ (*i.e.*, as Poincaré section we chose the image of the switching surface belonging to a zero-height step-down). We showed that the integration mapping ΠI is the optimal mapping in the sense that for some state x, $\Pi I(x)$ gives the most accurate information on the future behavior of the system.

Furthermore, we introduced a way of relating different types of disturbance to curves on the Poincaré section. If we evaluate the reaction of the walker at a few different magnitudes of a certain disturbance, and connect the thus obtained points on the Poincaré section, we get a curve associated with the disturbance. This curve necessarily goes through the fixed point and it gives insight in how the system will behave as a response to the disturbance. As an example, we showed the curves for two different disturbances, and by means of an experiment we showed that this method indeed provides good information on the expected behavior of the walker.

As for future work, the mapping to the Poincaré section gives us the ability to work with the Poincaré section and its derivative tools (*e.g.*, the stride function, the linearization thereof, and the basin of attraction) in the case of irregular floors,

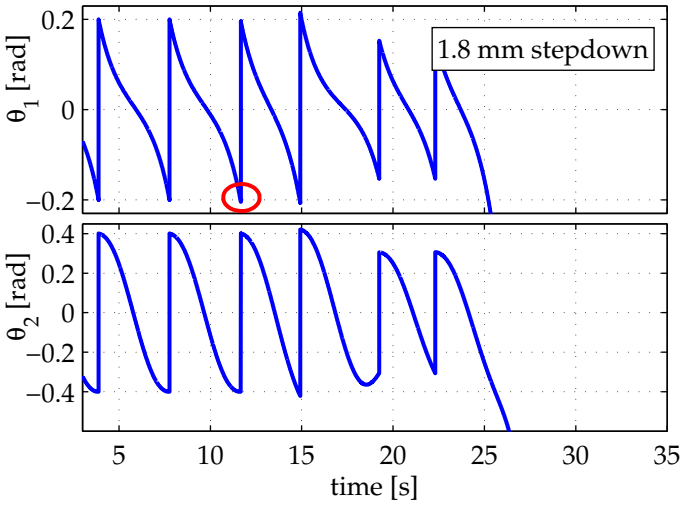

Figure 2.11: The stance leg angle θ_1 and inter-leg angle θ_2 (as a function of time) of the first walker model experiencing a step-down of 1.8 mm. After the step-down (encircled), the walker stumbles for three steps and then falls forward.

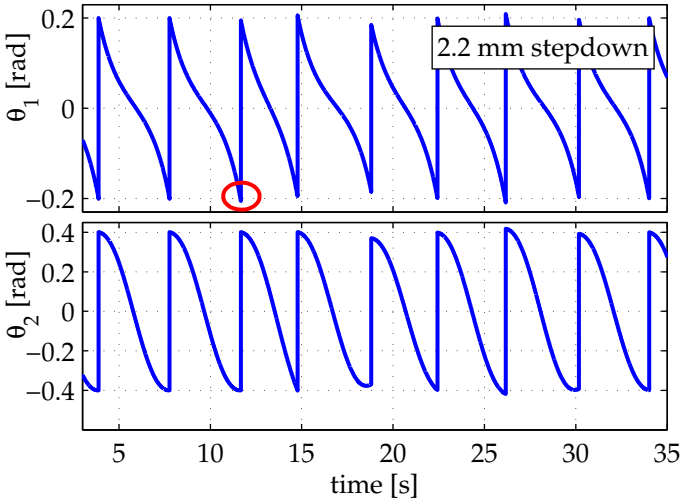

Figure 2.12: The stance leg angle θ_1 and inter-leg angle θ_2 (as a function of time) of the first walker model experiencing a step-down of 2.2 mm. After the step-down (encircled), the walker stumbles a little, but it keeps walking; eventually converging to the limit cycle again.

which opens a new field problems and solutions to be explored.

A natural extension to the (1D) curves associated with a disturbance is to introduce 2D planes associated with two disturbances. For example, one can make a combination of two different disturbances during the same step and check if they reinforce each other or cancel each other out. Another interesting feature would be to create a surface of the response to two sequential step-downs.

Chapter 3

Coordinate transformation as a help for analysis, simulation and controller design in walking robots

The contents of this chapter has not been published before.

Abstract—**In this chapter we show how a change of coordinates—in particular, the choice of the stance foot as reference body—can facilitate both model analysis and controller design for humanoid robots. Firstly, it is shown what the coordinate transformation looks like, all in directly applicable equations. Then a few examples are given of things that become easier due to the coordinate change.**

3.1 Introduction

In robotics it customary to describe the mechanics of the robot by means of a model. The model consists of the state (pose and velocity of each part of the robot) and equations of motion that tell how the state evolves in time.

In order to do calculations, the state needs to be expressed in numbers. For mobile robots, usually the pose and velocity of one body (called the *reference body* in this chapter) are taken as numerical entries in the state, as well as the (angular) positions and velocities of all joints. For walking robots the most obvious choice is to take the torso as reference body. This is often convenient because

1. the notion of 'position of the robot' is, intuitively, more related to the position of the torso than to to any of the other parts, and

2. it is symmetric with respect to left and right steps.

Sometimes however, it is useful to choose a different reference body, for example the stance foot. Advantages of this choice of reference body are, amongst others:

1. During normal walking, the stance foot is standing still on the ground. So, the reference body is fixed and its velocity is zero. This makes analysis of the system easier.

2. Forces acting on the reference body appear directly in the equations of motion. Choosing the stance foot as a reference body thus implies that ground reaction forces can easily be handled.

3. As will be shown in section 3.3.3, the form of the mass matrix in stance foot coordinates is much more useful than the original mass matrix.

More than in other literature, we explicitly denote how (in which coordinate representation, with respect to which body *etc.*) all elements of the equations are expressed. The reason for that is twofold. Firstly, the whole point of this chapter is in the difference between different representations. Therefore, it is important that there can be no confusion about which representation is used. Secondly, by explicitly denoting these things, it is easier to directly implement the equations, lowering the chance of mistakes.

In this chapter we combine some well-known principles (state representation, non-linear coordinate transformation and analysis tools from walking robots). We will show that, when using coordinate transformations, analysis algorithms on walking robots can become much easier, reducing the chance of errors when implementing. This is especially useful for actual realization of analysis algorithms in robot prototypes. Usually, in such prototypes, the state of the robot is calculated in only one representation. The equations in this chapter are ready-to-

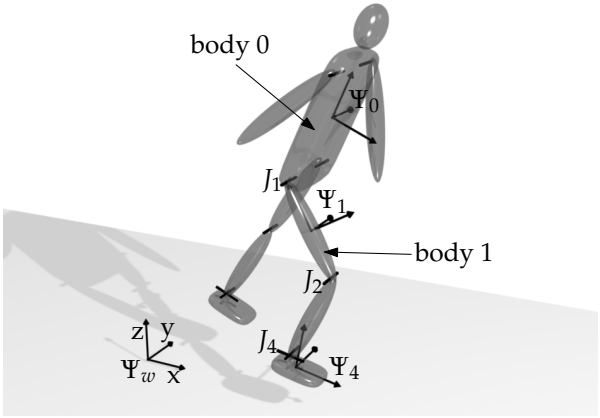

Figure 3.1: A rigid body mechanism floating in space.

use for transforming the state into another representation. The individual results in this chapter are not new, but the bundling can be helpful for those who are working hands-on with walking robots.

Basically, this chapter deals with 'just mathematical manipulation': everything we do here can also be done without coordinate transformation of the dynamics (transforming the controller instead). In many cases however, our method gives more insight and less chance to errors because it allows the user to see the model in the way he wants when developing a controller.

The chapter is structured as follows. Section 3.2 present a general representation of a rigid body system with its equations of motion, and then gives explicit equations for the coordinate transformation. In section 3.3 we present a few applications that, with the proper coordinate transformation, become easier to handle. A few notations used in this chapter, as well as some important identities, are listed in the appendix 3.A.

3.2 Coordinate transformation of the robot's dynamic equations

3.2.1 Dynamic equations of a floating rigid-body system

Consider a 3D, $(n+1)$–body, n–joint system that is floating in space (figure 3.1). We assume that all joints are rotational. This system has $N = 6 + n$ degrees of

freedom. If we choose some body 'a' as the reference body, the system's configuration can be denoted as

$$Q_{(\mathrm{a})} = (H_{\mathrm{a}}^{\mathrm{w}}; q)\,, \tag{3.1}$$

where $H_{\mathrm{a}}^{\mathrm{w}} \in \mathrm{SE}(3)$ denotes the pose of reference frame Ψ_{a} rigidly connected to body a (the superscript 'w' means that it is expressed in world coordinates), and $q \in \mathbb{R}^n$ denotes the vector of all joint angles. The subscript in parentheses in $Q_{(\mathrm{a})}$, indicates that we chose body 'a' as reference body. We will use this convention throughout the whole chapter.

We define the generalized velocity vector $v_{(\mathrm{a})}$ (again with body 'a' as reference body) as

$$v_{(\mathrm{a})} := \begin{pmatrix} {}^{\mathrm{w}}T_{\mathrm{a}}^{\mathrm{w}} \\ \dot{q} \end{pmatrix} \tag{3.2}$$

where ${}^{\mathrm{w}}T_{\mathrm{a}}^{\mathrm{w}}$ is the twist (Featherstone, 2007) of the reference body 'a', relative to the world frame Ψ_{w}, expressed in world coordinates of Ψ_{w}. The relation between ${}^{\mathrm{w}}T_{\mathrm{a}}^{\mathrm{w}}$ and the evolution of $H_{\mathrm{a}}^{\mathrm{w}}$ is given by

$${}^{\mathrm{w}}\tilde{T}_{\mathrm{a}}^{\mathrm{w}} = \dot{H}_{\mathrm{a}}^{\mathrm{w}}\, H_{\mathrm{w}}^{\mathrm{a}} \tag{3.3}$$

where $\tilde{T} \in \mathrm{se}(3)$ is as in (3.36). Note that $v_{(\mathrm{a})}$ is not the time derivative of $Q_{(\mathrm{a})}$, but there is a linear, bijective mapping between them:

$$v_{(\mathrm{a})} = \Phi_{(\mathrm{a})}(Q_{(\mathrm{a})})\, \dot{Q}_{(\mathrm{a})}. \tag{3.4}$$

We can write for the kinetic co-energy of the system:

$$E^*(q, v_{(\mathrm{a})}) = \tfrac{1}{2} v_{(\mathrm{a})}^T\, M_{(\mathrm{a})}(q)\, v_{(\mathrm{a})} \tag{3.5}$$

where $M(q)$ is the mass matrix of the system. An explicit expression for $M(q)$ is given by Stramigioli et al. (2009). Note that E^* is independent on the pose H of the reference body. The generalized momentum of the system can now be defined as

$$\bar{P}_{(\mathrm{a})}(q, v_{(\mathrm{a})}) := \begin{pmatrix} {}^{\mathrm{w}}P \\ p_{(\mathrm{a})} \end{pmatrix} = M_{(\mathrm{a})}(q)\, v_{(\mathrm{a})} \tag{3.6}$$

where ${}^{\mathrm{w}}P$ is the total momentum screw of the system (independent on the choice of reference body) expressed in world coordinates, and $p_{(\mathrm{a})}$ are the momenta associated with the system's internal joints (these *are* dependent on the choice of reference body).

Using the above we can write the dynamic equations of the system in a gravity field as

$$\dot{\bar{P}}_{(\mathrm{a})} = C_{(\mathrm{a})}(Q_{(\mathrm{a})}, \bar{P}_{(\mathrm{a})})\bar{P}_{(\mathrm{a})} + G_{(\mathrm{a})}(Q_{(\mathrm{a})}) + \bar{\tau}_{(\mathrm{a})} \tag{3.7}$$

where $C(Q, \bar{P})\bar{P}$ is a vector containing centrifugal, Coriolis and other internal components, $G(Q)$ contains the gravitational forces, $\bar{\tau}_{(\mathrm{a})} := \begin{pmatrix} {}^{\mathrm{w}}W^{\mathrm{a}} \\ \tau \end{pmatrix}$ are the generalized forces collocated with v, such that $\bar{\tau}^T v$ equals the power flowing into the system. By construction, the first six elements of $\bar{\tau}$, ${}^{\mathrm{w}}W^{\mathrm{a}}$, are the wrench (Featherstone, 2007) on the reference body; the last n elements are the joint torques. An external wrench acting on a different body (*e.g.*, body i) can be described as the linear combination

$$\bar{\tau}_{(\mathrm{a})} = \begin{pmatrix} I_{6\times 6} \\ \left({}^{\mathrm{w}}J_i^{\mathrm{a}}\right)^T \end{pmatrix} {}^{\mathrm{w}}W^{\mathrm{i}}, \tag{3.8}$$

where ${}^{\mathrm{w}}J_i^{\mathrm{a}} = {}^{\mathrm{w}}J_i^{\mathrm{a}}(q)$ is the geometric jacobian, mapping the joint velocities to the relative twist of body i:

$${}^{\mathrm{w}}T_i^{\mathrm{a}} = {}^{\mathrm{w}}J_i^{\mathrm{a}}(q)\,\dot{q}. \tag{3.9}$$

By integrating (3.7) we find an expression for $\bar{P}$ as a function of time. The velocity v can then be found with the inverse of (3.6), and finally the evolution of Q by (3.3).

The matrices M, C and vector G contain the model information; obtaining them can be hard. Fortunately, there are some modeling packages available that do the job (Controllab Products B.V., 2011; Dynasim, 2011). In a real robot it is often useful to have an accurate dynamic model of the plant available for the controller. The equations for M, C and G can be directly copied from the simulation model in that case.

3.2.2 The coordinate transformation

Presented here is a standard non-linear coordinate transformation, as explained in many textbooks on non-linear dynamics, such as those by Isidori (1995) and Nijmeijer and van der Schaft (1990). The equations are worked out for our special case: a multi-link rigid-body system, having, amongst others, a torso ('tor') and a stance-foot ('stf').

Assume that the variables and equations of motion are known in torso representation and we want to have the stance foot as our new reference body, *i.e.*, we

want to find the transformation that, given $Q_{(\text{tor})}$, $v_{(\text{tor})}$, $\bar{\tau}_{(\text{tor})}$ and (3.7), results in a $Q_{(\text{stf})}$, $v_{(\text{stf})}$, $\bar{\tau}_{(\text{stf})}$ and new equations of motion expressed in these variables.

There exists a (bijective) non-linear mapping between the configuration representations $Q_{(\text{stf})}$ and $Q_{(\text{tor})}$:

$$Q_{(\text{stf})} = \begin{pmatrix} H^{\text{w}}_{\text{stf}} \\ q \end{pmatrix} = S(Q_{(\text{tor})}) = \begin{pmatrix} \tilde{S}\left(Q_{(\text{tor})}\right) \\ q \end{pmatrix}. \tag{3.10}$$

The relation between $v_{(\text{stf})}$ and $v_{(\text{tor})}$ can be found by writing

$$\begin{aligned} v_{(\text{stf})} &= \begin{pmatrix} {}^{\text{w}}T^{\text{w}}_{\text{stf}} \\ \dot{q} \end{pmatrix} = \begin{pmatrix} {}^{\text{w}}T^{\text{w}}_{\text{tor}} + {}^{\text{w}}T^{\text{tor}}_{\text{stf}} \\ \dot{q} \end{pmatrix} = \begin{pmatrix} {}^{\text{w}}T^{\text{w}}_{\text{tor}} + {}^{\text{w}}J^{\text{tor}}_{\text{stf}}\,\dot{q} \\ \dot{q} \end{pmatrix} \\ &= E(Q_{(\text{tor})})\, v_{(\text{tor})} \end{aligned} \tag{3.11}$$

with

$$E(Q_{(\text{tor})}) = \begin{bmatrix} I_{6\times 6} & {}^{\text{w}}J^{\text{tor}}_{\text{stf}}(q) \\ 0_{n\times 6} & I_{n\times n} \end{bmatrix}. \tag{3.12}$$

Note that E is always invertible.

The kinetic co-energy is, of course, independent on our choice of coordinates, hence

$$\tfrac{1}{2} v^T_{(\text{stf})}\, M_{(\text{stf})}\, v_{(\text{stf})} = \tfrac{1}{2} v^T_{(\text{tor})}\, M_{(\text{tor})}\, v_{(\text{tor})} \tag{3.13}$$

which we can use to find the mass matrix and generalized momentum in new coordinates (dependencies of $Q_{(\text{tor})}$ are left out for brevity):

$$M_{(\text{stf})} = E^{-T}\, M_{(\text{tor})}\, E^{-1}, \tag{3.14}$$

$$\bar{P}_{(\text{stf})} = M_{(\text{stf})}\, v_{(\text{stf})} = E^{-T}\, \bar{P}_{(\text{tor})}. \tag{3.15}$$

We can now use (3.7) and (3.15) to find expressions for $C_{(\text{stf})}$, $G_{(\text{stf})}$ (dependencies of $Q_{(\text{tor})}$ and $\dot{q}$ are left out again):

$$\begin{aligned} \tfrac{\mathrm{d}}{\mathrm{d}t} \bar{P}_{(\text{tor})} &= C_{(\text{tor})} \quad \bar{P}_{(\text{tor})} \quad + G_{(\text{tor})} + \bar{\tau}_{(\text{tor})} \\ \tfrac{\mathrm{d}}{\mathrm{d}t} \left(E^T \bar{P}_{(\text{stf})} \right) &= C_{(\text{tor})}\, E^T \bar{P}_{(\text{stf})} + G_{(\text{tor})} + \bar{\tau}_{(\text{tor})} \\ E^T \dot{\bar{P}}_{(\text{stf})} + \dot{E}^T \bar{P}_{(\text{stf})} &= C_{(\text{tor})}\, E^T \bar{P}_{(\text{stf})} + G_{(\text{tor})} + \bar{\tau}_{(\text{tor})} \end{aligned} \tag{3.16}$$

so

$$\begin{aligned} \dot{\bar{P}}_{(\text{stf})} &= \underbrace{E^{-T}(C_{(\text{tor})} E^T - \dot{E}^T)}\, \bar{P}_{(\text{stf})} + \underbrace{E^{-T} G_{(\text{tor})}} + \underbrace{E^{-T} \bar{\tau}_{(\text{tor})}} \\ \dot{\bar{P}}_{(\text{stf})} &= \qquad\quad C_{(\text{stf})} \qquad\quad \bar{P}_{(\text{stf})} + \quad G_{(\text{stf})} \quad + \quad \bar{\tau}_{(\text{stf})}. \end{aligned} \tag{3.17}$$

An analytical expression for $\dot{E}$ can be found, as shown in appendix 3.B. With that, all elements of the coordinate transform are known analytically.

3.2.3 Interpretation of the coordinate transformation

The 'conventional representation' of the state, $(Q_{(\mathrm{tor})}, \bar{P}_{(\mathrm{tor})})$, is intuitive in the sense that one usually thinks as 'the pose and velocity of the robot' as being 'the pose and velocity of the torso'. This is understandable; the torso is the largest and heaviest part of the robot. The pose and velocity of the torso are directly available in this representation of state, as $H^{\mathrm{w}}_{\mathrm{tor}}$ and ${}^{\mathrm{w}}T^{\mathrm{w}}_{\mathrm{tor}}$ respectively.

The 'stance foot representation' of the state, $\left(Q_{(\mathrm{stf})}, \bar{P}_{(\mathrm{stf})}\right)$ does not give any direct information about the pose and velocity of the torso; instead it gives the pose and velocity of the stance foot. Since the stance foot is usually stationary, the pose $H^{\mathrm{w}}_{\mathrm{stf}}$ does not change during one step, and the velocity ${}^{\mathrm{w}}T^{\mathrm{w}}_{\mathrm{stf}}$ is zero. What remains in the state is only the joint angles and angular velocities. This is closely related to the actual situation: as long as the robot is standing on one foot, it behaves just like a fixed-in-the-world manipulator, having only rotational joints to take into account.

One may see this situation as follows: as long as the stance foot has contact with the ground, the foot may be considered to be rigidly connected to the ground. Consequently, the apparent mass of the foot will be increased by the ground, being infinite. Hence, the foot (with ground) is now the largest and heaviest part of the robot, which justifies the choice of the stance foot as reference body.

3.2.4 The double support phase

When the robot is in double support phase, there is a constraint on the relative movement of the two feet. This causes the number of usable degrees of freedom of the robot to decrease. Therefore, any state representation with the original number of degrees of freedom ($N = 6 + n$) is redundant. The equations of motion can then only be solved by applying constraint methods such as Lagrangian multipliers, or by introducing stiff spring-damper systems that force the constraint to be kept.

The coordinate transformation presented in this chapter is a bijective transformation, *i.e.*, for each state representation $(Q_{(\mathrm{tor})}, \bar{P}_{(\mathrm{tor})})$ there exists one unique state representation $\left(Q_{(\mathrm{stf})}, \bar{P}_{(\mathrm{stf})}\right)$ and vice versa. Hence, both state representations have the same number of degrees of freedom and are redundant in the double support phase. Of course, the transformed state representation is as valid as the original state representation (if the right constrains methods are applied), but the nice properties (as explained in the next section) disappear. Therefore, the coordinate transformation does not give any advantages (nor any disadvantages) in the double support phase. In the next section we assume that one and only one foot is on the ground.

3.3 Applications

In this section, a few examples are given of how the above math makes life easier for those who want to study bipedal walking.

3.3.1 Static analysis: joint torques and stability

Using (3.16), it is easy to find the joint torques needed to keep the robot static in a particular pose (as mentioned earlier, this method only works for open-chain systems, so the robot should have exactly only one foot on the ground). The information is useful for checking if the actuators you have chosen will suffice for this task. By setting $\dot{\bar{P}}_{(\text{stf})}$ and $\bar{P}_{(\text{stf})}$ to zero, we find

$$\bar{\tau}_{(\text{stf})} = \begin{bmatrix} {}^{\text{stf}}W^{\text{stf}} \\ \tau \end{bmatrix} = -G_{\text{stf}}(Q). \tag{3.18}$$

The torques τ are the joint torques needed to keep the robot in the position. Equation (3.18) can be evaluated for a set of different poses, giving a set of required torques. These are minimum requirements for the actuators (of course, dynamics may add additional requirements to the actuators).

It is also interesting to check if the robot, in a certain static pose, does not fall over. In addition to the above-mentioned joint torque conditions, a necessary condition is that the Foot Rotation Indicator[1] (FRI) (Goswami, 1999) must be within the convex hull of the stance foot (the two conditions together are sufficient as well). The coordinate transformation directly gives us the necessary wrench on the stance foot, ${}^{\text{stf}}W^{\text{stf}} = \begin{bmatrix} m_x & m_y & m_z & F_x & F_y & F_z \end{bmatrix}^T$. From this, the position of the FRI, expressed in coordinates of the stance foot's reference frame, can be found to be (see also (3.33))

$${}^{\text{stf}}p_{\text{fri}} = \begin{bmatrix} -m_y/f_z \\ m_x/f_z \\ 0 \end{bmatrix}. \tag{3.19}$$

Checking to see if the FRI is within the stance foot's convex hull is now easy because the FRI is already expressed in convenient coordinates. For example, if we consider a rectangular foot with length l and width w, the conditions for the

[1] The Foot Rotation Indicator is defined as the "point on the foot/ground surface, within or outside the support polygon, where the net ground reaction force *would have to act* to keep the foot stationary" (Goswami, 1999).

FRI being within the convex hull are

$$-l/2 < -m_y/f_z < l/2 \quad \text{and} \tag{3.20}$$

$$-w/2 < \; m_x/f_z \; < w/2. \tag{3.21}$$

3.3.2 Rigid foot contact

When simulating a walker, there are two options to model foot contact with the ground: compliant and rigid (Gilardi and Sharf, 2002) contact modeling. Compliant contacts are easier to model, but may be inaccurate and increase simulation time because they introduce high-frequency dynamics. Rigid contacts are generally faster in simulation but need more sophisticated math. In the field of bipedal walking, rigid contacts are usually assumed to be inelastic, which is also assumed here. Furthermore, we assume that the foot is exactly parallel to the ground during the collision (*i.e.*, all edges of the foot touch simultaneously). The process of simulating foot contact by means of a rigid contact model consists of three phases:

1. collision, by means of an impulsive ground reaction force,
2. 'resting contact', by means of a ground reaction force usually calculated with the aid of Lagrangian multipliers, and
3. contact loss.

These three phases are described in more detail below.

Stramigioli et al. (2009) explained how the impulsive ground reaction force $\bar{\tau}_{(\mathrm{a})} = \begin{pmatrix} {}^{\mathrm{a}}W^{\mathrm{a}} \\ \tau \end{pmatrix} = A_{(\mathrm{a})}^T \, \lambda(P,Q) \, \delta(t-t_i)$ (where $\delta(t-t_i)$ indicates a Dirac pulse at impact time t_i) can be found that brings the foot velocity ${}^{\mathrm{w}}T_{\mathrm{stf}}^{\mathrm{w}}$ to zero instantaneously in a coordinate system with arbitrary reference body a:

$$\lambda = -(A_{(\mathrm{a})} \, M_{(\mathrm{a})}^{-1} \, A_{(\mathrm{a})}^T)^{-1} A_{(\mathrm{a})} \, M_{(\mathrm{a})}^{-1} \, \bar{P}_{(\mathrm{a})}^-, \tag{3.22}$$

where $A_{(\mathrm{a})} = A_{(\mathrm{a})}(q) = \begin{bmatrix} I_{6\times 6} & {}^{\mathrm{w}}J_{\mathrm{stf}}^{\mathrm{a}} \end{bmatrix}$ and $\bar{P}_{(\mathrm{a})}^-$ is the generalized momentum vector just before impact. This leads to the post-impact momentum

$$P_{(\mathrm{a})}^+ = \left(I - A_{(\mathrm{a})}^T (A_{(\mathrm{a})} M_{(\mathrm{a})}^{-1} A_{(\mathrm{a})}^T)^{-1} A_{(\mathrm{a})} M_{(\mathrm{a})}^{-1} \right) P_{(\mathrm{a})}^- \tag{3.23}$$

and, by $v_{(\mathrm{a})}^+ = M_{(\mathrm{a})}^{-1} P_{(\mathrm{a})}^+$ and similar for $v_{(\mathrm{a})}^-$, we obtain

$$v_{(\mathrm{a})}^+ = \left(I - M_{(\mathrm{a})}^{-1} A_{(\mathrm{a})}^T (A_{(\mathrm{a})} M_{(\mathrm{a})}^{-1} A_{(\mathrm{a})}^T)^{-1} A_{(\mathrm{a})} \right) v_{(\mathrm{a})}^-. \tag{3.24}$$

When we choose the coordinate system with stance foot as the reference body, then (because by construction ${}^{\mathrm{w}}J_{\mathrm{stf}}^{\mathrm{stf}} = 0$) matrix A reduces to the constant matrix

$A = \begin{bmatrix} I_{6\times 6} & 0_{6\times n} \end{bmatrix}$ and thus $\bar{\tau}_{(\text{stf})} = \begin{pmatrix} {}^{\text{stf}}W^{\text{stf}} \\ \tau \end{pmatrix} = \begin{pmatrix} \lambda(P,Q)\,\delta(t-t_i) \\ 0 \end{pmatrix}$. This indicates that, when simulating an impact which instantaneously brings the foot velocity to zero, only an impulsive wrench on the stance foot is exerted, no joint impulses are generated by the impact. This is logical, because what is actually simulated is the just the impulsive force the ground exerts on the foot. Note however, that the impact does affect the velocities of the joints, which can be seen by closer inspection of (3.24).

Keeping the stance foot in place after it made contact with the ground can be done by using the technique of lagrangian multipliers. An expression for the acceleration $a_{(\text{stf})} = \dot{v}_{(\text{stf})}$ of the system is:

$$a_{(\text{stf})} = \begin{bmatrix} {}^{\text{stf}}\dot{T}^{\text{w}}_{\text{stf}} \\ \ddot{q} \end{bmatrix} = \dot{M}^{-1}_{(\text{stf})}\bar{P}_{(\text{stf})} + M_{(\text{stf})}\dot{\bar{P}}_{(\text{stf})}. \tag{3.25}$$

We can rewrite (3.16) as (where all $A = A_{(\text{stf})}$)

$$\dot{\bar{P}}_{(\text{stf})} = C_{(\text{stf})}\bar{P}_{(\text{stf})} + G_{(\text{stf})} + A'^{T}\tau + A^{T}\,{}^{\text{stf}}W^{\text{stf}} \tag{3.26}$$

where A is as above and A' is its 'opposite': $A' = \begin{bmatrix} 0_{n\times 6} & I_{n\times n} \end{bmatrix}$. ${}^{\text{stf}}W^{\text{stf}}$ is the unknown ground reaction force (wrench) that keeps the foot from accelerating. We demand that the first six elements of $a_{(\text{stf})}$ are zero, *i.e.*, $Aa_{(\text{stf})} = 0$. Therefore after pre-multiplying (3.25) by A, setting it to zero, inserting (3.26) and reordering, we find the wrench needed to keep the foot in place:

$$\begin{aligned} {}^{\text{stf}}W^{\text{stf}} = -(A{M_{\text{stf}}}^{-1}A^{T})^{-1}(A\dot{M}^{-1}_{(\text{stf})}\bar{P}_{(\text{stf})} + \\ AM^{-1}_{(\text{stf})}(C_{(\text{stf})}\bar{P}_{(\text{stf})} + G_{(\text{stf})} + A'^{T}\tau)). \end{aligned} \tag{3.27}$$

In order to find ${}^{\text{stf}}W^{\text{stf}}$, we need the time derivative of $M^{-1}_{(\text{stf})}$. Several techniques are available to find this (Muller, 2007).

It is not guaranteed that the floor can indeed deliver this required force to keep the foot stationary. If not, then the foot would accelerate and we would have contact loss (or at least contact change, if the foot starts to rotate about an edge). A good measure for detecting contact loss or change is the 'foot rotation indicator' (FRI) together with the sign of the local z-component of the ground reaction force (Goswami, 1999).

Especially when considering multiple contacts or impacts during contact of another part of the system, it becomes hard to find out when exactly there is contact loss. As an example, when a rigid body system already has some contact point while another points collides, the first point may or may not lose contact. This problem is addressed by Ruspini and Khatib (1997), where Linear Complementarity Problem (LCP) solving is used.

3.3.3 Mass matrix and P(I)D control

Using normal, fixed-coefficient PD or PID control (we will speak of PD control in the remainder of this section for brevity) on joints has the following two disadvantages:

1. due to coupling in the system, a torque on one joint will influence the movement of other joints as well, and
2. because the configuration of the robot is time-varying, the perceived inertia of each joint changes all the time. Hence, the performance of a PD controller on the joint will vary too.

By using the transformed mass matrix $M_{(\text{stf})}$, these two problems can be overcome.

Firstly, let us focus on the transformation of the mass matrix in a qualitative way. Given a bipedal robot hanging in the air, with the torso fixed. Now, if we want to give a foot some rotational acceleration, we need only a little actuator power in the ankle to do so; we only have to accelerate the foot's inertia. If we look at the mass matrix $M_{(\text{tor})}$, we will see that the associated element ($M_{(i+6)(i+6)}$ if the ankle joint is joint i) is small.

Now if we make the robot stand on this leg, the same rotational acceleration requires a much larger torque — the whole robot's inertia needs to be accelerated instead of only the foot's (or, from a different perspective, the inertia of the foot was increased by the earth's inertia). This is something which cannot be deduced from $M_{(\text{tor})}$. However, this information *is* correctly given in $M_{(\text{stf})}$: the associated element $M_{(i+6)(i+6)}$ naturally reflects the relation between torque and achieved rotational acceleration at all times.

The fact that we have a good representative of the mass matrix, gives us the opportunity to do true MIMO (multiple input, multiple output) control. Assume we want to steer joint q_i to a desired angle $\hat{q}_i(t)$ with a PD-controller, such that the *controller's contribution* to the joint's acceleration is $\ddot{q}_{C,i} = K(\hat{q}_i - q_i) + D\frac{\mathrm{d}}{\mathrm{d}t}(\hat{q}_i - q_i)$. Furthermore, the controller should not influence the other joints, so $\ddot{q}_{C,j} = 0$ for all $j \neq i$ (other forces and controllers may accelerate the joints, though). The joint torques τ needed to achieve the desired contribution to the acceleration on all these joints can be found by

$$\begin{bmatrix} {}^{\text{stf}}W^{\text{stf}} \\ \tau \end{bmatrix} = M_{(\text{stf})}\, \ddot{q}_C \tag{3.28}$$

where $\ddot{q}_C = \begin{bmatrix} 0 & \cdots & 0 & \ddot{q}_{C,i} & 0 & \cdots & 0 \end{bmatrix}^T$, or

$$\begin{bmatrix} {}^{\text{stf}}W^{\text{stf}} \\ \tau \end{bmatrix} = \left(M_{(\text{stf})}\right)_{\text{col}\, i}\, \ddot{q}_{C,i} \tag{3.29}$$

where $\left(M_{(\mathrm{stf})}\right)_{\mathrm{col}\,i}$ is the i-th column of $M_{(\mathrm{stf})}$. W indicates the additional ground reaction forces resulting from the joint torques and can be used to estimate if the desired acceleration causes the stance foot to move (which is generally undesired). By using this controller structure and the appropriate M, reflecting the current state of the robot, we can tune the desired behavior (bandwidth etc.) once by adapting K and D, and the performance of the controller will be the same, no matter what state the robot is in.

Similarly, it is also easy to do complete feed-forward, *i.e.*, calculating the required torques $\bar{\tau}_{(\mathrm{stf})}$ from the desired accelerations: one uses (3.25) to determine the desired $\dot{\bar{P}}_{(\mathrm{stf})}$ and then (3.16) to find the torques. However, in the field of dynamically walking robots, this is generally not desired; we want to *use* the natural dynamics, not destroy it.

3.4 Conclusions and future work

In this chapter we have presented explicit equations for a coordinate transformation which changes the reference body for a free-floating rigid-body structure. We showed, by means of some examples, that a change of reference body from torso to stance foot is useful in analysis (section 3.3.1), simulation (section 3.3.2) and control (section 3.3.3). The applications are not new, but they all become simpler because of the coordinate transformation.

By means of the coordinate transformation, the state of the robot is represented in a way that is 'more closely to what actually happens': interaction with the environment (*i.e.*, the ground), mainly goes through forces acting on the stance foot; these forces are directly visible in $\bar{\tau}_{(\mathrm{stf})}$. As long as the stance foot has full contact with the ground, the robot behaves like a fixed-to-the-world manipulator, which is exactly reflected in the transformed state. When applying a torque on a joint, the forces needed on the foot to make sure it stays on the ground can easily be calculated (section 3.3.2) and actually have a meaningful interpretation: these are really the forces that the ground exerts on the foot.

Future work will be twofold. Firstly, the 'tools' presented here will be used for developing new robust walking controllers. Secondly, it is expected that more sophisticated coordinate transformations may make other things easier, so we will certainly have a look into that. Priority is to find meaningful coordinate transformations for the double support phase.

3.A List of mathematical notations and identities

Proofs of the identities below can easily be found or derived with the help of textbooks on geometric dynamics such as (Featherstone, 2007).

$$H_i^j = \text{'Homogeneous matrix', expressing the pose (position and orientation) of frame } \Psi_i \text{ in coordinates of frame } \Psi_j. \tag{3.30}$$

$${}^cT_a^b = \text{Twist (generalized velocity) of body } a \text{ relative to body } b, \text{ expressed in the coordinate frame of body } c. \tag{3.31}$$

$${}^cW^a = \text{Wrench (generalized force) acting on body } a \text{ expressed in the coordinate frame of body } c. \tag{3.32}$$

$${}^cp_a = \text{Position of point } a \text{ expressed in coordinates of frame } \Psi_c, \tag{3.33}$$

$$\tilde{x} = \begin{bmatrix} 0 & -x_3 & x_2 \\ x_3 & 0 & -x_1 \\ -x_2 & x_1 & 0 \end{bmatrix} \text{ Same for } \tilde{p}, \tilde{v} \text{ and } \tilde{\omega} \tag{3.34}$$

$$H_i^j = \begin{bmatrix} R_j^j & p_i^j \\ 0 & 1 \end{bmatrix} \Leftrightarrow \mathrm{Ad}_H = \begin{bmatrix} R & 0 \\ \tilde{p}R & R \end{bmatrix} \tag{3.35}$$

$$T = \begin{bmatrix} \omega \\ v \end{bmatrix} \Leftrightarrow \tilde{T} = \begin{bmatrix} \tilde{\omega} & v \\ 0 & 0 \end{bmatrix} \tag{3.36}$$

$$T = \begin{bmatrix} \omega \\ v \end{bmatrix} \Leftrightarrow \mathrm{ad}_T = \begin{bmatrix} \tilde{\omega} & 0 \\ \tilde{v} & \tilde{\omega} \end{bmatrix} \tag{3.37}$$

$${}^jT_\bullet^\bullet = \mathrm{Ad}_{H_i^j}\,{}^iT_\bullet^\bullet \tag{3.38}$$

$${}^jW^\bullet = \mathrm{Ad}_{H_j^i}^T\,{}^iW^\bullet \tag{3.39}$$

$${}^jT_a^c = {}^jT_b^c + {}^jT_a^b \tag{3.40}$$

3.B Analytical expression for $\dot{E}$

The time derivative $\dot{E}$ can analytically be expressed as (the derivation is left behind):

$$\dot{E} = \begin{bmatrix} 0_{6\times 6} & {}^wj_{\mathrm{stf}}^{\mathrm{tor}}(q) \\ 0_{n\times 6} & 0_{n\times n} \end{bmatrix}, \tag{3.41}$$

where the i^{th} column of ${}^wj_{\mathrm{stf}}^{\mathrm{tor}}$, denoted as $\left({}^wj_{\mathrm{stf}}^{\mathrm{tor}}\right)_{\mathrm{col}\,i}$, (and associated with move-

ment of joint i) is equal to

$$\left({}^{\mathrm{w}}J^{\mathrm{tor}}_{\mathrm{stf}}\right)_{\mathrm{col}\,i} = \mathrm{ad}\left({}^{\mathrm{w}}T^{\mathrm{w}}_{\mathrm{tor}} + {}^{\mathrm{w}}J^{\mathrm{tor}}_{*(i)}\,\dot{q}\right)\,\left({}^{\mathrm{w}}J^{\mathrm{tor}}_{\mathrm{stf}}\right)_{\mathrm{col}\,i} \tag{3.42}$$

where $\mathrm{ad}_{(\bullet)}$ as in (3.37) and ${}^{\mathrm{w}}J^{\mathrm{tor}}_{*(i)}$ denotes the geometric jacobian of the 'parent' rigid body $*(i)$ to which joint i is attached (*e.g.*, in figure 3.1, joint 2 is attached to body 1 so $*(2) = 1$).

Chapter 4

Geometric interpretation of the Zero-Moment Point

This chapter is based on the following article (van Oort and Stramigioli, 2011):

Geometric interpretation of the Zero-Moment Point
Gijs van Oort and Stefano Stramigioli
Proc., IEEE International Conference on Robotics and Automation (ICRA'11)
pages 575–580, May 2011.

***Abstract*—In this chapter we show that the concept of screws and wrenches gives us tools to *geometrically* establish the relation between the ground reaction wrench and the Zero-Moment Point. In order to arrive at this, we show how a wrench can be decomposed into separate components. The proposed method gives a general, completely coordinate-free way to find the ZMP and contributes in improving the geometrical insight.**

4.1 Introduction

The Zero-Moment Point, ZMP (Vukobratović and Borovac, 2004), is widely known in the area of walking robots. Numerous researchers have investigated this point and have given their own definitions and interpretations of it (for references, see section 4.2). The theory on screws, introduced by Ball (1900) is a 6D generalization of velocity and force, being the Twist and Wrench respectively. This approach is coordinate-free, meaning that the equations and their results are invariant for the choice of coordinates. The absence of coordinates gives greater flexibility (the equations work for any orientation of the robot; they are not limited to a certain pose in the world), reduces the chance of errors (*e.g.*, one cannot be tempted to make assumptions like 'the robot will walk approximately in x-direction, so let's use the x-coordinate for the distance traveled' because the lack of coordinates implies that no x-direction was defined in the first place), and most importantly, mimics what happens in nature: nature does not have coordinates at all; the laws are completely dictated by the physics of the system, by nothing more. The concept is also called 'geometric dynamics', emphasizing the fact that everything follows from the geometric properties of the system (in a broad sense, *e.g.*, geometric mass and force distribution), not from the way you look at the system (*i.e.*, which coordinates you use).

In this chapter we combine the knowledge of the Zero-Moment Point and screw theory, to give a novel, geometric interpretation of the Zero-Moment Point. We will show how the position of the ZMP can be found from the ground reaction wrench (the generalization of the ground reaction force) and geometric rules on wrench decomposition. This leads to more insight in the position of the ZMP and how this relates to the ground wrench exerted on the foot.

The relation between ground reaction wrench and ZMP has been (indirectly) presented before (Takao et al., 2003; Park et al., 2005; Sardain and Bessonnet, 2004), but without any discussion nor proof. The mathematical expression for the ZMP has been known for over 40 years now, so in that sense the final result of this chapter is not new. The insightful, graphical way of achieving the result however is the real contribution of this chapter.

In sections 4.2 and 4.3 we introduce the key terms of this chapter further. We will address some issues of the ZMP, and show how a wrench can be shown uniquely in a graphical way. In section 4.4 we show and prove three ways of decomposing a wrench into two separate components (analogous to decomposition of a force into two components). In section 4.5 we present the main contribution of this chapter, being the geometric relation between the ground reaction wrench and the ZMP. In section 4.6 it will be shown that this leads to a simple explicit expression for the ZMP position. Conclusions are discussed in section 4.7.

4.2 The Zero-Moment Point

The Zero-Moment Point, ZMP, was introduced by M. Vukobratović and D. Juričić around 1969 (Vukobratović and Juričić, 1968, 1969) (although the term ZMP was only introduced a few years later). It should be noted that "...the notion of ZMP has never been introduced in the form of a formal definition..." (Vukobratović and Borovac, 2004). This has given rise to dozens of researchers giving their own definitions and interpretations to this point. In general, the definitions of the ZMP can be divided into two groups:

1. Definitions in which the position of the ZMP is related to gravity and inertia forces, *e.g.*:
   - "The ZMP is defined as that point, on the ground at which the net moment of the inertial forces and the gravity forces has no component, along the horizontal axes." (Dasgupta and Nakamura, 1999),
   - "The ZMP is the point on the ground where the tipping moment acting on the biped, due to gravity and inertia forces, equals zero, the tipping moment being defined as the component of the moment that is tangential to the supporting surface." (Sardain and Bessonnet, 2004),
2. Definitions in which the position of the ZMP is related to the ground-reaction force acting on the robot, *e.g.*:
   - "The ZMP (Zero-Moment Point) is defined to be a point on the ground at which the tangential component of the moment generated by the ground reaction force/moment becomes zero." (Harada et al., 2003),
   - "The pressure under supporting foot can be replaced by the appropriate reaction force acting at a certain point of the mechanism's foot. Since the sum of all moments of active forces with respect to this point is equal to zero, it is termed the Zero-Moment Point (ZMP)."[1] (Vukobratović et al., 2001).

Interestingly, both cited definitions in group 1 (as well as most others in this group) fail to include external disturbance forces (such as someone pushing the robot), which makes these definitions incomplete. After fixing this (for example, the first definition would become: The ZMP is defined as that point, on the ground at which the net moment of the inertial forces, the external disturbance and gravity forces has no component, along the horizontal axes), all definitions are correct

[1] At first glance, this definition seems incorrect because it is well-known that the existence of a moment around the ZMP *is* allowed as long as it is has no component along the ground surface. However, the author (the inventor of the ZMP) cleverly chose to use the 'pressure under supporting foot', which, by definition, only has a component perpendicular to the ground surface. This indeed results in an appropriate reaction force at the ZMP having no moment at all. The friction forces along the ground surface, that *would* give a vertical moment around the ZMP, were simply ignored.

and (necessarily) will give the same location for the ZMP. This location is equal to the location of the Center of Pressure (CoP). A sufficient amount of papers have already been written to prove all this (Sardain and Bessonnet, 2004; Goswami, 1999)[2], so we will not repeat that.

Contrary to what is stated in many papers, *e.g.*, Vukobratović and Borovac (2004), there is no direct relation between the ZMP lying strictly within the support polygon (as opposed to lying on the edge of it) and 'falling' of the robot. Two examples suffice to show this:

1. Consider a bipedal robot standing on one leg, having unactuated ankles. This system acts like an (unstable) inverted pendulum and thus the robot falls down. However, as no torques were exerted on the foot, the foot could remain on the ground without starting to rotate, so the ZMP was always inside the support polygon.
2. Consider a bipedal robot walking exactly like a human, without falling. Just like humans do, the robot will rotate its feet about the front and rear edge while walking, so the ZMP sometimes does lie on the edge of the support polygon (not strictly within it) although the robot is not falling.

To be short, the ZMP lying strictly within the support polygon only tells us that the stance foot (or feet, if the robot is in double-support phase) will not start to rotate about one of its edges. This is neither a sufficient nor a necessary condition for walking without falling (Pratt and Tedrake, 2006). It must be said however, that having the ZMP strictly within the support polygon makes continuous pose control of the robot a lot easier[3], which is probably the reason that so many people think that it is the only solution.

4.3 Wrench — a 6D force

In this chapter we will use the widely known concept of wrenches, from geometric mechanics (Ball, 1900; Murray et al., 1994). A wrench is a 6D generalization of a force. Any combination of forces and moments can be replaced by a single force and a moment in a plane perpendicular to the force (Poinsot's theorem (Ball, 1900)) and therefore by one wrench.

We will first introduce the notion of a *screw*. A screw S consists of an (undirected) axis $(\boldsymbol{\Delta})$ in space and an associated scalar $\lambda \in \mathbb{R}$ called the *pitch* (the unit of λ is

[2] In these papers it was assumed that there are no external disturbances, but the results still hold if there are.

[3] When the foot is rotating about one of its edges, we essentially have an underactuated system, which is hard to control exactly. Luckily, for walking without falling, we believe it is not necessary to exactly control the robot's pose at all times.

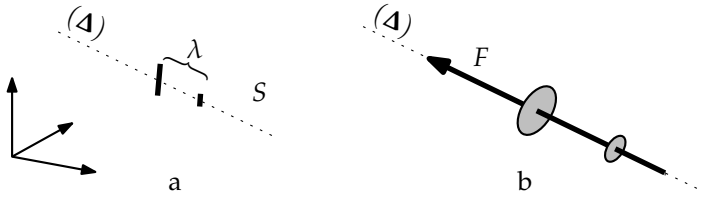

Figure 4.1: a) Graphical representation of a screw S. The pitch λ is shown with two small ticks on the axis (direction from the large to the small disk). b) Graphical representation of a wrench in a 3D space: the magnitude of force F along axis $(\boldsymbol{\Delta})$ is indicated by the length of the arrow. The magnitude of moment M along $(\boldsymbol{\Delta})$ is indicated by the distance between the two discs (direction from the large to the small disc). Note that we did not explicitly draw the pitch anymore, as drawing the magnitude of the moment directly gives the same information but in a more intuitive way.

[m]). The axis can be fully specified by the position r of some point on the axis and a (unit) direction vector ω, such that $(\boldsymbol{\Delta}) = \{r + \alpha\,\omega | \alpha \in \mathbb{R}\}$. A graphical representation of a screw is shown in figure 4.1a. Because the axis is undirected, the screw $S = (\omega, r, \lambda)$ is the same screw as $S^* = (-\omega, r, \lambda)$.

A wrench W, having *intensity* v, on a screw S (having axis $(\boldsymbol{\Delta})$ and pitch λ) can be interpreted as a combination of:

1. A (linear) force $F = v \cdot \omega$ along axis $(\boldsymbol{\Delta})$, and

2. A (rotational) moment $M = \lambda F = \lambda\, v \cdot \omega$ along axis $(\boldsymbol{\Delta})$.

The pitch λ is the ratio between amount of moment (in [Nm]) and amount of force (in [N]). In order for the wrench to be fully specified, the parameters of the screw S must be known, as well as the intensity v of the wrench. This is similar to the case of a linear force on an axis: there the parameters of the axis as well as the magnitude of the force are enough for the force to be fully specified. In order to specify the direction of the force (either towards one end of the axis or towards the other), we will use the direction of vector ω: if the force goes into the direction of ω, we will denote a positive v, otherwise a negative one.

A graphical representation of a wrench is shown in figure 4.1b. The magnitude of the force (which is equal to the intensity of the wrench) and magnitude of the moment are indicated with the lengths of the arrow and distance between the disks respectively. In order to have a meaning, 'reference lengths' must be provided, as shown in figure 4.2.

The numerical expression of the wrench depends on the choice of coordinates, thus on the chosen reference frame Ψ_{ref}. Hence, when expressing a wrench in

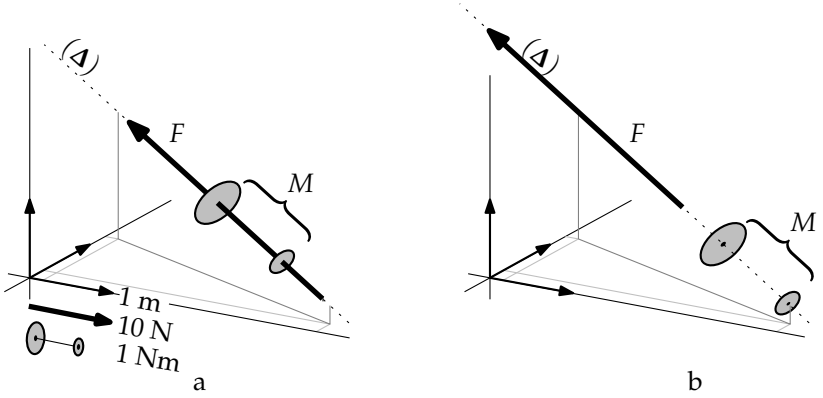

Figure 4.2: a) Introduction of reference lengths. In the lower left, a scale for meter, Newton and Newton meter are given. It can be deduced that this wrench has $|F| = 35\,\mathrm{N}$, $|M| = 2.4\,\mathrm{Nm}$ and (thus) $\lambda = -0.07\,\mathrm{m}$. The vector and discs can (independently) be freely translated along the axis without losing meaning, hence b) represents the same wrench. We will use the scaling shown in this figure for the other figures in this chapter.

numbers, the choice of coordinates *must* always be given, otherwise it is unclear what the numbers actually mean. In this chapter we use a pre-pended superscript to express the reference frame, in the following way:

${}^{a}W$: A wrench expressed in reference frame Ψ_a.

Note that it is necessary to denote the reference frame only when a wrench is expressed in numbers; not when drawing the wrench graphically (which makes drawing wrenches completely coordinate-free) or manipulating the equations.

One way to numerically represent a wrench is in so-called *Plücker coordinates* (Featherstone, 2007):

$$ {}^{\mathrm{ref}}W = \begin{pmatrix} m \\ f \end{pmatrix} = v \, (\underbrace{\begin{pmatrix} r \wedge \omega \\ \omega \end{pmatrix}}_{\text{linear force}} + \lambda \underbrace{\begin{pmatrix} \omega \\ 0 \end{pmatrix}}_{\text{moment}}), \tag{4.1} $$

where v refers to the intensity of the wrench, r is a vector from the reference frame's origin to some point on the screw axis, ω is the unit vector indicating the direction of the axis and λ is the pitch. The $\wedge$ denotes the cross product. m and f are (3×1) vectors. The coordinates $\left(\begin{smallmatrix} m \\ f \end{smallmatrix}\right)$ can be interpreted as follows: the wrench W is equal to a linear force f exerted at the origin of the reference frame, plus a moment m.

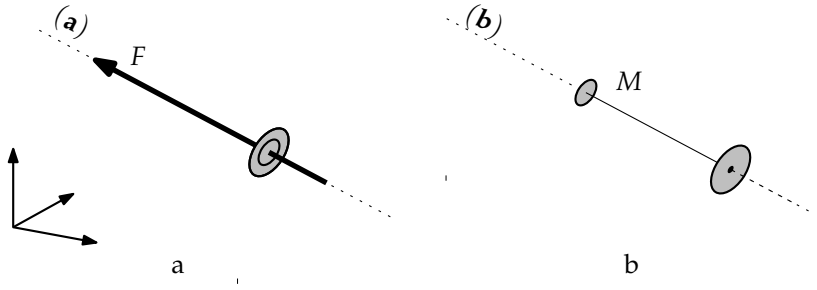

Figure 4.3: a) A wrench representation of a pure force ($\lambda = 0$). b) A wrench representation of a pure moment ($\lambda = \infty$). For reference lengths, see figure 4.2.

A pure force F along an axis $(\mathbf{a})$ can be represented by a wrench with intensity $v = |F|$ along a screw with axis $(\mathbf{a})$ and zero pitch. In Plücker coordinates this results in:

$$ {}^{\text{ref}}W^{\text{force}} = v \left(\begin{pmatrix} r \wedge \omega \\ \omega \end{pmatrix} + 0 \cdot \begin{pmatrix} \omega \\ 0 \end{pmatrix} \right) = v \begin{pmatrix} r \wedge \omega \\ \omega \end{pmatrix}. \tag{4.2} $$

So, even though this describes a pure force, the moment part in Plücker coordinates is non-zero due to the arm of the force with respect to the coordinates used. A pure moment M about an axis $(\mathbf{b})$ can be represented by a wrench with intensity $v \to 0$ along a screw with axis $(\mathbf{b})$ and infinite pitch $\lambda \to \infty$; such that the magnitude of the moment becomes a finite value: $v^* = \lambda v = |M|$. Here we introduced the *pseudo-intensity* v^* in order to circumvent problems with zero intensity. In Plücker coordinates we have:

$$ \begin{aligned} {}^{\text{ref}}W^{\text{mom}} &= \lim_{\substack{v \to 0 \\ \lambda v \to |M|}} v \left(\begin{pmatrix} r \wedge \omega \\ \omega \end{pmatrix} + \lambda \begin{pmatrix} \omega \\ 0 \end{pmatrix} \right) = \lambda v \begin{pmatrix} \omega \\ 0 \end{pmatrix} \\ &= v^* \left(\frac{1}{\lambda} \begin{pmatrix} r \wedge \omega \\ \omega \end{pmatrix} + \begin{pmatrix} \omega \\ 0 \end{pmatrix} \right) = v^* \begin{pmatrix} \omega \\ 0 \end{pmatrix}. \end{aligned} \tag{4.3} $$

From (4.3) it is clear that, indeed, a pure moment is invariant for translation of its axis: the position of the axis, indicated by r, falls out of the equation. In figure 4.3 the graphical representation of a pure force and a pure moment as wrench are shown.

The wrench is the dual of the Twist T, as generalized 6D velocity; *i.e.*, expressed in coordinates of any reference frame Ψ_a, the product $({}^aW^T \cdot {}^aT) \in \mathbb{R}$ equals the power supplied by W.

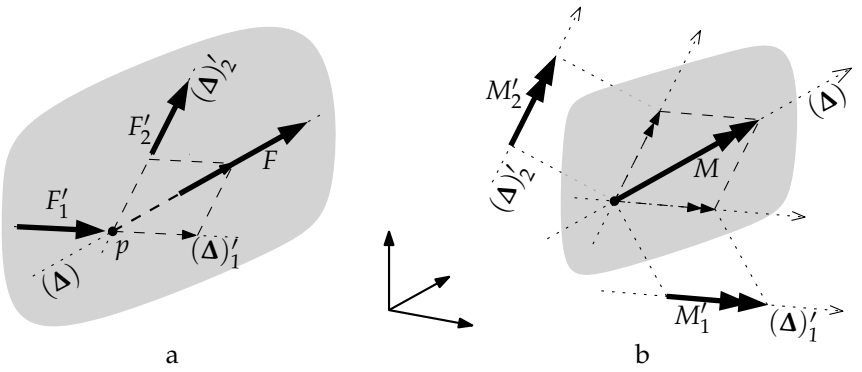

Figure 4.4: a) A linear force F, decomposed into two components F_1' and F_2'; b) A moment M, decomposed into two components M_1' and M_2'.

4.4 Decomposition of a wrench

The principle behind decomposition of wrench W is to find wrenches $W_1' \dots W_n'$ that, together, do the same work as W when applied on a moving rigid body for any motion. Mathematically this is not challenging at all, since wrenches represented in Plücker coordinates can be summed:

$$^{\text{ref}}W = \sum_i \left(^{\text{ref}}W_i' \right). \tag{4.4}$$

Geometrically however, the problem is much more interesting: given n screws $S_1' \dots S_n'$, do there exist wrench intensities $v_1' \dots v_n'$ such that the composition of the n wrenches together yields the original wrench W?

In this section, we give conditions for the decomposition of a wrench W on screw S into two components W_1', W_2' along screws S_1', S_2'. Decomposition into more than two forces is not considered because it is not needed in this chapter.

Firstly, we will review some decomposition rules for pure forces and pure moments:

DEC1 A pure force F along axis $(\boldsymbol{\Delta})$ can be decomposed into pure forces F_1' and F_2' along axes $(\boldsymbol{\Delta})_1'$ and $(\boldsymbol{\Delta})_2'$ if and only if:

1. either the axes $(\boldsymbol{\Delta})$, $(\boldsymbol{\Delta})_1'$ and $(\boldsymbol{\Delta})_2'$ intersect each other in one point p and the plane spanned by the direction vectors ω_1' and ω_2' (which must have distinct directions) contains the direction vector ω (figure 4.4a),

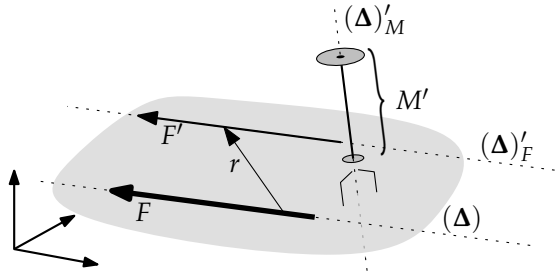

Figure 4.5: Decomposition of force F into (translated) force F' and moment M'. F and r are not necessarily perpendicular.

2. or all axes $(\boldsymbol{\Delta})$, $(\boldsymbol{\Delta})'_1$ and $(\boldsymbol{\Delta})'_2$ are parallel and lie in the same plane. This is the limit case for $p \to \infty$ of the first condition.

If $(\boldsymbol{\Delta})'_1$ and $(\boldsymbol{\Delta})'_2$ are different from each other, then the decomposition is unique, *i.e.*, there exists exactly one set of force magnitudes $\{|F'_1|, |F'_2|\}$ that yield a valid decomposition.

DEC2 A pure moment M along an axis $(\boldsymbol{\Delta})$ can be decomposed in pure moments M'_1, M'_2 along axes $(\boldsymbol{\Delta})'_1, (\boldsymbol{\Delta})'_2$ if and only if:

1. either the plane spanned by the direction vectors ω'_1 and ω'_2 (which must have distinct directions) contains the direction vector ω (see figure 4.4b),
2. or all axes $(\boldsymbol{\Delta})$, $(\boldsymbol{\Delta})'_1$ and $(\boldsymbol{\Delta})'_2$ are parallel.

In the first case, the decomposition is unique, in the second case it is not. Note that the decomposition rule for a pure force (DEC1) is a subset of the decomposition rule for a pure moment. Hence, a moment can always be decomposed along axes that fulfill the conditions for force decomposition.

DEC3 A force F along axis $(\boldsymbol{\Delta})$ can be decomposed into a force F' along axis $(\boldsymbol{\Delta})'_f$ and a moment M' about an axis $(\boldsymbol{\Delta})'_m$ if and only if $(\boldsymbol{\Delta}) \parallel (\boldsymbol{\Delta})'_f$ and $(\boldsymbol{\Delta})'_m$ is perpendicular to the plane spanned by $(\boldsymbol{\Delta})$ and $(\boldsymbol{\Delta})'_f$. Let r be a vector from some point on $(\boldsymbol{\Delta})$ to some point on $(\boldsymbol{\Delta})'_f$. Then $|F'| = |F|$ and $M' = -r \wedge F$. See figure 4.5.

For general wrenches, things are a bit more complicated: we do not only have restrictions on the axes, but also on the pitches of each screw. Firstly, we will present two trivial cases of a wrench decomposition into two components.

Theorem 1 *A wrench W on screw S can be decomposed into one wrench W'_f on screw S'_f representing a pure force ($\lambda'_f = 0$) plus one wrench W'_m on screw S'_m representing a pure moment ($\lambda'_m = \infty$), if axis $(\mathbf{\Delta})'_f$ coincides with $(\mathbf{\Delta})$ and axis $(\mathbf{\Delta})'_m$ is parallel to $(\mathbf{\Delta})$.*

Proof Assume that the conditions on axes $(\mathbf{\Delta})'_f$ (defined by ω'_f and r'_f) and $(\mathbf{\Delta})'_m$ (defined similarly) are met, *i.e.*, $\omega'_f = \pm\omega$; $r'_f = r$; $\omega'_m = \pm\omega$; $r'_m =$ arbitrary. Without loss of generality we can assume that $\omega'_f = \omega'_m = \omega$ (by changing the sign of the (pseudo-)intensities v'_f and $v^{*\prime}_m$ if necessary). By expressing the wrench in Plücker coordinates (and using (4.2) and (4.3)), we can show that indeed there exist intensities v'_f and $v^{*\prime}_m$ that give a valid decomposition $W = W'_f + W'_m$:

$$v \begin{pmatrix} r \wedge \omega \\ \omega \end{pmatrix} + \lambda v \begin{pmatrix} \omega \\ 0 \end{pmatrix} = v'_f \begin{pmatrix} r'_f \wedge \omega'_f \\ \omega'_f \end{pmatrix} + v^{*\prime}_m \begin{pmatrix} \omega'_m \\ 0 \end{pmatrix} \tag{4.5}$$

so choosing $v'_f = v$ and $v^{*\prime}_m = \lambda v$ will do. This is actually the way a wrench is built in the first place: it consists of a pure force $F = v \cdot \omega$ along axis $(\mathbf{\Delta})$ plus a pure moment $M = \lambda v \cdot \omega$ around this axis. ■

The converse of this theorem (decomposition is possible only if the screw axes satisfy the constraints) is not true. As a counter-example see DEC3, where a wrench (a pure force in this case) is decomposed into a pure force and pure moment while the screws are perpendicular instead of parallel.

Theorem 2 *A wrench W of intensity v on screw S, can be decomposed into two wrenches W'_1 and W'_2 on screws S'_1 and S'_2 if the axes $(\mathbf{\Delta})'_1$ and $(\mathbf{\Delta})'_2$ satisfy the conditions of DEC1 and the pitches satisfy $\lambda'_1 = \lambda'_2 = \lambda$.*

Proof Assume that all conditions are satisfied. Wrench W consists of a force F along $(\mathbf{\Delta})$ and a moment $M = \lambda F$ around it. According to DEC1, F can be decomposed into F'_1 and F'_2 along $(\mathbf{\Delta})'_1$ and $(\mathbf{\Delta})'_2$. The same holds for decomposition of M into $M'_1 = \lambda F'_1$ and $M'_2 = \lambda F'_2$. Now F'_1 and M'_1 can be taken together again to form wrench W'_1; similarly for W'_2. A more mathematical proof is given in the appendix. ■

The converse of this theorem is not true: there are many sets of screws $\{S'_1, S'_2\}$ along which a wrench can be decomposed that do not satisfy the above conditions.

A more general theorem can be stated, which will be useful for the determination of the ZMP later on:

Theorem 3 *A wrench W of intensity v on screw S, can be decomposed into a wrench W'_f on screw S'_f representing a pure force ($\lambda'_f = 0$) and a wrench W'_m on screw S'_m representing a pure moment ($\lambda'_m = \infty$) if and only if:*

- *axes $(\mathbf{\Delta})$ and $(\mathbf{\Delta})'_f$ are parallel (i.e., S'_f is obtained by translating S a certain distance $(r'_f - r)$), and*
- *the translation vector $(r'_f - r)$ is such that*

$$\Big(\omega \wedge (r'_f - r) + \lambda\omega\Big) \parallel \omega'_m. \tag{4.6}$$

Proof A valid decomposition can be made if and only if there exist (pseudo-) intensities v'_f and $v^{*\prime}_m$ such that $W = W'_f + W'_m$:

$$v \begin{pmatrix} r \wedge \omega \\ \omega \end{pmatrix} + v\lambda \begin{pmatrix} \omega \\ 0 \end{pmatrix} = v'_f \begin{pmatrix} r'_f \wedge \omega'_f \\ \omega'_f \end{pmatrix} + v^{*\prime}_m \begin{pmatrix} \omega'_m \\ 0 \end{pmatrix}. \tag{4.7}$$

The lower line of (4.7) implies that $v\omega = v'_f\omega'_f$, thus (because ω and ω'_f are unit vectors) $\omega'_f = \pm\omega$ and $v'_f = \pm v$. Again, without loss of generality we may assume that ω and ω'_f have the same direction (thus $v = v'_f$). The top line of (4.7) can now be written as

$$(r - r'_f) \wedge \omega + \lambda\omega = \frac{v^{*\prime}_m}{v}\,\omega'_m. \tag{4.8}$$

Indeed, a suitable $v^{*\prime}_m$ can be found if and only if the left hand side of (4.8) is parallel to ω'_m. ■

This result implies that for a given ω, ω'_m and $\lambda \neq 0$ there exists one location of screw S'_f for which a valid decomposition exists (any translation $(r - r'_f)$ which satisfies (4.8) gives the same axis location; only translated along the axis itself, for which the axis is invariant). If $\lambda = 0$ (W is a pure force), then there are two possibilities: either $\omega'_m \perp \omega$, in which case a valid decomposition exists for any translation of S perpendicular to ω'_2 (this is equivalent to DEC3), or no decomposition on S'_f and S'_m exists at all. If one would take $\omega'_m = \omega'_f = \omega$, then the system reduces to the system described in theorem 1, and indeed (4.8) only has a solution for $r'_f = r$, *i.e.*, the screws S and S'_f coincide.

4.5 Construction of the ZMP using the ground reaction wrench

If the ground reaction wrench W^{grf} is known, the Zero-Moment Point can quite easily be found geometrically. First we show how this is done; second we will

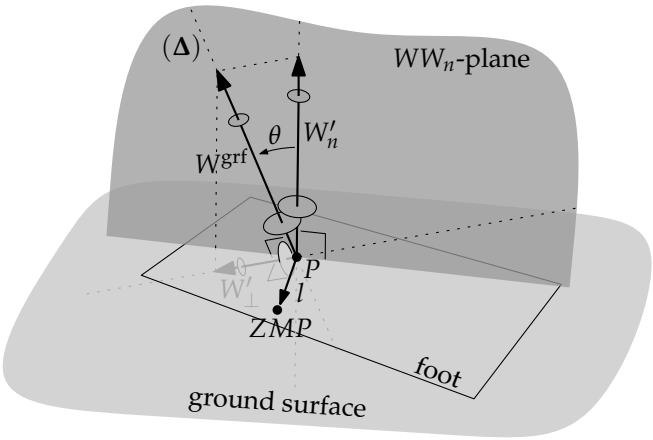

Figure 4.6: Geometric construction of the Zero-Moment Point from the ground contact wrench W^{grf}.

prove that indeed this algorithm gives us the ZMP.

1. Given the ground contact wrench W^{grf}, on screw S (defined by axis $(\boldsymbol{\Delta})$ and pitch λ), find the point P, being the intersection between $(\boldsymbol{\Delta})$ and the ground plane.
2. By using theorem 2, decompose W^{grf} (which has a force component f^{grf} and a moment component $m^{\text{grf}} = \lambda f^{\text{grf}}$) into a wrench W'_n normal to the ground surface plus a wrench $W'_\perp$ perpendicular to W^{grf}, intersecting each other in P. The force and moment components of the obtained wrenches are denoted $f'_n, f'_\perp$ and $m'_n, m'_\perp$ respectively. Note that $m'_n = \lambda f'_n$, $m'_\perp = \lambda f'_\perp$, $W'_n + W'_\perp = W^{\text{grf}}$ and thus $f'_n + f'_\perp = f^{\text{grf}}$ and $m'_n + m'_\perp = m^{\text{grf}}$.
3. Construct a vector l from P, perpendicular to the plane spanned by W^{grf} and W_n (this plane is denoted by WW_n), having magnitude $|l| = \lambda \frac{|f_\perp|}{|f^{\text{grf}}|}$ (the direction of l follows from applying the right-hand rule, going from W_n to W^{grf}).
4. Now l points to the Zero-Moment Point.

The whole procedure is also sketched in figure 4.6.

Proof The proof shows that the ground reaction wrench is equivalent to a pure force $\bar{f}$ acting on the ZMP plus a moment $\bar{m}_n$ that is perpendicular to the ground surface. We introduce a reference frame Ψ_0 somewhere in space with an arbitrary

orientation, a vector p pointing from its origin to point P and a vector $z = p + l$ pointing from its origin to the supposed position of the ZMP. $\bar{f}$ and $\bar{m}_n$ can be written as a wrench as $W^{\bar{f}} = \begin{pmatrix} z \wedge \bar{f} \\ \bar{f} \end{pmatrix}$ and $W^{\bar{m}_n} = \begin{pmatrix} \bar{m}_n \\ 0 \end{pmatrix}$ respectively.

Assume that indeed l points to the ZMP, then the above defined $\bar{f}$ and $\bar{m}_n$ should exist such that

$$\begin{gathered} W^{\text{grf}} = W^{\bar{f}} + W^{\bar{m}_n} \\ \begin{pmatrix} p \wedge f^{\text{grf}} \\ f^{\text{grf}} \end{pmatrix} + \lambda \begin{pmatrix} f^{\text{grf}} \\ 0 \end{pmatrix} = \begin{pmatrix} z \wedge \bar{f} \\ \bar{f} \end{pmatrix} + \begin{pmatrix} \bar{m}_n \\ 0 \end{pmatrix}. \end{gathered} \tag{4.9}$$

From this, it follows directly that $\bar{f} = f^{\text{grf}}$. Because $z = p + l$, we can write the top row of (4.9) as $p \wedge f^{\text{grf}} + \lambda f^{\text{grf}} = p \wedge \bar{f} + l \wedge \bar{f} + \bar{m}_n$ which can be simplified to ($\bar{f} = f^{\text{grf}}$)

$$\lambda f^{\text{grf}} = l \wedge f^{\text{grf}} + \bar{m}_n. \tag{4.10}$$

It can be shown that $l \wedge f^{\text{grf}} = m'_\perp$ by proving the following (sufficient) conditions:

1. $m'_\perp \perp l$ — l is perpendicular to W^{grf} and W'_n and, consequently, to any vector in the plane spanned by them. Now $W'_\perp$ is in this plane, and thus so is $m'_\perp$ (which has the same direction as $W'_\perp$).
2. $m'_\perp \perp f^{\text{grf}}$ — $W'_\perp$ was constructed perpendicularly to W^{grf}. By construction $m'_\perp \parallel W'_\perp$ and $f^{\text{grf}} \parallel W^{\text{grf}}$. Therefore we have indeed $m'_\perp \perp f^{\text{grf}}$.
3. $|l \wedge f^{\text{grf}}| = |m'_\perp|$ — because $l \perp f^{\text{grf}}$, we have $|l \wedge f^{\text{grf}}| = |l| \cdot |f^{\text{grf}}| = \lambda \frac{|f'_\perp|}{|f^{\text{grf}}|} \cdot |f^{\text{grf}}| = |\lambda f'_\perp| = |m'_\perp|$.
4. $l \wedge f^{\text{grf}} = m'_\perp$ follows the right-hand rule — by inspection of figure 4.6.

By using $l \wedge f^{\text{grf}} = m'_\perp$ and the identities of step 2 of the ZMP construction algorithm, (4.10) can be rewritten as

$$\lambda f^{\text{grf}} = m^{\text{grf}} = m'_\perp + m'_n = m'_\perp + \bar{m}_n \tag{4.11}$$

so we can conclude that indeed there exists an $\bar{f} = f^{\text{grf}}$ and $\bar{m}_n = m'_n$ (which is perpendicular to the ground surface) that satisfy (4.9), so indeed l points to the Zero-Moment Point. ■

Remark 1 *Both step 1 and 2 of the algorithm are only possible if* ($\boldsymbol{\Delta}$) *is not parallel to the ground plane. This is logical because if* ($\boldsymbol{\Delta}$) *were parallel to the ground plane, the ground does not exert a normal force; i.e., the ground does not support the foot and in that case the* ZMP *does not exist.*

Remark 2 *If $(\boldsymbol{\Delta})$ is almost vertical, i.e., the friction forces are much smaller than the normal force, we can approximate the magnitude $|l|$ as follows: let θ be the angle between f'_n and f^{grf} (see figure 4.6); then $\frac{|f'_\perp|}{|f^{\text{grf}}|} = \tan\theta \approx \theta \Rightarrow |l| \approx \lambda\theta$.*

Remark 3 *As l is perpendicular to W'_n (and thus to the ground's normal), it it automatically parallel to the ground surface. Therefore, l points to a point belonging to the ground surface; which is in agreement with the commonly-known fact that the* ZMP *is a point on the ground surface.*

Remark 4 *We never stated that the ground should be horizontal. In fact, we did not even draw the reference from which a 'world's horizontal plane' could be deduced. This method works for any orientation of the ground plane (and the orientation does not need to be known either). Of course, in order for the* ZMP *to make sense, the foot must make full contact with the ground surface and therefore the ground surface under the foot should be flat. It is however no problem to have different (possibly discontinuous) parts of flat ground where the robot steps on.*

Remark 5 *From a decomposition point of view, the algorithm can be interpreted as follows. The ground reaction wrench consists of a force f^{grf} and a moment m^{grf} along the same axis $(\boldsymbol{\Delta})$. In order to find the* ZMP*, we want to find a decomposition in a purely vertical moment and a pure force. The moment m^{grf} can be seen as the composition of a 'wanted' vertical component m'_n and an 'unwanted' remainder $m'_\perp$. In order to cancel the latter, we can translate f^{grf} (according to theorem 3) along l, which introduces a canceling moment $-m'_\perp$. The result is a translated version of f^{grf} and the sum of all moments $m'_n + m'_\perp + (-m'_\perp) = m'_n$. The intersection of the translated f^{grf} and the ground plane is the* ZMP*.*

4.6 Explicit expression for the ZMP position, given the ground reaction wrench

4.6.1 Expression for the ZMP

The purpose of this section is to show that, when the ground reaction force/moment is known as a wrench, the expression for the ZMP is simple. Of course, these equations give the same results as any ZMP other equation. Hence the expression presented here is most useful if the ground reaction force/moment is already available as a wrench (otherwise other ZMP equations are usually more direct and thus faster).

Consider an arbitrary walking robot in single support phase and a reference frame Ψ_0 attached to the ground surface, such that the frame's XY-plane coincides with the ground surface and the frame's z-axis points out of the ground (note that we do not require the ground surface to be horizontal). Let the ground reaction wrench ${}^0W^{\text{grf}}$ be known (see section 4.6.2), expressed in frame Ψ_0. By using (4.9), we can find an explicit expression for the position of the ZMP, as shown below. The ground reaction wrench can be written as (where we use $f = f^{\text{grf}}$ and $m = m^{\text{grf}}$)

$$ {}^0W^{\text{grf}} = \begin{pmatrix} {}^0m \\ {}^0f \end{pmatrix} = \begin{pmatrix} {}^0z \wedge {}^0\bar{f} \\ {}^0\bar{f} \end{pmatrix} + \begin{pmatrix} {}^0\bar{m}_n \\ 0 \end{pmatrix} \tag{4.12} $$

where ${}^0z$ (the position of the ZMP expressed in coordinates of Ψ_0) is the unknown. By using ${}^0\bar{f} = {}^0f$, ${}^0z \wedge {}^0\bar{f} = -{}^0\bar{f} \wedge {}^0z$ and expanding the cross product, we obtain for the top row of (4.12)

$$ \begin{pmatrix} {}^0m_x \\ {}^0m_y \\ {}^0m_z \end{pmatrix} = \begin{pmatrix} 0 & {}^0f_z & -{}^0f_y \\ -{}^0f_z & 0 & {}^0f_x \\ {}^0f_y & -{}^0f_x & 0 \end{pmatrix} \begin{pmatrix} {}^0z_x \\ {}^0z_y \\ {}^0z_z \end{pmatrix} + \begin{pmatrix} {}^0\bar{m}_{nx} \\ {}^0\bar{m}_{ny} \\ {}^0\bar{m}_{nz} \end{pmatrix}. \tag{4.13} $$

The chosen position and orientation of Ψ_0 implies that the coordinates of the ZMP, ${}^0z$, and the normal moment, ${}^0\bar{m}_n$, satisfy

$$ {}^0z = \begin{pmatrix} {}^0z_x \\ {}^0z_y \\ {}^0z_z \end{pmatrix} = \begin{pmatrix} \bullet \\ \bullet \\ 0 \end{pmatrix}; {}^0\bar{m}_n = \begin{pmatrix} {}^0\bar{m}_{nx} \\ {}^0\bar{m}_{ny} \\ {}^0\bar{m}_{nz} \end{pmatrix} = \begin{pmatrix} 0 \\ 0 \\ \bullet \end{pmatrix}. \tag{4.14} $$

By rewriting the first two rows of (4.13) and substituting the results from (4.14), we obtain the explicit equation for the position of the ZMP expressed in coordinates of frame Ψ_0:

$$ {}^0z = \begin{pmatrix} {}^0z_x \\ {}^0z_y \\ {}^0z_z \end{pmatrix} = \begin{pmatrix} -{}^0m_y / {}^0f_z \\ {}^0m_x / {}^0f_z \\ 0 \end{pmatrix}. \tag{4.15} $$

4.6.2 Obtaining the ground reaction wrench

In a robot, the ground reaction wrench should be measured in some way. An easy way to do this is by utilizing a 6D force sensor. By placing the reference frame Ψ_0 in the origin of the sensor, oriented such that the XY-plane is aligned to the sole of the foot, the forces and moments $f_x, f_y, f_z, m_x, m_y, m_z$ are directly the elements of ${}^0W^{\text{grf}}$. The fact that the reference frame may move relatively to the fixed world does not invalidate the results.

In simulation, the ground reaction wrench is usually already available in some form because it is needed anyway for simulating the foot-ground interaction.

4.7 Conclusions

In this chapter we have shown that the concept of screws and wrenches gives us tools to geometrically establish the relation between the ground reaction wrench and the Zero-Moment Point. In order to arrive at this, we showed how a wrench can be decomposed into separate components. The proposed method gives a general, completely coordinate-free way to find the ZMP. The power of coordinate-free analysis is broadly and recognized to prevent any kind of implicit (and possibly wrong) assumptions in the analysis. The method contributes to a better insight in the problem and gives support for graphical animation of locomotion.

4.A A more mathematical proof of theorem 2

Proof The screws S, S'_1 and S'_2 can be represented by axis locations r, r'_1 and r'_2, axis directions ω, ω'_1 and ω'_2 and common pitch $\lambda = \lambda'_1 = \lambda'_2$.

First condition — Without loss of generality we can assume that the location vectors point to the intersection point and thus $r = r'_1 = r'_2$. The condition that ω'_1 and ω'_2 span a plane which contains ω implies that there exist an α and β such that $\omega = \alpha\omega'_1 + \beta\omega'_2$. Now by choosing intensities $v'_1 = v\alpha$ and $v'_2 = v\beta$, we can write

$$\begin{aligned} W'_1 + W'_2 &= v'_1\left(\begin{pmatrix} r'_1 \wedge \omega'_1 \\ \omega'_1 \end{pmatrix} + \lambda'_1 \begin{pmatrix} \omega'_1 \\ 0 \end{pmatrix}\right) + v'_2\left(\begin{pmatrix} r'_2 \wedge \omega'_2 \\ \omega'_2 \end{pmatrix} + \lambda'_2 \begin{pmatrix} \omega'_2 \\ 0 \end{pmatrix}\right) \\ &= \begin{pmatrix} r \wedge (v'_1\omega'_1 + v'_2\omega'_2) \\ v'_1\omega'_1 + v'_2\omega'_2 \end{pmatrix} + \lambda \begin{pmatrix} v'_1\omega'_1 + v'_2\omega'_2 \\ 0 \end{pmatrix} \\ &= v\left(\begin{pmatrix} r \wedge \omega \\ \omega \end{pmatrix} + \lambda \begin{pmatrix} \omega \\ 0 \end{pmatrix}\right) \\ &= W \end{aligned} \tag{4.16}$$

which shows that indeed there exists a decomposition.

Second condition — All axes are parallel, thus $\omega = \omega'_1 = \omega'_2$. Without loss of generality we can assume that r, r'_1 and r'_2 lie on one line, thus there exists an α such that $r = \alpha\, r'_1 + (1 - \alpha)r'_2$. Now by choosing $v'_1 = v\alpha, v'_2 = v(1 - \alpha)$, we can

write

$$\begin{aligned} W_1' + W_2' &= v_1'\left(\begin{pmatrix} r_1' \wedge \omega_1' \\ \omega_1' \end{pmatrix} + \lambda_1' \begin{pmatrix} \omega_1' \\ 0 \end{pmatrix}\right) + v_2'\left(\begin{pmatrix} r_2' \wedge \omega_2' \\ \omega_2' \end{pmatrix} + \lambda_2' \begin{pmatrix} \omega_2' \\ 0 \end{pmatrix}\right) \\ &= \begin{pmatrix} (v_1' r_1' + v_2' r_2') \wedge \omega \\ (v_1' + v_2')\,\omega \end{pmatrix} + (v_1' + v_2')\,\lambda \begin{pmatrix} \omega \\ 0 \end{pmatrix} \\ &= v\left(\begin{pmatrix} r \wedge \omega \\ \omega \end{pmatrix} + \lambda \begin{pmatrix} \omega \\ 0 \end{pmatrix}\right) \\ &= W \end{aligned} \tag{4.17}$$

which shows that indeed there exists a decomposition. ■

Chapter 5

Compact analysis of 3D bipedal gait using geometric dynamics of simplified models

This chapter is based on the following article (Stramigioli et al., 2009):

Compact analysis of 3D bipedal gait using geometric dynamics of simplified models
Stefano Stramigioli, Vincent Duindam, Gijs van Oort and Ambarish Goswami
Proc., IEEE International Conference on Robotics and Automation (ICRA'09)
pages 1978–1984, May 2009.

Abstract—**The large number of degrees of freedom in legged robots give rise to complicated dynamics equations. Analyzing these equations or using them for control can therefore be a difficult and non-intuitive task. A simplification of the complex multi-body dynamics can be achieved by instantaneously reducing it to an equivalent single inertial entity called the *locked inertia*.**

In this chapter, we adopt the methods of geometric dynamics to analyze the gait using the locked inertia of the robot. The analysis includes the rolling of a biped on a 3D rigid foot and 3D impacts. An example of numerical optimization of foot shape parameters is shown.

Our long-term objective is to develop the theoretical framework and to provide the necessary tools for systematic analysis, design, and control of efficient biped robots.

5.1 Introduction

The fundamental nature of locomotion has been compactly captured as "a question of relating internal shape changes to net changes in position via a coupling mechanism, most often either through interaction with the environment or via some type of conservation law" (Marsden and Ostrowski, 1998). The use of geometric tools has been found to be very useful in generating insights into the complex dynamics of locomotion systems. Geometric dynamics is a coordinate-neutral framework which yields results only pertaining to the physics of the system.

The utility of reduced models that capture the essentials of gait dynamics is widely acknowledged. Simple biped models such as the different variations of the inverted pendulum models have been proven immensely beneficial for the study of gait and balance both for humans (Inman et al., 1981; Alexander, 1984, 1990; McMahon, 1984) and humanoid robots (Kajita and Tani, 1991; Kajita et al., 2002; Sugihara and Nakamura, 2003; Komura et al., 2005).

Reduced humanoid models allow one to ignore the non-central aspects of dynamics and to express the complex gait dynamics in a minimalist way. While at the final implementation stage one still needs to formulate control laws for the entire system, it is at the analysis and planning stage where such reduced models demonstrate their value. These models not only enhance our understanding of bipedal locomotion, but open the way to new classes of control laws, which would otherwise be difficult or impossible to conceive.

Many studies have been performed for 2D passive dynamic walkers, starting with the ground-breaking work of McGeer (1990b), and later on with various systematic approaches, *e.g.*, based on Poincaré mappings (Goswami et al., 1998; Garcia et al., 1998) and passivity (Spong and Bullo, 2005; Duindam and Stramigioli, 2005). Several successful three-dimensional walking robots have been built as well (Wisse and Schwab, 2001; Wisse, 2004; Collins et al., 2001), but most of these results were achieved relying more in engineering insight and smart designs rather than systematic analytical methods. The main difficulty when trying to use analytic methods for 3D robots is the sheer complexity of the mechanisms and their interaction with the 3D world.

Our present approach to tackling the complexity of 3D walking robots relies on the very useful concept of *locked inertia* (Marsden and Ostrowski, 1998), more commonly known in robotics as the *composite rigid body inertia* (Walker and Orin, 1982). The locked inertia of a humanoid robot is its instantaneous generalized inertia, assuming that all of its joints are frozen. It has the same structure as the generalized inertia of a single rigid body. We have recently shown (Lee and Goswami, 2007) how using this concept an entire humanoid can be mapped into

the much simpler entity called the Reaction Mass Pendulum (RMP). In this chapter the instantaneous locked inertia is used to model and to analyze the 3D gaits of humanoid robots including continuous dynamics, foot-ground impacts, and natural rolling motion of curved feet on a support surface.

This chapter is structured as follows: section 5.2 presents a general form of the dynamic equations of a walking robot and defines its locked inertia. Section 5.3 introduces a geometric description of 3D impacts. Section 5.4 presents the main contribution of this chapter. It shows how the previous concepts can be used to analyze and possibly to design the different phases of 3D gait of bipedal robots with curved feet. In section 5.5 we present in a simulation example the optimization of foot shape parameters, using the theory of section 5.4.

5.2 Dynamics of a Humanoid

A rigid body is characterized by its *inertia tensor*, which is a second order covariant positive definite tensor. This tensor has a constant numerical representation in any coordinate frame Ψ_b rigidly connected to the body (often called a body-fixed frame). Furthermore, if the frame is chosen with the origin at the center of mass and with the axes oriented along the principal axes of inertia, the matrix representation of this tensor becomes a 6×6 diagonal matrix of the form:

$$ {}^b\mathcal{I}_i = \begin{pmatrix} J & 0 \\ 0 & mI_3 \end{pmatrix} \tag{5.1} $$

where ${}^b\mathcal{I}_i$ denotes the inertia tensor of body i expressed in frame Ψ_b, m is the mass of the body, and the elements of

$$ J := \begin{pmatrix} J_x & 0 & 0 \\ 0 & J_y & 0 \\ 0 & 0 & J_z \end{pmatrix} $$

describe the magnitudes of moments of inertia around the three coordinate axes. If only the rotational dynamics are of interest, usually just the 3×3 tensor J is considered.

Consider now a floating mechanism composed of multiple rigid bodies, for example, a humanoid robot floating in space, as shown in figure 5.1. Let us index the bodies $i \in \{1, \ldots, n\}$, rigidly attach a frame Ψ_i to each body i, and align the frame axes with the principal inertia axes. ${}^i\mathcal{I}_i$ is the (constant) inertia of body i expressed in Ψ_i. In addition, let Ψ_0 denote an inertial (world) frame.

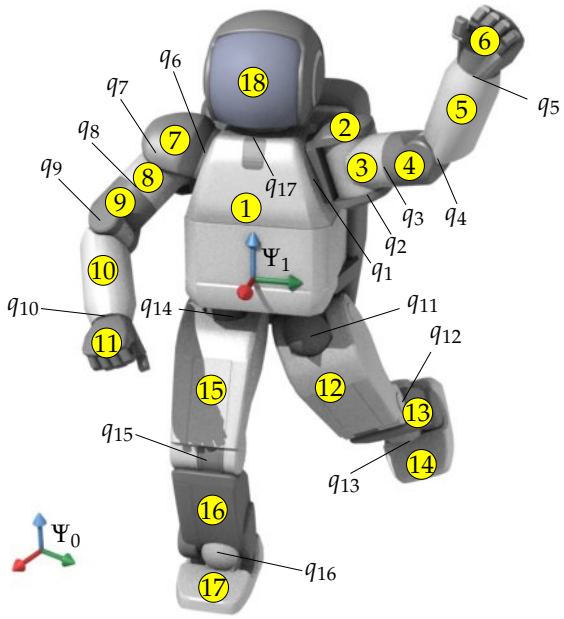

Figure 5.1: Setup and labeling of the n bodies and $n-1$ joints q_i in a general free-floating humanoid mechanism. Frame Ψ_0 is the inertial frame, Ψ_1 is attached to the torso, serving as a (non-inertial) reference frame.

5.2.1 Locked Inertia

If we lock all joints of this mechanism, we can calculate the total inertia of the entire mechanism in a static configuration just by summing the inertia tensors of the composing rigid bodies (since inertia is additive); this is the locked inertia of the mechanism. Expressing the locked inertia ${}^j\mathcal{I}_{\text{tot}}$ in some arbitrary coordinate frame Ψ_j, we can write

$$ {}^j\mathcal{I}_{\text{tot}} = \sum_{i=1}^{n} {}^j\mathcal{I}_i = \sum_{i=1}^{n} \text{Ad}_{H_i^j}^T \, {}^i\mathcal{I}_i \, \text{Ad}_{H_i^j} \tag{5.2} $$

where $\text{Ad}_{H_i^j}$ is the adjoint of the homogeneous transformation H_i^j from frame Ψ_i to frame Ψ_j (Murray et al., 1994; Stramigioli, 2001). Similar to that of a single rigid body, the locked inertia also possesses principal axes, and for a proper choice of coordinate frames, can be expressed in the simple form of (5.1). Therefore, once the joints are physically locked, the floating mechanism will obey the dynamics of a single rigid body with inertia ${}^j\mathcal{I}_{\text{tot}}$.

5.2.2 Dynamic Equations of a General Mechanism

Suppose that we have a general humanoid mechanism composed of an interconnection of rigid bodies. If we take one of the rigid bodies (typically a foot or the torso) as a reference with frame Ψ_1 (the base frame), the internal configuration or 'shape' of the humanoid is completely defined by a set of joint coordinates q. The total configuration of the robot is thus given by the configuration $H_1^0 \in \mathrm{SE}(3)$ of the reference frame plus the internal joint angles $q \in \mathbb{R}^n$. Similarly, a certain kinematic state of the system can be characterized by the twist ${}^1T_1^0 \in \mathrm{se}(3)$ of the reference body plus the joint velocities $\dot{q} \in \mathbb{R}^n$, where ${}^cT_a^b \in \mathrm{se}(3) \sim \mathbb{R}^6$ denotes the twist of body a with respect to body b expressed in coordinate frame Ψ_c. The reference body twist and the joint velocities can be combined in a vector of the form

$$\bar{T} := \begin{pmatrix} {}^1T_1^0 \\ \dot{q} \end{pmatrix}. \tag{5.3}$$

For each body i we can write its twist as

$${}^iT_i^0 = {}^iT_1^0 + {}^iT_i^1 = \mathrm{Ad}_{H_1^i(q)} \left({}^1T_1^0 + J_i(q)\dot{q} \right) \tag{5.4}$$

with $J_i(q)$ the geometric Jacobian mapping the internal shape speed to the twist of body i with respect to the reference body 1 expressed in frame Ψ_1. In particular, $J_1(q) \equiv 0$ by construction. Using these coordinates, we can write an expression for the kinetic co-energy as

$$E^*({}^1T_1^0, q, \dot{q}) = \frac{1}{2}\bar{T}^T M(q) \bar{T} \tag{5.5}$$

where the mass matrix $M(q)$, which is independent of H_1^0, has the following structure:

$$M(q) := \begin{pmatrix} \sum \mathrm{Ad}_{H_1^i}^T \, {}^i\mathcal{I}_i \, \mathrm{Ad}_{H_1^i} & \sum \mathrm{Ad}_{H_1^i}^T \, {}^i\mathcal{I}_i \, \mathrm{Ad}_{H_1^i} \, J_i \\ \sum J_i^T \, \mathrm{Ad}_{H_1^i}^T \, {}^i\mathcal{I}_i \, \mathrm{Ad}_{H_1^i} & \sum J_i^T \, \mathrm{Ad}_{H_1^i}^T \, {}^i\mathcal{I}_i \, \mathrm{Ad}_{H_1^i} \, J_i \end{pmatrix}. \tag{5.6}$$

The top-left 6×6 sub-matrix is seen to be exactly the locked inertia of (5.2) expressed in Ψ_1. Using the Boltzmann-Hamel equations we can then obtain the dynamics equations of the mechanism (see (Duindam and Stramigioli, 2008) for the details):

$${}^1\dot{P} = \mathrm{ad}_{({}^1T_1^0)}^T \, {}^1P + \sum_{i=1}^{n} {}^iW_i \tag{5.7}$$

$$\dot{p} = \gamma(q, \dot{q}, {}^1T_1^0) + \tau + \sum_{i=1}^{n} J_i^T \, {}^iW_i \tag{5.8}$$

where ${}^jW_i$ indicates the total external wrench applied to body i expressed in frame Ψ_j, τ_i indicates the torque applied at joint i, ${}^iP$ indicates the total momentum screw expressed in frame i, and γ is a vector of all Coriolis, centrifugal, and other nonlinear internal forces. p is the $n \times 1$ vector of generalized momentum coordinates such that

$$\bar{P} := \begin{pmatrix} {}^1P \\ p \end{pmatrix} = M\bar{T}. \tag{5.9}$$

For a free-floating humanoid with locked joints, the dynamics of (5.7) are equivalent to the dynamics of a single rigid body with inertia equal to the locked inertia, and (5.8) becomes void. Thus, the structure of the presented equations clearly separates the internal (5.8) from the external dynamics (5.7).

5.3 Impacts

When a foot of the robot touches the ground, an impact occurs. This is characterized by certain velocities, *i.e.*, the linear velocities of the impact point, instantaneously reducing to zero. In this section we first derive a projection matrix relating the pre-impact momentum to the post-impact momentum. Then, we show that also during impact, a locked multi-body chain behaves as a single rigid body.

5.3.1 Single Impacts on a Rigid Mechanism

Since the complete kinematic state of the robot is described using $\bar{T}$, the velocity $\dot{s}$ of any point on any of the bodies in the mechanism can be expressed as

$$\dot{s} = A(q)\,\bar{T} \tag{5.10}$$

where we can assume $A(q)$ a full row rank matrix. By construction, we will have for the velocity just after impact $\dot{s}_+ = 0$, and in general the velocity just before impact $\dot{s}_- \neq 0$. The dual impulsive force on the mechanism will be of the form

$$\begin{pmatrix} W \\ \tau \end{pmatrix} = A^T(q)\,\lambda\,\delta(t) \tag{5.11}$$

where λ is the magnitude of the impulsive force and $\delta(t)$ indicates a Dirac pulse at $t = 0$, which, without loss of generality, we assume to be the time of impact. The impulsive force of (5.11) applied to the dynamics of (5.7) and (5.8) can be written as

$$\bar{P}_+ - \bar{P}_- = A^T(q)\lambda. \tag{5.12}$$

Where subscript $-$ denotes the time just before impact, and subscript $+$ the time just after impact. Pre-multiplying by M^{-1} as defined in (5.6) we get

$$\bar{T}_+ - \bar{T}_- = M^{-1}A^T\lambda \tag{5.13}$$

which, pre-multiplied by A and using $\dot{s}_+ = 0$, gives

$$-A\bar{T}_- = AM^{-1}A^T\lambda \tag{5.14}$$

and finally, since M is positive definite and A has full row rank, we obtain an expression for λ as

$$\lambda = -(AM^{-1}A^T)^{-1}AM^{-1}\bar{P}_- \tag{5.15}$$

which can be substituted into (5.12) to obtain the total momentum projection operation

$$\bar{P}_+ = \mathbb{P}(q)\bar{P}_- \tag{5.16}$$

with projection matrix $\mathbb{P}(q)$ equal to

$$\mathbb{P}(q) := I - A^T(AM^{-1}A^T)^{-1}AM^{-1}. \tag{5.17}$$

This is a projection matrix acting on the momentum vector, but we can directly define the following projection $\mathbb{P}_T(q)$ acting on the velocity vector $\bar{T} = M^{-1}\bar{P}$, being

$$\mathbb{P}_T(q) := I - M^{-1}A^T(AM^{-1}A^T)^{-1}A \tag{5.18}$$

such that $\bar{T}_+ = \mathbb{P}_T(q)\bar{T}_-$.

5.3.2 Impacts in a Locked Mechanism

When the mechanism is locked and there is an external impact, intuitively it should behave like the single equivalent rigid body with inertia equal to the locked inertia. To prove this, we can write the impact constraints and equations of (5.10) as a set of two impact constraints: one is the impact from the ground forces, and one is the impulsive joint torques required to keep the joint velocities to zero:

$$\begin{pmatrix} \dot{s} \\ \dot{q} \end{pmatrix} = \begin{pmatrix} A_1(q) \\ A_2(q) \end{pmatrix} \bar{T} = \begin{pmatrix} A_{11}(q) & A_{12}(q) \\ 0 & I \end{pmatrix} \begin{pmatrix} {}^1T_1^0 \\ \dot{q} \end{pmatrix}. \tag{5.19}$$

Following the same derivations as before, we obtain an equation like (5.13), being

$$\bar{T}_+ - \bar{T}_- = M^{-1} \begin{pmatrix} A_{11}^T & 0 \\ A_{12}^T & I \end{pmatrix} \begin{pmatrix} \lambda_c \\ \lambda_i \end{pmatrix} \tag{5.20}$$

with subscript c for contact and i for internal. We first express the required internal locking torques λ_i as a function of λ_c, and then compute the external impact forces λ_c. Starting with the second constraint (internal locking), we pre-multiply (5.20) by A_2 and using the assumption that $\dot{q}_- = 0$ (the mechanism is locked before ground impact) to write

$$0 = -\dot{q}_- = \begin{pmatrix} 0 & I \end{pmatrix} M^{-1} \begin{pmatrix} A_{11}^T & 0 \\ A_{12}^T & I \end{pmatrix} \begin{pmatrix} \lambda_c \\ \lambda_i \end{pmatrix}. \tag{5.21}$$

If we structure the mass matrix of (5.6) as

$$M = \begin{pmatrix} F & G \\ G^T & H \end{pmatrix} \tag{5.22}$$

with F the locked inertia, and use the linear systems theory of block matrix inverses and Schur Complements (Strang, 1988), we can write the inverse of the mass matrix as

$$M^{-1} = \begin{pmatrix} F^{-1} + F^{-1} G S_F^{-1} G^T F^{-1} & -F^{-1} G S_F^{-1} \\ -S_F^{-1} G^T F^{-1} & S_F^{-1} \end{pmatrix} \tag{5.23}$$

with S_F the Schur complement of F. Substituting this into the right-hand side of (5.21), we obtain the relation between λ_c and λ_i as

$$0 = (-S_F^{-1} G^T F^{-1} A_{11}^T + S_F^{-1} A_{12}^T)\, \lambda_c + S_F^{-1} \lambda_i. \tag{5.24}$$

Continuing now with the first constraint, and again using the assumption that $\dot{q}_- = 0$, we pre-multiply (5.20) by $\begin{pmatrix} A_{11} & 0 \end{pmatrix}$ to find

$$-A_{11} ({}^1T_1^0)_- = \begin{pmatrix} A_{11} & 0 \end{pmatrix} M^{-1} \begin{pmatrix} A_{11}^T & 0 \\ A_{12}^T & I \end{pmatrix} \begin{pmatrix} \lambda_c \\ \lambda_i \end{pmatrix}. \tag{5.25}$$

Substituting M^{-1} from (5.23) and expressing λ_i as a function of λ_c using (5.21), we obtain

$$-A_{11} ({}^1T_1^0)_- = A_{11} F^{-1} A_{11} \lambda_c \tag{5.26}$$

which shows that, indeed, if the shape velocity $\dot{q}_-$ before impact equals zero and the mechanism is locked (through the impulsive joint torque λ_i), then the effect

of a ground impact with magnitude λ_c is just (5.15) with $A \to A_{11}$ and $M \to F = {}^1\mathcal{I}_{\text{tot}}$ (the locked inertia). It follows directly that the projection matrix (5.17) is

$$\mathbb{P}(q) = I - A_{11}^T \left(A_{11} ({}^1\mathcal{I}_{\text{tot}})^{-1} A_{11}^T \right)^{-1} A_{11} ({}^1\mathcal{I}_{\text{tot}})^{-1}. \tag{5.27}$$

5.4 Analysis of 3D Walking Cycles

We now have all the necessary ingredients to analyze and describe the kinematics and dynamics of 3D walking gaits of (simplified) bipedal robots with curved feet. This section presents equations and relations that apply to the various phases of locomotion. These relations can be used for straightforward simulation of a particular robot, but the ultimate goal is to apply them for optimal *design* of bipeds with specific desired gait properties.

In what follows we make the following assumptions

1. The double stance phase is instantaneous,
2. All internal joints are locked during impact,
3. The feet are perfectly rigid with convex, curved shape,
4. The stance foot rolls over the ground without slipping,
5. The inertial effect of the swing leg is either negligible or is compensated by proper motion of the torso or arms.

We are aware of the fact that some of these assumptions will not hold in general. Finding ways in which these assumptions (espcecially 1 and 5) can be relaxed without falling back to the original, complex full dynamics equations is future work.

In the next subsection we discuss high-level kinematic properties of 3D gaits. After that, kinematics and dynamics of the rolling stance phase are discussed.

5.4.1 High-level Kinematic Description of 3D Gait

The first aspects of a 3D walking cycle are the high-level kinematic properties. Concepts like walking direction, step length, and foot rolling direction are trivial in 2D walking and reasonably intuitive in 3D, but it is useful to describe the relation of these quantities to kinematic states of the robot, rather than implicitly through definition of a coordinate system with axes aligned in a specific way.

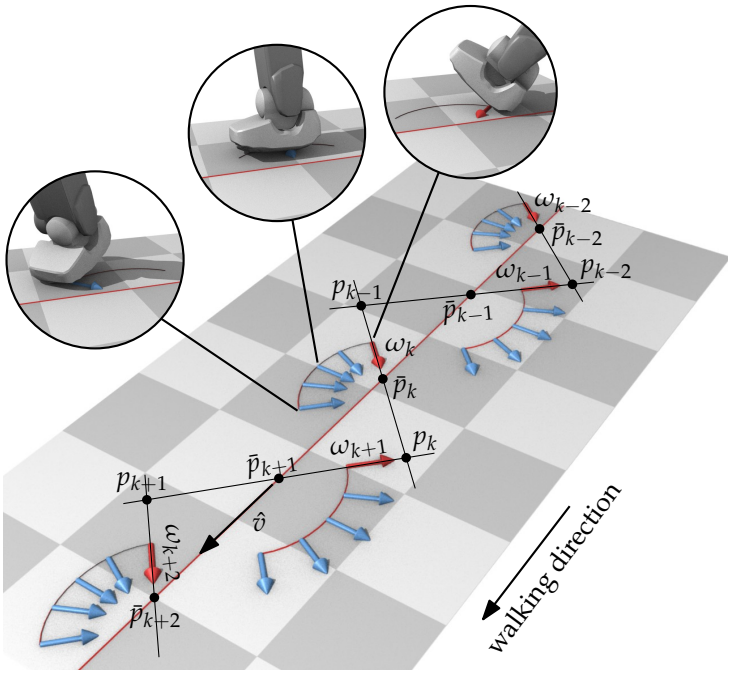

Figure 5.2: Geometric description of a symmetric walking gait. The stance foot rolls along a moving axis ω, with stride length described by the points $\bar{p}$, and $\hat{v}$ the direction of forward walking.

The momentum ${}^1P_+$ of a locked biped just after impact can be calculated using (5.27) and corresponds to a twist

$$\left({}^1T_1^0\right)_+ = ({}^1\mathcal{I}_{\text{tot}})^{-1}\,{}^1P_+. \tag{5.28}$$

Under assumptions 2–4, the motion of the locked biped right after impact will be a rolling motion on the stance foot, following a trajectory that depends on the shape of the foot and $\left({}^1T_1^0\right)_+$. The rolling motions corresponding to several steps in a symmetric gait are illustrated in figure 5.2. The k-th impact in the figure corresponds to an impact of the right foot, and the figure shows the moving axis ω_k around which the rolling motion occurs. For a slip-less pure rolling contact, the axis ω_k must be in the ground plane, orthogonal to the trajectory of the contact point of the foot with the ground.

For a (desirable) symmetric gait, there exists a a relation between consecutive steps in the walking cycle (and hence between consecutive rolling axes ω) and the global walking direction. If we denote by $\mathbf{e}_z$ a unit vector in z-direction (pointing

upwards) and by $\hat{v}$ the unit vector in the walking direction, it can be seen that

$$\hat{v} = \frac{(\omega_k \times \mathbf{e}_z) + (\omega_{k+1} \times \mathbf{e}_z)}{|| (\omega_k \times \mathbf{e}_z) + (\omega_{k+1} \times \mathbf{e}_z) ||} \tag{5.29}$$

where $\times$ denotes the vector product (think of $\mathbf{e}_z$ as a vector pointing from the ground up to some point of the robot, *e.g.*, the hip, and note that $\omega \times \mathbf{e}_z$ denotes the linear velocity of that point).

Let us assume that the shape of the curves traced by the contact points is outward, that is, during rolling, the contact points move away from the center line and then return (as in figure 5.2). For efficiency reasons, it is clear that this is a necessary property: through the outward bending shape, the final rolling axis of one foot just before impact will be more or less aligned with the initial rolling axis of the other foot just after impact. In this way, the motion continues reasonably smoothly across impacts and little energy is lost. If the trajectory of the contact point were to bend inward during rolling, the rolling axes just before and after impact would be misaligned, leading to significant energy loss. Because we can design the contact point trajectory ourselves (see section 5.5), we can design it in such a way that the assumption holds. In that case, we can use a simpler equation for the walking direction, being

$$\hat{v} = \frac{\omega_k + (-\omega_{k+1})}{||\omega_k + (-\omega_{k+1})||}. \tag{5.30}$$

If the locations of the impacts are known, we can define the points p_k in the figure as the intersections of the lines defined by the twist axes of two consecutive steps k and $k+1$. For a symmetric gait, the sequence of middle points

$$\bar{p}_k := (p_k + p_{(k-1)})/2 \tag{5.31}$$

will lie on a center line in the walking direction $\hat{v}$. The distance between subsequent points $\bar{p}_k$ corresponds to the longitudinal step length. The lateral distance of a point p_k describes how much the foot trajectories curve away from $\hat{v}$, *i.e.*, it depends on $\langle \hat{v}, \omega_k \rangle$.

5.4.2 Kinematics of 3D Rolling

Continuing now with the details of the rolling motion during the stance phase, suppose we have decided on a desired walking direction $\hat{v}$ and rolling twist ω_k after impact, and suppose we have chosen a desired trajectory of the contact point on the floor, for example a spline interpolating between the impact point and rolling direction and the release point and rolling direction.

Under these assumptions, we can write down a relation for the kinematics of 3D rolling of the foot such that the contact point between the foot and the floor follows the desired trajectory. If we take r to be the moving contact point, we know from previous work (Duindam and Stramigioli, 2003) that

$$\left(g_{1*} + H_0^1\, g_{0*}\, H_1^0\right) \dot{r}_1 = {}^1\tilde{T}_0^1\, g_1 - H_0^1\, g_{0*}\, {}^0\tilde{T}_1^0\, r_0 \tag{5.32}$$

with r_1 the contact point in body coordinates, r_0 the contact point in floor coordinates, g_1 the normal to the foot surface, and g_0 the normal to the floor. The tangent mappings g_{1*} and g_{0*} describe the local curvature of the foot and floor surfaces at the contact point. Since the floor is assumed fully flat $g_{0*} \equiv 0$ and the previous equation reduces to

$$\dot{g}_1 = g_{1*}\, \dot{r}_1 = {}^1\tilde{T}_0^1\, g_1 = -{}^1\tilde{T}_1^0\, g_1. \tag{5.33}$$

This equation gives a relation between the twist ${}^1T_1^0$ of the foot and the change $\dot{g}_1$ of the normal vector to the foot surface, which is equal to the foot curvature $g_{1*}\dot{r}_1$ in the direction of the trajectory of the contact point. Since $\dot{r}_1$ must be along the surface of the foot, we have an additional constraint

$$g_1^T\, \dot{r}_1 = 0. \tag{5.34}$$

Depending on the purpose of our analysis of the walking cycle, we can read these equations in several ways. First, they give us the possible relative motions ${}^1T_1^0$ for a given foot surface shape g_{1*}. It can be seen that these correspond to the three rolling directions around the contact point. Second, for given foot shape g_{1*} and relative motion ${}^1T_1^0$, the equations give us the motion of the contact point $\dot{r}_1$. Finally, and this is the most interesting application, (5.33) can give us design constraints for the foot: for given desired motions $\dot{r}_1$ of the contact point and rolling motion ${}^1T_1^0$, we can find local surface shapes g_{1*} that satisfy the equation. Since (5.33) only gives us a relation for the curvature in the direction of motion, the curvature in the orthogonal direction can be designed separately, *e.g.*, to increase stability or efficiency of the rolling motion.

5.4.3 Dynamics of 3D Rolling

The next step in the analysis of the stance phase is the dynamics of the rolling motion. Here, we use assumption 5 and neglect the inertial effect of the swing leg, or equivalently, we assume its effect is compensated by a counter-effect through motion of the torso or arms. These assumptions allow us to again study the biped through its locked inertia.

Under assumption 5, the inertia of the system is constant, hence we study the dynamics of the locked inertia, rolling on the stance foot. In other words, we look at

the dynamics of a rigid body with inertia equal to the locked inertia, with surface defined by the foot surface of the stance foot, rolling on a flat floor. As discussed before, the rolling constraint allows only motion around three rotation axes passing through the contact point, and hence we can write the allowed relative twist ${}^1T_1^0$ of the body with respect to the floor as

$$ {}^1T_1^0 = X(r)\omega := \begin{pmatrix} T_x(r) & T_y(r) & T_z(r) \end{pmatrix} \begin{pmatrix} w_x \\ w_y \\ w_z \end{pmatrix} \tag{5.35} $$

with $T_i(r)$ the twist describing rotation around axis i located at the contact point r and w_i the angular velocity around T_i. The columns of the matrix $X(r)$ give a basis for the space of allowed twists. Note that this is similar but opposite to the matrix A in (5.10) which gives a basis for the space of *constrained* velocities.

Theorem 4 *The dynamics of a locked biped with locked inertia tensor $\mathcal{I}$, external wrench W, and rolling on a foot with allowed twists given by ${}^1T_1^0$ as in (5.35) and moving contact point r, are given as*

$$ \bar{\mathcal{I}}\dot{w} + Cw = X^T W \tag{5.36} $$

with $\bar{\mathcal{I}} := (X^T \mathcal{I} X)$ and $C := X^T \mathcal{I} \dot{X} - X^T \operatorname{ad}_{Xw}(\mathcal{I}X)$.

Proof Since all the joints are locked, the behavior of the biped is the same as the behavior of a single rigid body, and its dynamics are therefore given by the dynamics equation for a rigid body (Stramigioli, 2001)

$$ \mathcal{I}\frac{d}{dt}\left({}^1T_1^0\right) - \operatorname{ad}_{{}^1T_1^0}(\mathcal{I}\,{}^1T_1^0) = W + W_c \tag{5.37} $$

where ${}^1T_1^0$ is the twist of the body, $\operatorname{ad}_{{}^1T_1^0}$ is its algebra representation adjoint, and W_c are the external wrenches due to the rolling contact with the floor. Since we can write ${}^1T_1^0 = X(r)w$ at all times, we can substitute this into (5.37) and write

$$ \mathcal{I}\frac{d}{dt}\left(X(r)w\right) - \operatorname{ad}_{X(r)w}\left(\mathcal{I}X(r)w\right) = W + W_c. \tag{5.38} $$

As the contact wrenches W_c are dual to the allowed twists Xw, we have by definition $X^T W_c \equiv 0$, and hence if we multiply the equation from the left by X^T, we obtain

$$ X^T\mathcal{I}\frac{d}{dt}\left(Xw\right) - X^T \operatorname{ad}_{Xw}\left(\mathcal{I}Xw\right) = X^T W \tag{5.39} $$

$$ X^T\mathcal{I}X\dot{w} + X^T\mathcal{I}\dot{X}w - X^T \operatorname{ad}_{Xw}\left(\mathcal{I}Xw\right) = X^T W \tag{5.40} $$

$$ \left(X^T\mathcal{I}X\right)\dot{w} + X^T\left(\mathcal{I}\dot{X} - \operatorname{ad}_{Xw}\mathcal{I}X\right)w = X^T W \tag{5.41} $$

which is the result in the theorem if we substitute the definitions of $\bar{\mathcal{I}}$ and C. ■

On a practical note, we can express $\dot{X}$ in terms of the kinematic states H_1^0 and w as

$$\dot{X} = \frac{\partial X}{\partial r}\dot{r}_1 \tag{5.42}$$

with $\dot{r}_1$ the velocity of the contact point. Using (5.33), (5.34), and the assumption that contact between the floor and the foot occurs only at a single point (since the foot is assumed convex), there is a unique solution $\dot{r}_1$ that satisfies the following equations

$$g_{1*}\,\dot{r}_b = -{}^1\tilde{T}_1^0\, g_1 = -\widetilde{(Xw)}\, g_1 \text{ and} \tag{5.43}$$

$$g_1^T\,\dot{r}_1 = 0. \tag{5.44}$$

The theorem gives an explicit differential equation that describes the dynamics of the locked biped (or any rigid body) with arbitrary foot shape and point contact with the ground, as a function of the relative configuration H_1^0 (which determines r) and the velocity state w. The external wrench W may include forces such as gravity or ankle actuation. Just as the equation for the kinematics of 3D rolling, this equation can be used for different purposes. The most straight-forward way is to use it as a model to predict the motion of a locked biped with a particular foot shape. A more interesting application, however, is to use it to *design* a foot shape, given a certain desired walking gait. As stated in the introduction, it is these applications that benefit most from reduced models such as the one presented here. The dynamics equations are relatively simple, and for a given trajectory (given H_1^0 and ${}^1T_1^0$ as functions of time), it can be used in optimization routines that adept the foot shape parameter g_{1*}. An example is shown in section 5.5.

For bipedal walking on a horizontal floor, the impacts of the feet with the ground will generally reduce the kinetic energy of the system (except for very specific motions for which the projection operator of (5.17) becomes the identity). In order to compensate for this and obtain a cyclic motion, energy needs to be injected into the system. One way that humans inject energy is through the use of ankle push-off. We can mimic this behavior and use an actuator in the ankle to slightly raise the center of mass of the biped at the beginning of each step, thus increasing the potential energy and making a cyclic motion possible. Since the inertia of the foot is small compared to the inertia of the rest of the biped, we can include ankle actuation into the dynamics as part of the external wrench W.

5.5 Simulation example

In this section we give a simple example of how the theory of section 5.4 can be applied for the design of a foot shape. We consider the design as a numerical

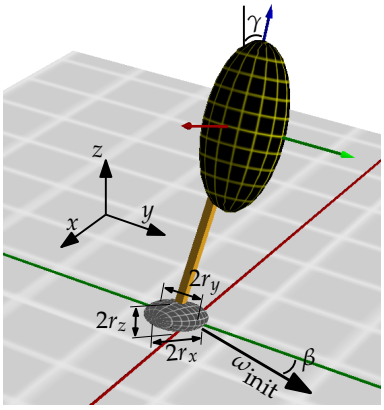

Figure 5.3: Simulation model for parameter optimization.

optimization problem with two parameters.

Consider a sytem of one rigid body (or, equivalently, a locked system of multiple bodies), having an ellipsoidal foot, as shown in figure 5.3. This system represents the robot's right foot, right leg and torso rigidly attached to each other.

Our target is to find a foot width ($2r_y$) and initial angular velocity magnitude $|\omega_{\text{init}}|$ that make the foot roll as shown in figure 5.2. We consider only one step and want a step time of $t_{\text{step}} = 1$ s. As the optimization criterion we use the Euclidean distance d between the foot's contact point $r_0(t)$ at $t = 1$ s and a certain chosen desired contact point location $r_{0,\text{des}} = [0.25 \quad 0 \quad 0]^T$ (without loss of generality we choose $r_0(0) = [0 \quad 0 \quad 0]^T$). The direction of the initial angular velocity β, the length ($2r_x = 0.3$ m) and height ($2r_z = 0.05$ m) of the foot, as well as the inertial properties $\mathcal{I}$ and initial orientation γ of the body are kept fixed during the experiment. In order to obtain a unique solution, we do not allow rotation around w_z (see (5.35)).

We used the simulation package 20-sim (Controllab Products B.V., 2011) to perform an automatic parameter optimization by first making a parameter sweep in both parameters (figure 5.4) and then optimize the best result by a steepest-descent method. The optimal solution was found at $2r_y = 0.274$ m, $|\omega_{\text{init}}| = 1.22$ rad/s. The final contact point r_0 was exactly our desired point $r_{0,\text{des}}$ ($d = 0$).

Although this is a simple example, it does show the application of the method. By choosing other optimization parameters and criteria (*e.g.*, incorporating the final orientation of the body or the final direction of ω), we may be able to design feet that maximize aspects like disturbance rejection during a step, or good performance over a range of gaits.

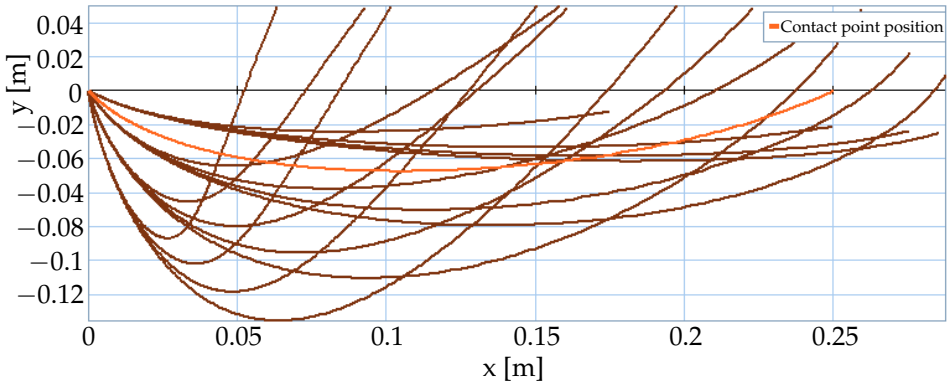

Figure 5.4: Foot contact point trails for different parameter values of $(2r_y) \in [0.1, 0.3\,\text{m}]$ and $|\omega_{\text{init}}| \in [1.1, 1.6\,\text{rad/s}]$ (dark lines) and the optimal solution as stated in the text (light line).

5.6 Conclusions and Future Work

In this chapter we presented a systematic dynamic analysis of 3D bipedal gait. The gait has a foot rolling phase and an instantaneous phase of foot/ground impact. We showed how these phases can be analyzed separately and described in approximation using simplified models described by the locked inertia and a momentum projection. The resulting equations are much simpler than the full robot dynamics and can be used as a starting point for analysis and foot shape design.

One feature of this analysis is the use of locked inertia, which is an instantaneous single rigid body equivalent of the full biped. Using this simplified model makes the complex multi-joint robot dynamics more manageable for theoretical probing. The authors believe that insight from geometric dynamics can potentially lead to a more efficient bipedal gait that exploits natural dynamics.

Our long-term objective is to continue to develop a theoretical framework of biped gait based on geometric dynamics. As applications of this framework, we will address several specific topics. We would like to start from a desired nominal locomotion pattern and compute the required shape of the rigid 3D feet. Furthermore, practical applications require disturbance robustness of gait cycles for which both the foot shape and a proper foot placement strategy need to be devised. Finally, previous research has used concepts such as the energy ellipsoid and momentum sphere to describe the dynamics of a rigid body, and it would be interesting to see how these ellipsoids and spheres change under the influence of rolling motion on a convex foot surface.

Part II

Control and actuation

Chapter 6

Using time-reversal symmetry for stabilizing a simple 3D walker model

This chapter is based on the following article (van Oort and Stramigioli, 2007):

Using time-reversal symmetry for stabilizing a simple 3D walker model
Gijs van Oort and Stefano Stramigioli
Proc., IEEE International Conference on Robotics and Automation (ICRA'07)
pages 4673–4678, April 2007.

Abstract—**A new method is presented for controlling the lateral foot placement of a simple 3D compass biped model. The method is based on the fact that, for the specific model used in this chapter, limit cycle is time-reversal symmetric and that, after a disturbance, the degree of asymmetry in the cycle is indicated by a single variable. This variable is used for feedback with a proportional controller. Simulation results show that the controller works very well for a large range of gaits, without any adaptation of the parameter values.**

6.1 Introduction

Dynamically walking robots (*e.g.*, Denise (Wisse, 2004), Dribbel (Duindam, 2006) and the Cornell Walker (Collins et al., 2001)), have the advantage over 'fully actuated' walkers that they consume far less energy. However, stability and robustness are serious problems for them. Particularly, the robustness of 3D dynamic walkers to lateral disturbances is still very poor. Lateral foot placement is generally seen as a promising method for increasing the robustness in the sideways direction.

This chapter presents a new method for controlling the lateral foot placement of a simple 3D compass biped model. It is based on the fact that, for the specific model used in this chapter, limit cycle is time-reversal symmetric and that, after a disturbance, the degree of asymmetry in the cycle is indicated by a single variable. This variable is used for feedback with a proportional controller.

In section 6.2 the model of the 3D compass walker is presented. The configuration of the walker is given, the environmental assumptions are summed up and the equations of motion as well as the impact equations are discussed. In section 6.3 the open-loop gait is analyzed. It is shown that the system has infinitely many limit cycles. One 'reference limit cycle' is chosen and by linearization of the stride function it is shown that the limit cycle is unstable. It is also shown that a few eigenvalues are intrinsic to the model and cannot be changed. In section 6.4 we show that each step is time-reversal symmetric when the walker is in its limit cycle. In section 6.5 we use this knowledge and propose a controller with one parameter K, and in section 6.6 we show by simulation that the controller can stabilize the walker well for a large range of gaits. We give a different view of the controller in section 6.7 and we end with conclusions and recommendations in section 6.8.

6.2 Model description

6.2.1 General

Consider a 3D compass biped model as sketched in figure 6.1. This biped consists of a pointmass at the hip, having mass m, and two massless legs of length ℓ; each with two degrees of freedom: φ_{hip} and φ_{splay} (the hip can thus be seen as a ball-joint). We distinguish the stance leg (subscripted st) and the swing leg (subscripted sw). The 'feet' are modeled as point contacts. Ground contact is inelastic and rigid, and since the legs are infinitely stiff, the support transfer is instantaneous. The ground is considered to have an infinite friction coefficient: no sliding of the feet can occur. In this chapter the following parameters were chosen: m=1 kg; ℓ=1 m; g=9.81 m/s^2 (gravitational acceleration).

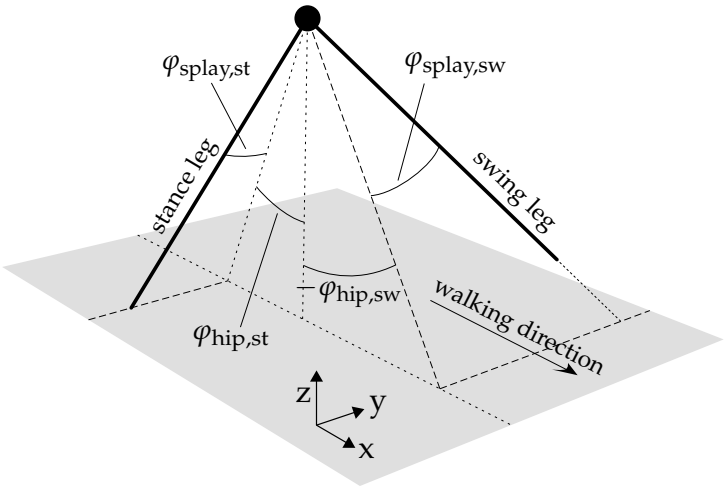

Figure 6.1: A sketch of the 'very simple 3D biped' used in this chapter. Walking direction is the positive x-direction.

The state of the system represents the position and velocity of the hip, relatively to the stance foot, and is denoted as follows: $\mathbf{x} = (\varphi_{\text{hip,st}}, \dot{\varphi}_{\text{hip,st}}, \varphi_{\text{splay,st}}, \dot{\varphi}_{\text{splay,st}})^T$. The state at the beginning of a step k, which is just after swing foot impact, when the rear foot leaves the ground, is denoted by $\mathbf{x}_k^+$ (the $+$ indicates 'post-impact'). The state at the end of the step, just before the new foot impact, is denoted by $\mathbf{x}_k^-$ (the $-$ indicates 'pre-impact'). Note that the state $\mathbf{x}_k^+$ occurs well before $\mathbf{x}_k^-$ and that $\mathbf{x}_k^-$ is immediately followed by $\mathbf{x}_{k+1}^+$ after the impact.

The only means of control of this model is giving the next pose for the swing leg. Because the legs are considered massless, the new configuration can be considered to be reached instantaneously and without any dynamic influence on the overall motion. The input of the system is defined as $\mathbf{u} = (\varphi_{\text{hip,sw}}, \varphi_{\text{splay,sw}})^T$. The input at the end of step k, before and during impact, is denoted by $\mathbf{u}_k$.

6.2.2 Equations of motion

During a step, the hip mass plus leg acts as a spherical inverted pendulum, pivoting around the stance foot. The corresponding equations of motion are

$$\begin{cases} \ddot{\varphi}_{\text{hip}} = \dfrac{\frac{g}{\ell}\sin(\varphi_{\text{hip}}) + 2\,\dot{\varphi}_{\text{hip}}\,\dot{\varphi}_{\text{splay}}\sin(\varphi_{\text{splay}})}{\cos(\varphi_{\text{splay}})} \\ \ddot{\varphi}_{\text{splay}} = \frac{g}{\ell}\cos(\varphi_{\text{hip}})\sin(\varphi_{sp}) - \dot{\varphi}_{\text{hip}}^2\cos(\varphi_{sp})\sin(\varphi_{sp}) \end{cases} \tag{6.1}$$

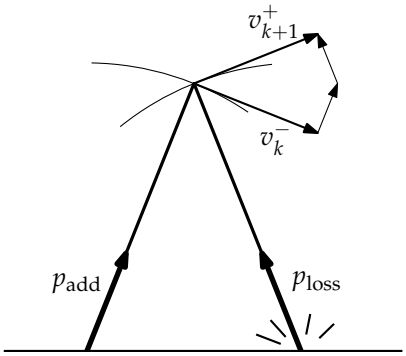

Figure 6.2: A 2D representation of the impulses during foot impact.

where all angles $\varphi_{\bullet}$ refer to the stance leg. These equations can be integrated to obtain the state of the system. Because the swing leg is massless, it does not influence the motion of the system during the step. Therefore, the input $\mathbf{u}$ does not appear in the equations.

6.2.3 Impact equations and energy injection

When the swing foot hits the ground (foot impact), energy is lost and velocity of the hip changes instantaneously. The inelastic, instantaneous collision is modeled as the ground applying an upward impulse p_{loss} to the walker, along the leg. The loss of kinetic energy due to this impulse is denoted by E_{loss}. In order to keep the internal energy of the walker at level, energy is added to the system by applying an upward impulse p_{add} along the posterior leg (which becomes the new swing leg), as shown in figure 6.2. This impulse can be interpreted as the equivalent of the push-off of the human ankle during a normal gait. The kinetic energy added to the system is denoted by E_{add}. In order to keep the energy level constant, we need to find a p_{add} such that $E_{\text{add}} = E_{\text{loss}}$. Since we consider the push-off with energy injection right before the swinging leg touches the floor, p_{loss} is dependent on p_{add}. To understand this, it is sufficient to consider the extreme case in which p_{add} would be extremely large. In this situation the walker would be launched and the front leg would not even touch the ground.

Given the state of the walker $(\mathbf{x}_k^-, \mathbf{u}_k)$ just before impact, the required impulse p_{add} can be calculated that makes $E_{\text{loss}} = E_{\text{add}}$ using (without proof)

$$p_{\text{add}} = m\ell \frac{\sin \mathbf{u}_2 \left(\dot{\varphi}_{\text{sp}}^- \cos \varphi_{\text{sp}}^- \right) + \cos \mathbf{u}_2 \left(\dot{\varphi}_{\text{sp}}^- \sin \varphi_{\text{sp}}^- \cos(\varphi_{\text{hip}}^- - \mathbf{u}_1) + \dot{\varphi}_{\text{hip}}^- \cos \varphi_{\text{sp}}^- \sin(\varphi_{\text{hip}}^- - \mathbf{u}_1) \right)}{1 - \sin \mathbf{u}_2 \sin \varphi_{\text{sp}}^- + \cos \mathbf{u}_2 \cos \varphi_{\text{sp}}^- \cos(\varphi_{\text{hip}}^- - \mathbf{u}_1)}$$

where all $\varphi_{\bullet}^{-}$'s refer to the (pre-impact) stance leg (and φ_{splay} was abbreviated to φ_{sp}). Note that the energy injection system is actually identical to the energy loss system: it is an impulse along the leg that adds a certain amount of velocity to the walker, in the direction of the leg. If time would be reversed (which makes the walker walk backward), the impulses take each others place, and the system would still walk. In other words: the impact (including energy injection) is time-reversal symmetric.

We can define the impact equations (including the energy injection) as a nonlinear function in the following way: $\mathbf{x}_{k+1}^{+} = \mathbb{P}(\mathbf{x}_k^{-}, \mathbf{u}_k)$. The input $\mathbf{u}_k$ defines the position of pre-impact swing leg, which becomes the post-impact stance leg. The position of this stance leg can directly be copied from $\mathbf{u}_k$ to two of the elements of $\mathbf{x}_{k+1}^{+}$. From this it follows that $\mathbf{x}_{k+1}^{+}$ always has the form

$$\mathbf{x}_{k+1}^{+} = \begin{pmatrix} \varphi_{\text{hip}}^{+} \\ \dot{\varphi}_{\text{hip}}^{+} \\ \varphi_{\text{splay}}^{+} \\ \dot{\varphi}_{\text{splay}}^{+} \end{pmatrix} = \mathbb{P}(\mathbf{x}_k^{-}, \mathbf{u}_k) = \begin{pmatrix} \mathbf{u}_{k,1} \\ \mathbb{P}_2(\mathbf{x}_k^{-}, \mathbf{u}_k) \\ \mathbf{u}_{k,2} \\ \mathbb{P}_4(\mathbf{x}_k^{-}, \mathbf{u}_k) \end{pmatrix}, \tag{6.2}$$

where the second and fourth element are non-linear functions of the input variables, and the first and third element are equal to the input itself. The equations are quite long and not included in this chapter. They can however be found in (van Oort, 2005).

6.2.4 Stride function

We define the *stride function* as

$$\mathbf{x}_{k+1}^{+} = \mathcal{S}(\mathbf{x}_k^{+}, \mathbf{u}_k) \tag{6.3}$$

which, given a certain initial state $(\mathbf{x}_k^{+}, \mathbf{u}_k)$ returns the state $\mathbf{x}_{k+1}^{+}$ at the beginning of the next step (if it exists). The stride function covers the equations of motion (section 6.2.2) as well as the impact equations and energy injection system (section 6.2.3). Similarly to (6.2), it can be found that the stride function has the form

$$\mathbf{x}_{k+1}^{+} = \begin{pmatrix} \varphi_{\text{hip}}^{+} \\ \dot{\varphi}_{\text{hip}}^{+} \\ \varphi_{\text{splay}}^{+} \\ \dot{\varphi}_{\text{splay}}^{+} \end{pmatrix} = \mathcal{S}(\mathbf{x}_k^{+}, \mathbf{u}_k) = \begin{pmatrix} \mathbf{u}_{k,1} \\ \mathcal{S}_2(\mathbf{x}_k^{+}, \mathbf{u}_k) \\ \mathbf{u}_{k,2} \\ \mathcal{S}_4(\mathbf{x}_k^{+}, \mathbf{u}_k) \end{pmatrix}. \tag{6.4}$$

It should be noted that, apart from disturbances, the internal energy of the system is always constant ($\dot{H} = 0$, where $H = E_{\text{kin}} + E_{\text{pot}}$). During the motion phase,

Eigenvalue	-2.26	1	0	0
Eigenvector	$\begin{pmatrix} 0 \\ -0.05 \\ 0 \\ -0.99 \end{pmatrix}$	$\begin{pmatrix} 0 \\ -0.99 \\ 0 \\ -0.08 \end{pmatrix}$	$\begin{pmatrix} 0 \\ 0.10 \\ 0.37 \\ -0.92 \end{pmatrix}$	$\begin{pmatrix} 0.46 \\ -0.89 \\ 0 \\ 0.05 \end{pmatrix}$

Table 6.1: The eigenvalues and eigenvectors of the uncontrolled walker, linearized around the 'reference gait'.

the system moves through a conservative (gravity) field, which of course does not alter the total internal energy. During impact, the amount of (kinetic) energy added by p_{add} is (by construction) exactly equal to the amount that is lost by p_{loss}. So, if a disturbance would raise (or lower) the total internal energy of the walker, the system has no way to restore the energy to the original level afterwards.

6.3 Analysis of the uncontrolled gait

For any fixed $\mathbf{u}$ within the range where the walker looks 'human-like', thus with the hip above the ground, swing leg pointing forward and step length larger than step width, this system has infinitely many limit cycles $\mathbf{x}_{k+1}^+ = \mathbf{x}_k^+$, which will be denoted by $\mathbf{x}^*$.

To understand this, realize that this model has its energy addition directly coupled to the energy loss. For each energy level the loss and addition are in equilibrium, which gives the possibility for a limit cycle for each energy level. This is different from most other walker models, that inject a fixed amount of energy into the system at each step, and can have a limit cycle only for a gait where the impact energy loss is equal to this fixed amount of injected energy.

For analysis it is convenient to choose a 'reference gait'. Quite arbitrarily a limit cycle is chosen having $\mathbf{u}^r = (-0.3, 0.05)^T$ and $\mathbf{x}^r = (-0.3, 1.5, 0.05, -0.0819)^T$. By linearizing the stride function $\mathcal{S}$ around $(\mathbf{x}^r, \mathbf{u}^r)$ and taking the eigenvalues of the obtained Jacobian matrix $J_x = \frac{\partial \mathcal{S}}{\partial x}$, it can be shown that this gait is unstable. The other limit cycle gaits in the 'human-like' range are also unstable. The eigenvalues and corresponding eigenvectors of the reference gait are shown in table 6.1. The eigenvalues are discussed below.

From (6.4) it can be seen that the first and third element of $\mathcal{S}$ are independent on $\mathbf{x}$, hence the first and third row of J_x will be entirely zero. J_x thus has rank 2 (the two other rows are linearly independent), so it can only have two non-zero eigenvalues (the other two will be zero).

If a disturbance would alter the magnitude of the velocity of the walker, the kinetic energy and thus the total energy H will also change (by, say, an amount of ΔH). By construction, the walker cannot restore its original energy level, so the deviation from the original energy level will always remain constant (equal to ΔH), which explains the eigenvalue 1.

The eigenvalue of -2.26 has to do with changes in direction of the velocity vector. This is inverted pendulum-like, unstable mode that needs to be stabilized by means of active control.

If the walker falls, we can distinguish the following cases:

- The walker is falling backward ($\dot{\varphi}_{\text{hip}} < 0$). This happens when not enough energy is present at the start of a step. As an indication, if for our reference input $\mathbf{u}^r$ the initial hip velocity $a = \dot{\varphi}_{\text{hip}} < 0.94$ rad/s, the walker will fall backwards.

- The walker is falling to the side. This happens if the splay velocity or the splay angle is too far off the limit cycle value.

- The walker goes so fast that the stance foot leaves the ground due to the vertical component of the ground reaction force becoming zero. This happens when the angular velocity of the hip (rotating around the stance foot) is so large that $m\ell\omega^2(\cos\varphi_{\text{hip}}\cos\varphi_{\text{splay}}) > mg$. As an indication, if for our reference input $\mathbf{u}^r$ the initial hip velocity $a = \dot{\varphi}_{\text{hip}} > 3.15$ rad/s, the walker will leave the ground. The walker cannot fall forwards, because it always instantaneously puts its swing leg forward.

6.4 Using time-reversal symmetry for the design of a controller

A special case for the impact equations (6.2) occurs when the position of the stance leg just before impact is equal but mirrored to the (fixed) input, which is the position of the swing leg, *i.e.*,

$$\mathbf{x}^- = \begin{pmatrix} \varphi^-_{\text{hip,st}} \\ \dot{\varphi}^-_{\text{hip,st}} \\ \varphi^-_{\text{splay,st}} \\ \dot{\varphi}^-_{\text{splay,st}} \end{pmatrix} = \begin{pmatrix} -\mathbf{u}_1 \\ a \\ \mathbf{u}_2 \\ b \end{pmatrix} = \begin{pmatrix} -\varphi_{\text{hip,sw}} \\ a \\ \varphi_{\text{splay,sw}} \\ b \end{pmatrix}, \tag{6.5}$$

with any positive angular velocities a and b. In this case, the plane spanned by

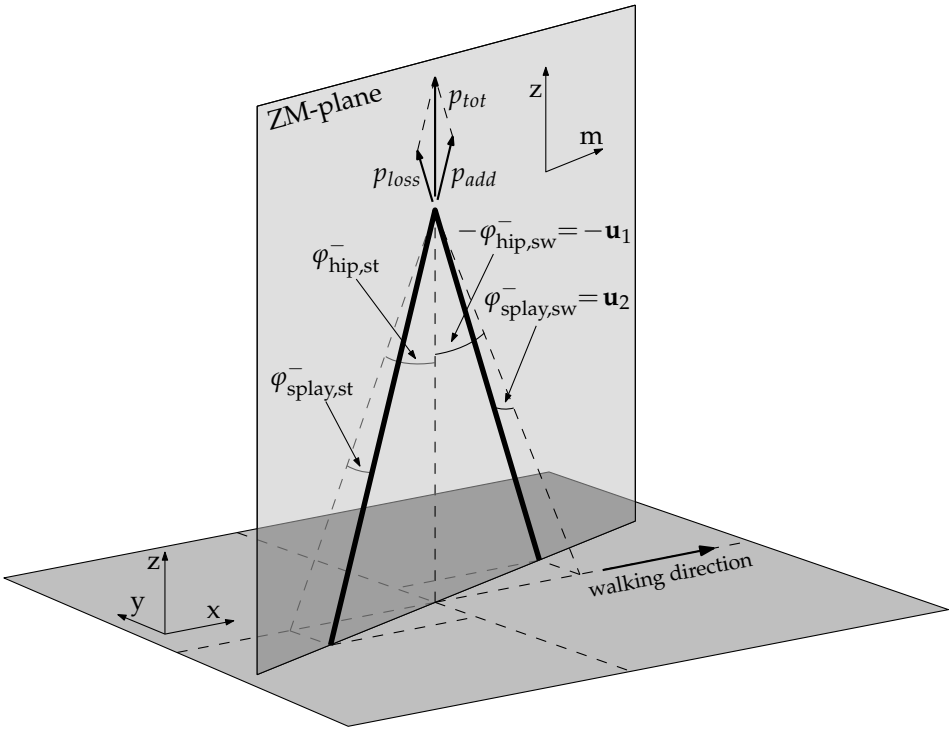

Figure 6.3: A special case for the impact equations: $\varphi^-_{\text{hip,st}} = -\mathbf{u}_1$, $\varphi^-_{\text{splay,st}} = \mathbf{u}_2$. In this case the legs span a plane that is exactly vertical.

the legs, indicated as the ZM-plane in figure 6.3, will be exactly vertical (the z-axis will be parallel to the world's z-axis and the m-axis will be parallel to the world's XY-plane. Because the two impact impulses p_{add} and p_{loss} are aligned with the legs, they also lie in the ZM-plane. Both impulses are equal in magnitude, so their z-components add up, while their m-components cancel each other out. So only the vertical velocity of the hip will change at impact; the forward and sideways velocities are unaffected. This makes the post-impact velocities be equal but mirrored (due to the splay sign change) to the pre-impact velocities, resulting in the post-impact state

$$\text{Equation (6.5)} \Longrightarrow \mathbf{x}^+ = \begin{pmatrix} \varphi^+_{\text{hip}} \\ \dot{\varphi}^+_{\text{hip}} \\ \varphi^+_{\text{splay}} \\ \dot{\varphi}^+_{\text{splay}} \end{pmatrix} = \begin{pmatrix} \mathbf{u}_1 \\ a \\ \mathbf{u}_2 \\ -b \end{pmatrix}, \tag{6.6}$$

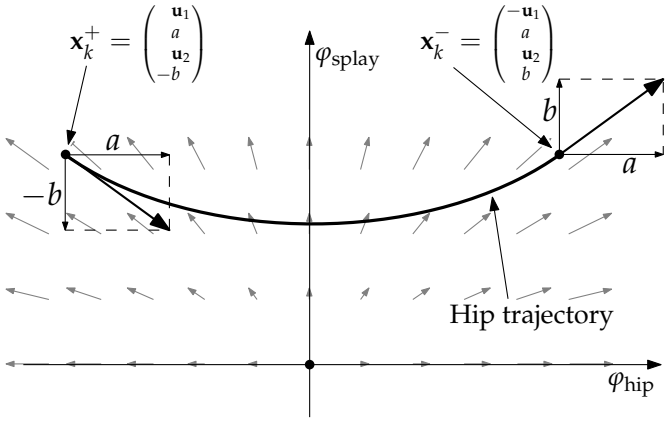

Figure 6.4: The trajectory traveled by the hip when going from the initial condition $\mathbf{x}_k^+$ to the final condition $\mathbf{x}_k^-$, along with an approximation of the (angular) acceleration vector field of (6.1). Because the conditions and the vector field are symmetric around $\varphi_{\text{hip}} = 0$, the trajectory is also symmetric.

which holds for any angular velocities a and b. If we can find values for a and b such that the equations of motion, when initialized with post-impact state $\mathbf{x}^+$, as defined in (6.6), will return a new pre-impact state $\mathbf{x}^-$ obeying (6.5), we obtain a limit cycle as schematically shown below:

$$\mathbf{x}_k^+ = \begin{pmatrix} \mathbf{u}_1 \\ a \\ \mathbf{u}_2 \\ -b \end{pmatrix} \overset{(6.1)}{\Longrightarrow} \mathbf{x}_k^- = \begin{pmatrix} -\mathbf{u}_1 \\ a \\ \mathbf{u}_2 \\ b \end{pmatrix} \overset{(6.2)}{\Longrightarrow} \mathbf{x}_{k+1}^+ = \begin{pmatrix} \mathbf{u}_1 \\ a \\ \mathbf{u}_2 \\ -b \end{pmatrix} \overset{(6.1)}{\Longrightarrow} \dots \tag{6.7}$$

In figure 6.4 the trajectory (the solution of the differential equation (6.1) with the given initial conditions $\mathbf{x}_k^+$ and final conditions $\mathbf{x}_k^-$) is sketched, along with an approximation of the acceleration vector field of (6.1).[1] Because the initial and final conditions as well as the vector field are symmetric around $\varphi_{\text{hip}} = 0$, the trajectory will also be symmetric. This symmetry implies that the sideways velocity $\dot{\varphi}_{\text{splay}}$ at $\varphi_{\text{hip}} = 0$ must be zero. At the same time, because the vector field is symmetric around $\varphi_{\text{hip}} = 0$, any trajectory having $\dot{\varphi}_{\text{splay}}\Big|_{(\varphi_{\text{hip}}=0)} = 0$ will be symmetric around $\varphi_{\text{hip}} = 0$, and, combined with the impact equations, will give

[1] The actual acceleration at a certain point also depends on the instantaneous velocity of the hip. However, for the velocities used, the influence is small.

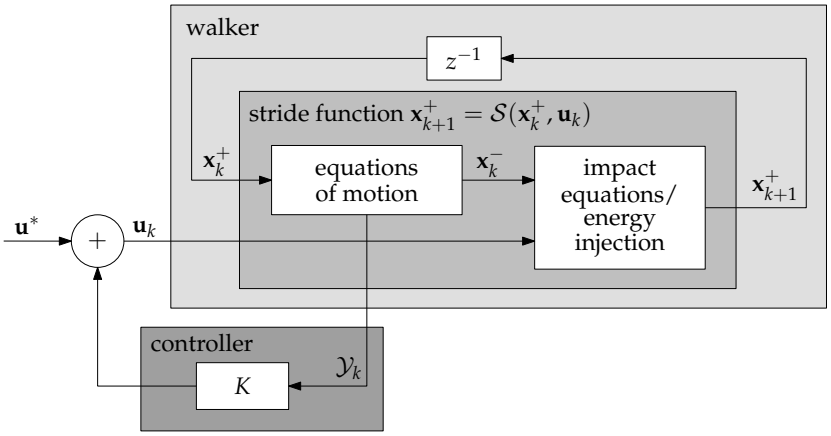

Figure 6.5: A block diagram of the controlled walker.

a limit cycle. So, for this walker, the condition $\dot{\varphi}_{\text{splay}}\Big|_{(\varphi_{\text{hip}}=0)} = 0$ is a sufficient condition for having a limit cycle. We introduce $\mathcal{Y}$ as a shorter notation:

$$\mathcal{Y} := \dot{\varphi}_{\text{splay}}\Big|_{(\varphi_{\text{hip}}=0)}. \tag{6.8}$$

6.5 Control

If the walker is walking in a limit cycle ($\mathcal{Y} = 0$), a disturbance will generally lead to a non-zero $\mathcal{Y}$. We can use the value of $\mathcal{Y}$ at step k (denoted as $\mathcal{Y}_k$) to control the input $\mathbf{u}_k$, such that the disturbance is suppressed (*i.e.*, $|\mathcal{Y}_{k+1}| < |\mathcal{Y}_k|$). Note that $\mathbf{u}_k$ is only used at the end of step k and that $\mathcal{Y}_k$ is already known halfway step k, so we won't run into problems here. A good choice for control would be to give a setpoint offset for the splay angle $\varphi_{\text{splay,sw}}$ proportional to $\mathcal{Y}$, *i.e.*,

$$\mathbf{u}_k = \begin{pmatrix} \varphi_{\text{hip,sw}} \\ \varphi_{\text{splay,sw}} \end{pmatrix} = \begin{pmatrix} \mathbf{u}_1^* \\ \mathbf{u}_2^* + K \cdot \mathcal{Y}_k \end{pmatrix}, \tag{6.9}$$

where K is the controller gain. A block diagram of the obtained system is shown in figure 6.5. Analysis of the effect of a disturbance, sketched in figure 6.6, shows that K should be positive. Because of the extensiveness of the equations of motion and the impact equations, no attempt was made to analytically prove that the walker can indeed be stabilized with this control law. However, simulation

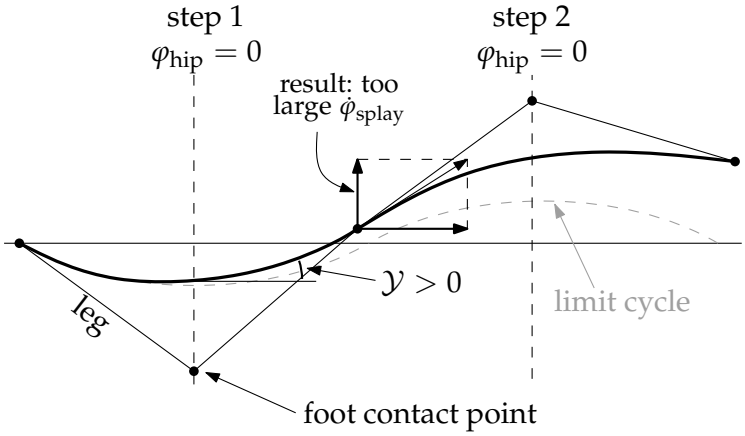

Figure 6.6: Analysis of the effect of a disturbance. A disturbance causing $\mathcal{Y}$ to be positive (as in the figure), leads to a too large $\dot{\varphi}_{\text{splay}}$. In order to compensate for this, the swing foot should be placed a little more outward.

results, described in the next section, have shown that it is indeed possible to stabilize the walker.

An advantage of the controller over the conventional technique of linearization and pole placement (*e.g.*, (Kuo, 1999)) is that no explicit knowledge of the limit cycle is needed in order to stabilize the walker (as $\mathbf{x}^*$ does not appear in the calculation of $\mathbf{u}_k$). Hence, the controller will work for a great range of limit cycles without adaptation of any parameter. Furthermore, only a single controller gain needs to be chosen, which simplifies the design and tuning.

6.6 Simulation results

In order to verify the correctness of the control strategy, simulations were done in Matlab. The results are presented in this section.

One criterion that could be used for choosing the 'optimal' value of K is trying to minimize the eigenvalues of the linearized controlled system. For a non-zero K, the third element of the stride function S will become dependent on $\mathbf{x}_k^+$ (because $\mathbf{u}_{k,2}$ is dependent on $\mathbf{x}_k^+$), so the third row of the Jacobian J_x will not be zero anymore. This results in an increase in rank of J_x and the possibility to have three non-zero eigenvalues. One of them is the (unchangeable) eigenvalue 1, which is still a system property. The two other eigenvalues can be influenced by varying K.

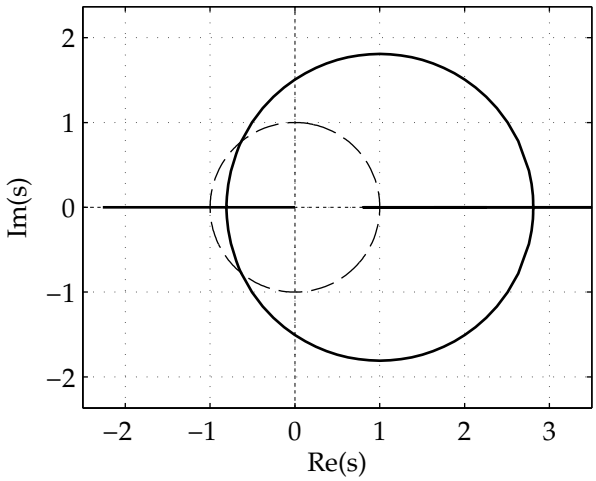

Figure 6.7: Root locus plot of the controlled reference gait. For $K = 0.252 \ldots 0.398$ all poles are within the unit circle, so the system is stable. The smallest eigenvalue is reached at $K = 0.259$.

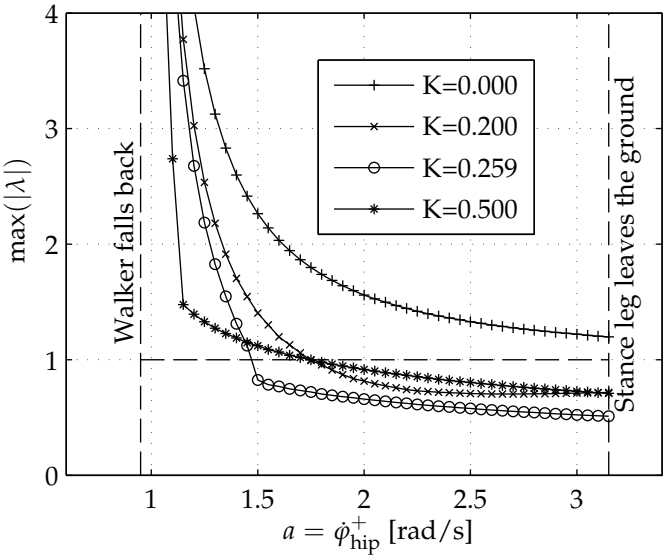

Figure 6.8: The eigenvalues of the controlled system for different gait velocities, with different values for K. It can be seen that $K = 0.259$ can not only stabilize our reference gait well, but also all gaits with higher velocity.

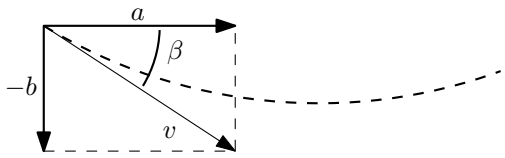

Figure 6.9: Representation of the velocity of the hip as (v, β).

In figure 6.7 the root-locus is drawn for our reference gait $(\mathbf{x}^r, \mathbf{u}^r)$. As can be seen, the system can indeed be stabilized with the controller: by choosing a proper K, we can put both eigenvalues inside the unit circle. The system is stable for a reasonably large range of K. The minimum eigenvalue of -0.81 is reached when $K = 0.259$.

In order to see how well the controller with a fixed K can handle different limit cycles (different values for a and b in (6.7)), figure 6.8 was made. It shows that indeed a single value for K can stabilize a large region of limit cycles. We also see that the K that gave the lowest eigenvalues for our reference gait does really well in stabilizing faster gaits.

Eigenvalues only give insight in the behavior under small disturbances. For a nonlinear system such as a walker, the behavior under large disturbances is also very interesting. We are particularly interested in the *basin of attraction* (Schwab and Wisse, 2001): how large can a disturbance be before the walker falls?

For investigation of the basin of attraction, it is useful to represent the velocity of the hip in polar coordinates v and β (see figure 6.9). A disturbance acting on β (affecting the direction of the velocity vector) will not affect the internal energy of the system, therefore the system can return to its original limit cycle. A disturbance acting on v (affecting the magnitude of the velocity vector) does affect the internal energy and will cause the walker to converge to a different limit cycle (if (v, β) is within the basin of attraction, that is). Note that in the limit cycle, b is small relative to a, which makes $v \approx a$.

Figure 6.10 shows a slice of the basin of attraction of the controlled system with $K = 0.259$. As can be seen, for low velocities the walker cannot be stabilized with this controller (there exists a limit cycle for these low velocities, but it is unstable). With increasing velocity the basin of attraction increases. From this we can conclude that fast walking more robust than slow walking. As most real walking robots have a relatively slow gait, this suggests that a bit of extra robustness could be obtained with relative ease by just making the robot walk faster.

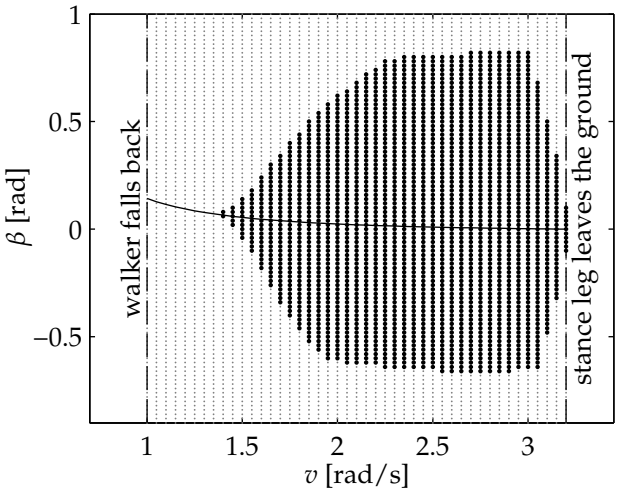

Figure 6.10: The basin of attraction of the controlled system with controller gain $K = 0.259$. On the horizontal axis the velocity $v = \sqrt{a^2 + (-b)^2}$ is put, on the vertical axis we have $\beta = \text{atan}(\frac{-b}{a})$ (see also figure 6.9). Each dot represents a simulation run with initial condition $\mathbf{x}^+ = (\mathbf{u}_1^r, a, \mathbf{u}_2^r, -b)$. Thick dots indicate that the initial condition is inside the basin of attraction. The curve in the graph shows the set of all limit cycles having $\mathbf{x}^* = (\mathbf{u}_1^r, \bullet, \mathbf{u}_2^r, \bullet)$. Note that for small velocities v the system is unstable and has no basin of attraction.

6.7 Interpretation as a standard discrete nonlinear controller

When looking at the block diagram of the system (figure 6.5), it does not look like a standard discrete controller. However, $\mathcal{Y}_k$ is actually only dependent on $\mathbf{x}_k$ (via the equations of motion). So we can write: $\mathcal{Y}_k = f(\mathbf{x}_k)$ with f being a nonlinear function. This gives

$$\mathbf{u}_k = \begin{pmatrix} \varphi_{\text{hip,sw}} \\ \varphi_{\text{splay,sw}} \end{pmatrix} = \begin{pmatrix} \mathbf{u}_1^* \\ \mathbf{u}_2^* + K f(\mathbf{x}_k) \end{pmatrix}, \tag{6.10}$$

which is simply a conventional nonlinear controller. It is a special one however: because the value of $f(\mathbf{x}_k)$ has a clear geometrical meaning, this is much more insightful than just a nonlinear formula.

6.8 Conclusions and future work

A new method has been described for controlling lateral foot placement of a 3D compass biped model, based on time-reversal symmetry of the limit cycle. If a disturbance occurs, the step becomes asymmetric. It was shown that $\mathcal{Y} := \dot{\varphi}_{\text{splay}}\Big|_{(\varphi_{\text{hip}}=0)}$ is a good measure for the degree of asymmetry of the step, and can be used for feedback. A proportional controller was proposed where the splay angle offset is proportional to $\mathcal{Y}$ (with controller gain K).

Simulation results showed that the controller can stabilize the walker in a large range of gaits (at different velocities) without any adjustment of the parameter, and that the basin of attraction is large, especially for fast walking. It was shown that the controller is actually a conventional nonlinear controller, with the additional property that the non-linear function has a clear geometrical meaning, which gives more insight in the actual control strategy.

The control method as described here works well with the compass model, but it cannot directly be used for more complex models, because generally the gait of such models is not time-reversal symmetric. This study will be continued by investigating how the method can be generalized to work with other walker models as well. Our goal is to build a real 3D biped soon, which will, amongst others, make use of the lateral foot placement control method.

Chapter 7

Dynamic walking stability of the TUlip robot by means of the extrapolated center of mass

This chapter is a major revision of the following article (Bouwman et al., 2010):

Dynamic walking stability of the TUlip robot by means of the extrapolated center of mass
Windel M. Bouwman, Gijs van Oort, Edwin C. Dertien,
Jan F. Broenink and Raffaella Carloni
Proc., 12th Mechatronics Forum Biennial International Conference
pages 197–204, June 2010.

Abstract—**The humanoid robot TUlip was created to participate in the 'teen-size' league of Robocup. It is a bipedal robot intended for dynamic walking. It has six degrees of freedom in each leg: three at the hip, one at the knee and two at the ankle. This chapter elaborates on the algorithm for the sideways control during gait. The algorithm uses the 'extrapolated center of mass' (XCOM) to achieve limit cycle stability. The algorithm was tested in simulation using a linear inverted pendulum and, then, experimentally applied to TUlip. The result is an adaptive behavior of the robot, promising for future application to legged robot stability.**

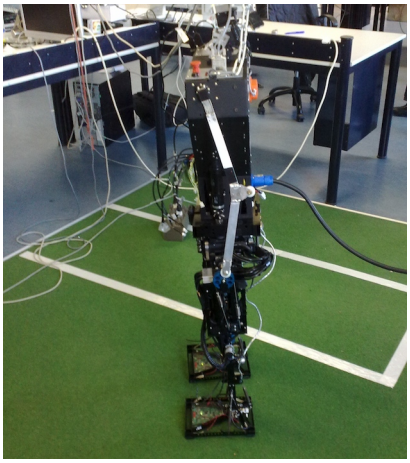

Figure 7.1: TUlip in stable stance mode.

7.1 Introduction and motivation

The robot *TUlip* (figure 7.1) is a 'teensize' humanoid robot, which has been designed to walk dynamically and to compete in the RoboCup soccer league. The development of the robot is a collaboration between the three technical universities of the Netherlands: University of Twente, Eindhoven University of Technology and Delft University of Technology.

The link structure of the robot is shown in figure 7.2a. The figure also shows the choice for axes: the x-axis points into walking direction; y-axis points left (as seen from the robot) and the z-axis points upward. Each leg has six degrees of freedom: three in the hip, one in the knee and two in the ankles. The joints relevant for this chapter are named. The sagittal joints (rotation about y-axis) are all constructed as a series elastic actuator (SEA), (Pratt and Williamson, 1995). This means that a compliance is intentionally put in between the motor shaft and the joint shaft. Series elastic actuators allow for torque control and protect the DC motors by absorbing the shocks from foot impact. The lateral ankle joints are unactuated: passive springs pull the feet towards their default position but are compliant enough to allow excursions of a few tens of a radian (figure 7.2b). The feet are rectangular and flat of shape. Pressure sensors on each of the corners are used to determine impact.

In order to make TUlip walk without falling, a controller is needed. Hof (2008) described a simple controller, called *constant offset controller*. This controller is based on the *extrapolated center of mass* (XCOM), (Hof et al., 2005), which is also

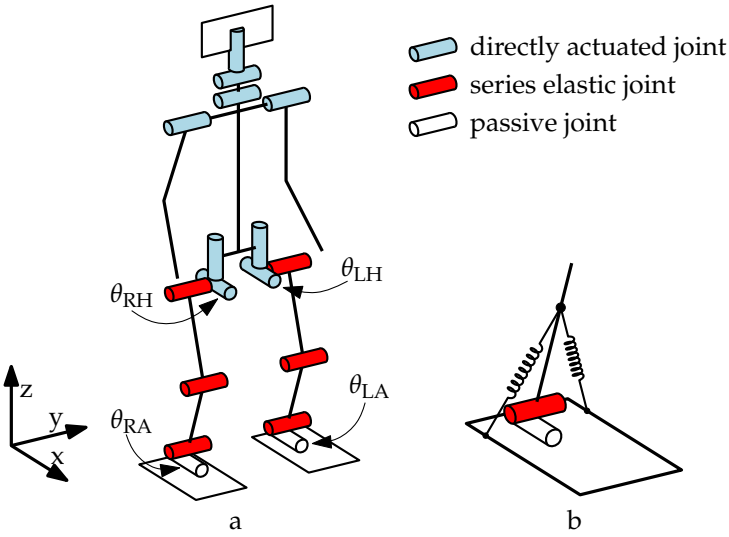

Figure 7.2: TUlip. a) The joint structure of TUlip. The joints that are important for this chapter are named. b) The passive lateral ankle joint.

known as the *instantaneous Capture Point* (Pratt et al., 2006). In this chapter the constant offset controller is first evaluated by applying it to a simple linear inverted pendulum. Then it is applied to TUlip in order to get lateral stability.

This chapter is organized as follows. Section 7.2 presents the extrapolated center of mass and describes how the constant offset controller is applied to an inverted pendulum in simulation. Section 7.3 elaborates on the modifications needed on the controller for implementation on TUlip and section 7.4 describes some experimental results that were obtained.

7.2 The XCOM and the constant offset controller applied to a linear inverted pendulum

Consider a two-dimensional 'linear inverted pendulum' (LIP) in the YZ plane, as shown in figure 7.3, being a point mass m on a stick. The position of the center of mass (COM), is denoted by $C = [C_y \quad C_z]^T$. The structure can be interpreted in two ways: either as a linearization of a normal inverted pendulum by small angle approximation ($\sin\theta \approx \theta$, $\cos\theta \approx 1$) or as an exact model of a variable-stick-length inverted pendulum in which the stick length r is controlled such that the mass is always at a constant height, *i.e.*, $C_z = l$. The projection of the center of

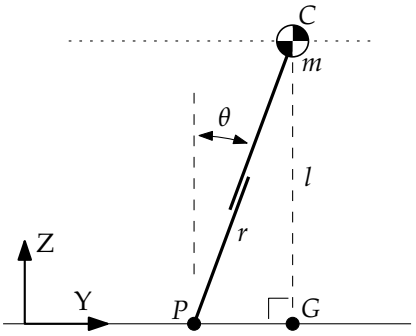

Figure 7.3: Linear inverted pendulum model. Height l remains constant for all possible angles of the pendulum.

mass onto the (flat) ground is denoted by $G = [G_y \quad G_z]^T = [C_y \quad 0]^T$. The center of pressure (COP) of this system is denoted by point $P = [P_y \quad P_z]^T$ with $P_z = 0$ and is (necessarily) the point where the stick contacts the ground.

The LIP has only one degree of freedom, being the y-position of the center of mass, C_y. The equation of motion is

$$\frac{\mathrm{d}^2}{\mathrm{d}t^2} C_y = \omega_0^2 (C_y - P_y) \tag{7.1}$$

where ω_0 is the natural oscillation frequency of the pendulum, *i.e.*, $\omega_0 = \sqrt{\frac{g}{l}}$. This system is unstable (it has poles in $-\omega_0$ and $+\omega_0$). This model can be seen as a very simple model of a walking robot. The stick represents the stance leg and the point mass represents the robot mass; no swing leg is modeled. Support transfer from one leg to the other is done by instantaneously moving the end of the stick (thus, moving the center of pressure P) to another position on the ground.

The *extrapolated center of mass* (XCOM), (Hof et al., 2005), denoted by $\xi = [\xi_y \quad \xi_z]^T$ with $\xi_z = 0$, is defined as the point on the (flat) ground that, when the COP is placed and held there, the system would exactly come to a standstill in its (unstable) equilibrium. The position of the XCOM is dependent on the position and velocity of the COM and can be determined by

$$\xi_y = C_y + \frac{1}{\omega_0} \frac{\mathrm{d}}{\mathrm{d}t} C_y. \tag{7.2}$$

This point has also independently been described by Pratt et al. (2006) under the name *instantaneous capture point*. The linear inverted pendulum and all points defined in this section (including the XCOM) can be straightforwardly extended

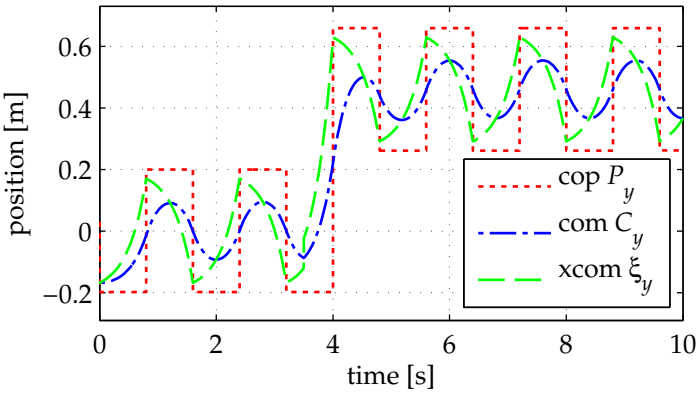

Figure 7.4: Simulation of the constant offset control strategy applied to a linear inverted pendulum. The COP changes instantaneously. Both COM and XCOM trajectories are bounded and are limit cycle stabilized by the control strategy. For the simulation the following parameters were used: $g = 9.81$ m/s, $l = 1$ m, (hence $\omega_0 = 3.13$ rad/s), $T_s = 0.8$ s and $b_y = 0.03$ m. At $t = 3.5$ s an impulsive push is given to the mass, resulting in an instantaneous velocity increase of $\Delta v = 0.3$ m/s.

to 3D. For example, the position of the XCOM in a three-dimensional space is denoted as $\xi = [\xi_x \quad \xi_y \quad \xi_z]^T$.

It was shown by Hof (2008) that the LIP can be stabilized by a 'foot placement' algorithm, called *constant offset control*, which is based on the XCOM. In this chapter the focus is on the lateral stabilization, thus rocking from side to side. At the start of each step n a new position is calculated for the 'foot' (*i.e.*, the COP), being

$$P^n_{y,des} = \xi^n_y + (-1)^n b_y, \tag{7.3}$$

where n is the step number, ξ^n_y is the y-position of the XCOM at the start of the new step and b_y is a constant which offsets the COP from the XCOM (hence the name of the controller).

The applicability of the controller was verified on a LIP model in simulation. The results are shown in figure 7.4. The simulated steps were made at a fixed rate, using a step time $T_s = 0.8$ s. Once each step the position of the COP was changed instantaneously. It can be observed that the XCOM has a bounded trajectory and that the COM trajectory is also bounded. Also the system recovers after a disturbance (at $t = 3.5$ s). The simulation was performed using the simulation package 20-sim (Controllab Products B.V., 2011).

7.3 Stability by foot placement applied to TUlip

The constant offset controller has been designed with an ideal linear inverted pendulum in mind. In order to be able to use it for controlling the robot TUlip, some adaptations need to be made to it because TUlip differs from a LIP in the following ways:

- TUlip has a double support phase during walking during which the COP gradually moves from one foot to the other. The LIP has instantaneous support transfer and therefore instantaneous relocation of the COP;
- The legs of TUlip cannot be positioned arbitrarily fast, while the 'leg' of the LIP can;
- The duration of each step, T_n, is unknown a priori and is a result of the system dynamics. Therefore, the step time is influenced by disturbances. This is in contrast to the LIP, where the step time is a control choice, *i.e.*, a new step can be initiated at any moment in time;
- Contrary to the LIP, the region where the foot of TUlip can be placed is limited due to physical constraints;
- During single support, the COP P moves around within the convex hull of the stance foot. In the sagittal plane P_x can be moved actively by control. In the lateral plane P_y is a function of the stance ankle angle $\theta_{\bullet\mathrm{A}}$.

The unknown step time issue would not seem like a problem because in the control law (7.3) no notion of timing is used. However, because the legs of TUlip cannot be moved arbitrarily fast, the step time *is* an important factor because the leg should be moved to the right position within this time. In order to provide a solution, a minimum step time $T_{\min}$ should be determined experimentally ($T_{\min} = \min(T_n)$) or estimated.

7.3.1 State machine of the gait

The gait cycle of TUlip consists of four states, described shortly below. After that, in the subsequent sections, implementation details are discussed. For robot and controller parameters, see table 7.1.

- **Double stance, left push-off**. At the start of the new step, the left foot pushes off with the ankle. Because during this phase both feet are on the ground, lateral foot movements are impossible. Exit condition for this state is that the left heel has lost contact with the floor and $t > T_{\text{push-off}}$.

Description	Name	Value
Dist. COM – ankle joint	l	0.68 m
Half width between hips	a	0.09 m
Leg length	r	0.57 m
Constant offset	b_y	0.06 m
Push-off duration	$T_{\text{push-off}}$	0.2 s
Swing duration	T_{swing}	0.65 s

Table 7.1: A few dimensions of TUlip and parameters of the controller.

- **Left swing**. In this state, the left leg is controlled forward (in the sagittal plane) using a fixed motion profile with a duration of $T_{\text{swing}} = (T_{\text{min}} - T_{\text{push-off}})$, while accounting for proper ground clearance by bending the knee slightly. After this period, the leg is kept in place in the sagittal plane. Lateral foot placement using the constant offset control is gradually turned on from $t = \frac{1}{2}T_{\text{swing}}$ according to an activation function f_{act}. The angle of the stance hip, θ_{RH}, is controlled to zero. Note that the constant offset controller is not used for sagittal control. Transition to the next state is partial touchdown of the swing foot.

- **Double stance, right push-off** is a mirrored version of double stance, left push-off.

- **Right swing** is a mirrored version of Left swing.

7.3.2 Calculation of the XCOM

To be able to use the control law (7.3), the lateral position of the COM and the XCOM of the robot need to be known. In order to minimize calculation load, the COM is approximated using a simple linearized mass-on-a-stick model of the robot as is shown in figure 7.5 (if needed, the position of the COM can be calculated more accurately by incorporating the full system state). In case of the left foot being the stance foot (figure 7.5a), the sagittal location of the COM location is approximated as

$$(C_y - A_y) = (\theta_{\text{LA}} - \delta)\, l \tag{7.4}$$

where A_y is the lateral position of the stance ankle, θ_{LA} is the angle of the sagittal joint of the left ankle and l is the estimated distance between the ankle and the COM. It is assumed that the left hip angle can be kept exactly at $\theta_{\text{LH}} = 0$ by

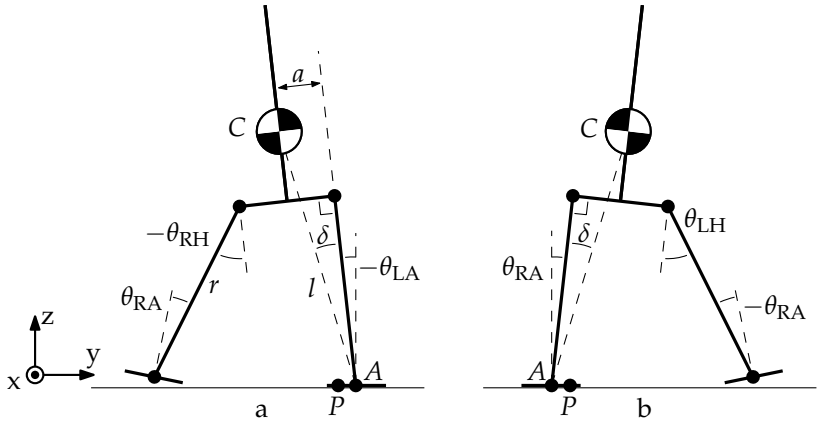

Figure 7.5: Front view of the simplified model of TUlip. a) Left leg is stance leg. $\theta_{LH} = 0$; b) Right leg is stance leg. $\theta_{RH} = 0$. The stance ankle is indicated with A; its lateral position is A_y. The center of pressure P is not necessarily exactly at A.

control. δ is a small constant angle, being

$$\delta = \arcsin(\frac{a}{l}) \approx 0.09 \text{ rad} \tag{7.5}$$

where a is the horizontal distance between the center line of the robot and the hip joint. When the right foot is stance foot (figure 7.5b) the equation for C_y is

$$(C_y - A_y) = (\theta_{RA} + \delta)\, l. \tag{7.6}$$

It should be noted that the absolute value of neither C_y nor A_y is known to the controller, because the controller has no notion of any fixed world. Only the difference between the two, $(C_y - A_y)$, is relevant and is stored as such in the computer running the controller (in a variable called `com_rel_to_stance_ankle`).

Once the lateral position of the COM is determined, the lateral position of the XCOM, ξ_y, is calculated by differentiating $(C_y - A_y)$ with a second order state variable filter (cut-off frequency of $\omega_{svf} = 60$ rad/s ≈ 9.45 Hz) and using (7.2). Every time a new step is started, a jump in the value of $(C_y - A_y)$ occurs (see figure 7.8 on page 120). In order to avoid spikes in the differentiated signal, the state variable filter is re-initialized at the beginning of each new step.

7.3.3 Foot placement

Equations (7.2) and (7.3) can be combined into one equation representing the desired lateral distance between the target position of the swing foot and the COM

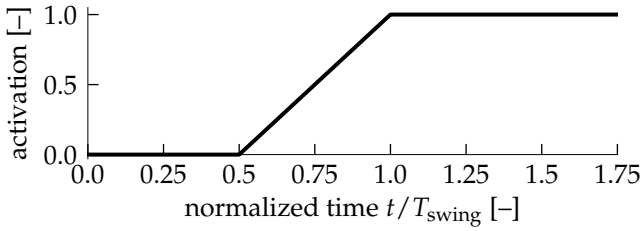

Figure 7.6: Activation function $f_{\text{act}}(t)$ for the setpoint of the lateral hip joint. This function gradually activates the output of the XCOM controller from halfway the swing motion.

at the start of step n as

$$(P^n_{y,des} - C^n_y) = \frac{1}{\omega_0}\frac{\mathrm{d}}{\mathrm{d}t}C^n_y + (-1)^n\, b_n, \tag{7.7}$$

where C^n_y and its time derivative are the lateral position and velocity of the COM at the start of that new step. This can be converted to a desired swing hip angle $\bar{\theta}^n_{\bullet\text{H},des}$ by the following approximations:

$$\bar{\theta}^n_{\text{RH},des} = \arcsin\frac{(P^n_{y,des} - C^n_y) + a}{r} = \arcsin\frac{\left(\frac{1}{\omega_0}\frac{\mathrm{d}}{\mathrm{d}t}C^n_y + (-1)^n\, b_n\right) + a}{r} \tag{7.8}$$

if the right leg is the swing leg, and

$$\bar{\theta}^n_{\text{LH},des} = \arcsin\frac{(P^n_{y,des} - C^n_y) - a}{r} = \arcsin\frac{\left(\frac{1}{\omega_0}\frac{\mathrm{d}}{\mathrm{d}t}C^n_y + (-1)^n\, b_n\right) - a}{r} \tag{7.9}$$

if the left leg is the swing leg. r is the leg length. Note that at the start of a new step the stance ankle angle (θ^n_{LA} or θ^n_{RA}) is almost zero, so the approximation is actually quite accurate.

As already stated, the step time of the robot is uncertain. Therefore, it can not be known on beforehand when exactly a new step will start and what the actual value of C^n_y and its derivative will be at that time. A solution to this is to assume that the new step may start at any time $t \geq T_{\text{swing}}$ and keep $\bar{\theta}_{\bullet\text{H},des}$ up to date constantly, *i.e.*,

$$\bar{\theta}_{\bullet\text{H},des}(t) = \arcsin\frac{\left(\frac{1}{\omega_0}\frac{\mathrm{d}}{\mathrm{d}t}C_y(t) + (-1)^n\, b_n\right) \pm a}{r}. \tag{7.10}$$

For $t < T_{\text{swing}}$, we don't need to steer the leg directly to $\bar{\theta}_{\bullet\text{H},des}$, because there is no chance anyway that a new step is going to be started then. Moreover, at the

first half of the step, the XCOM is not at the right place anyway. From halfway the step, we want to gradually move the leg towards the XCOM. In order to to this, the output of the XCOM controller (7.10) is multiplied with an *activation function* f_{act}, being (see also figure 7.6)

$$f_{\text{act}}(t) = \begin{cases} 0 & \text{if } 0 < t \leq \frac{1}{2}\, T_{\text{swing}}, \\ 2\,(t - \frac{1}{2}\, T_{\text{swing}}) & \text{if } \frac{1}{2}\, T_{\text{swing}} < t \leq T_{\text{swing}}, \\ 1 & \text{if } t > T_{\text{swing}}, \end{cases} \tag{7.11}$$

to get to the real lateral hip setpoint $\theta_{\bullet\text{H},des}$ which is used during the full swing phase. Furthermore, the resulting angle is limited to a small range in order to prevent leg collisions and over-stretching. The final desired swing leg angle is thus calculated as

$$\begin{aligned} \theta_{\text{LH},des}(t) &= \text{Limit}\left(f_{\text{act}}(t) \cdot \bar{\theta}_{\text{LH},des}(t),\ 0,\ 0.3\right) \text{ or} \\ \theta_{\text{RH},des}(t) &= \text{Limit}\left(f_{\text{act}}(t) \cdot \bar{\theta}_{\text{RH},des}(t),\ -0.3,\ 0\right), \end{aligned} \tag{7.12}$$

depending in which leg is the swing leg. Both lateral hip joints are controlled to their respective setpoints using PD control:

$$\tau = K_p\, e + K_d\, \dot{e} + FF_{\text{grav}} \tag{7.13}$$

where $e = \theta_{\bullet\text{H},des} - \theta_{\bullet\text{H}}$ and FF_{grav} is a feed forward term to compensate for the mass of the torso in case of the stance leg. FF_{grav} is increased to a value with a constant rate when stance leg is detected and set to zero in case of the swing leg. During the push-off states the hip setpoints $\theta_{\bullet\text{H},des}$ are decreased to zero with a constant rate.

In figure 7.7 an overview is given of the control strategy used in TUlip during normal gait.

7.4 Experimental results

The algorithm as described was implemented and tested on TUlip. The experiment done consisted of making the robot take a sequence of steps. During these steps the robot was sustained, because total limit cycle stability is not yet achieved. This type of walking is denoted by *sustained walk*.

In figure 7.8 the lateral behavior of the COM and XCOM are shown, together with the resulting setpoint for the hip joint of the stance leg. Note that the COM and XCOM positions are relative to the stance ankle position A_y (which changes each step), not to some fixed-world point. For interpretation of the results this is inconvenient, but for the controller inside the robot it makes sense: this controller

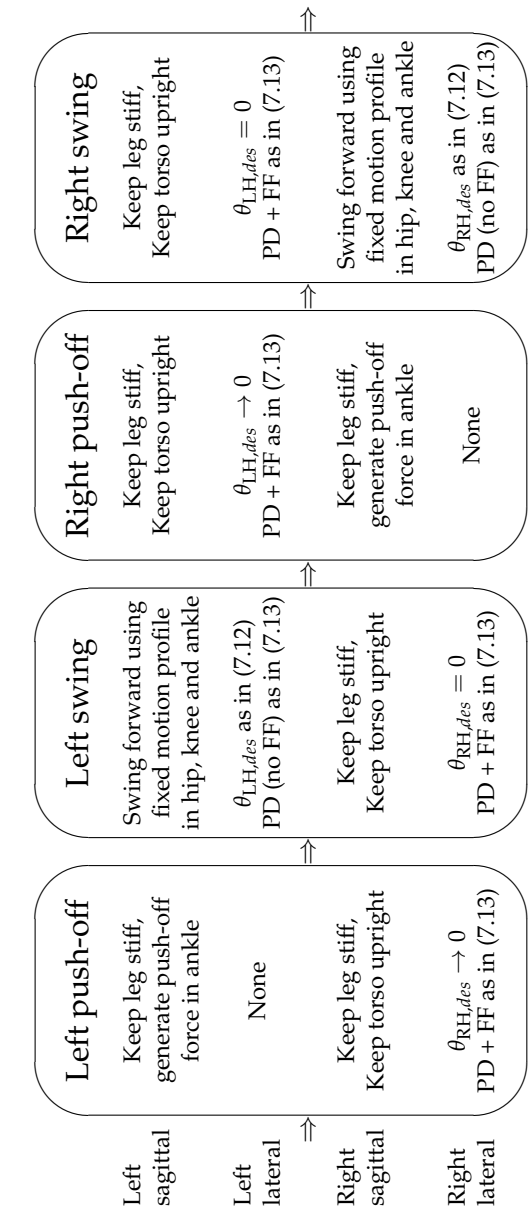

Figure 7.7: Overview of the control strategy of TUlip for each of the four phases of the gait.

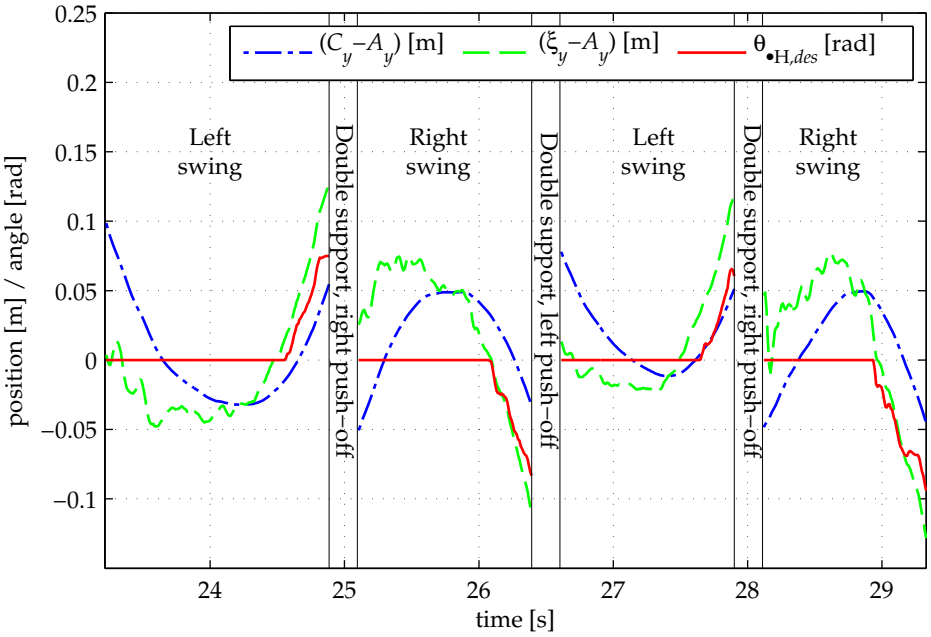

Figure 7.8: The logged COM $(C_y - A_y)$, XCOM $(\xi_y - A_y)$ and setpoint for the hip joint of the swing leg $\theta_{\bullet H,des}$ during a sustained walk consisting of four steps. The COM and XCOM positions are relative to the stance ankle position A_y. As the stance ankle changes each step, A_y changes too. Therefore, the COM and XCOM make jumps at each step transition.

should be invariant for the robot's absolute position, and therefore there is no need to have any notion of world position in this controller[1]. During double support, none of the signals are plotted. The reason is that during this period there is no unambiguous definition of the signals: as both legs are on the ground, there are actually two stance ankle positions and no swing leg angle. Moreover, the signals are not so meaningful during double stance because they are not used for control anyway.

In figure 7.9 the center of mass and extrapolated center of mass are again shown, but now relatively to the fixed world. In order to get these values, the lateral position of the stance ankle A_y was determined manually for each step and added to the values from figure 7.8, *e.g.*, C_y in figure 7.9 was obtained by calculating $(C_y - A_y) + A_y$.

[1]Of course, for other (higher-level) controllers, the robot's *should* have some notion of it's position in the world. For example, when playing a soccer match it is important to know where you are in the soccer field.

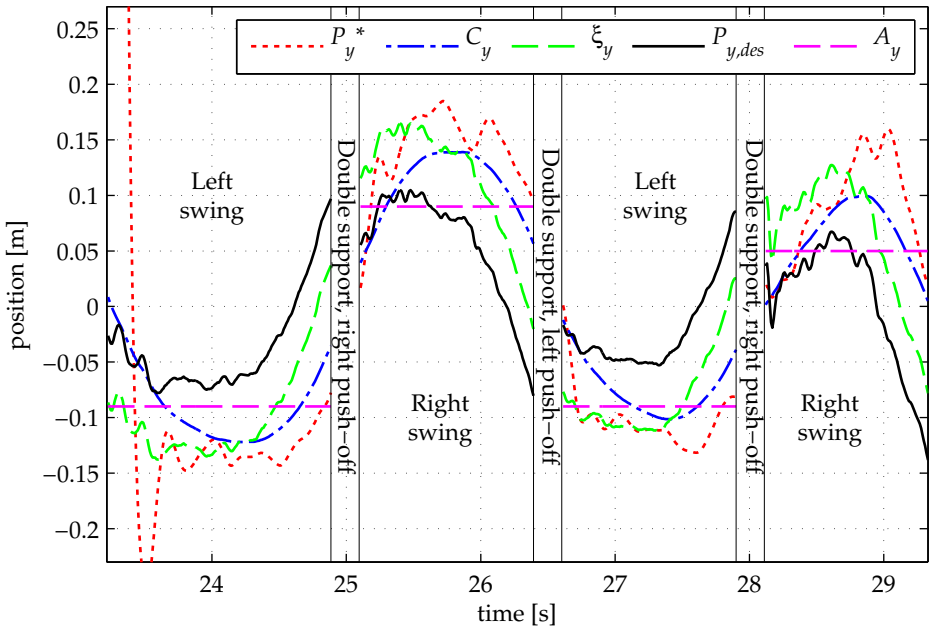

Figure 7.9: Various signals of the sustained walk experiment, represented relatively to the fixed world. P_y^* is an estimate of the center of pressure, C_y and ξ_y are the COM and XCOM respectively. $P_{y,des}$ is the desired lateral swing foot position (7.3). A_y is the lateral position of the stance ankle.

The estimate of the center of pressure, P_y^* was determined by double differentiation of C_y with two second order state variable filters ($\omega_{\text{svf1}} = 30$ rad/s and $\omega_{\text{svf2}} = 15$ rad/s respectively) and then applying the inverse of (7.1). The value of P_y^* fluctuates heavily. Especially around $t = 24$ s a damped oscillation can be seen; this is due to unaccounted oscillations in the hip joint θ_{RH}. However, it can still be observed that the COP indeed lies quite close to the stance ankle (but not exactly on it), just as expected.

The center of mass traverses according to the same pattern as the simulated center of mass of figure 7.4. The XCOM differs somewhat; this can be attributed to the fact that the center of pressure can move around on the sole of the foot and to various other unmodeled effects. The desired lateral swing foot position $P_{y,des}$ is interesting: it grows exponentially near the end of the step. Although this can be expected from the theory and simulation, it is inconvenient because it means rapid leg movements. In future work we will address this problem. It can also be observed that the leg positioning is quite accurate: the ankle position A_y is always within a few centimeters of the desired position $P_{y,des}$ just before ground

contact. From an investigation of figures 7.8 and 7.9, it can be seen that the swing leg does not follow the entire trajectory of $P_{y,des}$; thanks to the limitation of the hip angle, only the last part of each step is followed.

7.5 Conclusions

Lateral stability by foot placement was implemented in our walking robot TUlip by using a *constant offset controller*: a controller which is based on the extrapolated center of mass (XCOM). First the control strategy as proposed by (Hof, 2008) was verified in a computer simulation. The algorithm was then adapted to suit TUlip. Finally an experiment was carried out that shows lateral stability and resemblance with the simulation. We therefore conclude that the constant offset control is usable in the control for bipedal robots.

In the experiment, TUlip required additional energy input (a gentle push from the human guiding the robot) to remain in limit cycle gait. In future work the push-off phase of TUlip will be improved in order to insert more energy in the dynamic walking system. Also an effort will be put in predicting the required lateral leg position $P_{y,des}$ earlier during the step so that sudden movements during the end of the step are not necessary anymore.

Chapter 8

A concept for a new energy efficient actuator

This chapter is based on the following article (Stramigioli et al., 2008):

A concept for a new energy efficient actuator — in pursuit of the ideal actuator
Stefano Stramigioli, Gijs van Oort and Edwin Dertien
Proc., IEEE/ASME International Conference on Advanced Intelligent Mechatronics (AIM'08)
pages 671–675, July 2008.

Abstract—**In this chapter a novel concept of embedded robotic actuator is presented which has been named the Very Versatile Energy Efficient (V2E2) actuator. This actuator stores energy during any force profile which generates negative work on the load and it does therefore have unprecedented potentials for robotics applications.**

8.1 Introduction

For mobile robotics and powered prosthetics, the energy consumption is a crucial factor for usability. A reduction of the amount of energy consumed can yield longer operation on a mobile energy source (*e.g.*, a battery), or can allow for use of smaller energy storage devices.

There are a number of strategies for reducing energy consumption. One approach is to increase the mechanical efficiency of a device. A second method is to limit waste of energy. Normally, mechanical energy is wasted in a system when doing negative work. Adding a buffer element for storage of mechanical energy, such as a spring, seems a logical solution.

The development of actuators incorporating elastic elements has got a lot of attention in the recent years. One of the first and well known examples is the Series Elastic Actuator (SEA) as developed by Pratt and Williamson (1995). Also a number of compliant actuators with tunable elastic elements are under development, such as the MACCEPA by van Ham et al. (2005) or the 'Jack Spring'^{TM} by Hollander et al. (2005), which allow adjustment of the zero-position of a series elastic element. Another approach is to enable adjustment of the spring constant, by varying the pre-tension of a system using non-linear springs. This approach has been used in for example the VSSEA (Variable Stiffness SEA) by Thorson et al. (2007) and the AMASC by Hurst et al. (2004). An elaborate overview of the current state of the art is given in by Ham et al. (2009).

An actuator able to intelligently store energy whenever negative work is done, and able to reuse this energy whenever necessary would be a great breakthrough in the robotic and active prosthetics world. In this chapter a concept of an actuator is presented which does address the energy efficiency explicitly.

This chapter is organized as follows. Section 8.2 elaborates on actuators in general. Then, in section 8.3, the concept of our new actuator is introduced, step by step. Section 8.4 and 8.5 describe two specific aspects on the realization and control and the chapter end with conclusions and discussion in section 8.6.

8.2 Reflections on actuators

Usually an actuator is considered as a 'signal processor' which translates a command generated by a controller to a physical quantity which is applied on the plant, like a force or torque. More correctly, acting on a physical system, energy is exchanged and in order to describe this properly, it is better to consider an actuator as a controlled device that converts energy from a certain domain in which

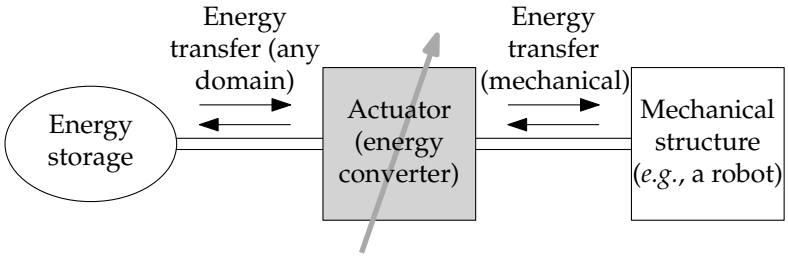

Figure 8.1: An ideal actuator is just an energy converter from any domain in which energy is stored to the mechanical domain and vice versa.

energy is stored (*e.g.*, electrical, chemical battery or even mechanical storage) to mechanical energy, as schematically shown in figure 8.1. The double lines in the figure represent the energy flow. In an ideal situation, the energy conversion is lossless, no energy is stored in the device, the device has no dynamic effects and the energy flow can be in both directions.

The arrow through the actuator in figure 8.1 represents the fact that the amount of energy converted from one domain to the other can be varied (*e.g.*, by varying the control input signal of the actuator).

Let us consider for example a normal DC motor, which converts electrical into mechanical energy. The amount of energy converted depends on the load and the input current. An external controller (such as a switching regulator) can modulate the motor's input current, and thereby influence the the amount of converted energy.

In order to allow for a more formal discussion we introduce the concept of power ports. Each block in figure 8.1 represents an entity which has one or more power ports. In each domain the power port consists of a coupled pair of variables called effort and flows. In the electric domain these are the voltage v (which is an effort) and current i (which is a flow), in the mechanical domain these are a force or torque τ (which is an effort) and a velocity or angular velocity ω (which is a flow). In all situations, the product of the effort and the corresponding flow, which are called power conjugate variables, gives the power P which is instantaneously transferred through that port.

In energy converters, we distinguish two types: transformers (the output effort is proportional to the input effort) and gyrators (the output effort is proportional to the input flow). The DC motor (figure 8.2a) is an example of the latter one. Mathematically, an ideal DC motor can be expressed as

$$\begin{bmatrix} \tau_A \\ v \end{bmatrix} = \begin{bmatrix} k & 0 \\ 0 & k \end{bmatrix} \begin{bmatrix} i \\ \omega_A \end{bmatrix}. \tag{8.1}$$

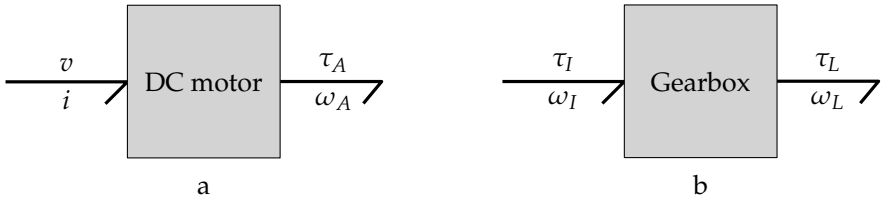

Figure 8.2: Block diagrams; a) A DC motor has two ports: electrical (v, i) and mechanical (τ_A, ω_A); b) A gearbox has two mechanical ports: (τ_I, ω_I) and (τ_L, ω_L). The direction of the half-arrow (called a *bond*) indicates the direction in which the energy flows if the power, which is the product of the port variables ($v \cdot i$, for example) is positive; if it is negative, the energy flows into the other direction.

where τ_A and ω_A are the port variables associated with the motor axis, v and i are the applied voltage and current and k is the motor constant (in Nm/A). More generally, for any gyrator, k is called the 'gyration ratio'. It does not need to be constant (however, it *is* constant in the case of a DC motor), and can sometimes be used to steer the energy flow. It can be observed that $\tau_A \cdot \omega_A = v \cdot i$ (even if k would be time-varying), proving that indeed the energy conversion is lossless and no energy is stored in the ideal actuator.

An ideal gearbox with 'transformation ratio' n can be modeled similarly; it is a transformer (figure 8.2b). It has two mechanical ports (port I, which is usually attached to a source of torque and port L which is usually attached to the inertial load), and can be described mathematically by

$$\begin{bmatrix} \tau_L \\ \omega_I \end{bmatrix} = \begin{bmatrix} n & 0 \\ 0 & n \end{bmatrix} \begin{bmatrix} \tau_I \\ \omega_L \end{bmatrix}. \tag{8.2}$$

In some sense one can regard a gearbox as an actuator: it converts energy from some domain (which happens to be the mechanical domain) of port I to the mechanical domain of port L. Again, n does not need to be constant (however, it *is* constant in the case of a normal gearbox).

An ideal actuator would have the following features:

1. Only energy from the energy storage is used if positive work is done on the output port.

2. If negative work is done on the output port, energy flows back into the energy storage. So, there is no loss of energy.

3. If the actuator is controlled in such a way that no energy transfer takes place, the output shaft of the actuator is either perfectly stiff ($\omega = 0$) and can

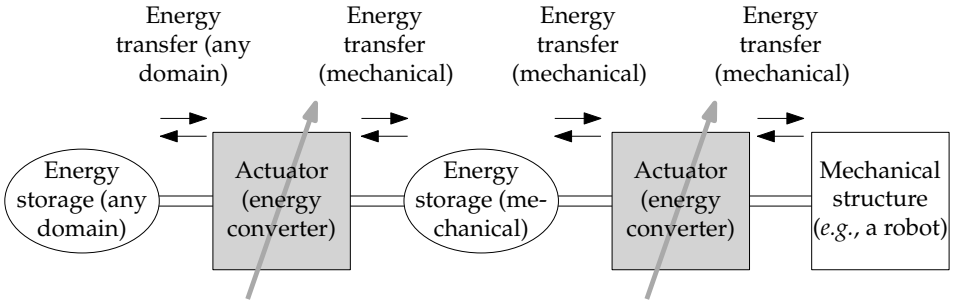

Figure 8.3: Our new actuation concept: an intermediate mechanical energy storage device.

deliver any (static) force or perfectly free-moving and will exert no force to the system ($\tau = 0$). The latter situation is called 'fully backdrivable'. In both cases, no mechanical work is done ($P = \tau \cdot \omega = 0$), so the energy storage does not need to supply any energy.

An ideal actuator can of course never be made, however, we search for solutions that approach (certain aspects) of it. For the moment, we restrict our search to solutions in which the energy storage domain is the electrical domain (or at least, has an electrical interface). We can think of the energy storage device as being a battery or a (large) capacitor. The most versatile converter from electrical to mechanical energy is the DC motor, which behaves as a non-ideal gyrator.

In many applications like legged locomotion, the actuation is approximately periodic[1]. An example of such a periodic movement is given in figure 8.7 on page 134. This data has been taken from the hip joint of our 2D walking robot (Dertien, 2006). The mechanical structure (the leg) has a low and continuously varying velocity in which the direction of movement often changes sign. In this region of operation, a DC motor is an inefficient device: either it needs to run slowly with high torque (in the case of a gearbox with small gear ratio) resulting in a large and heavy motor and bad energy efficiency, or it needs a gearbox with large gear ratio (in case of a better-suited motor) resulting in non-negligible dynamic effects. In the range of operation needed, a DC motor is not a good choice towards an ideal actuator.

We introduce a new actuator concept: an actuator which uses mechanical energy storage as an intermediate step (figure 8.3). In particular, we will focus on a concept which combines a normal DC motor, a rotational spring and an Infinitely Variable Transmission to form an actuation module which we will call the 'V2E2 actuator', which stands for Very Versatile Energy Efficient actuator (figure 8.4).

[1] If the actuation were exactly periodic, simple solutions exist, *e.g.*, a continuously rotating shaft, actuated by a standard DC motor in its most efficient region of operation, with a mechanical mechanism behind it that converts the rotating motion into the desired periodic motion.

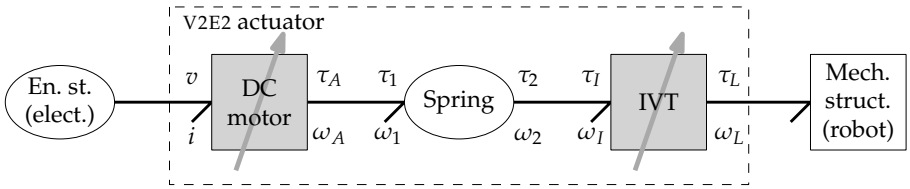

Figure 8.4: Block diagram of the V2E2 actuator.

As will be clear from the discussion below, this approach differs from the use of the elastic element in a Series Elastic Actuator. In the following section the steps to arrive at the new actuator concept are described separately.

8.3 The V2E2 actuator

8.3.1 Using an IVT to modulate actuation torques

The general way to approach control of mechanical systems is to use an actuator (*e.g.*, a DC motor) which generates a time-variant torque $\tau_A(t) = k\,i(t)$ which will be transformed by a fixed gearbox ($\tau_I = \tau_A$) with transformation ratio n to generate an output torque

$$\tau_L = n \cdot \tau_I(t) = n \cdot k\,i(t) \tag{8.3}$$

which will be applied to an inertial load (the interconnection of the two blocks of figure 8.2a and b).

Suppose now that instead of using a fixed gearbox, we take an Infinitely Variable Transmission (IVT). An IVT is a variable transmission unit with the special property that its transmission ratio $n(t)$ can range from a negative to a positive value (*i.e.*, $n(t) \in [n_{min}, n_{max}]$ with $n_{min} < 0 < n_{max}$). We assume the IVT to be ideal, *i.e.*, it does not have any losses and is purely kinematical. Then the output torque τ_L is

$$\tau_L = n(t) \cdot \tau_I(t) = n(t) \cdot k\,i(t). \tag{8.4}$$

Now we have two ways of varying the output torque: either vary the transmission ratio $n(t)$ or vary the actuator output torque $\tau_I(t)$ (or both). Because $n(t)$ can be both positive and negative, it is possible to achieve positive and negative output torques with a constant (non-zero) τ_I.

At first, this does not seem to be interesting, but it does become interesting if one realizes that the torque τ_I can be provided by any system; it does not need to be a simple actuator such as a DC motor. One of the possibilities is to attach the IVT to a rotational spring, as explained in the next subsection.

8.3.2 Adding a spring

An ideal spring is an energy storage element, having a mechanical power port with torque τ_S and (rotational) velocity ω_S. It has a state φ_S and spring stiffness K. It can mathematically be described by the following equations:

$$\varphi_S = \int \omega_S \, \mathrm{d}t, \tag{8.5}$$

$$\tau_S = K\varphi_S. \tag{8.6}$$

If we replace the DC motor of the previous subsection by spring, such that $\tau_I = \tau_S$, we obtain for the torque on the load

$$\tau_L = n(t) \cdot \tau_S = n(t) \cdot K\, \varphi_S(t). \tag{8.7}$$

Note that $\varphi_S(t)$, the internal state of the spring, can not be changed instantaneously; only the rate of change $\dot{\varphi}_S$ can be controlled arbitrarily. By controlling in real time $n(t)$ and supposing that the spring state would never be empty ($\varphi_S \neq 0$), it would be possible to achieve any desired torque τ_L on the load by a proper control of $n(t)$, namely

$$n(t) = \frac{\tau_L}{K\, \varphi_S}. \tag{8.8}$$

This would seem a very complicated way of achieving a desired torque on the load, but by doing so, in case negative work is done on the load ($\tau_L\, \omega_L < 0$), this work would not be lost but instead stored in the spring! We could for example make this actuator behave exactly as a physical (non-linear) damper, but the energy, instead of being lost, would be stored in the spring. A problem which needs some attention is that the idea would not work in case the spring state $\varphi_S = 0$, or in other words if the spring would be unloaded. This can be easily solved as explained in the next section.

8.3.3 Preventing the singular situation $\varphi_S = 0$

A spring is actually a nodic element, which means that it actually has two attaching points (point 1 and 2) and that its internal change of state depends on the relative motion of these points (figure 8.5), *i.e.*,

$$\dot{\varphi}_S = \omega_S = \omega_1 - \omega_2, \tag{8.9}$$

$$\tau_1 = \tau_2 = \tau_S = K\, \varphi_S. \tag{8.10}$$

We can therefore attach one side of the spring to the IVT as explained in the previous subsection, but instead of fixing the other side to a fixed body, we could

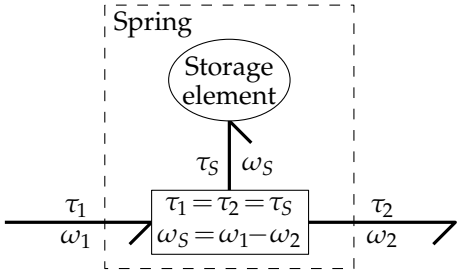

Figure 8.5: The block diagram of an ideal spring: a nodic element with two ports. In bond graph terms the lower block interconnecting the three bonds would be a 0-junction.

attach it to an electrical drive and control this drive in such a way that the stored energy of the spring would not go under a certain level. In this case, the singular situation $\varphi_S = 0$ could be avoided. Furthermore, the electrical drive will only have to supply the extra energy which is needed for the load or which should be used to compensate for friction. In case of a periodic motion of the load like many robotics application in leg locomotion, the net to energy exchange between the load and the actuator would be small or equal to zero and such a motor could be dimensioned small. More on the use of this idea for periodic motions was written by Stramigioli and van Dijk (2008).

8.3.4 Static load compensation

In many applications in robotics, it is also necessary to keep a certain force constant. Using normal electrical drives this implies a constant loss of energy as heat in the electrical drive. In the presented approach, a constant force will correspond to a certain value n of the IVT and the force will be completely generated by the elastic element and no electrical loss will be involved.

In order to allow this, the motor has to be non-backdrivable. As explained previously, the elastic element will be connected on one side to the IVT and on the other side to an electrical drive which may in some situations be used as generator. On this side, for efficiency purposes, it should be possible to latch this side of the spring and keep it in place without having to generate a force with the electrical drive. This would be necessary in most situations when the spring is working in its nominal region. This latching can be implemented with a small electromechanical clutch on the axis which should be activated only if the angular velocity is zero. This is an interesting hybrid optimal control problem.

8.3.5 Electrical storage

The elastic element which will be used for mechanical energy storage will in general be nonlinear and have a maximum amount of energy it can store. This nonlinear behavior can be taken into account, but physically we would reach a problem if the storage would saturate by getting into a region where the spring simply cannot deform elastically anymore and starts to deform plastically. This problem can be tackled by using the electrical motor, which is used to prevent the complete unloading of the elastic storage, as a generator. While it is most efficient to do energy storage without domain conversion, it would be a waste of energy if the surplus in mechanical storage would simply be dissipated. By releasing the clutch between fixed world and the spring, the motor can be used as a generator, driven by the spring. A reversible motor amplifier has to be used to boost up the generated voltage, and charge a battery.

8.4 The IVT

The most crucial part for the realization of a V2E2 actuator, is an efficient realization of an IVT. The IVT should have a range of continuously variable gains between a positive and a negative value, *i.e.*, $n \in [n_{min}, n_{max}]$ with $n_{min} < 0 < n_{max}$. A proper design will have to be such that changing the gain n in real time would cost very little energy. Furthermore, for the usage presented, the IVT should be connected in such a way that the gain n would correspond to a zero torque on the load and no motion on the spring side and not the other way around, otherwise operation would not be possible.

A rotary IVT can be made with by a combining a planetary gear, a Continuously Variable Transmission (CVT) (which has a gear ratio $m \in [m_{min}, m_{max}]$, with $0 < m_{min} < m_{max}$) and a normal gear reduction with gear ratio N. Figure 8.6 shows the configuration of a planetary gear system. We distinguish four parts:

1. the *annulus*, the outer ring, having radius r_a and angular velocity ω_a,

2. the *sun* the inner ring, having radius r_s and angular velocity ω_s,

3. the *planets*, the small gears connecting the sun to the annulus, having radius r_p and angular velocity ω_p (about their own axis), and

4. the *carrier*, which is connected to the planets, having rotational velocity ω_c (this is the angular velocity with which the planets circle around the sun).

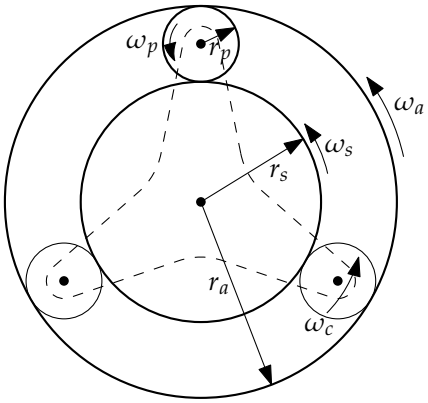

Figure 8.6: Configuration of a planetary gear.

The relation between the angular velocities of the annulus, sun and carrier is

$$\omega_s = \left(\frac{r_a}{r_s} + 1\right) \omega_c - \left(\frac{r_a}{r_s}\right) \omega_a = (\alpha + 1)\, \omega_c - \alpha\, \omega_a \tag{8.11}$$

where $\alpha > 1$. By attaching the input axis of the gear reduction to the sun, the output axis will have angular velocity

$$\omega_o = \frac{1}{N}\, \omega_s. \tag{8.12}$$

We attach the CVT between two axes of the planetary gear, such that we get the relation

$$\omega_c = m\, \omega_a. \tag{8.13}$$

By combining (8.11), (8.12) and (8.13), we find the relation between input angular velocity ω_a and output angular velocity ω_o, which is the IVT reduction ratio n, being

$$n = \frac{\omega_o}{\omega_a} = (m - 1)\, \frac{\alpha}{N} + m\, \frac{1}{N}. \tag{8.14}$$

We can achieve a desired IVT range $n \in [n_{min}, n_{max}]$ with a given CVT range $m \in [m_{min}, m_{max}]$ by solving the following equation for the parameters α and N:

$$\begin{bmatrix} \dfrac{\alpha}{N} \\ \dfrac{1}{N} \end{bmatrix} = \begin{bmatrix} (m_{min} - 1) & m_{min} \\ (m_{max} - 1) & m_{max} \end{bmatrix}^{-1} \begin{bmatrix} n_{min} \\ n_{max} \end{bmatrix}. \tag{8.15}$$

Description	parameter	value
Given CVT range	$[m_{min}, m_{max}]$	$[\ 0.3 \dots 1.0]$
Desired IVT range	$[n_{min}, n_{max}]$	$[-0.5 \dots 0.5]$
Planetary gearhead ratio	$\alpha = \frac{r_a}{r_s}$	1.86
Gear reduction	N	2

Table 8.1: A numerical example of parameter selection for the IVT according to (8.15). The resulting parameters, are very feasible.

In order to show that the resulting parameters are feasible, table 8.1 shows a numerical example.

8.5 Control

At the moment we are working on the design of an optimal controller for the proposed actuator. The control strategy can be divided into two separate tasks: Recharging the spring and controlling the output torque with the IVT.

The control of the clutch causes the need for a hybrid control solution with two states. The challenge in the design of the controller is to find the optimal point when to switch on the motor. A large part of the gain in energy efficiency of the proposed V2E2 system lies in the fact that the DC motor can be used in its optimal (most efficient) point while recharging the spring. Depending on the energy transfer at the output shaft, the motor can be periodically switched on at its maximum efficiency. As an additional control law, it is necessary to stay away from the state $\varphi_S = 0$ at all times. The clutch does not necessarily need to be a controlled version. Its primary functioning can also be mechanically solved by using a one-way clutch, in the same way as the winding mechanism of a clock or a wind-up toy.

The IVT ratio is used for control of the output torque. Depending on the desired actuation profile, the ratio can be set at a fixed value, or needs to be changed during a (periodic) motion. Different control schemes apply for different actuation profiles. Consider the control of a walking (humanoid) robot. During a normal walking gait, the hip joint is powered using a periodic profile, requiring a large torque to start the swing-phase of a leg, and braking this motion at the end of the swing phase. For this profile, periodic switching of the IVT will be necessary, from a high gear ratio for the swing-phase torque to a reverse ratio at the end, enabling storage of braking energy in the spring. An example of this movement is shown in figure 8.7. This data has been taken from a simulation model of our

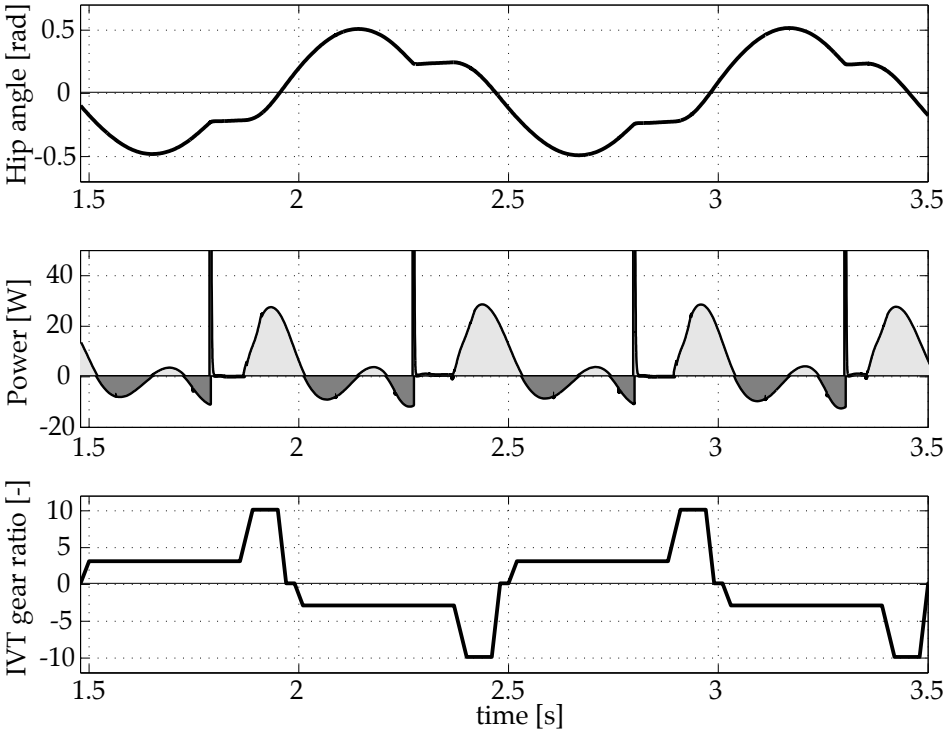

Figure 8.7: Simulation data of the 2D powered dynamic walker 'Dribbel', showing hip angle, injected power by the hip motor and IVT ratio when using the proposed V2E2 actuator.

2D walking robot (Dertien, 2006). The top graph shows the hip angle during a walking motion, the middle graph shows the power that is being injected by a DC motor in the hip (the part that lies below the zero line is the negative work that can be stored in the spring), the third graph shows an impression of the used IVT ratio. The spikes in the power graph are caused by the mechanical locking of the passive knee mechanisms.

During normal walking, the knee joint does not need to be powered (Collins et al., 2001; Dertien, 2006), so a very low ratio ($\approx [\infty : 1]$) can be used, resulting in zero torque as described in the previous section (however, adding a little power can increment the ground-clearance and may improve robustness). When the robot has to do other types of movement with the same joints, such as sitting down or standing up, high gear ratio's will be required because of the high torques involved. In this case it is not necessary to change the IVT ratio with a very high bandwidth.

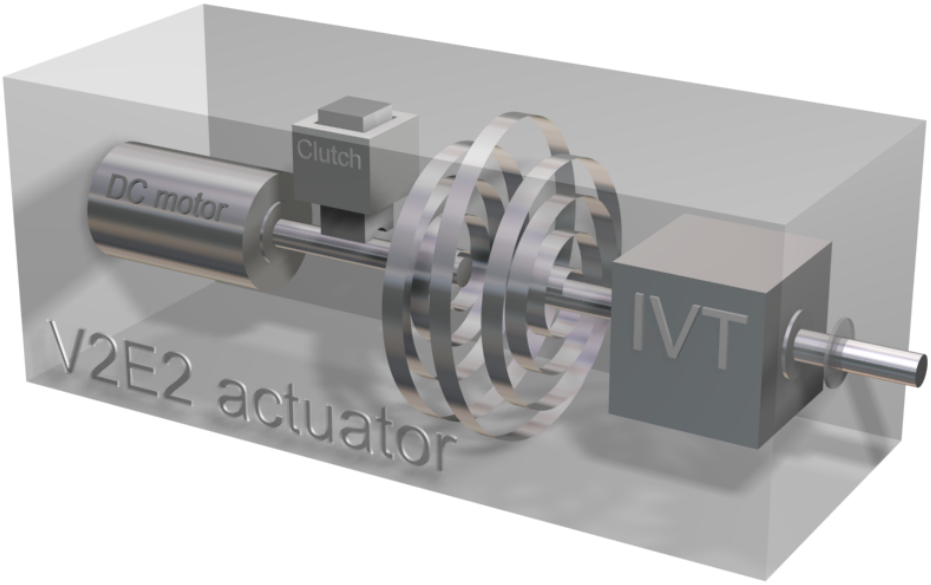

Figure 8.8: Conceptual sketch of the V2E2 actuator.

8.6 Conclusions and discussion

8.6.1 Proposed system

The concept for a novel embedded V2E2 actuator has been presented which is able to store negative work and create constant forces without conceptually any or small losses of energy. This device will have, in its final form a mechanical and an electrical interface. The mechanical interface will be used as a usual actuator. The electrical interface will have a power connection which will be used bidirectionally to use or charge a battery and a signal control to specify the desired torque on the axis. Internally, with a low power micro-controller, the actuator will take care of steering the device as required, controlling the electric DC motor, the IVT and the clutch. In figure 8.8 we have sketched the mechanical part of the new actuator.

8.6.2 Consequences for robotics

The future will learn how efficient the IVT under study will be. Other practical implementations and problems in the realization of the proposed actuator have

yet to be tackled, but if this will be successful, the implications for robotics will be substantial. In legged locomotion people either develop highly geared, fully actuated, robust but not efficient machines or minimally actuated, not robust, but extremely energy efficient machines. A machine which has the robustness of the first group and the energy efficient of the second as yet to come. Such actuators could drastically change this and this was originally the idea which brought the author to conceive V2E2 actuators. We could make a fully V2E2 actuated machine and control it using the most advanced nonlinear control methods without having to worry about the efficiency since the actuators would take care of that. Such devices would therefore bridge the gap which is still existing between advanced but complex and inefficient nonlinear control methods and simple non-robust minimalistic efficient approaches. In the opinion of the authors, this would be a major achievement for robotic locomotion.

8.6.3 Ongoing work

Some practical problems have still to be solved before the proposed concept will be applicable, first of all the realization of an efficient Infinitely Variable Transmission. A lot of progress has been made in this direction and the team of the authors is currently working on a patent. The authors believe that if the practical problems will be overcome, such an actuator could cause a revolution in the world of many robotic applications especially in legged locomotion and prosthetics.

8.A Acknowledgments

The authors would like to thank MSc. student Jos Ansink who worked on the IVT design and made vital contributions to the ideas expressed in this chapter.

Part III

Design

Chapter 9

Design and realization of an energy efficient knee-locking mechanism for a dynamically walking robot

This chapter is based on the following article (van Oort et al., 2011a):

An energy efficient knee locking mechanism for a dynamically walking robot
Gijs van Oort, Raffaella Carloni, Dian J. Borgerink and Stefano Stramigioli
Proc., IEEE International Conference on Robotics and Automation (ICRA'11)
pages 2003–2008, May 2011.

Abstract—**In this work, we present the design and the implementation of an innovative knee locking mechanism for a dynamically walking robot. The mechanism consists of a four-bar linkage that realizes a mechanical singularity for locking the knee when the leg is in the extended position. Once extended, the knee remains locked without energy consumption, while unlocking it only costs a small amount of energy. Tests showed that the robot walks robustly and that the energy consumption of the new system is low.**

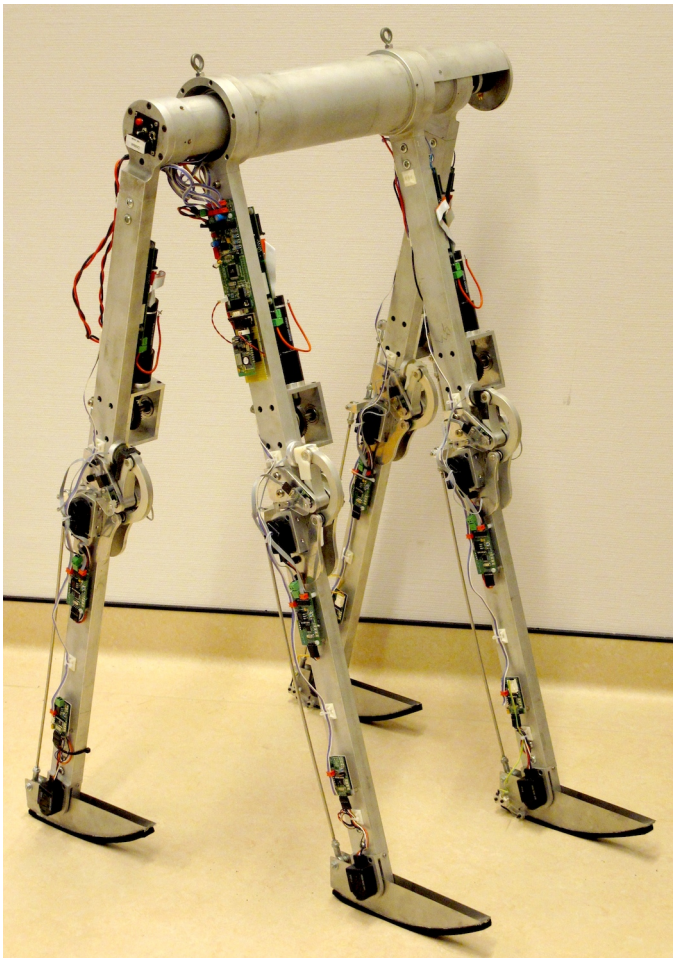

Figure 9.1: The dynamically walking robot Dribbel.

9.1 Introduction

The energy efficient bipedal walking robot Dribbel (figure 9.1), developed at the Control Engineering group of the University of Twente, has been built in order to demonstrate the potential dynamic walking (Dertien, 2005). Dribbel has a mass of 16.1 kg and its leg length is 0.95 m. Instead of using heavily geared motors, the knees of Dribbel have no motor at all. Nevertheless, the robot is able to produce a stable dynamic gait. In order to keep the legs extended during stance phase, the knees of Dribbel are equipped with a locking system.

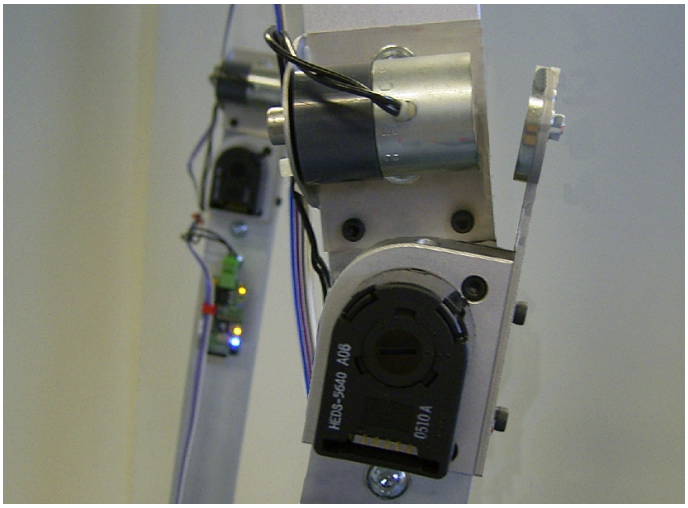

Figure 9.2: The old knee locking mechanism of Dribbel: An electomagnet pulling an iron disk (top right) towards itself. The magnet had to be turned on permanently in order to keep the knee locked.

The original knee lock design (figure 9.2) used electromagnets to keep the leg stretched. With these knee locks Dribbel was able to walk, but sometimes it stumbled, due to the fact that the mechanism failed to fix the leg. When, for example, the lower leg swung too fast, the electromagnets could not absorb all kinetic energy, resulting in a rebound of the leg.

Another problem of the knee locking mechanism was that the locking force was limited. The ankle push-off mechanism made by Franken (2007) (a bi-articular one, *i.e.*, the force runs over the knee and the ankle) produces large knee torques, sometimes resulting in a spontaneous unlocking of the knee.

A third disadvantage of the previous knee lock was that the mechanism consumed a significant amount (55 %) of the total energy of the robot (the electromagnets were switched on for 77 % of the time and consumed 17 of the total 31 W used by Dribbel).

We have conducted a study on different knee locking mechanisms (Reinink, 2009). Based on that, an innovative design was made, which uses a mechanical singularity to lock the knee — effortless. The advantages of the new mechanism over the previous electromagnet version are:

- Chances of rebound of the lower leg are much smaller,
- The mechanism uses only a small amount of energy to keep locked,

- The locking force is independent on the energy consumption of the mechanism; it is only dependent on the mechanical strength of the mechanism.

A prototype of the new knee mechanism has been built and tested (Borgerink, 2008). The results of these tests show that indeed the new knee mechanism is more reliable, stronger and more efficient than the electromagnet precursor. Based on these tests, a final design was made and implemented on Dribbel, which can now walk safer and more energy efficiently than before.

All dynamically walking robots with knees suffer from the problem of needing a knee mechanism. The first kneed walker, by McGeer (1993), did not have any locking mechanism at all; it only had a de-bouncing mechanism and an endstop. The 2D biped Mike, byWisse and van Frankenhuyzen (2003), used a mechanical latch and a solenoid for unlocking. The 3D walker by Collins and Ruina (2005) has an electromagnetic release system for a movable latch. At MIT, Baines developed a knee mechanism with a DC motor for actuation and an electromagnetic clutch for uncoupling the actuator from the knee (Baines, 2005). This mechanism was later improved by Reynolds (2006) by using bevel gears. Trifonov and Hashimoto (2007) tried a totally passive locking system with permanent magnets, but this could not be tuned well enough. Later they developed a mechanism with a locking hook.

In the world of prosthetics there are many patents on knee mechanisms. Many describe four-bar linkages that create a virtual rotation point outside the mechanism, or a virtual rotation point that moves during the flexion of the knee (Marlow, 1990; Townsend, 1994; Kramer, 1998). Generally, these systems are constructed such that exerting a pressure on the knee (*i.e.*, leaning on the extended leg) helps locking the system. Another four-bar mechanism is found in (Radcliffe, 1992), where the mechanism is constructed such that it acts as a pivot lock. A knee system with a dedicated locking hook is described by Townsend (2002). A locking system using a mechanical singularity is described by Hieronymus (2003), although it has noting to do with prostheses or robots (it is used for printing or varnishing machines).

This chapter is organized as follows. In section 9.2 we state the design requirements for our new knee lock. Then, in section 9.3 we present the new knee locking system and discuss some of the features. A few tests and measurements done on the new actuator itself and on Dribbel are described in section 9.4. Finally, before concluding, we show in section 9.5 how mechanical play (backlash) appears to be advantageous.

9.2 Design requirements

In this chapter, the knee angle, φ, is defined as the angle between upper and lower leg, where $\varphi = 0$ corresponds to a fully extended (*i.e.*, straight, not bent) leg, and a bent knee will give a positive value for φ.

In order to be suitable for our research on dynamically walking robots, the new knee locking mechanism has to meet the following requirements:

- The knee locking mechanism should be able to lock the knee when the leg becomes fully extended, preventing it from flexing again,
- When the knee is flexed (during swing phase), the mechanism's influence on the dynamics of the leg should be minimal,
- The mechanism should be energy efficient, lightweight and robust against falling.

The maximum amount of flexing torque expected is due to the push-off. From measurements on Dribbel, it is deduced the maximum flexing torque is in the range of 3–5 Nm. The lock mechanism should be able to withstand this. As no movement at all is needed during this torque, it would be logical to use a high transmission ratio n between the actuator used and the knee. Clearly, this is only needed when the leg is straight ($\varphi = 0$).

Dribbel has been designed to have a passive-dynamic walking gait, which means that the passive dynamics of the system dominate the movements (as opposed to actuators dominating the movement). Hence, the influence of the new knee lock on the dynamics should be minimized. Minimizing the mass of the mechanism is therefore important, as well as minimizing the added moment of inertia. It is desirable to have only a small transmission ratio n between the actuator and the knee, since a large transmission ratio would increase the apparent inertia of the actuator by n^2. This is important especially during the swing phase, when there is most movement of the leg and the leg is bent ($\varphi > 0$).

It is clear that we have contradicting requirements: on one hand the transmission ratio between the actuator and knee should be high in order to achieve a large locking torque with a small actuator, on the other hand it should be low in order to minimize the added inertia. Fortunately, these two requirements are needed in two different regions of the knee angle: large transmission ratio when the leg is extended ($\varphi = 0$), and small transmission ratio when the leg is flexed ($\varphi > 0$). Therefore, a system that links the transmission ratio and the knee angle may give us the best of both worlds.

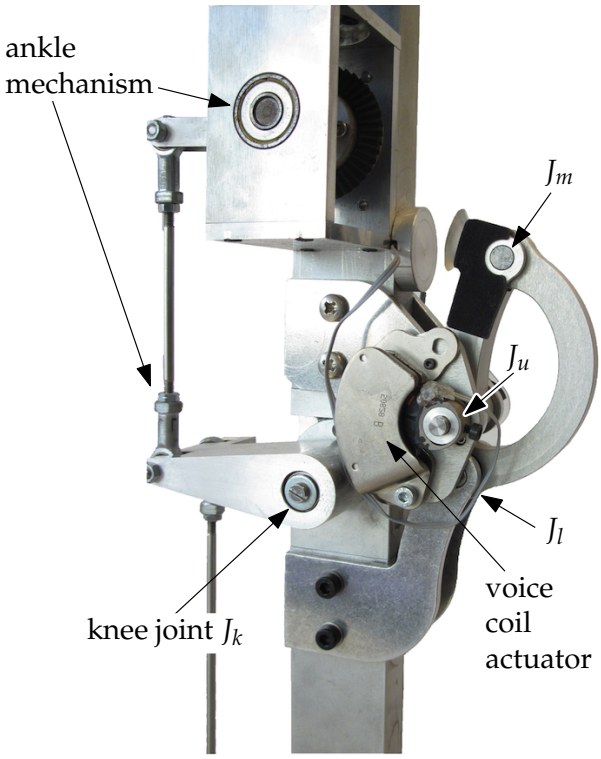

Figure 9.3: The new knee locking mechanism.

9.3 The new knee locking mechanism: The 'Beugel'

Figures 9.3 and 9.4 show the new knee locking mechanism. The mechanism (which is basically a four-linkages mechanism) consists of two rods, called the *motor arm* and the *connection rod*, connecting the upper and lower leg through rotational joints J_u (on upper leg), J_l (on lower leg) and J_m (on motor arm). The fourth joint is the knee joint J_k itself. The dimensions of the mechanism are shown in table 9.1. A voice coil actuator (VCA) (Buttolo et al., 1994) from a hard disk can exert a torque τ_{VCA} around J_u onto the motor arm. The angle of the motor arm is called α. At the end of the motor arm a suction cup with a small hole is mounted that can contact the end stop on the upper leg. There are also end stops on the lower leg which limit its range to $0 \leq \varphi \leq \pi/2$ rad.

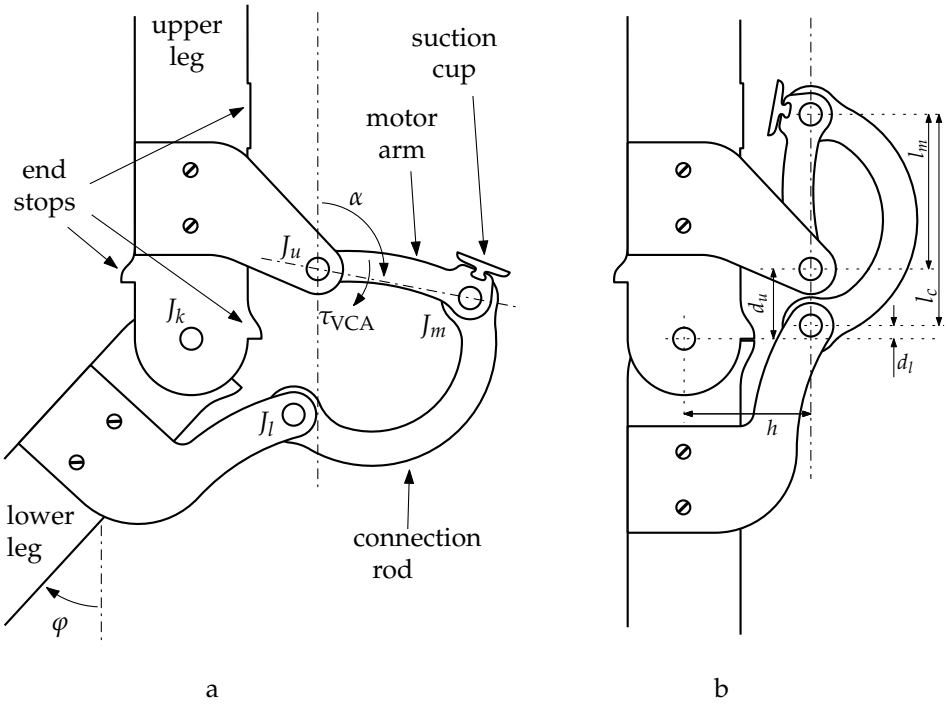

Figure 9.4: The new knee locking mechanism. a) Leg in flexed position; b) System in singularity (joints J_m, J_u and J_k lie on one line).

Description	Dimension	Length
Horizontal offset of J_u and J_l	h	45 mm
Vertical offset of J_u	d_u	25 mm
Vertical offset of J_l	d_l	5 mm
Motor arm length	l_m	55 mm
Connection rod length	l_c	75 mm

Table 9.1: Dimensions of the mechanism (see also figure 9.4).

9.3.1 Four-linkages mechanism

There is a fixed relation between the motor arm angle and the lower leg angle, as shown in figure 9.5. This relation is dependent on the exact geometry of the mechanism and was found using numerical optimization by Reinink (2009). The transmission ratio $n(\varphi)$ between motor arm angle (on which the actuator is mounted) and knee angle is the slope $n = \mathrm{d}\alpha/\mathrm{d}\varphi$ and is shown in figure 9.6. Indeed, we have the best of both worlds: a very large (even infinity) transmission ratio near $\varphi = 0$ and a small transmission ratio for a bent knee. The torque on the lower leg (around J_k) that the system can generate is $\tau_l = n(\varphi) \cdot \tau_{\mathrm{VCA}}$.

Figure 9.4a shows the leg in a flexed state. When the lower leg rotates, the motor arm (and thus the actuator) rotates with it at relatively low angular velocity ($\dot{\alpha} \approx \dot{\varphi}$). This does not influence the motion of the lower leg very much. When the knee is almost extended (φ is small), the motor arm will be almost vertical. A small angular displacement of the knee will now result in a large angular displacement of the motor arm (large transmission ratio, *i.e.*, $\dot{\alpha} \gg \dot{\varphi}$), and conversely, the actuator can exert a high torque on the lower leg.

Figure 9.4b shows the system in its mechanical singularity. The transmission ratio is infinity, implying that the lower leg cannot rotate at all and, irrespective of the (external) torque on the knee, the motor arm can be kept in place with minimum energy consumption. This is an unstable equilibrium.

The motor arm can go through the singularity, such that $\alpha < 0$. This way, the suction cup on the motor arm can contact the end stop on the upper leg. The lower leg is then flexed a minimal small amount. If an (external) flexing force acts on the knee, it will cause the motor arm to be pressed harder against the end stop. Hence the knee cannot be flexed any further, *i.e.*, the knee is locked.

The *apparent inertia* of a body, for example the leg, can be expressed as $I_{\mathrm{app}} = \frac{\tau}{\ddot{\varphi}}$ (where τ is the torque exerted on the joint), or, in words, the amount of torque needed for one unit acceleration. The apparent inertia of the lower leg (including the foot) consists of two parts: the inertia of the lower leg itself (including the foot) and the inertia added by the knee mechanism with actuator: $I_{\mathrm{app}} = I_{\mathrm{leg}} + I_{\text{knee-mech}}$. The former is fixed and was measured to be $I_{\mathrm{leg}} = 0.095\ \mathrm{kgm}^2$. The latter is heavily dependent on the transmission ratio $n(\varphi)$ and can be approximated by $I_{\text{knee-mech}} = n^2(\varphi) \cdot I_{\text{motor-arm}}$, for which we measured $I_{\text{motor-arm}} = 4.5 \cdot 10^{-5}\ \mathrm{kgm}^2$. In figure 9.7 the apparent inertia as a function of the leg angle is shown. Indeed, the influence of the mechanism in negligible for almost the whole range of motion of the lower leg, which is exactly what we desired. For very small leg angles (the leg almost extended), the inertia becomes large, which is not a problem because the leg does not need to swing freely anyway around those angles. Over the whole stroke of the system, the connection rod keeps more

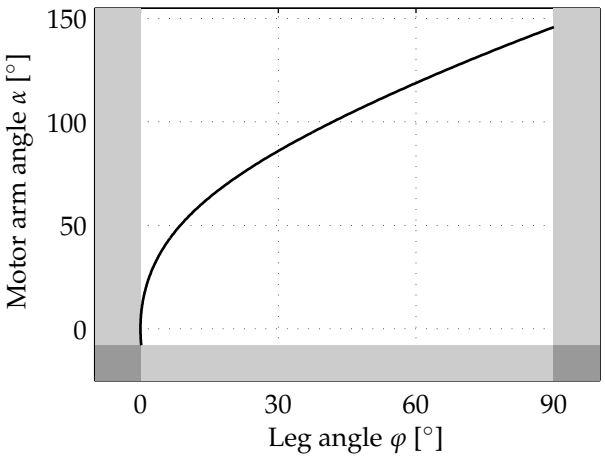

Figure 9.5: The relation between motor arm angle α and leg angle φ. The gray areas are areas where the system cannot go because of the end stops. The areas at the side are due to the end stops at the knee joint; the area at the bottom is due to the suction cup end stop.

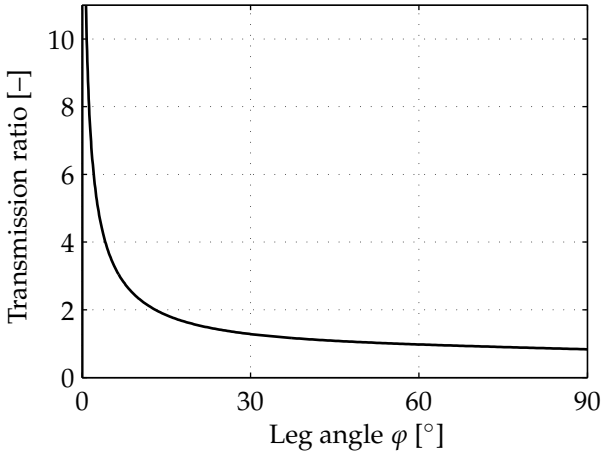

Figure 9.6: The transmission ratio between motor arm angle (where the actuator is situated) and leg angle. For very small leg angles (near leg extension) the transmission ratio is high — a large torque can be exerted. When the leg is flexed, the transmission ratio quickly decreases, allowing free leg swing. After the motor arm has past its singularity, the transmission ratio becomes negative. This is out of the the scale of the graph.

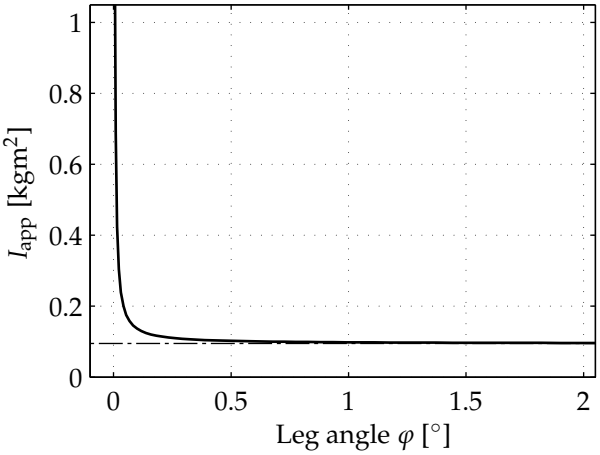

Figure 9.7: The apparent inertia I_{app} of the lower leg as a function of the leg angle. The dash-dotted line indicates the inertia of the lower leg $I_{leg} = 0.095\,\text{kgm}^2$ itself. When the leg is flexed, the knee locking mechanism barely increases the inertia, so its influence to the dynamics are negligible. When the leg is almost extended, the apparent inertia increases rapidly.

or less the same orientation; it only translates. This does not add much to the inertia at all and was therefore neglected.

The *impedance* of the knee actuator, as seen from the leg, can be expressed as $Z_{\text{knee-mech}}(j\omega) = \frac{\tau(j\omega)}{\dot{\varphi}(j\omega)} = j\omega I_{\text{knee-mech}}$. As $I_{\text{knee-mech}}$ is variable, the impedance is also variable. So, with right, we can say that we have a variable impedance actuator. However, instead of being able to vary the impedance separately (which is normally the case for a variable impedance actuator (Tonietti, 2005)), it is cleverly coupled to the leg angle, such that for each angle an appropriate impedance is obtained.

Although using the mechanical singularity of a four-bar linkage has, to our best knowledge, never been used to make passive knee locking systems for robots or prostheses, the idea to use mechanical singularities to lock things is not new, and it is frequently used. Our direct inspiration came from our local beer brewery Grolsch, that ships their beer in so-called 'swing top bottles[1]' (*Grolsch Beugels* in Dutch, hence the name for our device). Another example is the mechanism used to open and close small windows. These two examples are shown in figure 9.8. For comparison, we put the names used in this chapter on the equivalent parts in the mechanisms.

[1]The swing top bottle was invented in 1875 by De Quillfeldt (1875).

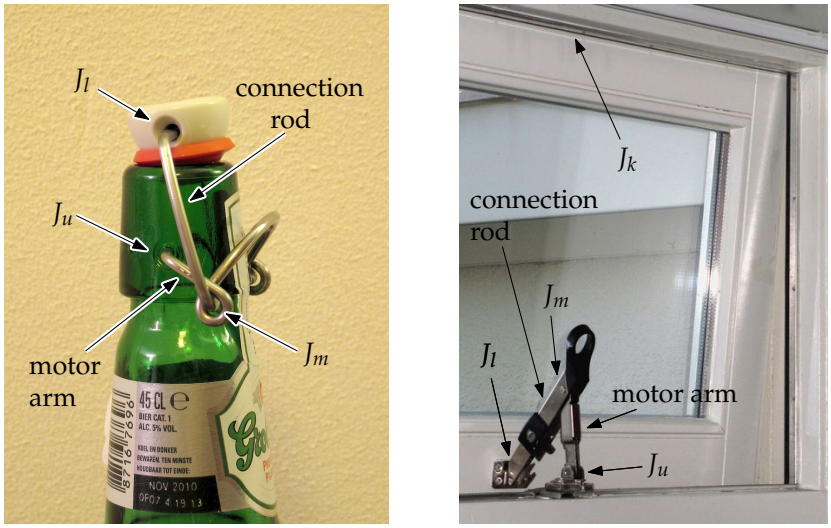

a b

Figure 9.8: Examples of other four-bar mechanisms using the mechanical singularity for locking. a) The Grolsch swing top bottle. The equivalent of J_k is absent; the mechanism only keeps J_l pulled towards J_u. b) A window opener.

9.3.2 Suction cup

Consider the event of locking the knee. When, during the end of the swing phase, the leg extends with velocity $\dot{\varphi}$, the motor arm will have an angular velocity $\dot{\alpha} = n\,\dot{\varphi}$. With the leg almost extended, n is very large and so will $\dot{\alpha}$ be. Because of its own inertia (which is small but not zero), the motor arm will still have a substantial angular momentum when hitting the end stop. It is essential that the motor arm does not bounce back too far, otherwise the system may become unlocked again. This is where the suction cup comes into play. A suction cup with a small hole in it is known to be able to absorb a lot of kinetic energy during collision, while having a minimum effect during non-collision. They were first used in McGeer's planar walking model with knees (McGeer, 1993). The working principle is as follows. At collision, the suction cup is pressed firmly against the end stop, squeezing out all air between the suction cup and end stop, generating a vacuum. The environmental air pressure then presses the suction cup against the end stop. A conventional (and ideal) suction cup would stick to the end stop forever, preventing the lock from opening during the next step. The small hole in our suction cups however, allows air to slowly leak into the space between the suction cup and end stop again, and after a while (typically a few tens of a second) the suction cup can be moved around freely again.

9.3.3 Actuator

The stroke of a typical voice coil motor from a hard disk is quite small (the one we used was 45°); from figure 9.5 it can be seen that the stroke of the VCA should be at least 155° (as it it fixed to the motor arm, it should be capable of rotating through the full range of α). Therefore, one of the end stops of the actuator was removed so that the voice coil can leave the magnet housing of the VCA when the lower leg flexes. Outside the magnet housing, the VCA cannot generate any torque. However, this is not a problem, because the knee should not be actuated when the leg is flexed anyway. In the range ($\alpha < 31°$) the VCA can exert torques, such that the system can be actuated. This is described in more detail in section 9.4.2.

9.3.4 Mechanical integration

Dribbel has been designed with modularity in mind. Mechanically, each joint is a separate unit which can be fit onto the robot with just eight (knee) or four (ankle) bolts. The new knee lock continues on this modularity. It was designed such that it does not require major adaptations on the robot itself. It forms an add-on that can easily be mounted using the eight bolts that fix the knee joint in the upper and lower leg.

9.3.5 Electronics

Dribbel's electronics are also modular. It has one master module, the main controller board, containing an ATMega128 microcontroller and 13 slave boards: a hip actuator module, four ankle actuator modules, four knee joint modules and four ankle sensor modules. Each slave module is equipped with an ATMega8 microcontroller to perform local tasks such as interfacing with sensors, doing elementary calculations and passing its status or other data to the main controller. Communication is done using a TWI field bus.

The original knee joint modules were designed to simply turn on or off the electromagnet through a power transistor. The modules were adapted to the new knee lock by adding a full H-bridge. This allows both positive and negative actuation of the VCA's, as well as PWM regulation.

9.3.6 Sensors

In order to properly control the knee mechanism, the angle of the motor arm needs to be known. An encoder was already available on Dribbel to measure

State	Motor arm region	Actuator action
Lock	Unlocked, out of VCA range	None
	Unlocked, within VCA range	Negative direction
	Locked	None
Unlock	Unlocked, out of VCA range	None
	Unlocked, within VCA range	Positive direction
	Locked	Positive direction

Table 9.2: Control strategy for the mechanism. For each of the two states the system can be in, the actuator action is shown for the different regions of the motor arm.

the knee angle, but this cannot be used to calculate the angle of the motor arm because the relation $\varphi = \varphi(\alpha)$ is non-injective (*i.e.*, for some knee angles φ there are multiple possible values for α). It would be possible to move the encoder from the knee to the motor arm and then calculate the knee angle from the motor arm angle, but in that position it is more vulnerable when the robot falls.

Therefore, a new, simple sensor was added to get information about the angle of the motor arm. A small study showed that for the type of control conducted at this moment, it sufficed to divide the total stroke of the motor arm into three regions and only know in which region the motor arm is. The regions are:

- Unlocked, out of actuation range: $\alpha \geq 31^\circ$,
- Unlocked, within actuation range: $0^\circ \leq \alpha < 31^\circ$,
- Locked: $\alpha < 0^\circ$.

A custom sensor was made using two simple optical sensors. Two small non-transparent plates connected to the motor arm move through these sensors to indicate in which region the motor arm is. The plates can easily be adjusted to fine-tune the system. It is also possible to save energy by turning the optical switches off when it is not important to know in which region the motor arm is (*e.g.*, during swing phase when is it certain that the knee is unlocked).

The control that is currently implemented in the new knee mechanism is straightforward. The knee locking system has two states: *lock* (try to lock the knee and keep it locked) and *unlock* (similarly defined). The main controller determines which state each knee should be in and sends the appropriate signals to the knee modules.

When the main controller sends the signal to lock, the VCA is actuated at full power in negative direction whenever the motor arm is not in the 'locked' region. In the 'locked' region, the VCA is turned off; as long as the motor arm is past

the singularity there is no chance for the leg to flex, thus no reason to actuate the mechanism. Also, the VCA is not powered if the motor arm is in the 'unlocked, out of actuation range'-region.

When the main controller sends the signal to unlock, the VCA is actuated at full power in positive direction until the motor arm is in the 'unlocked, out of actuation range'-region. In that region, the VCA is not actuated at all. Note that the controller always steers the system towards a low/no power region. Therefore, the current consumption is only large during the state transitions, not when in a state for a longer time. Table 9.2 gives an overview of the control strategy.

9.4 Tests and measurements on Dribbel

9.4.1 Locking strength

One of the problems of the old, magnetic knee lock was the limited locking strength. Theoretically, it should have been able to withstand a flexing force of 10 Nm (Dertien, 2005), but due to elasticity of the materials, the magnet and iron disk would un-align under the flexing force, thereby reducing the locking strength to only 3.5 Nm.

As stated earlier, the locking strength of the new system is independent on the actuator strength; it only depends on the mechanical strength of the parts, in particular the connection rod and the knee axis J_k. It is hard to measure how strong a system really is without irreversibly damaging it, so we only did a non-destructive test to determine a minimum strength. Therefore, we clamped the upper leg in a horizontal position and exerted a downward force on the foot (at a distance of 0.43 m from the knee joint). The maximum force we applied was 60 N, *i.e.*, 26.1 Nm. The mechanism could withstand this force with ease. Hence, at this aspect the new knee mechanism is at least seven times as good as the old one.

9.4.2 Torque of the actuator

As stated earlier, the voice coil actuator cannot exert torques over the whole stroke. An experiment was done to investigate this. A positive voltage of 12 V was put on the VCA and the resulting torque τ_{VCA} was measured for a range of angles, see figure 9.9. There is a negative torque range around $\alpha = 0^\circ$ and a less powerful positive torque range (around $\alpha = 60^\circ$). At $\alpha = 31^\circ$ the actuator provides no torque. In figure 9.10 it is shown how this torque translates to a torque

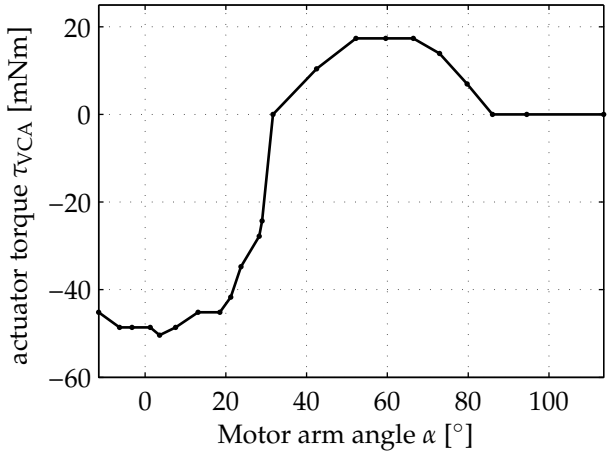

Figure 9.9: The torque of the VCA τ_{VCA} as a function of the motor arm angle α for a voltage of 12 V.

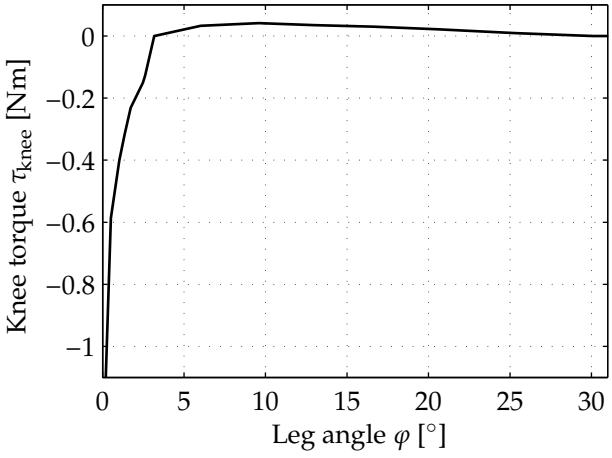

Figure 9.10: The torque on the knee joint τ_{knee} that the knee mechanism can generate.

around the knee joint, by using $\tau_{knee} = n(\varphi) \cdot \tau_{VCA}$. We chose to only use the range $\alpha < 31°$ (thus $\varphi < 3°$) for actuation, since the torque for larger angles is very small. Of course, within the region $\alpha < 31°$, positive torques can be exerted by applying a negative voltage.

9.4.3 Power consumption of the knee mechanisms during normal gait

When fully powered ($U = 12$ V), the VCA of the knee mechanism takes approximately $I = 0.39$ A, which results in a power consumption of $P_{\text{VCA}} = U \cdot I = 4.7$ W for each actuator. This is a significant amount, but it should be remembered that most of the time the actuators don't have to work at full power. During a normal walk, we measured the average actuation time for each actuator to be approximately 10 % of the gait cycle, which implies that the four knee locks together consume approximately 1.9 W.

9.4.4 Total power consumption, specific cost of transport

The specific cost of transport C_{et} is a non-dimensional indicator of the energy-efficiency of transportation. It equals the amount of (electrical) energy needed to transport a unit weight over a unit distance:

$$c_{et} = \frac{E}{m \cdot g \cdot d} = \frac{P_{\text{avg}}}{m \cdot g \cdot v_{\text{avg}}} \tag{9.1}$$

where E is the energy used, m the mass of the system, g the earth's gravitational acceleration, d the distance traveled, P_{avg} the average power consumed and v_{avg} the average velocity.

In order to obtain the average power consumption, we made Dribbel walk and recorded the power consumption as a function of time. Over four typical, consecutive steps, we measured an average power consumption of 27.7 W. The hip actuator was controlled by a simple PD controller that instantaneously switches the setpoint for the inter-leg angle when the front foot touches the ground (similar to Wisse et al. (2005), but with the difference that we used very low controller gains such that the swing phase more or less resembles natural swinging motion).

Dribbel's velocity was measured by making it walk 14 consecutive steps, covering a distance of 4.0 m. This took 14.0 s, giving an average velocity of $v_{\text{avg}} = 0.29$ m/s. Together with the mass of Dribbel being 16.1 kg, we find a specific cost of transport of $c_{et} = 0.60$. Table 9.3 shows some important specifications of Dribbel.

9.5 How mechanical play is —for once— our friend

When we first implemented the new knee mechanisms on Dribbel, the system did not work entirely as expected. Often, the motor arm did not pass its singularity

Description	Value	
Average step length	0.29	m
Average step time	1.0	s
Average velocity	0.29	m/s
Power consumption	27.7	W
Specific cost of transport	0.60	–

Table 9.3: Specifications of the gait of Dribbel.

during knee-strike, and when it did, it did not go to the end stop but was pushed back towards the singularity (which is unwanted because a small disturbance on the motor arm could cause it to move into the unlocked region again). The behavior was also heavily non-reproducible: one day it could work very well; the other day it could fail all the time. We identified the source of the problems: the singularity itself.

For the motor arm not passing the singularity during knee-strike, we found two opposing causes. The system was designed such that it could be fine-tuned easily (the positions of J_l and J_u can be changed a few mm by loosening and retightening the eight construction bolts, resulting in a slight change of the relation between the lower leg angle and motor angle (the curve of figure 9.5 would be shifted a little). However, it was very hard to tune it such that the curve would *exactly* go through the point $(\alpha, \varphi) = (0, 0)$. Moreover, temperature changes, shocks or falls of the robot could de-tune the system easily. The actual relation could be such that when $\alpha = 0$ then $\varphi < 0$, *i.e.*, the curve is shifted somewhat to the left. The end stop in the knee would not allow the lower leg to have a negative angle, implying that the motor arm could never pass the singularity. Oppositely, the relation could be such that when $\alpha = 0$ then $\varphi > 0$, *i.e.*, the curve is shifted somewhat to the right. In this case, the motor arm can move through its whole stroke. Near the singularity, the lower leg exerts a large force on the motor arm, perpendicularly to its moving direction. This force creates a lot (theoretically: infinity) of friction in the rotational joints. Because of this friction, the motor arm would stop moving, again not passing its singularity.

From figure 9.5 it can be seen that when some external torque on the lower leg would force it to be fully extended, the motor arm will be pushed towards the singularity, diminishing the robustness of the lock (the motor arm could easily go past the singularity, thereby unlocking). The VCA could of course be used to counteract this movement, but this consumes power, which is unwanted.

In order to solve all these problems, we deliberately created play into the system: we made the hole on joint J_l approximately half a millimeter larger than the axis. The result is that the motor arm and lower leg are now able to move a little,

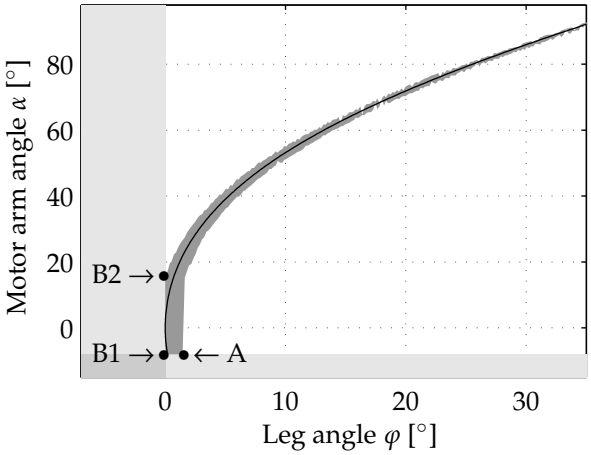

Figure 9.11: Measurement of the relation between the motor arm angle and lower leg angle. Due to the mechanical play, there is no exact coupling between the two. The black line indicates the theoretical no-play situation. Point A: self-locking point when there is a bending moment on the lower leg. Line B1B2: The range of motor arm angles 'compatible' with a fully extended leg.

independently from each other. Figure 9.11 shows all possible combinations of motor arm and lower leg angles. From the figure, a few interesting observations can be made. There is still a single point (point A) where the bending moment of the knee self-locks. Due to the play it has moved a little bit (the leg is more flexed), but practically this cannot be noticed. The real benefit is in the line B1B2. This line shows that, when the leg is fully extended ($\varphi = 0$, against the leg's end stop), the motor arm can move freely all the way from its end-stop (B1) to a point past the singularity (B2): as long as $\varphi = 0$, the motor arm movement is fully uncoupled from the leg for a quite large stroke.

Fine-tuning (or accidental de-tuning), may still shift the curve (which is now actually a region) of figure 9.11, but now there is a tuning margin for which the point $(\alpha, \varphi) = (0, 0)$ is within the region. Hence, the motor arm is always able to pass the singularity when the leg is fully extended. Moreover, when the leg is fully extended by an external torque, all torque is counteracted by the leg's end stop; the leg does not exert any force on the motor arm anymore. This way, we have got rid of the friction issues and the motor arm will not be pushed back towards the singularity. The motor arm can be held against its end stop easily by a small amount of power on the VCA, greatly reducing the chances of accidental unlocking.

This means that by creating play in the system, we made it more robust and far less sensitive to tuning. A super-simple solution with great benefit!

9.6 Conclusions and future work

We have designed, implemented and tested a new knee locking mechanism for the energy efficiently walking robot Dribbel. It uses a four-bar mechanism and a mechanical singularity for locking the knee in extended position. Once extended, the knee remains locked without energy consumption, while un-locking only costs a small amount of energy. We used suction cups for passive de-bouncing of the system, which has been proven to be an effective method. A simple controller was implemented that is locally executed by the knee-module. The tests showed that the knee locks function well, that the energy consumption indeed has decreased and the robot walks robustly.

Future work will focus on improving the control algorithm. Firstly, the energy consumption could be further decreased by actively monitoring the exact movement of the motor arm, and only activate the VCA if strictly necessary. For example, when locking, if the motor arm is already moving towards the end stop with enough velocity, it is not necessary to help it by turning on the VCA. Secondly, the VCA could be used for active de-bouncing. If, when locking, the motor arm goes really fast, the VCA could be used to decelerate it, reducing the chance of a rebound. Both enhancements require more accurate measurement of the motor arm angle α, which will be provided by a more accurate sensor.

Chapter 10

New ankle actuation mechanism for a humanoid robot

This chapter is based on the following article (van Oort et al., 2011b):

New Ankle Actuation Mechanism for a Humanoid Robot
Gijs van Oort, Roelof Reinink and Stefano Stramigioli
Proc., 18th IFAC World Congress (IFAC'11)
August 2011.

***Abstract*—In this chapter we discuss the design of a new ankle actuation mechanism for the humanoid robot TUlip. The new mechanism consists of two coupled series-elastic systems. We discuss the choice of actuators according to calculations for maximum achievable walking speed. Some control issues, MIMO and non-linearities are also discussed.**

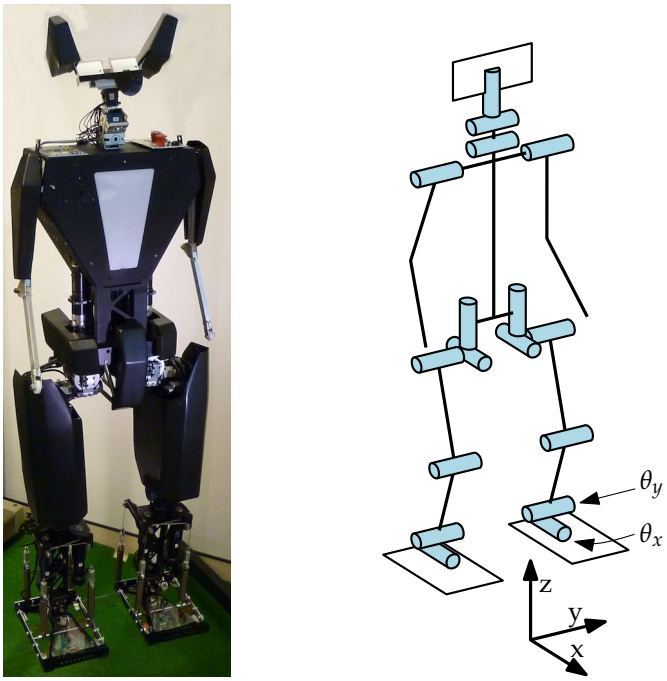

a b

Figure 10.1: a) The humanoid robot TUlip; b) Overview of the degrees of freedom of TUlip, the definition of the x-, y- and z-axis and indication of the ankle joints θ_x and θ_y.

10.1 Introduction

The field of humanoid robots gets more and more attention nowadays. As batteries, actuators and computers have become better, it has been increasingly more easy to build nice-looking well-working robots from off-the-shelf components.

In a collaboration project, the three Technical Universities of the Netherlands (University of Twente, University of Delft and University of Eindhoven) are developing a humanoid robot called TUlip (figure 10.1a). The robot was designed to compete in the RoboCup robotic soccer competition. Contrary to most other humanoid robot projects, where the focus lies on developing advanced controllers for a mechanical system based on very simple principles[1], we try to follow the

[1] Although these robots are, from a mechanical point of view, amazingly nicely designed, the underlying principle is old-fashioned: just heavily geared motors on each of the joints. This is in contrast to humans, which have a great level of compliancy in their muscles.

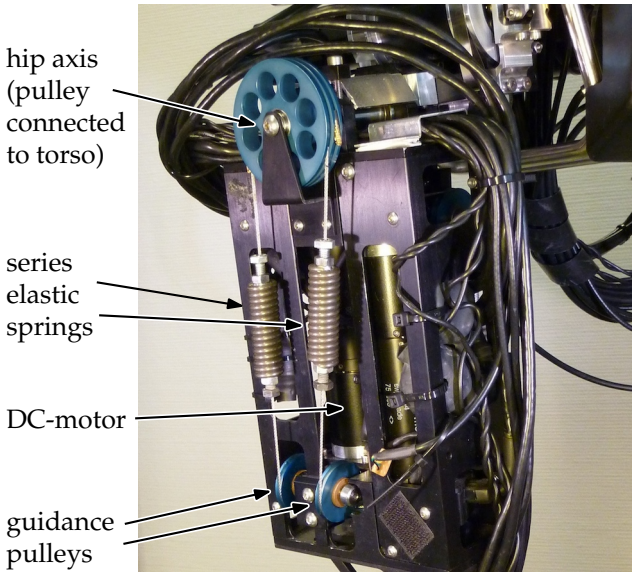

Figure 10.2: The series-elastic joint for the hip motion. Inside the upper leg a DC motor is situated (with its output axis pointing downward). On the output axis there is a pulley that actuates the cables with springs. The large pulley is fixed to the torso.

more mechatronic approach: solve each problem in the domain where it can be solved best. As an example, the hips and knees of TUlip are actuated by a *series elastic actuator* (SEA) (Williamson, 1995). Amongst others, this makes the system less vulnerable for shocks, for example on foot impact. Hence, at the control we don't have to cope with avoiding shocks anymore.

The main research goal for TUlip is research on 'limit cycle walking' (Hobbelen, 2008). In limit cycle walking, the goal is not to be stable at each time instant, but just have a stable cycle; during the cycle the robot can be unstable, *i.e.*, 'falling' for some time. This is in contrast to the so-called ZMP-type of walking, where tight control makes sure that the robot is always fully supported by the floor.

TUlip is 1.37 m in height and has a mass of 19 kg. It has 17 degrees of freedom: six in each leg, one in each arm and three in the neck (figure 10.1b). The sagittal (fore-aft) motion of the hip and the knee are equipped with a series elastic actuator as shown in figure 10.2.

The original ankle mechanism on the robot had one active degree of freedom (sagittal, rotation around the y-axis, called 'ankle-y') and one passive degree of freedom(lateral; rotation around the x-axis; 'ankle-x'). Due to the passive degree of freedom, the robot could not balance on one leg; it would fall sideways. Also

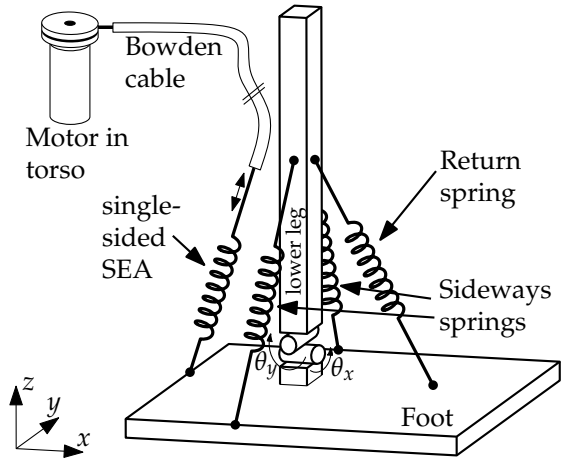

Figure 10.3: Schematic view of the old ankle mechanism. The rotation joints for sagittal movement (θ_y) and lateral movement (θ_x) are decoupled. There is no actuation for lateral movement; instead the foot is kept more or less in its default position by two stiff springs.

the actuation principle for ankle-y was far from satisfactory. In order to improve the performance of TUlip, a new ankle mechanism was designed and built, which is the topic of this chapter.

This chapter is organized as follows. In section 10.2 the previous design of the ankle is described. We show what was wrong with it and how it could be solved. Then, in section 10.3 we will investigate in more detail what the new ankle actuation mechanism should be capable of. The design is discussed in 10.4. Before concluding we dive into control issues of the system in section 10.5.

10.2 Old ankle design

A schematic view of the old ankle design is shown in figure 10.3. There are two rotation axes involved: 'ankle-x' (for sideways movement) and 'ankle-y' (for fore-aft movement). As shown in the figure, these are not coupled. The two joints are discussed one by one here.

10.2.1 Lateral joint (ankle-x)

There is no actuator for lateral (sideways) movement; instead the foot is kept more or less in its default position by two springs ($K \approx 15$ kN/m). The springs

are not strong enough to stabilize the robot passively when standing on one leg; neither were they intended to. The idea behind this set-up was to allow the robot to rock from one foot to the other (instead of going to a stable equilibrium on one leg); a prerequisite for dynamic walking. The rocking frequency can be tuned by changing the equilibrium position of the springs.

However, standing on one foot during a kick is really hard. Using Acrobot-like control (Hauser and Murray, 1990) was considered nearly impossible, due to the limited actuation range in the hip and the need to do other tasks simultaneously, such as ball kicking. Moreover, severe torso motions make it impractical or even dangerous to catch the robot when it is falling. Therefore, we decided not to try this and improve the mechanics instead.

10.2.2 Sagittal joint (ankle-y)

The sagittal (fore-aft) motion is unilaterally actuated, *i.e.*, the foot can be rotated actively in one direction but not in the other. A DC motor placed in the torso is connected to a bowden cable with series-elastic spring, which in turn is connected to the rear of the foot. Pulling the bowden cable makes the foot plantarflex (*i.e.*, toes down). A return spring on the front of the foot makes the foot dorsiflex (*i.e.*, toes up) again when the cable is loosened again.

The main reason why this design choice was made was to keep the weight of the lower leg and foot as low as possible. By putting the motor in the torso, the lower leg and foot only had to be some structural pieces of aluminum, without any heavy structures for actuation. The system however did not work as expected. In order to be able to dorsiflex the foot with a large enough torque, the return spring had to be quite stiff. This implied that the actuator had to deliver a large torque just to keep the foot still (in order to obtain a zero resultant torque). The induced tension in the bowden cable in its turn caused an enormous amount of friction, which made it virtually impossible to do precise control.

10.3 Requirements for new design

For the new actuator mechanism we had a few qualitative as well as quantitative requirements. Qualitatively, the system should not suffer from the problems described in the previous section, so unilateral actuation, bowden cables and underactuation were not an option. Furthermore, the system should be robust and as lightweight as possible. If mounted on the lower leg, its position should be as high as possible in order not to disturb the passive-dynamic swing properties of the leg too much (Franken, 2007). One of the demands is that the actuation is

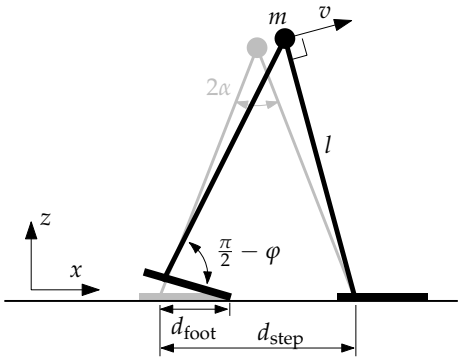

Figure 10.4: Simple 2D model of our robot: a compass walker with feet.

done in a series-elastic way. This reduces shock loads on the motors and gives us the possibility to mimic zero-torque control.

Quantitatively, the most demanding task for the system is supplying enough energy during push-off in order to compensate for the energy lost during impact. This is not only a matter of much torque, but also of speed: the foot must plantarflex fast enough in order to stay in contact with the ground during push-off. For the determination of these requirements, we look at the system as if it were a 'simplest walker' (Garcia et al., 1998) with flat feet: a 2D, bipedal walker with leg length l, a point mass m at the hip and negligible foot mass (figure 10.4). The inter-leg angle is denoted by 2α, the angle between the rear foot and leg by $(\frac{\pi}{2} - \varphi)$. The distance from ankle to toe is d_{foot} and the velocity of the hip is denoted by v. We assume post-impact push-off, which is the first strategy that we want to implement using the new ankle mechanism[2]. The model used implies an instantaneous inelastic swing foot collision. Contrary to the simplest walker without feet, the double support phase of this model is not instantaneous: the toe of the new swing foot keeps in touch with the ground for a short period T_p. During this period, the ankle actuator can exert a torque which results in an acceleration of the hip. The quantitative requirements regarding acceleration and velocity of the actuator are derived in the following two subsections. As the objective the maximum walking velocity is taken. A few important parameters of the actual robot (that are used in the compass model as well) are listed in table 10.1.

[2]Pre-impact push-off has been shown to be more energy efficient than post-impact push-off (Kuo, 2002), so if the new mechanism can achieve post-impact push-off, it is also able to do pre-impact push-off.

Parameter	Name	Value
Leg length	l	0.55 m
Step length	d_{step}	0.40 m
Mass	m	19 kg
Foot length	d_{foot}	0.145 m
Foot rotation limit	$-0.37 < \varphi < 0.18$	rad
Foot rotation stroke	$\Delta\varphi$	0.55 rad

Table 10.1: Robot parameters for the compass walker model.

10.3.1 Acceleration dependency

In this subsection the relation between rotational acceleration of the foot (during push-off) and achievable walking velocity is derived. Denote the velocity of the hip by v and its acceleration by a. Assume that just before foot impact the velocity of the walker is v_{pre}. Because of impact loss, the velocity just after impact (but before push-off) is $v_{\text{post}} = v_{\text{pre}} \cos(2\alpha)$ (Garcia et al., 1998). So the kinetic energy loss is

$$E_{\text{impact-loss}} = \tfrac{1}{2} m (v_{\text{pre}}^2 - v_{\text{post}}^2) = \tfrac{1}{2} m (1 - \cos^2(2\alpha))\, v_{\text{pre}}^2. \tag{10.1}$$

By applying a push-off torque on the ankle, the ankle actuator can inject energy into the system, being the product of the exerted torque and the stroke. If we use a constant push-off torque τ, we obain

$$E_{\text{injected}} = \tau \cdot \Delta\varphi = J\ddot{\varphi} \cdot \Delta\varphi \tag{10.2}$$

where J is the apparent moment of inertia, *i.e.*, the amount of torque required for one unit rotational acceleration, which can be calculated as follows. The relation between hip velocity v and foot rotational velocity $\dot{\varphi}$ and between acceleration a and $\ddot{\varphi}$ are approximately

$$v \approx -\frac{d_{\text{foot}}}{\sin 2\alpha}\dot{\varphi} \Rightarrow a \approx -\frac{d_{\text{foot}}}{\sin 2\alpha}\ddot{\varphi}. \tag{10.3}$$

Because we assume the only mass is in the hip, all power delivered by the ankle actuator will flow into acceleration of the mass, *i.e.*,

$$P = \tau\,\dot{\varphi} = F_v\, v \Rightarrow J\ddot{\varphi}\,\dot{\varphi} = ma\, v \tag{10.4}$$

where F_v is the component along the velocity vector v of the resulting force on the hip. Filling in (10.3) yields

$$J \approx \left(\frac{d_{\text{foot}}}{\sin 2\alpha}\right)^2 m. \tag{10.5}$$

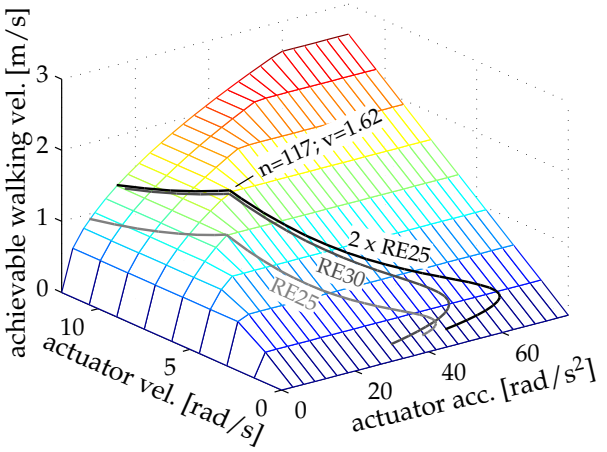

Figure 10.5: The maximum achievable walking velocity as a function of the maximum actuator angular acceleration and angular velocity, as described in section 10.3. The three thick lines correspond to a single Maxon RE25 motor, two RE25's (differential setup) and a single Maxon RE30 motor, with varying gear reduction ratios (section 10.4.3). The best walking velocity ($v = 1.62$ m/s) is obtained for the differential setup of two RE25 motors with (twice) a gearbox reduction of 1:117.

In order to obtain a limit cycle, it is necessary that the kinetic energy of each step is the same. This implies that the amount of injected energy should equal the amount of lost energy, *i.e.*, $E_{\text{impact-loss}} = E_{\text{injected}}$. Combining (10.1) and (10.2), we can calculate the achievable walking velocity v_{pre} for any foot acceleration $\ddot{\varphi}$:

$$v_{\text{pre,achievable,acc}} = \sqrt{\frac{2J\Delta\varphi}{m(1-\cos^2(2\alpha))}\ddot{\varphi}} \approx \frac{d_{\text{foot}}\sqrt{2\,\Delta\varphi}}{\sin^2(2\alpha)}\sqrt{\ddot{\varphi}}. \tag{10.6}$$

10.3.2 Velocity dependency

At the end of the push-off phase, the foot must rotate fast in order to keep the toe on the floor (otherwise, it is not able anymore to push-off). Equation (10.3) tells us that, when we have a certain maximum rotational velocity $\dot{\varphi}$, the walker can walk at a certain maximum velocity, being

$$v_{\text{pre,achievable,acc}} \approx -\frac{d_{\text{foot}}}{\sin 2\alpha}\dot{\varphi}. \tag{10.7}$$

In order to walk at a desired velocity v, we need both a minimum acceleration (equation (10.6)) and a minimum velocity (equation (10.7)), *i.e.*,

$$v_{\text{achievable}} = \min(v_{\text{pre,achievable,acc}}, v_{\text{pre,achievable,vel}}). \tag{10.8}$$

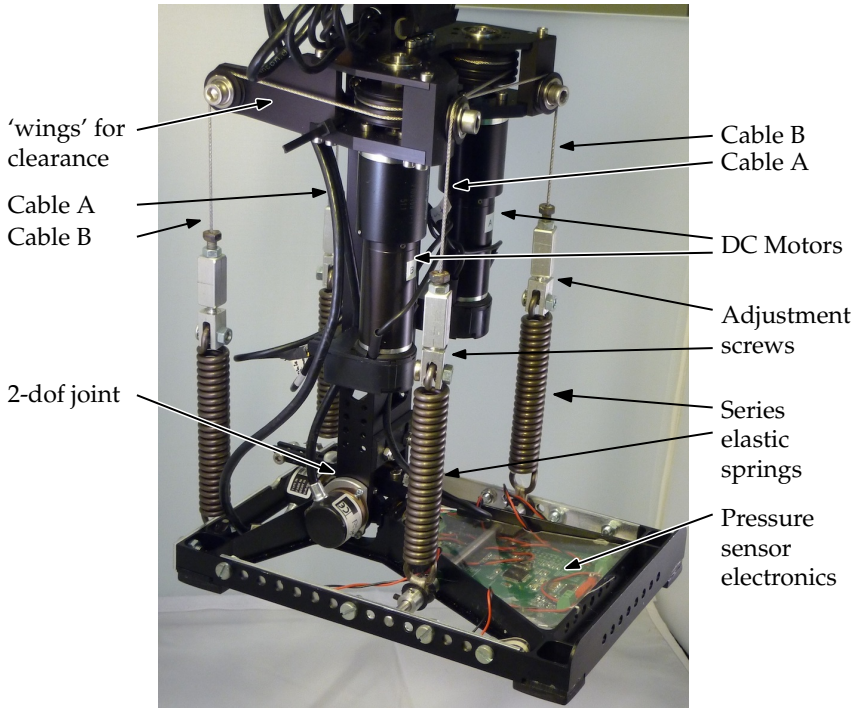

Figure 10.6: The new ankle actuation system of TUlip.

In figure 10.5 the maximum achievable velocity for our walker is shown as a function of the maximum acceleration and velocity that an actuator can generate. Now, for any choice of actuator, we can calculate the maximum velocity and acceleration and, from the graph, read out the maximum achievable walking velocity. This will be done in section 10.4.3.

10.4 New design

In this section we describe the innovative design of the new ankle actuation mechanism. Firstly we give an overview of the system, then we discuss some of the properties in more detail.

Figure 10.6 shows our new system. Two Maxon RE25 DC motors (A and B) are connected to the foot through cables with series-elastic springs. The motors are mounted in a differential set-up: both motors act on both the x-axis and y-axis simultaneously. The cables are guided along 'wings', mounted on the sides of the leg, so that the lower leg can flex without the wings touch the upper leg.

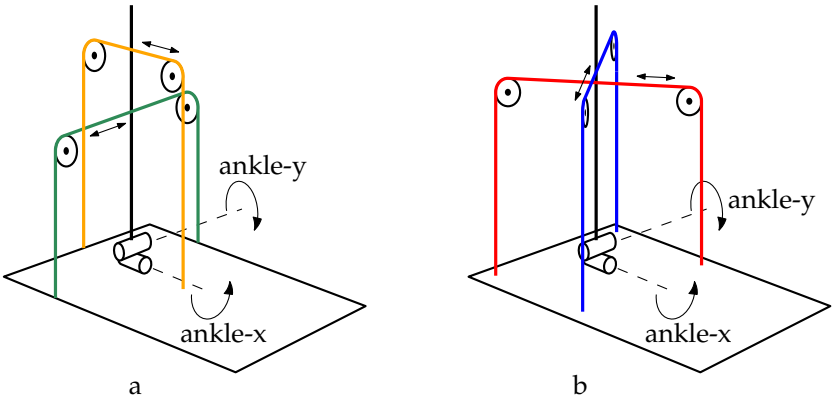

Figure 10.7: Ankle actuation concepts. (a) In an uncoupled setup, one motor drives the ankle-x and another the ankle-y joint. (b) In a differential setup the sum of the actuator motions drives the ankle-y and the difference the ankle-x.

10.4.1 Series elastics

Series elastic actuation can be implemented in different ways. For the new ankle actuation design, the same implementation is used as on the other SEA joints on TUlip: a system consisting of pulleys and cables with springs. It has proved to function well, and routing of the cables gives freedom in the placing of the actuator at a convenient place.

10.4.2 Differential setup

Conventionally, one would simply use one motor for actuation of the x-axis and the other motor for actuation of the y-axis (figure 10.7a). We chose however to merge the two axes in a so-called *differential setup*, where both motors act on both axes (figure 10.7b). When the motors turn in the same direction, the foot rotates about the y-axis; when they turn in different directions, the foot rotates about the x-axis.

The advantage of the differential setup is that both motors can work together in the joint direction that has the largest demand on the torque. Therefore the required maximum torque per motor is lower and lighter motors can be used for the same performance. A consequence is that the maximum torque in diagonal direction decreases to the torque of a single one of the actuators. Also, a more complex (MIMO) controller has to be designed because the motions of the x-axis and y-axis are coupled.

10.4.3 Actuator choice

For TUlip the RE line-up of motors by Maxon is used. They have a good performance versus weight ratio and there is good experience with them at the department. We considered two motors: the RE25 (a 20 W motor) and the RE30 (a 60 W motor). Smaller motors are unlikely to be powerful enough and stronger models are unlikely to be needed, and would certainly be too heavy.

The amount of acceleration that a motor can produce is not only dependent on the amount of torque it can generate, but also on the actuator's own inertia (this is the reason that we expressed the actuator demands in acceleration instead of torque in section 10.3.1). The angular acceleration that can be achieved by a DC motor with maximum motor torque $\tau_{\text{mot,max}}$, gearbox ratio n and gearbox efficiency $\eta = 0.7$ is

$$\ddot{\varphi}_{\max} = \frac{n\,\tau_{\text{mot,max}}\,\eta}{J + n^2 J_{\text{mot}}}, \tag{10.9}$$

where J is the moment of inertia of the load and J_{mot} is the moment of inertia of the motor and gearbox. The maximum angular velocity of an actuator is simply

$$\dot{\varphi}_{\max} = \frac{1}{n}\,\omega_{\text{mot,max}}, \tag{10.10}$$

where we assume that the friction in the joint is negligible relative to the motor friction (this is a valid assumption because the joint velocity is small relatively to the motor velocity and we use ball bearings in the joint axes). With these two equations and the motor parameters (table 10.2), we can plot a point in figure 10.5 and read, for the specific actuator, the maximum achievable walking velocity. In the figure we have plot three lines, representing a single Maxon RE25, a Maxon RE25-pair in differential setup and a single Maxon RE30 motor, all with varying gearbox ratio.

It seems that we can get approximately the same performance for a single RE30 and two RE25s in differential setup. The difference is that, in the case of one RE30 driving ankle-y we need another motor (an RE25) for ankle-x, while in the differential setup, two smaller motors suffice for both axes. Hence, the total system is lighter without giving in on performance.

The ideal transmission ratio of 1:117 should be the total ratio between revolutions of the DC motor axis and the foot. On top of the gearbox, there is also a small pulley-system involved, of which the transfer ratio can be freely chosen (up to some limits). The total ratio is then the product of the gearbox ratio and the pulley system ratio.

Parameter	Name	RE25	RE30	Unit
Rotor inertia	J_{mot}	10.7	33.3	gcm^2
Nominal speed	$\omega_{\text{mot,max}}$	875	842	rad/s
Maximum torque*	$\tau_{\text{mot,max}}$	129	259	mNm
Mass	m_{mot}	130	238	g

* For the RE25 we took half the stall torque as the maximum torque (this is already much more than the allowable continuous torque). For the RE30 we took the torque at $I = 10$ A as maximum torque, as that is the maximum that our motor amplifiers can deliver.

Table 10.2: Parameters of the Maxon RE25 and Maxon RE30 motors.

10.5 Control

Control of 'normal' series elastic actuation systems, such as in the hips and knees of TUlip (figure 10.2) has been studied intensively (Williamson, 1995; Robinson, 2000). Our new ankle actuation system differs from the 'normal' series elastics in two ways:

- The system consists of two coupled series elastics, *i.e.*, it is a multiple-input-multiple-output (MIMO) system,
- The system is nonlinear with respect to ankle position.

We will address these issues one by one: firstly we will consider the coupled system assuming that it is linear, after that we will introduce the non-linearities.

10.5.1 Linear control of the coupled Series Elastic Actuator

Firstly, we look at the system linearized around its 'home' position: $(\theta_x, \theta_y) = 0$. Therefore we use the small angle approximation $\sin\theta_\bullet \approx \theta_\bullet$ and $\cos\theta_\bullet \approx 1$. In that case, the following equations hold:

$$\begin{aligned} J_m\,\ddot{\varphi}_A &= \tau_A + r\,(F_{AF} - F_{AR}), \\ J_m\,\ddot{\varphi}_B &= \tau_B + r\,(F_{BF} - F_{BR}), \end{aligned} \tag{10.11}$$

and

$$\begin{aligned} \tau_x &= r_x\,\left((F_{AR} - F_{AF}) - (F_{BR} - F_{BF})\right), \\ \tau_y &= r_y\,\left((F_{AR} - F_{AF}) + (F_{BR} - F_{BF})\right), \end{aligned} \tag{10.12}$$

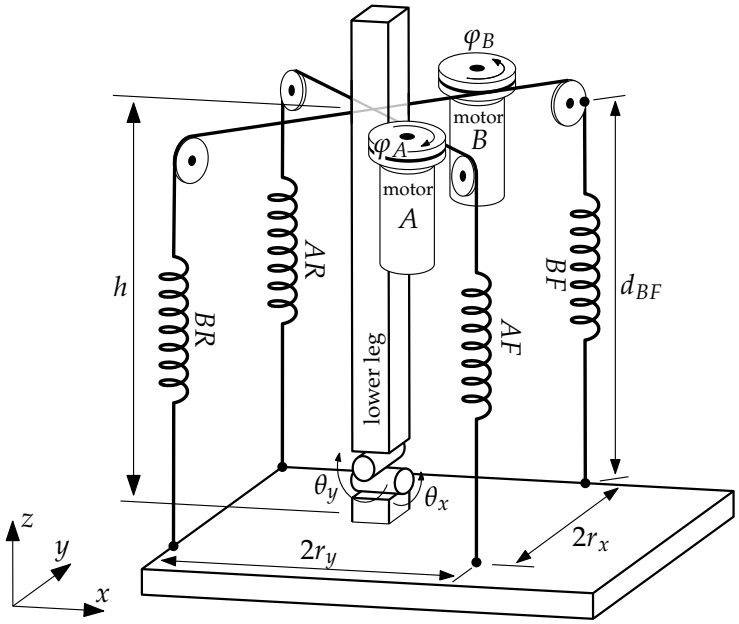

Figure 10.8: Sketch of the new ankle mechanism.

where J_m is the apparent inertia of each actuator, $\tau_{A/B}$ is the actuator torque of motor A/B (on the output shaft of the gearbox), $\tau_{x/y}$ is the resulting torque on the x- and y-axis of the foot, r the radius of the pulley on each actuator, $r_{x/y}$ the arm about which the cables exert their force on the foot and $F_{\bullet F}$ and $F_{\bullet R}$ represent the contracting force of the front and rear springs in cables A and B respectively. Note that we ignore motor friction throughout this chapter. The elongation of each of the springs, $\Delta l_\bullet$, can be determined by

$$\Delta l_{BF} = -r\varphi_B + (d_{BF} - d_{BF,0}), \tag{10.13}$$

and similarly for the other springs (with care for the minus-sign in front of r). Here, d_{BF} is the euclidean distance between the attachment point of the spring on the foot and the top pulley, as indicated in figure 10.8 and $d_{BF,0} = h$ is the initial distance (at $\theta_x = \theta_y = 0$). In order to make sure that there is always a positive tension on each of the cables, we use springs having a pre-tension F_{pre}. So the contracting force of the each spring is equal to

$$F_\bullet = k\,\Delta l_\bullet + F_{\text{pre}} \tag{10.14}$$

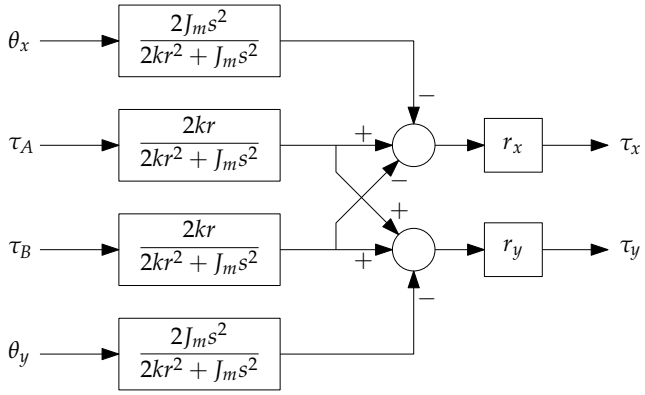

Figure 10.9: Linear plant model of the coupled series elastic ankle actuation system.

where k is the spring constant of each of the springs. In the case of a linear approximation, we have, explicitly

$$\begin{aligned} F_{AF} &= k\,(-r\varphi_A + r_x\theta_x + r_y\theta_y) + F_{\text{pre}}, \\ F_{AR} &= k\,(\ \ r\varphi_A - r_x\theta_x - r_y\theta_y) + F_{\text{pre}}, \\ F_{BF} &= k\,(-r\varphi_B - r_x\theta_x + r_y\theta_y) + F_{\text{pre}}, \\ F_{BR} &= k\,(\ \ r\varphi_B + r_x\theta_x - r_y\theta_y) + F_{\text{pre}}. \end{aligned} \tag{10.15}$$

By manipulating these equations we find

$$\begin{aligned} T_x &= \frac{2kr_x\ \left(rT_A - rT_b - 2J_m r_x \Theta_x s^2\right)}{2kr^2 + J_m s^2}, \\ T_y &= \frac{2kr_y\ \left(rT_a + rT_b - 2J_m r_y \Theta_y s^2\right)}{2kr^2 + J_m s^2}, \end{aligned} \tag{10.16}$$

where $T_\bullet$ and $\Theta_\bullet$ are the Laplace transforms of $\tau_\bullet$ and $\theta_\bullet$ respectively. If we look at the static case, *i.e.*, $\lim_{s\to 0}$, we find for the input sensitivity S, *i.e.*, the ratio between input torque $\tau_{A/B}$ and output torque $\tau_{x/y}$:

$$\begin{aligned} S_{xA} &= \frac{\partial \tau_x}{\partial \tau_A} = \ \ \frac{r_x}{r}, & S_{yA} &= \frac{\partial \tau_y}{\partial \tau_A} = \frac{r_y}{r}, \\ S_{xB} &= \frac{\partial \tau_x}{\partial \tau_B} = -\frac{r_x}{r}, & S_{yB} &= \frac{\partial \tau_y}{\partial \tau_B} = \frac{r_y}{r}. \end{aligned} \tag{10.17}$$

The linearized model of the plant is shown in figure 10.9. For controlling the system it is relatively straightforward to invert the transfer functions and take them as a feed-forward term, such as in (Williamson, 1995). Then, by linear feedback,

disturbances and model mismatch can be suppressed. However, as we will see in the following subsection, the non-linear effects are so large that it is wise to compensate for them with a decent non-linear feed-forward controller.

10.5.2 Nonlinearity

In the system we recognize two main sources of non-linearity:

1. The cable attachment points on the foot describe a sphere under variation of θ_x and θ_y, *i.e.*, the small angle approximation for these variables does not hold exactly,

2. The rotation axes of the foot are not in the same plane as the cable attachment points, which also gives rise to non-linearities.

The goal of the following subsections is to investigate how bad the non-linearities are and (thus) how much effort should be put in compensating for these non-linearities (especially because we don't want to use too much computational power or look-up tables, if unnecessary). It should be noted that the 'top' part of the system (the motors with pulleys) does show linear behavior and we consider the springs as having a linear force-elongation relationship. Therefore, (10.11), (10.13) and (10.14) still hold during the non-linear analysis. The other equations of section 10.5.1 are linear approximations and will be replaced by non-linear equivalents.

10.5.3 Nonlinearity — releasing the small-angle approximation

The effect of releasing the small angle approximation can be investigated by replacing (10.12) by

$$\begin{aligned} \tau_x &= (r_x \cos\theta_x)\,(F_{AR} + F_{BF} - F_{AF} - F_{BR}), \\ \tau_y &= (r_y \cos\theta_y - r_x \sin\theta_x \sin\theta_y)\,(F_{AR}{+}F_{BR}{-}F_{AF}{-}F_{BF}) \end{aligned} \tag{10.18}$$

and replacing $r_x\theta_x$ and $r_y\theta_y$ in (10.15) by $(r_x \sin\theta_x \cos\theta_y)$ and $(r_y \sin\theta_y)$ respectively. We assume here that the cables still pull exactly vertically (which can be assumed valid if $h \gg r_x\theta_x, r_y\theta_y$). By doing the math we find

$$\begin{aligned} \tau_x &= \frac{r_x}{r}\cos\theta_x(\tau_A - \tau_B), \\ \tau_y &= \frac{r_y}{r}\cos\theta_y(\tau_A + \tau_B) - \frac{r_x}{r}\sin\theta_x \sin\theta_y(\tau_A - \tau_B) \end{aligned} \tag{10.19}$$

Parameter	Name	Value
Arm x-rotation	r_x	5.5 cm
Arm y-rotation	r_y	6.0 cm
Motor pulley radius	r	1.65 cm
Mechanism height	h	22.5 cm
x-axis height	H_x	0.5 cm
y-axis height	H_y	1.6 cm
Spring pretension	F_{pre}	500 N
Spring stiffness	k	50 kN/m
Rotation range x	θ_x	$[-23^\circ \dots 20^\circ]$
Rotation range y	θ_y	$[-32^\circ \dots 35^\circ]$

Table 10.3: Some important dimensions of the ankle mechanism.

and the input sensitivity S for the static case with nonlinearity, being

$$\begin{aligned} S_{xA} &= \frac{\partial \tau_x}{\partial \tau_A} = \frac{r_x}{r}\cos\theta_x, & S_{yA} &= \frac{\partial \tau_y}{\partial \tau_A} = \frac{r_y}{r}\cos\theta_y - \frac{r_x}{r}\sin\theta_x \sin\theta_y, \\ S_{xB} &= \frac{\partial \tau_x}{\partial \tau_B} = -\frac{r_x}{r}\cos\theta_x, & S_{yB} &= \frac{\partial \tau_y}{\partial \tau_B} = \frac{r_y}{r}\cos\theta_y + \frac{r_x}{r}\sin\theta_x \sin\theta_y. \end{aligned} \tag{10.20}$$

Due to this non-linearity, the input sensitivity of the system has become dependent on de foot angle. Note however, that the system is still linear in $\tau_{A/B}$ (*i.e.*, the system can be written as

$$\begin{aligned} \tau_x &= S_{xA}(\theta_x)\ \tau_A + S_{xB}(\theta_x)\ \tau_B, \\ \tau_y &= S_{yA}(\theta_x, \theta_y)\,\tau_A + S_{yB}(\theta_x, \theta_y)\,\tau_B. \end{aligned} \tag{10.21}$$

For the dimensions of our system, as stated in table 10.3, the input sensitivity S_{yA} is shown in figure 10.10. The maximum deviation from the linear case is approximately 32%, which is substantial.

10.5.4 Nonlinearity — off-plane rotation axes

Figure 10.8 shows that the rotation axes of the ankle are not exactly in the plane of the cable attachment points; they are a little higher (also indicated by H_y in figure 10.11). The reason that we designed it like this is that we wanted to foot to be as light as possible, thus make it not too high. The rotation axes need some clearance from the ground however, otherwise the encoders would touch the ground. This gives rise to extra non-linearities, and as we will see in this section, even instability.

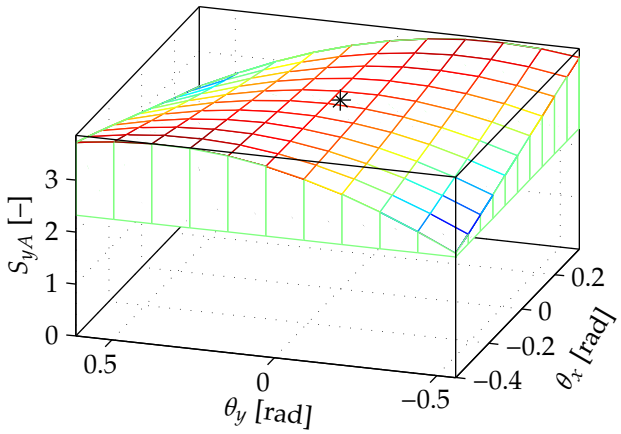

Figure 10.10: The input sensitivity $S_{yA} = \frac{\partial \tau_y}{\partial \tau_A}$ as a function of the foot angles θ_x and θ_y, for the non-linearity described in section 10.5.3. In the fully linear case, the surface would be exactly flat, meaning that the relation between τ_y and τ_A is constant, thus independent on the foot angles. The point $(\theta_x, \theta_y) = (0, 0)$ is indicated with a star.

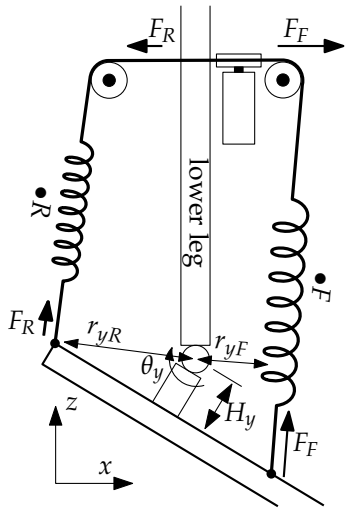

Figure 10.11: Example of positioning the foot at an angle θ_y. Because the rotation axis does not lie in the plane of the spring attachment points, the arms r_{yF} and r_{yR} are dependent on θ_y. As a result, in order to get zero torque on the rotation axis, the spring tensions F_R and F_F are not equal, resulting in an acceleration of the motor (unless a counteracting torque $\tau_{A/B}$ is applied).

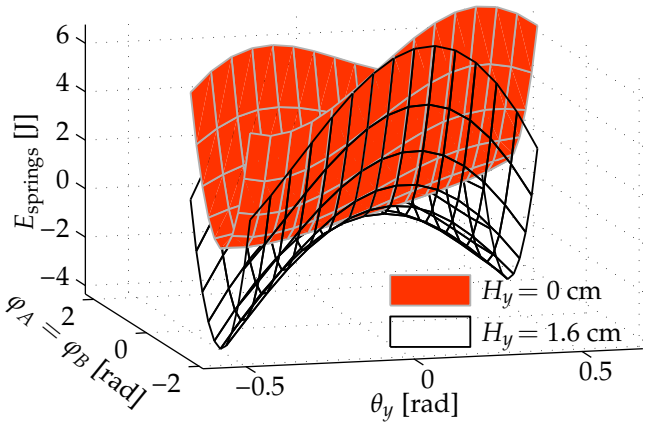

Figure 10.12: The total potential energy E_{tot} of the four springs together as a function of θ_y and $\varphi_{A/B}$. for a system where the rotation axis lies in ($H_y = 0$ cm) and outside ($H_y = 1.6$ cm) the plane with the spring attachment points. The other parameters used are the actual parameters of our robot.

In order to be able to visualize everything, we will limit ourselves here to rotation about the y-axis, thus throughout this section we assume that $\theta_x = 0$ and that (by proper control) $\varphi_A = \varphi_B$ (which we will denote as $\varphi_{A/B}$) and $\tau_A = \tau_B$ (ditto). Both springs AF and BF act identically; the same holds for springs AR and BR. We will denote them here as $\bullet F$ and $\bullet R$. Furthermore, again we only consider the static case.

Assume that the foot is at some angle θ_y and we want to keep it there by making sure that $\tau_y = 0$ (see figure 10.11). From the figure it immediately becomes clear that $F_{\bullet F} \neq F_{\bullet R}$ because the arms for the front and rear springs are different. From (10.11) it follows that, in order to get no motor acceleration ($J_m \ddot{\varphi}_{A/B} = 0$), we need a static torque $\tau_{A/B}$ to compensate for the force mismatch in the springs. Apparently, due to this non-linearity, the system is not linear in torque anymore: for a zero torque τ_y we need a non-zero $\tau_{A/B}$. We will investigate this phenomenon in more detail. Instead of approaching Δl linearly, we now look at the fully nonlinear function $\Delta l = f(\theta_x, \theta_y, \varphi_A, \varphi_B)$, which in our 2D case reduces to $\Delta l = f(\theta_y, \varphi_{A/B})$. Analytically, this function is quite long, but numerically it can easily be calculated. The potential energy of one pre-tensioned spring can be written as

$$E(\theta_y, \varphi_{A/B}) = \tfrac{1}{2} k \, \Delta l^2 + F_{\text{pre}} \, \Delta l \tag{10.22}$$

and the total potential energy contained in the four springs together as

$$E_{\text{tot}}(\theta_y, \varphi_{A/B}) = E_{AF} + E_{BF} + E_{AR} + E_{BR}. \tag{10.23}$$

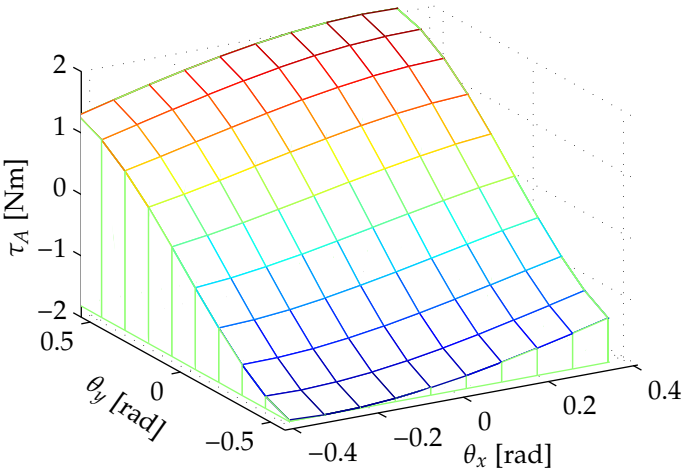

Figure 10.13: The torque $\tau_A = \frac{\partial E}{\partial \varphi_A}$ 'generated' by the non-linearity in the system. The torque τ_B has a similar profile but is mirrored around $\theta_x = 0$.

Figure 10.12 shows the total potential energy E_{tot} as a function of its variables for the case where the rotation axis is on ($H_y = 0$ cm) and off ($H_y = 1.6$ cm) the plane of the spring attachment points. We discuss both cases separately, starting with $H_y = 0$ cm. As the system naturally strives towards minimum energy, it will flow towards the valley and stay there; the system has reached a neutral equilibrium (this is actually a way to control the angle θ_y: control the motors to an angle $\varphi_{A/B}$ for which $(\theta_y, \varphi_{A/B})$ is a minimum of the energy function. The system then will converge to the desired foot angle). For $H_y = 1.6$ cm, there is only one (even unstable) equilibrium point: $(\theta_y, \varphi_{A/B}) = (0, 0)$. For any non-zero foot angle, the system is unstable; it will diverge towards one of the end stops. The force with which this occurs is linearly dependent on the pretension in the springs. The partial derivative

$$\frac{\partial E_{\text{tot}}}{\partial \varphi_A} = \tau_A \tag{10.24}$$

tells us the amount of torque on the motor axis that is 'generated' by the non-linearity. This torque is shown in figure 10.13, as a function of both foot angles. In order to not let the motor axis accelerate by this torque, we can make our controller counteract it with an opposite (feed forward) torque. As can be seen in the figure, the torques are substantial (and render the system unstable), up to 2 Nm. Therefore it is important to indeed compensate for it.

10.6 Conclusions

In this chapter we discussed the design and control of a new ankle mechanism for the humanoid robot TUlip. It has been shown that the problems of the previous design could be eliminated by using a differential motor setup, resulting in a coupled MIMO system. Calculations were done to determine the best motor and gearbox ratio, where achievable walking speed was chosen as optimization criterion. Some issues on controlling the system were discussed, mainly the non-linearities induced by the system.

We have not yet been able to do intensive testing with the new ankle system, therefore, we cannot tell yet how well the system behaves. Mechanically, we think the new system will easily outperform its predecessor. From a control point of view, the non-linearities can be compensated in software, but we will probably also try to reduce the amount of non-linearity in the system by moving the cable attachment points such that the rotation axes are in the same plane.

Chapter 11

Conclusions

In this chapter the main conclusions from this thesis are recapitulated. After that, the work is discussed and recommendations for future work are given.

11.1 Conclusions

In section 1.4.1 five research goals for this thesis were formulated, being:

1. How can we analyze the behavior of a 2D passive dynamic walker that is walking on rough terrain?

2. By looking at the robot from a different 'perspective', can we gain more insight in its dynamics?

3. How can we control a walking robot in order to stabilize it in the lateral (sideways) direction?

4. How can we improve the actuators in order to get minimum energy consumption?

5. How can we design parts of a walking robot optimally?

In this section each research goal will be reviewed and evaluated separately. For more detailed conclusions about a specific subject, please look at the conclusion sections at the end of each chapter. At the end of this section some overall conclusions will be stated.

Analyze behavior of 2D passive dynamic walker on rough terrain

In chapter 2 it was shown that the commonly used post-impact Poincaré section for walking robots can not be used directly in the case of irregular terrain because on an irregular floor the post-impact states of all steps do not lie on one Poincaré section. A solution was provided that extends the applicability of the post-impact Poincaré section to rough terrain by means of the *Integration mapping* ΠI, which maps any post-impact state to a state on the post-impact Poincaré section associated with a flat floor.

Furthermore, a method was introduced to relate disturbances of different magnitude to curves on the Poincaré section. This gives more insight in the effect of the disturbance on the gait and it gives hints on where to extend the Poincaré section in order to increase the robustness for the specific disturbance.

The methods presented open new possibilities for disturbance analysis using the Poincaré section and its derivative tools such as the stride function and the basin of attraction.

Gaining more insight by looking from different 'perspective'

In chapter 3 it was shown that a proper coordinate transformation makes the equations of motion and analysis easier. Ready-to-use equations were provided to do the coordinate transformation. The method has successfully been used in the programming of our limit cycle walker TUlip.

In chapter 4 it was shown that the concept of screws and wrenches gives us tools to geometrically establish the relation between the ground reaction wrench and the Zero-Moment Point. The coordinate-free nature of the method has the advantage of preventing implicit (and possibly wrong) coordinate-related assumptions in the analysis.

In chapter 5 a systematic dynamic analysis was presented of the 3D bipedal gait. The analysis was done using simplified models in which the robot is described as a single rigid body, called the 'locked inertia'. The phases of the gait (foot rolling phase and impact phase) were discussed separately and explicit equations for both were given. Because of the simplified models the equations became manageable and a good starting point for theoretical probing.

The three chapters introduced different ways of looking at the dynamics of walking robots. Indeed, the presented methods give more insight in the dynamics: by application of them, the analysis of the walker's gait becomes easier and the results are better understandable.

Control for lateral stabilization

In this thesis two ways were investigated to stabilize a walking robot laterally (sideways). The methods differ in control type and application, but they share the fact that *lateral foot placement* is used to stabilize the robot.

Chapter 6 described a very simple model of a 3D walker (a point mass in the hip, two massless legs and impulsive push-off) which has the special feature that, in the limit cycle, the gait is time-symmetric. If a disturbance occurs, the gait becomes asymmetric. The sideways velocity of the hip at mid-stance was shown to be a good indicator of the amount of asymmetry. A proportional controller was proposed that relates the sideways offset of the foot position directly to the sideways velocity of the hip. Through parameter analysis it was shown that the proposed controller could stabilize the walker for a wide range of velocities an disturbances.

Chapter 7 described the application of the extrapolated center of mass (XCOM), also known as instantaneous capture point, on our 3D robot TUlip. By means of simulations on an inverted pendulum and measurements on the real robot it was shown that the method, called *constant offset control* can indeed stabilize a real walking robot in the lateral direction.

Improve actuators for minimum energy consumption

An electric DC motor can be very efficient, if it is working at its optimum angular velocity. However, for walking robot applications, the motors work at very low velocity (often even zero velocity); a range in which a DC motor is inefficient.

In chapter 8 a concept for a new actuator was introduced that has the potential to be energy efficient. Negative work is stored mechanically and can be re-used later. An infinitely variable transmission (IVT) transforms the spring force to the desired output torque. The actuator is able to deliver a static torque at zero cost; something which a DC motor can not do at all. Transferring energy from the battery into the spring (which is done with a normal DC motor) can be done quickly and efficiently.

On paper, the concept indeed has the potential to be energy efficient. The big challenge is to build an IVT that transfers the energy without too much loss and allows fast and efficient transmission ratio changes. A first prototype of such an IVT has been designed (Ansink, 2008) and built at the group (figure 11.1). Although it does not have the desired efficiency yet, the principle behind the system (which is being patented) is promising.

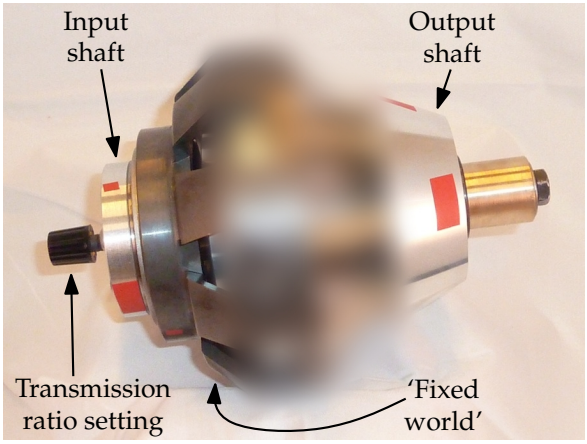

Figure 11.1: The Infinitely Variable Transmission (IVT), designed at the Control Engineering Group. The length of the device is approximately 20 cm. Part of the picture has been blurred in order not to reveal the internals which are being patented.

Design of parts of walking robot

Chapters 9 and 10 presented an innovative knee locking mechanism and an integrated 2-dof ankle mechanism respectively. Both are a good example of a design that is optimized for a specific task in walking.

The knee locking mechanism is based on a mechanical singularity: a four-bar mechanism that locks in a certain configuration. Some extra features of the mechanism were discussed in the chapter: a suction cup to prevent re-bouncing of the mechanism when it locks, a voice coil actuator to help the system lock and unlock, a discrete-state controller that minimizes energy consumption and deliberately added mechanical play that makes the system actually work. The mechanism was implemented on our 2D robot Dribbel and functioned well.

The ankle mechanism, which allows the foot to rotate around the x-axis (inversion/eversion) and y-axis (plantar-/dorsiflexion), is designed as a coupled Series Elastic Actuated system. The differential set-up of two small DC motors allows both motors to work together to deliver maximum push-off force. The Series Elastics absorb the impact shocks and make accurate torque control possible. The control of the system was discussed and it was shown that different non-linearities are present in the mechanics.

11.2 Recommendations for future work

After five years of research, resulting in this thesis, many questions have answered. The answers have however led to many new questions and ideas for future research. Some of them are discussed below, organized by topic.

Analysis

- Research on the Poincaré section and its derivative tools should be continued. An example is the applicability of the post-impact Basin of Attraction (BOA) to walkers with feedback control. Often, it is assumed that the robustness against disturbances and the size of the BOA are correlated. In chapter 2 it was already shown that this does not have to be the case. For an actuated walker however, there is another reason to question this assumption. A walker is robust against a disturbance if the disturbance leads the walker to a state on the post-impact Poincaré section which is inside the BOA. From this it follows that there are actually two ways to increase robustness: either enlarging the BOA by making a controller that can handle large deviations from the fixed point on the Poincaré section, or making sure that deviations from the fixed point as a result of the disturbance are not too large by making a controller that immediately reacts on the disturbance. The latter may work best because the controller reacts earlier, thereby preventing that the deviation from the limit cycle grows too much. It would be interesting to see if there is a BOA-like property that can successfully compare the robustness of a walker for both situations.

- For many-dof robots it is convenient to reduce the control problems to a 'state space' with less dimensions than the number of degrees of freedom. Therefore research should be continued on (bijective) coordinate transformations, focusing on transformations that split the state into a relevant part and a non-relevant part (analogous to the 'null space') for the specific control task.

- The approximation of a many-dof walker by a locked inertia (chapter 5) is somewhat crude. Firstly, the foot of a robot would not be rigidly attached to the leg, and secondly the torso would be approximately upright and not rotate with the leg. A logical extension to the model presented in the chapter would therefore be to approximate the robot by two or three locked inertias instead of one. It should be investigated how well such a model can represent the real behavior of the walker and if analytical conclusions still can be drawn from the simplified model.

- Even after years of research in this field, measures for 'performance' of a walking robot are still vague. On one hand this is no wonder because judging the performance is highly subjective and dependent on the specific task (which often is also vague). On the other hand it is strange because having a good performance criterion is essential when doing optimization or comparison between walkers. It is therefore suggested that more research should be dedicated to finding *meaningful* performance measures. Some ideas about this will be discussed now.

  A performance measure, or *metric*, should be homeomorphic to $\mathbb{R}$ (or a subset of it) so that two walkers can unambiguously be compared: the one with the higher score is is the best. If multiple of criteria are considered, they should be scaled in some way to get to one single metric. This scaling is an important design choice and should be chosen with care.

  The meaningfulness of a metric is a point which is often paid only little attention to. Assumptions are often made that some measurable property (*e.g.*, the largest eigenvalue) of the walker is correlated to a less measurable property like robustness or efficiency — without proof, and without elaborating on what exactly is meant with robustness or efficiency. Some commonly used performance measures said to be related to robustness are the area of basin of attraction (which is, mathematically speaking, not even defined), maximum allowable relative deviation from the limit cycle (which is highly dependent on the arbitrary choice of coordinates) and maximum eigenvalue. The *specific resistance*, the energy consumption per distance traveled per kilogram mass per gravity (Wisse et al., 2004) (also known as the *specific cost of transport*) is a good example of an unfortunate choice as an efficiency metric when used for a passive dynamic walker: when used as an optimization criterion it will come up with a walker walking at an infinitely low speed (Garcia et al., 2000; Chatterjee and Garcia, 2000).

  For metrics indicating robustness against a disturbance, the author thinks the only good solution is to really test the walker against the disturbance and record the maximum magnitude of the disturbance for which the walker does not fall. The 'maximum step-down' seems therefore a good metric, although it should be noticed that the metric only tells us something about the robustness against drops in floor height and not against other disturbances such as pushes.

  Some commonly used metrics (such as the specific resistance) are scaled by mass and/or length of the walker, such that walkers of different size (in the case of the specific resistance even walkers on different planets; the metric is scaled by gravity too) can be compared to each other. For simple systems such as models of 3-dof limit cycle walkers, this is okay, but in the opinion of the author, this method should be abandoned for more sophisticated walk-

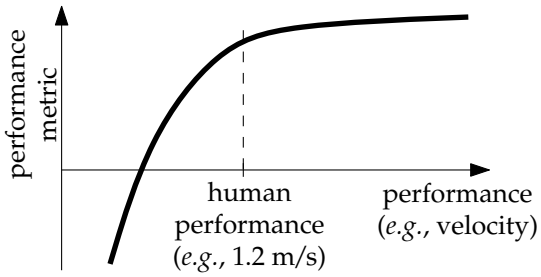

Figure 11.2: Non-linear relation between a performance criterion and its associated performance metric. The metric saturates when the performance of a human is approached.

ers. The reason is that, in such cases, it is possible to alter the measured performance of the walker (*e.g.*, by putting on a hat to make the walker taller) while practically the walker performs still the same. Therefore, the author thinks that it would be good if, for more sophisticated walkers, the performance measures are not dependent on the walker's properties, only on the environment. As an example, if two walkers, both designed to walk around in an office environment, are capable of handling a door step of maximum 2 cm, they should have the same performance rating for that, even if one robot is twice as tall as the other.

Coming up with a good overall performance metric for a walker, thus incorporating robustness, efficiency as well as speed, is a difficult task: which property should be preferred above the other? The author tends to think, qualitatively, of the questions 'Which robot would you buy? And why?'. Although there are no unique answers to these questions, the answers seem to be dependent on the relation to human performance. If a choice should be made between a robot that has human-like velocity and energy consumption and one that is four times as efficient but also twice as slow[1], probably the first would be favorable. However, a robot that walks twice as fast as a human but also uses four times as much energy would be less attractive because of its extraordinary energy consumption. Indeed, when striving for a human-like walking robot, it makes sense to use performance criteria that saturate when the human performance is approached. Furthermore, if the performance for a specific criterion is very poor, it should be penalized strongly so that it can not be compensated by exorbitant other performance criteria. Therefore, a non-linear relation between the performance criterion (*e.g.*, walking velocity) and the metric (how is the walking velocity rated), as shown in figure 11.2, seems to be a good idea. The over-

[1]Energy consumption per second required for walking E_{walk} (in [W]) and walking speed v (in [m/s]) in humans are related in a square fashion, $E_{\text{walk}} \propto v^2$; $E_{\text{tot}} = E_0 + E_{\text{walk}}$, where E_0 is the human energy consumption while walking as slowly as possible (Ralston, 1958).

all performance can then be taken as the sum of all individual performance metrics. More research is needed on this topic in order to find the best performance metrics.

Control and actuation

- The two foot placement controllers described in this thesis are both a little limited. The XCOM-controller only controls lateral foot placement; not sagittal. The time-reversal controller does control both, but is based on an over-simplified model of a 3D robot. Combining control of both planes, including coupling, rotation about the vertical axis and push-off could improve the gait and make it more robust.

- Most humanoid walking robots use only their legs and (counterswinging) arms for stabilizing the gait; the upper body remains vertical all the time. For rejection of large disturbances however, the upper body may be of great help. Thanks to its large moment of inertia, rotational acceleration of the upper body can — momentarily — shift the Center of Pressure towards a convenient place, thereby preventing a fall. The Reaction Mass Pendulum (Lee and Goswami, 2007) theory will be useful in designing such controllers.

- The idea behind limit cycle walking is to let the passive dynamics do most of the work and not to influence it too much by control. However, in order to stabilize a walker, control *is* needed. In order to benefit from the passive dynamics, the precise position control for stabilization should be abandoned and replaced by some new form of control that at the same time is functional but respects the passive dynamics as much as possible. This field of controllers needs to be explored further.

- For high-magnitude disturbances, people use different strategies to recover. Examples are taking extra steps within a short period of time and landing with a bent knee. Both strategies allow for fast dissipation of excess kinetic energy. Walking robots often have difficulty with taking many steps per second because of their limited actuation power. Therefore it would be nice to investigate the ability of walking robots to land with a bent knee in order to recover from high-magnitude disturbances.

- In this thesis a conceptual study was presented on the the Very Versatile Energy Efficient (V2E2) actuator. In order for such an actuator to meet our requirements (especially, efficiency of all the sub-parts), firstly the IVT needs to be optimized. Furthermore, a prototype of the whole actuator should be built and tested, especially to find out how to control the unit in an energy efficient way.

- It is the author's belief that DC motors are not the type of actuators that are suitable for driving humanoid robots. The two main problems is that they are highly inefficient at low angular velocities and that, in the case of large gear reduction, they are not backdrivable. In order to bring humanoid robots to the next level, new types of actuators should be used, which are more muscle-like.

  Pneumatic muscles (Daerden and Lefeber, 2002) have been around for quite a long time. Some walking robots have successfully been constructed with them, but the disadvantages, such as weight of the valves and air tank, inefficiency and non-linearity of the stiffness make them unsuitable for advanced control (Wisse, 2004, chap. 9).

  Research is being conducted on different types of artificial muscles based on deformation of materials.

  - *Shape Memory Alloys* (SMAs) are wires that change length when heated (Kratz et al., 2007; Sangbae et al., 2009), but the contraction speed is not very good (Ishikawa and Nakada, 2010).
  - *Electroactive Polymers* (EAPs) react on an electrical stimulation. Two types exist: electronic (driven by Coulomb forces) and ionic (driven by the transport of ions). The first can generate a static displacement without consuming energy, but needs a huge voltage to work on (in the order of kV). The second only requires a few Volts to operate but suffer from low electromechanical coupling (Bar-Cohen et al., 2007). Examples of EAP's are *Dielectric elastomers* (DE) (Chuc et al., 2009), and *Carbon nanotubes* (Mirfakhrai et al., 2007).
  - Experiments have also been done with using *living muscle* in robotics (Herr and Dennis, 2004; Dennis and Herr, 2005).

  The current state of the art in artificial muscles is not good enough yet to reliably use them in walking robots; additional research in this field is essential for the progression in walking robot research.

Design

- Specifically for the ankle mechanism described in chapter 10 a recommendation is to try to reduce the amount of non-linearity, especially the sources that render the system unstable. A few extra mechanical parts on the foot should be sufficient for that.

- When working on TUlip, one of the things the author noticed was that attempts to do precise control not always resulted in the desired movements. This was partly due to the control in which some simplifications were made,

but also partly due to non-optimal design. For example, at some places in the robot sliding bearings were used instead of ball bearings. In order to make a well-working robot, it is important to make everything as good as can be; any concessions done in the mechanical design will be directly noticed in degradation of performance.

- The two designs presented in this thesis were both inspired by mechanical possibilities, not by looking at nature. Although we can learn a great deal from nature, the author thinks that this is more useful for general principles (such as walking or flying), not so much for mechanical solutions of a specific problem. There are several reasons for this thought.
  1. During evolution most body parts have been optimized. Most body parts have multiple functions however, and as long as we're not exactly replicating human beings, it is likely that not all functions are needed in the robot, so the optimization criteria differ from nature's criteria.
  2. The building materials are different for nature and robots. Therefore the optimal constructions are too.
  3. Nature has no ball bearings. And it does not have the possibility to create rotating parts (if it did, ducks probably would have had the equivalent of a propeller and some land animals would certainly have had a set of wheels). In that sense, mechanics offers more possibilities than nature does.

  It is suggested to always look at nature to see how it solves complex design problems. However, a clever mechanical solution may outperform nature's solution on a very specific task; therefore it is encouraged to always be creative and explore all the possibilities that mechanics offers.

Bibliography

R. M. Alexander. The gaits of bipedal and quadrupedal animals. *International Journal of Robotics Research*, 3(2):49–59, 1984.

R. M. Alexander. Three uses for springs in legged locomotion. *International Journal of Robotics Research*, 9(2):53–61, 1990.

J. Ansink. Design and analysis of an infinitely variable transmission for energy efficient actuation. Msc thesis, Control Laboratory, University of Twente, Apr. 2008.

A. Baines. Knee design for a bipedal walking robot based on a passive-dynamic walker. Technical report, Massachusetts Institute of Technology, June 2005. URL `http://mit.dspace.org/handle/1721.1/32883`.

R. S. Ball. *A treatise on the theory of screws*. Cambridge University Press, Cambridge, 1900.

J. Bar-Cohen, K. J. Kim, H. R. Choi, and J. D. W. Madden. Electroactive polymer materials. *Smart Materials and Structures*, 16(2), 2007.

N. Beekman. Analysis and development of a 2d walking machine. Msc thesis, Control Laboratory, University of Twente, Dec. 2004.

D. J. Borgerink. Design and implementation of a knee mechanism for walking robots. BSc thesis 027CE2008, University of Twente, Dec. 2008.

W. M. Bouwman, G. van Oort, E. C. Dertien, J. F. Broenink, and R. Carloni. Dynamic walking stability of the TUlip robot by means of the extrapolated center of mass. In *Proc., 12th Mechatronics Forum Biennial International Conference*, pages 197–204, June 2010. ISBN 078-3-033-02507-3.

F. Bullo and A. D. Lewis. *Geometric Control of Mechanical Systems*, volume 49 of *Texts in Applied Mathematics*. Springer Verlag, New York-Heidelberg-Berlin, 2004. ISBN 0-387-22195-6.

P. Buttolo, D. Y. Hwang, P. H. Marbot, and B. Hannaford. Hard-disk actuators for mini-teleoperation. In *Proc., SPIE Telemanipulator and Telepresence Technologies Symposium*, pages 55–61, Oct. 1994.

J. Camp. Powered "passive" dynamic walking. Master's thesis, Cornell University, Aug. 1997.

A. Chatterjee and M. Garcia. Small slope implies low speed for McGeer's passive walking machines. *Dynamics and Stability of Systems*, 15(2):139–157, 2000. ISSN 0268-1110.

V. F. H. Chen. Passive dynamic walking with knees : a point foot model. Master's thesis, Massachusetts Institute of Technology, 2007.

N. H. Chuc, J. K. Park, N. H. L. Vuong, D. Kim, J. C. Koo, Y. Lee, J. Nam, and H. R. Choi. Multi-jointed robot finger driven by artificial muscle actuator. In *Robotics and Automation, 2009. ICRA '09. IEEE International Conference on*, pages 587–592, May 2009.

S. Collins, A. Ruina, R. Tedrake, and M. Wisse. Efficient bipedal robots based on passive-dynamic walkers. *Science*, 307(5712):1082–1085, 2005.

S. H. Collins and A. Ruina. A bipedal walking robot with efficient and human-like gait. In *Proceedings of IEEE International Conference on Robotics and Automation*, pages 1995–2000, 2005.

S. H. Collins, M. Wisse, and A. Ruina. A three-dimensional passive-dynamic walking robot with two legs and knees. *The International Journal of Robotics Research*, 20(7):607–615, 2001.

Controllab Products B.V. 20-sim Website, 2011. URL `http://www.20sim.com`. Accessed May 2011.

F. Daerden and D. Lefeber. Pneumatic artificial muscles: actuators for robotics and automation. *European Journal of Mechanical and Environmental Engineering*, 47(1):11–21, Mar. 2002.

A. Dasgupta and Y. Nakamura. Making feasible walking motion of humanoid robots from human motion capture data. In *ICRA*, pages 1044–1049, 1999.

C. De Quillfeldt. Improvement in bottle-stoppers. U.S. Patent No. 158406, Jan. 1875.

R. G. Dennis and H. Herr. Engineered muscle actuators: Cells and tissues. In Y. Bar-Cohen, editor, *Biomimetics Mimicking and Inspired by Biology*, chapter 9, pages 243–266. CRC Press, 2005.

E. C. Dertien. Realisation of an energy-efficient walking robot. MSc thesis 022CE2005, University of Twente, June 2005.

E. C. Dertien. Dynamic walking with dribbel — design and construction of a passivity-based walking robot. *IEEE Robotics and Automation Magazine*, 13(3): 118–122, Sept. 2006. ISSN 1070-9932.

V. Duindam. *Port-Based Modeling and Control for Effiecient Bipedal Walking Robots*. PhD thesis, University of Twente, Mar. 2006.

V. Duindam and S. Stramigioli. Modeling the kinematics and dynamics of compliant contact. In *Proc., IEEE International Conference on Robotics and Automation (ICRA'03)*, pages 4029–4034, Sept. 2003. ISBN ISBN 0-7803-7737-0.

V. Duindam and S. Stramigioli. Port-based control of a compass-gait bipedal robot. In *Proc., 16th IFAC World Congress (IFAC'05)*, July 2005.

V. Duindam and S. Stramigioli. Singularity-free dynamic equations of open-chain mechanisms with general holonomic and nonholonomic joints. *IEEE Transactions on Robotics*, 24(3):517–526, June 2008.

Dynasim. Dymola website, 2011. URL `http://www.dymola.com/index.htm`. Accessed May 2011.

G. T. Fallis. Walking toy ('improvement in walking toys'). U.S. Patent No. 376,588, Jan. 1888.

R. Featherstone. *Rigid Body Dynamics Algorithms*. Springer-Verlag New York, Inc., Secaucus, NJ, USA, 2007. ISBN 0387743146.

M. C. J. Franken. Ankle actuation for planar bipedal robots. MSc thesis 012CE2007, University of Twente, Apr. 2007.

M. C. J. Franken, G. van Oort, and S. Stramigioli. Analysis and simulation of fully ankle actuated planar bipedal robots. In *Intelligent Robots and Systems, 2008. IROS 2008. IEEE/RSJ International Conference on*, pages 634–639, Sept. 2008.

C. Fu and K. Chen. Gait synthesis and sensory control of stair climbing for a humanoid robot. *Industrial Electronics, IEEE Transactions on*, 55(5):2111–2120, May 2008. ISSN 0278-0046.

M. Garcia, A. Chatterjee, and A. Ruina. Efficiency, speed, and scaling of two-dimensional passive-dynamic walking. *Dynamics and Stability of Systems*, 15(2): 75–99, 2000.

M. Garcia, A. Chatterjee, A. Ruina, and M. Coleman. The simplest walking model: Stability, complexity, and scaling. *ASME Journal of Biomechanical Engineering*, 120(2):281–288, 1998.

G. Gilardi and I. Sharf. Literature survey of contact dynamics modelling. *Mechanism and Machine Theory*, 37(10):1213–1239, 2002. ISSN 0094-114X.

A. Goswami. Postural stability of biped robots and the Foot-Rotation Indicator (FRI) point. *Int. J. Robotic Research*, 18(6):523–533, 1999.

A. Goswami, B. Espiau, and A. Keramane. Limit cycles and their stability in a passive bipedal gait. In *Robotics and Automation, 1996. Proceedings., 1996 IEEE International Conference on*, volume 1, pages 246–251, Apr. 1996.

A. Goswami, B. Thuilot, B. Espiau, and L. G. Gravir. A study of the passive gait of a compass-like biped robot: Symmetry and chaos. *International Journal of Robotics Research*, 17:1282–1301, 1998.

J. W. Grizzle, G. Abba, and F. Plestan. Asymptotically stable walking for biped robots: analysis via systems with impulse effects. *Automatic Control, IEEE Transactions on*, 46(1):51–64, Jan. 2001. ISSN 0018-9286.

R. v. Ham, T. Sugar, B. Vanderborght, K. W. Hollander, and D. Lefeber. Compliant actuator designs. *IEEE Robotics Automation Magazine*, 16(3):81–94, september 2009. ISSN 1070-9932.

K. Harada, S. Kajita, K. Kaneko, and H. Hirukawa. ZMP analysis for arm/leg coordination. In *Intelligent Robots and Systems, 2003. (IROS 2003). Proc. IEEE/RSJ Int. Conf. on*, volume 1, pages 75–81, 2003.

J. Hass, J. M. Herrmann, and T. Geisel. Optimal mass distribution for passivity-based bipedal robots. *The International Journal of Robotics Research*, 25(11):1087–1098, 2006.

J. Hauser and R. M. Murray. Nonlinear controllers for non-integrable systems: the acrobot example. *American Control Conference*, pages 669–671, May 1990.

H. Herr and R. Dennis. A swimming robot actuated by living muscle tissue. *Journal of NeuroEngineering and Rehabilitation*, 1(1):6, 2004. ISSN 1743-0003.

J. Hieronymus. Edge folding device having self-locking mechanism. U.S. Patent No. 6588341, July 2003.

H. Hirukawa, S. Hattori, K. Harada, S. Kajita, K. Kaneko, F. Kanehiro, K. Fujiwara, and M. Morisawa. A universal stability criterion of the foot contact of legged robots — adios ZMP. In *Robotics and Automation, 2006. ICRA 2006. Proceedings 2006 IEEE International Conference on*, pages 1976–1983, May 2006.

D. Hobbelen. *Limit Cycle Walking*. PhD thesis, University of Delft, 2008.

D. Hobbelen, T. de Boer, and M. Wisse. System overview of bipedal robots flame and tulip: Tailor-made for limit cycle walking. In *Intelligent Robots and Systems, 2008. IROS 2008. IEEE/RSJ International Conference on*, pages 2486–2491, Sept. 2008.

D. Hobbelen and M. Wisse. A disturbance rejection measure for limit cycle walkers: The gait sensitivity norm. *Robotics, IEEE Transactions on*, 23(6):1213 –1224, Dec. 2007. ISSN 1552-3098.

D. G. E. Hobbelen and M. Wisse. Ankle actuation for limit cycle walkers. *The International Journal of Robotics Research*, 27(6):709–735, 2008.

A. L. Hof. The 'extrapolated center of mass' concept suggests a simple control of balance in walking. *Human Movement Science*, 27(1):112–125, 2008.

A. L. Hof, M. G. J. Gazendam, and W. E. Sinke. The condition for dynamic stability. *Journal of Biomechanics*, 38(1):1–8, 2005. ISSN 0021-9290.

K. W. Hollander, T. G. Sugar, and D. E. Herring. A robotic "Jack Spring"™ for ankle gait assistance. In *Proc., ASME International Design Engineering Technical Conferences and Computers and Information in Engineering Conference (IDETC/CIE'05)*, pages 25–34, Sept. 2005.

K. Hosoda and K. Narioka. Synergistic 3D limit cycle walking of an anthropomorphic biped robot. In *Intelligent Robots and Systems, 2007. IROS 2007. IEEE/RSJ International Conference on*, pages 470–475, Oct. 2007.

W. Huang, C.-M. Chew, Y. Zheng, and G.-S. Hong. Pattern generation for bipedal walking on slopes and stairs. In *Humanoid Robots, 2008. Humanoids 2008. 8th IEEE-RAS International Conference on*, pages 205–210, December 2008.

J. W. Hurst, J. E. Chestnutt, and A. A. Rizzi. An actuator with physically variable stiffness for highly dynamic legged locomotion. In *Proc., IEEE International Conference on Robotics and Automation (ICRA'04)*, pages 4662–4667, Apr. 2004.

V. T. Inman, H. J. Ralston, and F. Todd. *Human Walking*. William and Wilkins, Baltimore, 1981.

T. Ishikawa and T. Nakada. Shape Memory Alloy actuator for artificial muscle. *Journal of Environment and Engineering*, 5(1):105–113, 2010.

A. Isidori. *Nonlinear Control Systems*. Springer-Verlag New York, Inc., Secaucus, NJ, USA, 1995. ISBN 3540199160.

S. Ito, S. Amano, M. Sasaki, and P. Kulvanit. A zmp feedback control for biped balance its application to in-place lateral stepping motion. *Journal of Computers*, 3(8):23–31, 2008.

Y. Jeon, Y.-s. Park, and Y. Park. Global stability analysis for plane limit cycle walking models with feet and actuation. In *SICE Annual Conference 2010, Proceedings of*, pages 1812 –1814, Aug. 2010.

S. Kajita, F. Kanehiro, K. Kaneko, K. Fujiwara, K. Harada, K. Yokoi, and H. Hirukawa. Biped walking pattern generation by using preview control of Zero-Moment Point. In *Robotics and Automation, 2003. Proceedings. ICRA '03. IEEE International Conference on*, volume 2, pages 1620–1626, Sept. 2003.

S. Kajita, F. Kanehiro, K. Kaneko, K. Fujiwara, K. Yokoi, and H. Hirukawa. A real-time pattern generator for biped walking. In *Proc., IEEE International Conference on Robotics and Automation (ICRA'02)*, pages 31–37, 2002.

S. Kajita and K. Tani. Study of dynamic biped locomotion on rugged terrain. In *Proc., IEEE International Conference on Robotics and Automation (ICRA'91)*, pages 1405–1411, 1991.

K. Kaneko, F. Kanehiro, M. Morisawa, K. Miura, S. Nakaoka, and S. Kajita. Cybernetic human HRP-4C. In *Humanoid Robots, 2009. Humanoids 2009. 9th IEEE-RAS International Conference on*, pages 7–14, Dec. 2009.

H. Komsuoglu, A. Majumdar, Y. O. Aydin, and D. E. Koditschek. Characterization of dynamic behaviors in a hexapod robot. In *International Symposium on Experimental Robotics*, Dec. 2010.

T. Komura, A. Nagano, H. Leung, and Y. Shinagawa. Simulating pathological gait using the enhanced linear inverted pendulum model. *IEEE Transactions on Biomedical Engineering*, 52(9):1502–1513, Sept. 2005. ISSN 0018-9294.

T. Koolen. Capturability-based analysis and control of legged locomotion. Master's thesis, Delft University of Technology, Mar. 2011.

S. Kramer. Knee joint mechanism for knee disarticulation prosthesis. U.S. Patent no. 5746774, 1998.

R. Kratz, M. Stelzer, M. Friedmann, and O. von Stryk. Control approach for a novel high power-to-weight robotic actuator scalable in force and length. In *Advanced intelligent mechatronics, 2007 IEEE/ASME international conference on*, pages 1–6, Sept. 2007.

A. D. Kuo. Stabilization of lateral motion in passive dynamic walking. *The International Journal of Robotics Research*, 18(9):917–930, 1999.

A. D. Kuo. Energetics of actively powered locomotion using the simplest walking model. *ASME Journal of Biomechanical Engineering*, 124(1):113–120, 2002.

A. D. Kuo. The six determinants of gait and the inverted pendulum analogy: A dynamic walking perspective. *Human Movement Science*, 26(4):617–656, 2007. ISSN 0167-9457. European Workshop on Movement Science 2007, European Workshop on Movement Science 2007.

S.-H. Lee and A. Goswami. Reaction Mass Pendulum (RMP): An explicit model for centroidal angular momentum of humanoid robots. In *Robotics and Automation, 2007 IEEE International Conference on*, pages 4667–4672, Apr. 2007.

N. Liu, J. Li, and T. Wang. The effects of parameter variation on the basins of attraction of passive walking models. In *Mechatronics and Automation, 2007. ICMA 2007. International Conference on*, pages 1908–1913, Aug. 2007.

R. Z. Marlow. Artificial knee with improved stable link-type knee joint. U.S. Patent No. 4911709, Mar. 1990.

J. E. Marsden and J. Ostrowski. Symmetries in motion: Geometric foundations of motion control. *Nonlinear Science Today*, 1998.

T. McGeer. Powered flight, child's play, silly wheels and walking machines. In *Robotics and Automation, 1989. Proceedings., 1989 IEEE International Conference on*, volume 3, pages 1592–1597, May 1989.

T. McGeer. Passive bipedal running. *Proceedings of the Royal Society of London. Series B*, Jan 1990a.

T. McGeer. Passive dynamic walking. *The International Journal of Robotics Research*, 1990b.

T. McGeer. Passive walking with knees. In *Robotics and Automation, 1990. Proceedings., 1990 IEEE International Conference on*, volume 3, pages 1640–1645, 13-18 1990c.

T. McGeer. Passive dynamic biped catalogue, 1991. In *The 2nd International Symposium on Experimental Robotics II*, pages 463–490. Springer-Verlag, London, UK, 1993.

T. A. McMahon. Mechanics of locomotion. *International Journal of Robotics Research*, 3(2):4–28, 1984.

T. Mirfakhrai, J. Oh, M. Kozlov, E. C. W. Fok, M. Zhang, S. Fang, R. H. Baughman, and J. D. W. Madden. Electrochemical actuation of carbon nanotube yarns. *Smart Materials and Structures*, 16(2):S243–S249, 2007.

K. Mitobe, M. Satoh, and G. Capi. A ZMP control of a powered passive dynamic walking robot. In *World Automation Congress (WAC), 2010*, Sept. 2010.

A. Muller. Partial derivatives of the inverse mass matrix of multibody systems via its factorization. *Robotics, IEEE Transactions on*, 23(1):164–168, Feb. 2007. ISSN 1552-3098.

R. M. Murray, Z. Li, and S. S. Sastry. *A Mathematical Introduction to Robotic Manipulation*. CRC, Mar. 1994. ISBN 0849379814. URL `http://www.worldcat.org/isbn/0849379814`.

S. Nakaoka, F. Kanehiro, K. Miura, M. Morisawa, K. Fujiwara, K. Kaneko, S. Kajita, and H. Hirukawa. Creating facial motions of cybernetic human hrp-4c. In *Humanoid Robots, 2009. Humanoids 2009. 9th IEEE-RAS International Conference on*, pages 561–567, Dec. 2009.

H. Nijmeijer and A. van der Schaft. *Nonlinear dynamical control systems*. Springer-Verlag New York, Inc., New York, NY, USA, 1990. ISBN 0-387-97234-X.

J. A. Norris, A. P. Marsh, K. P. Granata, and S. D. Ross. Revisiting the stability of 2D passive biped walking: Local behavior. *Physica D: Nonlinear Phenomena*, 237 (23):3038–3045, 2008. ISSN 0167-2789.

J. Park and Y. Youm. General ZMP preview control for bipedal walking. In *Robotics and Automation, 2007 IEEE International Conference on*, pages 2682–2687, Apr. 2007.

J. Park, Y. Youm, and W. Chung. Control of ground interaction at the zero-moment point for dynamic control of humanoid robots. In *Robotics and Automation, 2005. ICRA 2005. Proceedings of the 2005 IEEE International Conference on*, pages 1724–1729, April 2005.

G. A. Pratt and M. M. Williamson. Series elastic actuators. In *Intelligent Robots and Systems (IROS), Proceedings. 1995 IEEE/RSJ International Conference on*, volume 1, pages 399–406, Aug. 1995.

J. E. Pratt, J. Carff, S. V. Drakunov, and A. Goswami. Capture point: A step toward humanoid push recovery. In *Humanoid Robots, 2006 6th IEEE-RAS International Conference on*, pages 200–207, Dec. 2006.

J. E. Pratt and R. Tedrake. Velocity-based stability margins for fast bipedal walking. *Fast Motions in Biomechanics and Robotics*, pages 299–324, 2006.

C. Radcliffe. Knee brace with pivot lock. U.S. Patent No. 5168865, Dec. 1992.

H. J. Ralston. Energy-speed relation and optimal speed during level walking. *Int. Z. angew. Physiol. einschl. Arbeitsphysiol.*, 17:277–283, 1958. ISSN 0301-5548. 10.1007/BF00698754.

R. Reinink. Knee locking systems for a walking robot. BSc thesis 012CE2009, University of Twente, Aug. 2009.

A. Reynolds. Design and control of a clutch for a minimally-actuated biped based on the passive-dynamic simple walker. Bsc report, Massachusetts Institute of Technology, June 2006.

D. W. Robinson. *Design and analysis of series elasticity in closed-loop actuator force control*. PhD thesis, Massachusetts Institute of Technology, 2000.

A. Ruina. Website Biorobotics and Locomotion Lab — Cornell University, 2010. URL `http://ruina.tam.cornell.edu/research/topics/locomotion_and_robotics/index.php`. Accessed December 2010.

J. Rummel, Y. Blum, H. M. Maus, C. Rode, and A. Seyfarth. Stable and robust walking with compliant legs. In *IEEE Int. Conf. on Robotics and Automation (ICRA)*, pages 5250–5255, May 2010.

D. C. Ruspini and O. Khatib. Collision/contact models for the dynamic simulation of complex environments. In *Proc., IEEE/RSJ International Conference on Intelligent Robots and Systems (IROS'97)*, Sept. 1997.

K. Sangbae, E. Hawkes, C. Kyujin, M. Joldaz, J. Foleyz, and R. Wood. Micro artificial muscle fiber using niti spring for soft robotics. In *Intelligent Robots and Systems, 2009. IROS 2009. IEEE/RSJ International Conference on*, pages 2228–2234, Oct. 2009.

P. Sardain and G. Bessonnet. Forces acting on a biped robot. Center of Pressure—Zero Moment Point. *Systems, Man and Cybernetics, Part A: Systems and Humans, IEEE Transactions on*, 34(5):630–637, Sept. 2004. ISSN 1083-4427.

E. Schuitema, M. Wisse, T. Ramakers, and P. Jonker. The design of LEO: A 2D bipedal walking robot for online autonomous reinforcement learning. In *Intelligent Robots and Systems (IROS), 2010 IEEE/RSJ International Conference on*, pages 3238–3243, Oct. 2010.

A. L. Schwab and M. Wisse. Basin of attraction of the simplest walking model. In *Proceedings of ASME Desgin Engineering Technical Conferences 2001*, Sept. 2001.

A. Seyfarth, F. Iida, R. Tausch, M. Stelzer, O. von Stryk, and A. Karguth. Towards bipedal jogging as a natural result of optimizing walking speed for passively compliant three-segmented legs. *The International Journal of Robotics Research*, 28(2):257–265, 2009.

M. W. Spong and G. Bhatia. Further results on control of the compass gait biped. In *Intelligent Robots and Systems, 2003. (IROS 2003). Proceedings. 2003 IEEE/RSJ International Conference on*, volume 2, pages 1933 – 1938 vol.2, Oct. 2003.

M. W. Spong and F. Bullo. Controlled symmetries and passive walking. *IEEE Transactions on Automatic Control*, 50(7):1025–1031, July 2005.

S. Stramigioli. *Modeling and IPC Control of Interactive Mechanical Systems: a Coordinate-free Approach*. Springer-Verlag, 2001.

S. Stramigioli, V. Duindam, G. van Oort, and A. Goswami. Compact analysis of 3D bipedal gait using geometric dynamics of simplified models. In *Robotics and Automation, 2009. ICRA '09. IEEE International Conference on*, pages 1978–1984, May 2009.

S. Stramigioli and M. van Dijk. Energy conservative limit cycle oscillations. In *Proc., 17th IFAC World Congress (IFAC'08)*, pages 15666–15671, July 2008.

S. Stramigioli, G. van Oort, and E. C. Dertien. A concept for a new energy efficient actuator. In *Proc., IEEE/ASME International Conference on Advanced Intelligent Mechatronics (AIM'08)*, pages 671–675, July 2008.

G. Strang. *Linear Algebra and its Applications*. Brooks Cole, third edition, 1988.

T. Sugihara and H. Nakamura. Variable impedant inverted pendulum model control for a seamless contact phase transition on humanoid robot. In *Proc., IEEE International Conference on Humanoid Robots (Humanoids'03)*, Oct. 2003.

S. Takao, Y. Yokokohji, and T. Yoshikawa. FSW (feasible solution of wrench) for multi-legged robots. In *Robotics and Automation. (ICRA '03). Proc. IEEE Int. Conf. on*, volume 3, pages 3815–3820, Sept. 2003.

I. Thorson, M. Svinin, S. Hosoe, F. Asano, and K. Taji. Design considerations for a variable stiffness actuator in a robot that walks and runs. In *Proc., JSME Conference on Robotics and Mechatronics (*ROBOMEC*'07)*, May 2007.

G. Tonietti. *Variable impedance actuation*. PhD thesis, Univ. of Pisa, 2005.

J. H. Townsend. Multiaxis controlled motion knee brace with a four bar joint and method for producing same. U.S. Patent No. 5330418, July 1994.

J. H. Townsend. Orthopedic knee brace joint assembly having a trigger locking mechanism. U.S. Patent No. 6500139, Dec. 2002.

K. Trifonov and S. Hashimoto. Active knee-lock release for passive-dynamic walking machines. *Proceedings of IEEE International Conference on Robotics and Biomimetics*, pages 958 – 963, 2007.

R. van Ham, B. Vanderborght, M. van Damme, B. Verrelst, and D. Lefeber. MACCEPA: the actuator with adaptable compliance for dynamic walking bipeds. In *Proc., 8th International Conference on Climbing and Walking Robots (CLAWAR'05)*, pages 759–766, Sept. 2005.

G. van Oort. Strategies for stabilizing a 3d dynamically walking robot. Msc thesis, Control Laboratory, University of Twente, June 2005.

G. van Oort, R. Carloni, D. J. Borgerink, and S. Stramigioli. An energy efficient knee locking mechanism for a dynamically walking robot. In *Proc., IEEE International Conference on Robotics and Automation (ICRA'11)*, pages 2003–2008, May 2011a.

G. van Oort, R. Reilink, and S. Stramigioli. New ankle actuation mechanism for a humanoid robot. In *Proc., 18th IFAC World Congress*, Aug. 2011b.

G. van Oort and S. Stramigioli. Using time-reversal symmetry for stabilizing a simple 3D walker model. In *Proc., IEEE International Conference on Robotics and Automation (ICRA'07)*, pages 4673–4678, Apr. 2007. ISBN ISBN 1-4244-0601-3.

G. van Oort and S. Stramigioli. Geometric interpretation of the zero-moment point. In *Proc., IEEE International Conference on Robotics and Automation (ICRA'11)*, pages 575–580, May 2011.

G. van Oort and S. Stramigioli. The Poincaré section and basin of attraction of a 2D passive dynamic walker on an irregular floor. Submitted to: IEEE International Conference on Robotics and Automation (ICRA'12), 2012.

B. Vanderborght. *Dynamic stabilisation of the biped Lucy powered by actuators with controllable stiffness*. PhD thesis, Vrije Universiteit Brussel, May 2007.

B. Verrelst, R. van Ham, B. Vanderborght, F. Daerden, D. Lefeber, and J. Vermeulen. The pneumatic biped "Lucy" actuated with pleated pneumatic artificial muscles. *Autonomous Robots*, 18(2):201–213, 2005. ISSN 0929-5593.

Viactors. VIACTORS website, 2011. URL `http://www.viactors.org`. Accessed April, 2011.

M. Vukobratović and B. Borovac. Zero-Moment Point — thirty five years of its life. *International journal of humanoid robotics*, 1(1):157–173, 2004.

M. Vukobratović, B. Borovac, and D. Surdilovic. Zero-moment point — proper interpretation and new applications. *Int. Conf. on Humanoid Robots*, 2001.

M. Vukobratović and D. Juričić. Contribution to the synthesis of biped gait. *Proc. IFAC Symp. Technical and Biological Problem and Control*, 1968.

M. Vukobratović and D. Juričić. Contribution to the synthesis of biped gait. *Biomedical Engineering, IEEE Transactions on*, 16(1):1–6, Jan. 1969. ISSN 0018-9294.

M. W. Walker and D. Orin. Efficient dynamic computer simulation of robotic mechanisms. *ASME Journal of Dynamic Systems, Measurement, and Control*, 104: 205–211, Sept. 1982.

Q. Wang, Y. Huang, and L. Wang. Passive dynamic walking with flat feet and ankle compliance. *Robotica*, 28(03):413–425, 2010.

Q. Wang, Y. Huang, L. Wang, and L. Dongjiao. Stability and adaptability of passivity-based bipedal locomotion with flat feet and ankle compliance. In *North American Congress of Biomechanics*, Aug. 2008.

B. J. Whipp and K. Wasserman. Efficiency of muscular work. *Journal of Applied Physiology*, 26(5):644–648, May 1969.

M. M. Williamson. Series elastic actuators. Master's thesis, Massachusetts Institute of Technology, June 1995.

M. Wisse. *Essentials of dynamic walking; Analysis and design of two-legged robots*. PhD thesis, TU Delft, 2004.

M. Wisse and A. L. Schwab. A 3D passive dynamic biped with roll and yaw compensation. *Robotica*, 19:275–284, 2001.

M. Wisse, A. L. Schwab, and F. C. T. van der Helm. Passive dynamic walking model with upper body. *Robotica*, 22:681–688, 2004.

M. Wisse, A. L. Schwab, R. Q. van der Linde, and F. C. T. van der Helm. How to keep from falling forward: elementary swing leg action for passive dynamic walkers. *IEEE Transactions on Robotics*, 21(3):393–401, June 2005. ISSN 1552-3098.

M. Wisse and J. van Frankenhuyzen. Design and construction of MIKE; a 2D autonomous biped based on passive dynamic walking. In *Proc., International Symposium of Adaptive Motion and Animals and Machines (AMAM'03)*, 2003.

Dankwoord

Een van de doelen van promoveren is laten zien dat je op eigen houtje een gedegen onderzoek kan uitvoeren. Nou heb ik inderdaad veel zelf zitten doen, maar gelukkig had ik al die tijd een boel mensen om me heen — op mijn werk en in de privésfeer — die op een of andere manier hebben geholpen om van de afgelopen vijf jaar vijf fijne jaren te maken. Enkele van hen wil ik graag specifiek bedanken.

Allereerst een woord van dank aan mijn promotor, Prof. dr. ir. Stramigioli. Stefano, enorm bedankt voor alles wat je voor me gedaan en geregeld hebt afgelopen jaren. Tijdens mijn jaren als promovendus heb ik heel veel met je kunnen kletsen over interessante wiskunde en geometrische dynamica. Ik heb ontzettend veel van je geleerd! Jouw onuitputtelijke en aanstekelijke enthousiasme, enorme betrokkenheid (zowel zakelijk als privé) en aangename persoonlijkheid hebben ervoor gezorgd dat ik me als promovendus onder jouw hoede helemaal op mijn plek voelde. Een fijnere 'baas' en collega had ik niet kunnen wensen! Ook heb ik erg genoten van de momenten dat we samen muziek maakten. De repetities van onze vakgroepband 'Out of Control' waren soms wat ongestructureerd, maar altijd erg leuk. Stefano, bedankt!

Dan mijn beste vriend en collega, Edwin. Wat hebben we samen een boel gedaan! Meer dan tien jaar samen in Drienerlalala gezongen (met vanaf ons afstuderen iedere dinsdagavond pannenkoeken met wijn in de vakgroepkeuken), vijf jaar Gonnagles en nog steeds af en toe samen achtergrondmuziek. Ook in de techniek blijven we elkaar tegenkomen: als collega's op de vakgroep waar we samen tientallen studenten begeleid hebben en aan Dribbel en TUlip sleutelden, 'voor de hobby' (muziekdoosjes), en sinds juni ook bij Kunst- en Techniekwerk. Hopelijk kan ik daar na het schrijven van mijn boekje wat vaker komen werken. Edwin, bedankt voor je steun in goede en in slechte tijden. Ik weet zeker dat we in de toekomst nog veel meer leuks gaan beleven!

I would also like to thank all co-authors of the articles we have produced. It has been a pleasure to work with you! Andy, Martijn, Job, Bart Koopman and Pieter Jonker, thank you very much for taking place in my graduation committee. I hope you enjoyed reading my thesis and I look forward to see you in real life

and answer all the difficult questions you undoubtedly will have for me. Paranimfen Wietse en Edwin, fijn dat jullie me bij willen staan tijdens de verdediging tegenover de hierboven genoemde Professoren.

Raffaella, thanks for helping me with a lot of things and taking over much work when I didn't have time for it. Ludo, buurman die altijd een luisterend oor had en mee wilde denken als ik er weer eens niet uitkwam, ik heb veel aan je gehad! Michel, dank voor alle informatie die je me verstrekt hebt over het regelen van de promotie. I also want to thank all colleagues of the group, Controllab and Dutch Robotics (also TUD and TU/e) for all the fun; it was a pleasure working with you all.

Enkele bachelor- en masterstudenten die ik begeleid heb wil ik speciaal bedanken. Eddy, als een van de eerste studenten die ik (samen met Edwin) begeleidde, heb jij óns uitstekend begeleid in het leren om begeleider te zijn. Windel, Roelof en Bart, de gezamenlijke hackavondjes als voorbereiding op ons RoboCup-avontuur in Graz (en Graz zelf ook) waren super.

Vincent, ondanks dat we maar zo kort samen hebben gewerkt, heb je een onuitwisbare indruk op mij achtergelaten. Het gemak waarmee jij de moeilijkste wiskunde begrijpelijk op papier weet te zetten en vooral je altijd ontspannen indruk maakten jou als een soort voorbeeldpromovendus voor mij. Bedankt ook voor het mogen gebruiken van je mooie LaTeX-template voor dit proefschrift.

Parkweggers & uitpandige inboedel, Gonnagles en Bragi-vrienden (hoewel ik niet eens bij Bragi gezeten heb…), met veel plezier denk ik terug aan alle Maandagavondjes, feestjes, zeilweekenden, optredens, reisjes, repetities, concertjes, trouwpartijen, oud-en-nieuw'en en andere activiteiten met jullie!

Misschien is het wat raar om dingen te bedanken, maar voor de Sagitta, de boot van Opa Jan en Oma Keetje, maak ik graag een uitzondering. Boot, bedankt voor de weekjes 'extended thuiswerken'. Midden in de Biesbosch op mijn laptop aan een paper schrijven terwijl Marlies in de voorkajuit aan haar harprepertoire werkt; idyllischer kan toch niet?

Papa en mama, jullie onvoorwaardelijke steun betekent heel veel voor me; wat ik ook doe, ik weet dat jullie altijd achter me staan, met raad en daad. Bart & Cox, Marleen & Peter & kinderen, Opa Boerdijk en Oma Keetje, wat fijn dat jullie mijn familie zijn! Bedankt voor jullie support, interesse en gezellige afleiding!

Tot slot, Marlies, niets is zo fijn als na een lange dag werken weer thuiskomen. Dat komt door jou, jij bent mijn thuis. Ook al die dagen dat ik op de studeerkamer zat te werken en jij me kopjes koffie, thee en paaseitjes kwam brengen en beneden pedaalharp speelde waren heerlijk. Jouw motivatie, betrokkenheid en goede zorgen hebben me enorm gesteund en zullen me altijd steunen. Wat een genot om altijd bij je te mogen zijn! Marlies, dank je wel dat je er bent.

About the author

Gijs van Oort was born on November 29th, 1978 in Nijmegen. In 1985 he and his family moved to Eindhoven. During secondary school at the Eckart College in Eindhoven, he spent most of his free time making music (flute and saxophone) and building 'technical things' at *De Jonge Onderzoekers Eindhoven*. He participated in some national and international Contests for Young Scientists. In 1997 he won the *Dutch Physics Olympiad* and participated in the International Physics Olympiad in Canada.

In 1997 he started his studies Electrical Engineering at the University of Twente. He completed the first year cum laude. During his studies he participated in the technical design contest *Createch*, in the local qualification rounds as well as the national finals (three times). He founded the a cappella group *Drienerlalala* and sang in various choirs. For two years he was a member of the board of the *Drienerloos Vocaal Ensemble*.

During his internship in 2004 at the *Deutsches Zentrum für Luft- und Raumfahrt* (DLR) in Munich, he worked on the localization of a mobile platform using a SICK laser scanner. In 2005 he obtained his M.Sc. degree Electrical Engineering, with specialization in mechatronics, at the Control Engineering group of the University of Twente, under supervision of Stefano Stramigioli.

After working as an employee at the University for nine months (modeling a positioning system for a marine vessel), he started his Ph.D. on walking robots at the Control Engineering group in June 2006. His supervisor was Stefano Stramigioli. Meanwhile he continued building 'technical things' (this time muziekdoosjes) and became sound engineer of the folk band the *Gonnagles*.

After his Ph.D. contract ended in June 2011, he worked at the Control Engineering group on the walking robot TUlip, until October 2011. He will continue his career at the Biomechanical Engineering group of the UT, where he will work on the development of LOPES, an exoskeleton device for gait rehabilitation.